



**Filipa da Rosa
Carvalho Sequeira**

**Sensores em POF baseados em intensidade para a
avaliação da qualidade de águas**

**Intensity based POF sensors for water quality
assessment**



**Filipa da Rosa
Carvalho Sequeira**

**Sensores em POF baseados em intensidade para a
avaliação da qualidade de águas**

**Intensity based POF sensors for water quality
assessment**

Tese apresentada à Universidade de Aveiro para cumprimento dos requisitos necessários à obtenção do grau de Doutor em Engenharia Física, realizada sob a orientação científica da Doutora Lúcia Maria Botas Bilro, Investigadora Auxiliar do Instituto de Telecomunicações e co-orientação do Professor Doutor Rogério Nunes Nogueira, Investigador Principal do Instituto de Telecomunicações e da Doutora Alisa Rudnitskaya, Investigadora Auxiliar do departamento de Química da Universidade de Aveiro.

o júri

presidente

Doutor Vítor António Ferreira da Costa
Professor Catedrático, Universidade de Aveiro

Doutor Marcelo Martins Werneck
Professor Catedrático, Universidade Federal do Rio de Janeiro

Doutor José Luís Campos de Oliveira Santos
Professor Catedrático, Universidade do Porto

Doutora Margarida Maria Resende Vieira Facão
Professora Auxiliar, Universidade de Aveiro

Doutor Manuel Filipe Pereira da Cunha Martins Costa
Professor Auxiliar, Universidade do Minho

Doutora Lúcia Maria Botas Bilro
Investigadora Auxiliar, Instituto de Telecomunicações, Universidade de Aveiro

agradecimentos

O sucesso deste trabalho deve-se à colaboração de várias pessoas de áreas científicas distintas. Agradeço o convite que me foi feito e que culminou neste agora, agradeço a presença e as discussões saudáveis. Agradeço também a dinâmica criada nas alturas mais difíceis, e também o menos fácil, que me fez crescer.

Um agradecimento com carinho para o Paulino, a Nair e a Marta, pela amizade e pelo sorriso * Um agradecimento de Sol para o Nunzio e para o Gino, grandes Seres, que não abrem só o laboratório mas também os braços e o coração. Sem vocês isto não estava a acontecer assim. Agradeço de coração ao Francesco, que um dia o possa fazer pessoalmente. Tive o prazer (e também alvoroço) de passar por vários sítios, pessoas diferentes, laboratórios distintos. Concluo sempre o mesmo, o mais importante são as pessoas.

Aos de cá, aos de lá, e aos que já estão do outro lado, um grande abraço com sorriso, gratidão por nos termos cruzado. Até já *

Agradeço o apoio financeiro da Fundação para a Ciência e Tecnologia – FCT através da bolsa SFRH/BD/88899/2012 e do projeto INITIATE - IF/FCT - IF/01664/2014/CP1257/CT0002, que permitiu a concretização de missões de curta duração no âmbito de colaborações nacionais e internacionais. Agradeço também ao Instituto de Telecomunicações, IT-Aveiro.

palavras-chave

Fibra óptica polimérica, sensores em fibra óptica, índice de refração, sensores químicos, biossensores, modulação de intensidade, tecnologias de baixo-custo, avaliação da qualidade de águas, monitorização ambiental.

resumo

Hoje em dia há uma necessidade de soluções simples e de baixo custo para a avaliação da qualidade de águas e que permitam a monitorização remota de contaminantes, no local e em tempo real. As tecnologias baseadas em POF podem oferecer essa possibilidade através de sistemas de interrogação óptica adequados, combinados com camadas sensíveis especialmente desenvolvidas para detecção química.

As plataformas ópticas baseadas em POF foram desenvolvidas e caracterizadas com soluções aquosas com diferentes índices de refração. Os sensores foram otimizados através da variação do comprimento e/ou rugosidade da região sensível.

A capacidade de detecção química das plataformas ópticas desenvolvidas foi avaliada através do revestimento com camadas sensíveis, nomeadamente polímeros molecularmente impressos (PMI), utilizando diferentes técnicas de deposição. A dependência da imobilização de proteínas na superfície de POFs modificadas foi avaliada com o objectivo de desenvolver biossensores para detecção química.

Um sensor POF para detecção química, em configuração D-shape, foi desenvolvido com sucesso através do revestimento com um PMI, permitindo a detecção de perfluorooctanoato (POFA/PFO⁻) em soluções aquosas com um limite de detecção entre 0.20 – 0.28 ppb.

A colaboração com investigadores de diferentes áreas foi essencial para o sucesso do trabalho desenvolvido.

keywords

polymeric optical fibres (POFs), optical fibre sensors (OFSs), refractive index (RI), chemical sensors, biosensors, intensity modulation, low-cost technology, water quality assessment, environmental monitoring.

abstract

Nowadays there is the need for low-cost and user-friendly solutions for water quality assessment which can allow for remote, in-site and real-time monitoring of water contaminants. POF sensing technologies combined with specially developed sensitive layers for chemical detection may offer these possibilities, with proper interrogation systems.

POF sensing platforms based on low-cost procedures were developed and characterized using aqueous solutions of different refractive indices (RI). The POF RI sensors were optimized by varying the length and/or roughness of the sensing region.

The suitability of these sensing platforms for chemical detection was evaluated through the coating with sensitive layers, namely molecularly imprinted polymers (MIPs) using different deposition techniques. The dependency of proteins immobilization on the POF's surface was evaluated aiming future developments in chemical detection using POF biosensors.

A D-shaped POF chemical sensor was successfully developed using a sensitive MIP layer, allowing the detection of perfluorooctanoate (POFA/PFO⁻) in aqueous media with a limit of detection of 0.20 – 0.28 ppb.

The collaboration of researchers from different areas was essential for the success of the developed work.

Glossary of acronyms

List of symbols and constants

| | |
|--|-----------|
| Chapter 1 Introduction..... | 1 |
| 1.1 Motivation | 1 |
| 1.2 Main objective and outline..... | 1 |
| 1.3 Structure of the thesis..... | 2 |
| 1.4 Main contributions | 3 |
| | |
| Chapter 2 Sensing with POFs targeting chemical detection | 7 |
| 2.1 Introduction..... | 7 |
| 2.2 Light-matter interaction | 8 |
| 2.3 Polymeric Optical fibres (POFs) and light propagation | 12 |
| 2.3.1 Acceptance angle and numerical aperture | 14 |
| 2.3.2 Types of fibres and refractive index profile | 15 |
| 2.3.3 POF's designation and materials | 17 |
| 2.3.4 Optical attenuation | 19 |
| 2.3.5 Mechanical and thermal properties..... | 21 |
| 2.3.6 Chemical resistance..... | 22 |
| 2.4 Optical fibre sensing principles | 22 |
| 2.4.1 Intensity based sensing | 24 |
| 2.4.2 Surface plasmon resonance (SPR)..... | 30 |
| 2.5 Chemical sensing and biosensing | 32 |
| 2.5.1 Direct (label-free) and indirect (label-based) sensing methods..... | 33 |
| 2.5.2 Sensitive layers..... | 33 |
| 2.5.3 Molecularly Imprinted Polymers (MIPs) | 35 |
| 2.6 Applications of intensity based POF sensors and POF-MIP based chemical sensing | 43 |
| 2.6.1 Physical POF sensors | 43 |
| 2.6.2 Refractive index sensing..... | 44 |
| 2.6.3 Chemical sensing..... | 46 |
| 2.6.4 POF-MIP based sensing | 50 |
| 2.6.5 POF biosensing | 52 |
| 2.7 Conclusions..... | 53 |
| | |
| Chapter 3 Preliminary study of POF-MIP based sensors | 55 |
| 3.1 Introduction..... | 55 |
| 3.2 Preliminary studies..... | 56 |
| 3.2.1 Optical fibres | 57 |
| 3.2.2 Chemical reagents..... | 57 |
| 3.2.3 MIP and NIP preparation and grafting | 57 |
| 3.2.4 Optical characterization – mPOF-MIPs | 59 |
| 3.2.5 Conclusions..... | 61 |

| | | |
|--|--|------------|
| 3.3 | Materials and methods | 62 |
| 3.3.1 | Optical fibres | 62 |
| 3.3.2 | Length of the sensing region | 62 |
| 3.3.3 | Removal of the fluorinated cladding..... | 63 |
| 3.3.4 | Analyte solutions..... | 65 |
| 3.4 | Immobilization of the initiator on the unclad POF's surface..... | 71 |
| 3.4.1 | Chemical reagents..... | 71 |
| 3.4.2 | Initiator immobilization..... | 71 |
| 3.4.3 | Characterization of AAPH immobilization on POF samples | 71 |
| 3.5 | MIP & NIP grafting on POF's surface | 76 |
| 3.5.1 | Chemical reagents..... | 76 |
| 3.5.2 | Grafting procedures | 76 |
| 3.5.3 | POF selection and NIP optimization..... | 77 |
| 3.5.4 | POF's functionalization by MIP grafting..... | 81 |
| 3.6 | Stability of unclad POF samples immersed in solvent..... | 85 |
| 3.6.1 | General procedures..... | 85 |
| 3.6.2 | Optical microscopy..... | 86 |
| 3.6.3 | Thickness variation..... | 88 |
| 3.6.4 | Mass variation | 89 |
| 3.6.5 | Conclusions..... | 90 |
| 3.7 | MIP grafting on PMMA slabs..... | 90 |
| 3.8 | Optical sensing setup and data processing | 93 |
| 3.9 | Sensors characterization | 96 |
| 3.9.1 | Response of unclad POFs with temperature variation | 96 |
| 3.9.2 | Initiator immobilization and MIP's grafting on PMMA surface | 97 |
| 3.9.3 | Effect of solvent at polymerization conditions | 98 |
| 3.9.4 | Response to the template analyte (NH_4^+) | 100 |
| 3.9.5 | POF-MIP sensor response to interferents – NaCl and D-(+)-glucose | 104 |
| 3.9.6 | Sensitivity to refractive index variation | 106 |
| 3.10 | Conclusions and future developments..... | 109 |
| Chapter 4 Intensity based POF refractive index sensors – performance and optimization | | 111 |
| 4.1 | Introduction..... | 111 |
| 4.2 | D-shaped POF RI sensors..... | 111 |
| 4.2.1 | General manufacturing procedures..... | 111 |
| 4.2.2 | Preliminary results | 112 |
| 4.2.3 | Optimization..... | 118 |
| 4.2.4 | Conclusions and future work | 139 |
| 4.3 | Straight POF RI sensors..... | 140 |
| 4.3.1 | Roughness of the sensing region | 140 |
| 4.3.2 | Curvature of the sensing region - straight vs U-bent configurations..... | 151 |
| 4.3.3 | Conclusions and future work | 153 |
| 4.4 | Conclusions..... | 154 |

| | |
|---|------------|
| Chapter 5 POF chemical sensing and biosensing | 155 |
| 5.1 Introduction..... | 155 |
| 5.2 D-shaped POF chemical sensors for the detection of perfluorooctanoate (PFOA/PFO ⁻)..... | 155 |
| 5.2.1 Introduction and state of the art | 155 |
| 5.2.2 Optical sensing platform | 158 |
| 5.2.3 Refractive index characterization..... | 159 |
| 5.2.4 Sensitive MIP layer | 161 |
| 5.2.5 PFOA/PFO ⁻ detection..... | 165 |
| 5.2.6 Conclusions..... | 169 |
| 5.3 Protein immobilization on POF's surface | 170 |
| 5.3.1 Introduction and state of art..... | 171 |
| 5.3.2 Optical sensing platform | 174 |
| 5.3.3 Buffer, protein and staining solutions..... | 175 |
| 5.3.4 Influence of the immersion time..... | 177 |
| 5.3.5 Influence of the buffer solutions: phosphate and Tris..... | 188 |
| 5.3.6 Influence of the temperature..... | 196 |
| 5.3.7 Conclusions..... | 199 |
| 5.4 Conclusions..... | 200 |
| | |
| Chapter 6 Conclusions and future developments | 201 |
| 6.1 Major conclusions | 201 |
| 6.2 Future developments | 203 |
| | |
| References | 205 |

| | |
|------------------|--|
| A a | |
| AAPH | 2,2'-Azobis(2-methylpropionamidine) dihydrochloride |
| AIBN | 2,2-Azobisisobutyronitrile |
| ATR | Attenuated Total Reflection |
| D d | |
| DBDS | Dibenzyl disulphide |
| DNA | Deoxyribonucleic acid |
| DTT | 1,4-Dithiothreitol |
| E e | |
| EDMA | Ethylene glycol dimethacrylate |
| F f | |
| 2-FAL | Furfural |
| FBG | Fibre Bragg Grating |
| FIM | (N-(2-(6-4-methylpiperazin-1-yl)-1,3-dioxo-1 H-benzo[de]isoquinolin-2(3H)-yl-ethyl)acrylamide) |
| fMIPs | Fluorescent MIPs |
| FOCS | Fibre Optic Chemical Sensor |
| FPI | Fabry–Pérot Interferometer |
| FTIR | Fourier-Transform Infrared Spectroscopy |
| G g | |
| GO | Graphene oxide |
| rGO | Reduced graphene oxide |
| GOF | Glass Optical Fibre |
| I i | |
| IR | Infrared |
| L l | |
| LED | Light Emitting Diode |
| LMR | Lossy Mode Resonance |
| LOD | Limit of Detection |
| LPG | Long Period Grating |
| LSPR | Localized Surface Plasmon Resonance |
| M m | |
| MAA | Methacrylic acid |
| MIP | Molecularly Imprinted Polymer |
| MM | Multimode |
| MMA | Methyl Methacrylate |
| MMI | Multimode Interference |
| mPOF | Microstructured POF |
| MW | Microwaves |
| MZI | Mach-Zehnder Interferometer |
| N n | |
| NA | Numerical Aperture |
| NIP | Non-Imprinted Polymer |
| NMR | Nuclear Magnetic Resonance |
| NP | Nanoparticle |
| O o | |
| OFS | Optical Fibre Sensor |
| OLED | Organic Light Emitting Diode |
| OSA | Optical Spectrum Analyser |
| P p | |
| PAHs | Polycyclic Aromatic Hydrocarbons |
| PC | Polycarbonate |
| PCF | Photonic Crystal Fibre |
| PECVD | Plasma-Enhanced Chemical Vapour Deposition |
| PFASs | Perfluorinated Alkylated Substances |
| PFDA | 1H,1H,2H,2H-Perfluorodecyl acrylate |
| PFO ⁻ | Perfluorooctanoate |
| PFOA | Perfluorooctanoic acid |

Glossary of acronyms

| | |
|---------------------|--|
| PFO-NH ₄ | Ammonium perfluorooctanoate |
| PFOS | Perfluorooctanesulfonic acid |
| PMMA | Poly(methyl methacrylate) |
| POF | Polymer Optical Fibre (or Plastic Optical Fibre) |
| PS | Polystyrene |
| PVA | Poly(vinyl alcohol) |
| PVC | Poly(vinyl chloride) |
| PVDF | Poly(vinylidene fluoride) |
| PVP | Poly(vinylpyrrolidone) |
| R r | |
| RH | Relative Humidity |
| Rh B ITC | Rhodamine B isothiocyanate |
| Rh 6G | Rhodamine 6G |
| RI | Refractive Index |
| RIU | Refractive Index Units |
| RNA | Ribonucleic acid |
| S s | |
| SRB | Sulphate-Reducing Bacteria |
| SEM | Scanning Electron Microscopy |
| SI | Step-Index |
| SM | Single Mode |
| SPR | Surface Plasmon Resonance |
| T t | |
| THF | Tetrahydrofuran |
| TIR | Total Internal Reflection |
| TFBG | Tilted Fibre Bragg Grating |
| TNT | 2,4,6-Trinitrotoluene |
| Tris | Tris(hydroxymethyl)aminomethane |
| U u | |
| UV | Ultraviolet |
| V v | |
| VIS | Visible |
| VBT | (Vinylbenzyl) trimethylammonium chloride |
| VOC | Volatile Organic Compound |

| | |
|-----------------|--|
| A a | |
| A | Absorbance |
| A_r | Area |
| A_t | Optical attenuation |
| C c | |
| c_0 | Speed of the light in vacuum |
| c | Molar concentration |
| D d | |
| D | Thickness of the sensing region |
| D_{aP} | Thickness of the sensing region after polymerization |
| D_{bP} | Thickness of the sensing region before polymerization |
| D_n | Dry samples |
| d | Diameter of the optical fibre |
| d_p | Penetration depth of the evanescent field |
| G g | |
| G | Gain |
| H h | |
| H_n | Hydrated samples |
| I i | |
| I | Transmitted light |
| I_{source} | Current of the power supply |
| I_0 | Incident light |
| J j | |
| J_x | Jacketed POF |
| K k | |
| K_{inc} | Propagation constant of the evanescent wave |
| K_{SP} | Surface plasmon wave propagation constant |
| k | Self-referenced transmitted signal |
| k_{avg} | Average value of k_{norm} (replicated measurements) |
| k_{norm} | Normalized self-referenced transmitted signal |
| L l | |
| L, l | Length, distance |
| M m | |
| M | Number of modes |
| m | Mass |
| N n | |
| NA | Numerical aperture |
| NJ _x | Unjacketed POF |
| n | Refractive index |
| n_{clad} | Refractive index of the fibre cladding |
| n_{co} | Refractive index of the fibre core |
| n_{ext} | Refractive index of the external medium |
| n_{mol} | Number of mol |
| n_s | Refractive index of the sensing (dielectric) layer |
| P p | |
| P | Optical power |
| R r | |
| R | Resistance |
| R_λ | Responsivity of the photodetector |
| RT ₋ | Sample's modification at room temperature |
| r_c | Curvature radius of the POF's sensing region |
| r_f | Radius of the optical fibre |
| S s | |
| S | Sensitivity |
| S_{PSL} | Sensitivity - preliminary study with the length of D-shaped POFs |
| T t | |
| T | Transmittance |

List of symbols and constants

| | |
|-------------------------------------|---|
| T_g | Glass transition temperature |
| T_- | Sample's modification at 57 °C |
| V v | |
| V | Volume |
| $V_{multimeter}$ | Output voltage measured with the multimeter |
| V_{number} | V-number |
| V_{sensor} | Output voltage of the sensor signal |
| V_{source} | Voltage of the power supply |
| V_{ref} | Output voltage of the reference signal |
| V_0 | Output voltage for the unpolished POF sample |
| v | Speed |
| A α | |
| α | Attenuation coefficient |
| $\Delta \delta$ | |
| ΔD | Variation of the sensing region thickness |
| Δm | Mass variation |
| Δn | Resolution |
| $\delta(\Delta D)$ | Associated error of ΔD |
| $\delta(\Delta m)$ | Associated error of Δm |
| δD_{aP} | Standard deviation of D_{aP} |
| δD_{bP} | Standard deviation of D_{bP} |
| δk | Standard deviation of k |
| δk_{avg} | Standard deviation of k_{avg} |
| δk_{avg_max} | Maximum value of δk_{avg} obtained for all the sensors |
| δk_{norm} | Error of k_{norm} |
| δk_{norm_max} | Maximum value of δk_{norm} obtained for all the sensors |
| δn_{ext} | Standard deviation of n_{ext} |
| E ϵ | |
| ϵ | Molar absorptivity |
| ϵ_{mr} | Real part of the metal dielectric constant |
| $\Theta \theta$ | |
| θ_c | Complementary angle of φ_c |
| θ_{max} | Maximum angle of the acceptance cone (acceptance angle) |
| θ_r | Angle of reflection |
| θ_{res} | Angle of incidence for resonance condition |
| θ_1 | Incident angle |
| θ_2 | Angle of refraction |
| $\Lambda \lambda$ | |
| λ | Wavelength |
| λ_{DR} | Spectral resolution of the interrogation system |
| λ_{max} | Wavelength at which occurs maximum absorption |
| λ_{res} | Resonance wavelength |
| $\Phi \varphi$ | |
| φ | Incidence angle at the core-cladding interface |
| φ_c | Critical angle |

Chapter 1 Introduction

1.1 Motivation

Nowadays, the assessment of water quality is of outermost relevance for sustainable living and biodiversity. The water bodies, namely sea, lakes, subterranean and superficial waters are commonly contaminated with chemical species from various sources, including industrial wastes, agricultural effluents due to the excessive use of herbicides and fertilizers, sewage and marine dumping, among others. Despite constant technological developments, waste water treatment plants still do not have the capability of detection and removal of all the contaminants that are present in the waste waters and which, unfortunately, end up in the water bodies (Le *et al.*, 2017)(Garcia-Ivars *et al.*, 2017)(Li *et al.*, 2017). The development of sensors for water quality assessment, which would allow remote and on site measurements, can promote a new page in environmental monitoring. Nowadays there is still the need of sample collection and analysis in a certificated laboratory with the use of high resolution and expensive equipment (Gholizadeh, Melesse and Reddi, 2016)(Richardson and Ternes, 2018).

Optical fibre sensors (OFSs) can overcome these drawbacks as they allow for highly sensitive remote sensing, can be used in harsh environments and may be used as chemical sensors and biosensors through the use of selective and active layers (Wang and Wolfbeis, 2016)(Pospíšilová, Kuncová and Trögl, 2015)(Elosua *et al.*, 2017). Plastic optical fibres (POFs) are a good option in comparison with glass optical fibres (GOFs) for the development of sensors as they are more flexible, easier to handle and manipulate, allowing low-cost sensing systems through the use of fibres with large diameters, which can be connected to low-precision and low-cost connectors. This brings about the possibility of low-cost sensing systems based on intensity modulation (Bilro *et al.*, 2012)(Jin and Granville, 2016).

The principle of operation of optical fibre chemical sensors and biosensors is based on the variations of the properties of the sensitive layer deposited on the fibre. One commonly employed property is refractive index (RI), which changes when a specific target (chemical specie or family) binds to the sensitive layer, altering the guiding characteristics of the light in the POF (N. Cennamo *et al.*, 2017)(Lopes *et al.*, 2018). Light absorption (Foguel *et al.*, 2015)(Khalaf *et al.*, 2017)(Azkune *et al.*, 2018) or emission such as fluorescence (Rivera *et al.*, 2009)(Ton *et al.*, 2015) are also optical principles which can be employed in chemical sensing or biosensing with POF.

1.2 Main objective and outline

This work aimed at the development of low-cost POF chemical sensors and biosensors using simple, low-cost and fast procedures. In order to perform chemical detection, the sensor must be selective and this is directly dependent on the sensitive layer. For selectivity, molecularly imprinted polymers (MIPs) were chosen as active and selective layers. The MIP possesses cavities with affinity to the selected target molecule and can be tailored to be selective to a chemical specie or family.

Firstly, preliminary studies were conducted using a POF with straight configuration and grafting of a molecularly imprinted polymer on the POF's surface. These studies led to a variety of questions which were the basis of the developed work.

Different optical platforms will be presented, one based on a D-shaped POF and other in modified straight POFs. These sensors were characterized with aqueous solutions with different refractive indices allowing to verify their viability for refractive index sensing. The performance of the sensors was evaluated and optimized.

After the validation of the POF sensing platforms, the deposition of selective layers previously studied and validated was foreseen for chemical and biochemical sensing. An MIP was deposited in the surface of a D-shaped POF sensor which was further characterized with solutions of the target analyte. The immobilization of proteins on the surface of modified straight POFs was studied and validated, aiming future deposition of modified and selective proteins for chemical detection.

1.3 Structure of the thesis

This thesis is organized in six chapters.

This **first chapter** includes the motivation and main objectives as well as the mainly contributions of the developed work.

The **second chapter** describes scientific aspects related with POF's sensing technology targeting chemical detection. First, an overview is given of light matter interactions, as they allow for the applicability of POFs in sensing technology. The main characteristics of POFs will be described, including light propagation. An overview on sensing technologies with POFs will be described, with special attention to the intensity based sensing. POF chemical sensors can be developed through the combination with sensitive layers as well as intrinsic properties of the target analyte or labels, therefore a brief description will be given on these aspects. Molecularly imprinted polymers (MIPs) will be described in more detail since this kind of sensing layer was chosen for the development of POF chemical sensors. Finally, the state of the art of intensity based sensors will be addressed, with a special focus on refractive index sensors, chemical sensors and biosensors and specially POF-MIP based sensors.

The **third chapter** contains the preliminary studies of POF-MIP based sensors for chemical detection. The chemical procedures and experimental conditions are described and the grafting of POFs with MIPs is evaluated. MIP layer was synthesized using thermal polymerization and POF-MIP sensors were further characterized in solutions with varying refractive index including solutions of the template, ammonium chloride, as well as other chemical species such as sodium chloride, glucose and sucrose. These works allowed to conclude that new studies were needed: (i) optimization of the optical platform, namely the POF, including the development of new geometries; (ii) study of the viability of the selective layer to perform selective binding to allow selective chemical detection by the optical platform; (iii) assessment of the sensitive layer deposition on POF's surface by optical characterization. These paved the way for the work developed and reported in the subsequent chapters.

The **fourth chapter** describes the development and performance optimization of two optical platforms for refractive index sensing. A D-shaped POF sensing platform was developed in collaboration with Dr. Nunzio Cennamo and Dr. Luigi Zeni from the University of Campania Luigi

Vanvitelli in Aversa, Italy. The obtained results showed the viability of this platform for low-cost RI sensing using simple and fast manufacturing procedures. The performance optimization of this D-shaped POF platform was a continuation of the previous work by Bilro et. al with a side-polished POF sensor for curvature and RI sensing (Bilro, Alberto, *et al.*, 2010)(Lúcia Bilro *et al.*, 2011). A modified straight POF sensor was also developed and presented. The performance optimization of this sensor was based in the increase of the interaction of light with the external medium by modifying the POF structure and lowering the transmission capability in a controlled way. This was possible by changing the roughness of the sensing region of an unclad POF. These two POF sensors allowed to obtain a resolution of $10^{-3} - 10^{-4}$ RIU, dependent on the external refractive index, revealing their viability for future developments on chemical sensing and biosensing.

After the positive results achieved with the optical platforms described in the fourth chapter, the conditions were finally created for the development of POF chemical sensors and biosensors through the deposition of selective layers. These studies are presented in the **chapter five**. Firstly, an MIP was deposited in the surface of a D-shaped POF sensor which allowed the detection of perfluorooctanoate (PFOA/PFO⁻) with a LOD of 0.20 – 0.28 ppb, showing the viability of this POF platform to act as a chemical sensor. This MIP was validated (Nunzio Cennamo, D'Agostino, *et al.*, 2018) prior to the deposition on the D-shaped POF platform. Secondly, the immobilization of proteins on the surface of modified POFs was conducted and validated. Studies were performed to evaluate the effect of the experimental conditions on proteins immobilization. This was possible through a collaboration with Dr. Teresa Santos-Silva from the UCIBIO, Faculty of Sciences and Technology, Nova University of Lisbon, Portugal.

These studies validate the capability of these low-cost POF sensors for water quality assessment. Sensing properties, such as response time, sensitivity, limit of detection, reversibility and reproducibility, are directly dependent on the chemical sensitive layer.

The **sixth chapter** describes the main conclusions and suggestions for future developments.

1.4 Main contributions

Two optical platforms based on POFs were manufactured. The performance and optimization of these platforms were conducted and their viability for chemical detection was analysed.

In summary, the main contributions of this work are:

- development of a D-shape POF sensor for RI sensing;
- optimization of the D-shaped POF sensor based on the variation of the length and roughness of the sensing region;
- development of D-shaped POF-MIP sensor for the detection of perfluorooctanoate (PFOA/PFO⁻) in water;
- development of a modified straight POF sensor for RI sensing;
- optimization of the modified straight POF sensor based on the variation of the roughness and bending of the sensing region;
- analysis and validation of protein immobilization on the modified POF surface.

The conducted studies led to the presentation of thirteen papers in international conferences, publication of three peer-reviewed articles in open-access journals and two book chapters:

Book Chapters

F. Sequeira, R.N. Nogueira, L. Bilro, 'Chemical Sensing with POF', Chapter in, *Plastic Optical Fiber Sensors: Science, Technology and Applications*, Marcelo M. Werneck, Regina Célia S. B. Allil, Taylor & Francis, Boca Raton, 2019.

R. Oliveira, F. Sequeira, L. Bilro, R.N. Nogueira, 'Polymer Optical Fiber Sensors and Devices', Chapter in, *Handbook of Optical Fibers*, Gang Ding Peng, Springer, Singapore, Singapore, 2018.

Papers in journals

F. Sequeira, N. Cennamo, A. Rudnitskaya, R.N. Nogueira, L. Zeni, L. Bilro, 'D-Shaped POF Sensors for Refractive Index Sensing—The Importance of Surface Roughness', *Sensors*, Vol. 19, No. 11, pp. 2476 - 2476, May, 2019. doi: 10.3390/s19112476

N. Cennamo, G. D'Agostino, F. Sequeira, F. Mattiello, G. Porto, A. Biasiolo, R.N. Nogueira, L. Bilro, L. Zeni, 'A Simple and Low-Cost Optical Fiber Intensity-Based Configuration for Perfluorinated Compounds in Water Solution', *Sensors*, Vol. 18, No. 9, pp. 3009 - 3009, September, 2018. doi: 10.3390/s18093009

F. Sequeira, D. Duarte, L. Bilro, A. Rudnitskaya, M. Pesavento, L. Zeni, N. Cennamo, 'Refractive Index Sensing with D-Shaped Plastic Optical Fibers for Chemical and Biochemical Applications', *Sensors*, 16(12), pp. 2119, December, 2016. doi:10.3390/s16122119

N. Lopes, F. Sequeira, M.T.S.R. Gomes, R. Nogueira, L. Bilro, O.A. Zadorozhnaya, A.M. Rudnitskaya, 'Fiber optic sensor modified by grafting of the molecularly imprinted polymer for the detection of ammonium in aqueous media', *Scientific and Technical Journal of Information Technologies, Mechanics and Optics*, vol.15, no. 4, pp. 568–577, 2015. doi: 10.17586/2226-1494-2015-15-4-568-577.

Papers in conferences

N. Cennamo, F. Arcadio, C. Perri, L. Zeni, F. Sequeira, L. Bilro, R.N. Nogueira, G. D'Agostino, G. Porto, A. Biasiolo, 'Water monitoring in smart cities exploiting plastic optical fibers and molecularly imprinted polymers. The case of PFBS detection', *IEEE International Symposium on Measurements and Networking, M&N*, Catania, Italy, July, 2019. doi: 10.1109/IWMN.2019.8805049

F. Sequeira, D. Duarte, R. Nogueira, L. Bilro, 'Low-Cost Sensing with Plastic Optical Fibers—From Turbidity and Refractive Index to Chemical Sensing'. *Proceedings 2019*, 15, 12; *In "Proceedings of 7th International Symposium on Sensor Science"*. doi: 10.3390/proceedings2019015012

F. Sequeira, R. Nogueira, L. Bilro, T. Santos-Silva, 'Coating of modified plastic optical fibers with proteins for chemical sensing and biosensing: preliminary studies', *Proc. SPIE 11028, Optical Sensors 2019*, 110282O, SPIE Optics + Optoelectronics, Prague, Czech Republic, April, 2019. doi: 10.1117/12.2522347

N. Cennamo, G. D'Agostino, F. Sequeira, F. Arcadio, G. Porto, A. Biasiolo, C. Perri, R.N. Nogueira, L. Bilro, L. Zeni, 'An optical fiber intensity-based sensor configuration for the detection of PFOA in water', in 26th International Conference on Optical Fiber Sensors. Washington, September, 2018 D.C.: OSA, p. ThE37. doi: 10.1364/OFS.2018.ThE37

F. Sequeira, N. Cennamo, A. Rudnitskaya, R.N. Nogueira, L. Zeni, L. Bilro, 'Comparative analysis between refractive index POF Sensors for Chemical Sensing', International Conference on Plastic Optical Fibers POF, Seattle, United States, September, 2018.

N. Cennamo, G. D'Agostino, F. Sequeira, F. Mattiello, G. Porto, A. Biasiolo, R.N. Nogueira, L. Bilro, L. Zeni, 'Molecular Imprinted Polymer on a D-shaped Plastic Optical Fiber for the selective detection of Perfluorooctanoate', EUROPT(R)ODE XIII, Naples, Italy, pp. 181, March, 2018.

F. Sequeira, R.N. Nogueira, A. Rudnitskaya, N. Cennamo, L. Zeni, L. Bilro, 'Sensitivity optimization of POF sensors based on an intensity low-cost configuration targeting chemical and biochemical sensing', International Conference on Plastic Optical Fibres - POF, Aveiro, Portugal, paper 90: 1-4, September, 2017.

F. Sequeira, L. Bilro, A. Rudnitskaya, M. Pesavento, L. Zeni, N. Cennamo, 'Optimization of an Evanescent Field Sensor based on D-Shaped Plastic Optical Fiber for Chemical and Biochemical Sensing', 30th Eurosensors Conference, Budapest, Hungary, Procedia Engineering, Vol. 168, pp. 810 - 813, September, 2016. doi: 10.1016/j.proeng.2016.11.279

F. Sequeira, D. Duarte, R.N. Nogueira, A. Rudnitskaya, N. Cennamo, L. Zeni, L. Bilro, 'Analysis of the roughness in a sensing region on D-shaped POFs', Proceedings of the 25th International Conference on Plastic Optical Fibres - POF 2016, Aston University, Birmingham, United Kingdom, September, 2016.

F. Sequeira, D. Duarte, A. Rudnitskaya, M.T.S.R. Gomes, R.N. Nogueira, L. Bilro, 'Ammonium sensing in aqueous solutions with plastic optical fiber modified by molecular imprinting', European Workshop on Optical Fibre Sensors - EWOFs, Limerick, Ireland, Vol. 9916, pp. 99161I-1 - 99161I-4, May, 2016. doi: 10.1117/12.2236941

F. Sequeira, A. Rudnitskaya, M.T.S.R. Gomes, R.N. Nogueira, L. Bilro, 'Ammonium sensing with plastic optical fiber modified by molecular imprinting', EUROPT(R)ODE XIII, Graz, Austria, pp. 184, March, 2016.

F. Sequeira, A. Rudnitskaya, M.T.S.R. Gomes, R.N. Nogueira, L. Bilro, 'Plastic optical fiber sensor modified by molecular imprinting for ammonium sensing', XVIII European Conference in Analytical Chemistry EUROANALYSIS, Bordeaux, France, September, 2015.

Chapter 1 Introduction

F. Sequeira, N. Lopes, M.T.S.R. Gomes, A. Rudnitskaya, R.N. Nogueira, L. Bilro, 'Molecularly imprinted polymer grafted on a polymeric optical fibre for ammonium sensing', International Conf. on Applications of Optics and Photonics - AOP, Aveiro, Portugal, pp. 72, May, 2014.

Chapter 2 Sensing with POFs targeting chemical detection

This chapter intends to give an overview of the principles and characteristics of the low-cost polymeric optical fibre (POF) chemical sensors as well as the state of the art of the intensity based POF chemical sensors and biosensors.

First, light-matter interactions and the characteristics of light propagation in POFs will be described. An overview of the sensing principles which allow to develop POF sensors will be given, focusing on intensity based sensing.

Chemical detection with POFs is possible due to intrinsic properties of the target analyte(s) or using active and selective layers or labels. Therefore, a brief description of these aspects will be given. A special attention will be given to Molecularly Imprinted Polymers (MIPs) as this kind of selective layer was chosen for the development of POF chemical sensors.

Finally, the state of the art of intensity based POF sensors will be addressed, with a special focus on refractive index sensors, chemicals sensors and biosensors.

2.1 Introduction¹

What is a sensor? This may seem a meaningless question although this is an important aspect that worth's to be clarified. Sensors are present in everyday life even without being noticed, as they are so common nowadays. A sensor is expected to give a reliable output of a certain parameter that is aimed to be detected and/or measured, in a repeatable way and in real-time, without interferences of the external medium.

When diving into optical chemical sensors, also known as optodes or optrodes, this means that a sensing device based on light can be used to determine the presence (on/off) or also the properties of a specific chemical specie over time, i.e. concentration. Chemical sensors are expected to be small, act reversibly, free from sample treatment, work in complex samples (selective) and give a response in short time. The life time of the sensor is also an important parameter to be addressed. In on/off sensing the disposable sensors can be of interest (although they are less sustainable and cheap), where the reversibility and life time (in operation) are no longer an issue.

Chemical sensing with optical fibres allows fast and real-time detection, with the possibility of using low-cost equipment and simple procedures. Moreover, it is possible to develop several in-line remote sensing systems with real-time monitoring. Chemical analysis is usually time consuming, performed in a laboratory by a skilled operator using expensive equipment or complex procedures, critical aspects that can be overcome with optical fibre sensing. Nowadays, smaller and miniaturized components are being developed with high quality leading to enhanced performance of fibre optic chemical sensors (FOCSs).

The basic design of an optical sensing system includes a light source, a medium or waveguide where the light propagates, optical detector and data acquisition module, see Figure 2.1. The changes in the light propagation can therefore be monitored as a consequence of its interaction with the external medium. A transduction mechanism is necessary in chemical sensing, responsible

¹ (Sequeira, Nogueira and Bilro, 2019)

for the conversion of the desired quantity to be detected in a property that can be measured, in this case optical property (absorption, fluorescence, diffraction, scattering, etc.).



Figure 2.1 Basic design of an optical sensing system – schematic representation.

POF technology is a good solution when short lengths of sensing elements are foreseen, due to the high attenuation of light in the POF in comparison with glass optical fibres (GOFs). This attenuation is dependent on the length and material of the fibre as well as the wavelength of the light source. Usually the selection of the light source, and respective wavelength, has to take into account the window of lower attenuation of the selected POF. Therefore, wavelengths around 600 nm are commonly used in sensing schemes with POFs. Nevertheless, POFs are especially advantageous due to their excellent flexibility, easy handling, high numerical aperture and large diameters (Cennamo *et al.*, 2016), which makes them suitable to use with low-cost Light Emitting Diodes (LEDs) allowing easier and cheaper alignment and interconnection. Computers or microprocessors are used to control the optical instrumentation and are employed to analyse the output signals.

Chemical sensing with POFs means that a chemical specie will be detected and /or measured through optical detection, therefore two basic operation principles can be present: label-free (an intrinsic property of the analyte allows for its detection without the use of labels or indicators) or label based (when the analyte does not possess an intrinsic property that can be used for sensing and so there is the need of labels or indicators). Furthermore, the POF can act only as a waveguide for light propagation (extrinsic sensing) or can also act as the substrate/sensing platform (intrinsic sensing) together with the sensing layer, which can be immobilized on the surface or end-face of the fibre.

Intrinsic fibre optic chemical sensors have been reported in the scientific literature since 1946 (Lieberman, 1993). Hesse described an oxygen sensor in 1974 (Baldini *et al.*, 2006) and, in 1975, Lübbers and Opitz developed a carbon dioxide and oxygen sensors used in biological fluids and giving rise to optical fibre-based biosensors (Biran, Yu and Walt, 2008). The first POF chemical sensors have been reported by Sawada *et al.* in 1989 and by Zhou *et al.* in 1991. These POF chemical sensors were developed by doping fibre with fluorescent materials or covalently bond selective chemical indicators systems to the POF (respectively), allowing the detection of various chemical parameters, both in gas and liquid media (Sawada, Tanaka and Wakatsuki, 1989)(Zhou, Tabacco and Rosenblum, 1991). In 1991, eighteen articles were presented at a SPIE conference related to plastic optical fibres and their applications in sensing, photonic switches, optical fibre materials, local area networks and automotive applications (Kitazawa, Kreidl and Steele, 1991).

2.2 Light-matter interaction²

Light propagates in vacuum at a speed of 2.998×10^8 m/s (c_0). To simplify, the value of 3×10^8 m/s is generally assumed for the speed of propagation in air. When light propagates in a

² (Sequeira, Nogueira and Bilro, 2019)

medium optically denser than air, the propagation speed will be lower and the ratio between the two propagating speeds is known as refractive index of the medium, n . The refractive index is specific to each material and varies with the wavelength (λ). The higher the medium's refractive index, the lower will be the speed, v , at which the light travels in the medium:

$$v = \frac{c_0}{n} \quad \text{Equation 2.1}$$

Light, incident on an interface between two mediums, can be reflected, transmitted and refracted, scattered and/or absorbed. As depicted in the Figure 2.2 the angle of reflection (θ_r) is equal to the incident angle (θ_i) according to the law of reflection and the angle of refraction (θ_2) is dependent on the refractive index of the mediums according to the Snell's Law:

$$n_1 \cdot \sin \theta_1 = n_2 \cdot \sin \theta_2 \quad \text{Equation 2.2}$$

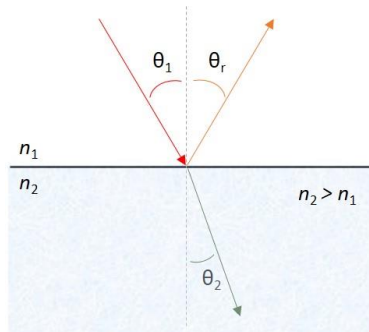


Figure 2.2 Light ray reflected and refracted after incidence on an interface between two mediums.

Smooth and flat surfaces allow specular (mirror-like) reflections, while rough and irregular surfaces give rise to diffuse reflections, as depicted in Figure 2.3.



Figure 2.3 Representation of (a) specular reflection and (b) diffuse reflection, after incidence on a smooth flat surface and on a rough and irregular surface, respectively.

When light interacts with matter a redirection of the light may occur, with the same or higher wavelength (lower energy) and it may have different polarization. When the scatterer has the same dimensions than the wavelength of the incident light, or higher, all wavelengths are equally scattered, known as Mie scattering – when light from the Sun interacts with the water droplets in a cloud, all the wavelengths of the visible light are scattered in a similar way making clouds white. When the dimensions of the scatterer are much smaller than the wavelength of the light, the light

can be absorbed and reemitted in a different direction with the same (Rayleigh scattering) or longer (Raman scattering) wavelength. In the last case, the molecule absorbs light and gets into an excited state, energy that is reemitted later when the molecule returns to the ground state (lower energy). The air molecules like di-oxygen (O₂) and di-nitrogen (N₂) are much smaller than water droplets and scatter more effectively shorter wavelengths, like blue and violet, which gives us the impression that the sky is blue (Rayleigh scattering).

Absorption is very common. When visible light hits an object, its colour will be the set of the various wavelengths that are reflected, which corresponds to the so-called complementary colour of the wavelength(s) that is/are absorbed. Absorption is therefore an optical property that can also be used for sensing, from microwaves (MW) to the infrared (IR), visible (VIS) and ultraviolet (UV) (Menzies and Chahine, 1974)(Barringer and Davies, 1977). Although when sensing with POFs the windows of transmission (low attenuation) are usually centred in the visible part of the light spectrum, from 400 nm to 800 nm, depending on the characteristics of the POF. In order to obtain transmission of light with low losses in other regions of the electromagnetic spectrum, POFs can be doped or produced with special materials and geometries.

Absorption is a transfer of energy from the light wave to the atoms or molecules of the medium. Due to the absorption of energy the electrons that constitute the atoms can be transferred to higher energy states (excited state) and, in the case of molecules, vibration or rotational states can be present. Infrared (IR) radiation is not energetic enough to excite electrons, but this radiation is absorbed generally by all organic molecules causing excitations in the vibrational energies. The IR absorption spectra of compounds are a unique signature of their molecular structure. Therefore, IR absorption in specific bands allow the development of sensors for gases and pollutants such as carbon dioxide (CO₂), methane (CH₄) and other hydrocarbons, sulphur dioxide (SO₂) and nitrogen oxides (NO_x). Ultraviolet (UV) absorption allow monitoring of nitrate (NO₃⁻) and nitrite (NO₂⁻) with absorption bands around 300 nm and 350 nm, respectively (Moo *et al.*, 2016), or organic compounds in water such as polycyclic aromatic hydrocarbons (PAHs) (Axelsson *et al.*, 1995) or potassium hydrogen phthalate (Kim *et al.*, 2016).

Simple optical configurations can be used in absorption studies, a light source and an optical detector are basic instruments that allow to perform the analysis. As the incident light (I_0) is absorbed, less light is transmitted (I) and a decrease in the light that reaches the detector is observed, see Figure 2.4. The transmittance (T) and absorbance (A) can be easily calculated through the following equations:

$$T = \frac{I}{I_0} \quad \text{and} \quad A = -\log(T) \quad \text{Equation 2.3}$$

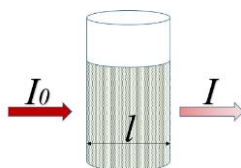


Figure 2.4 Light absorption by a chemical specie in a sample ($I < I_0$) when the light travels through an absorbing medium with length l .

When the detection and monitoring of chemical species are foreseen a finer analysis must be performed. If the target analyte has a characteristic absorption at a specific wavelength, intensity decrease will be observed at the absorbed wavelength in the broad spectrum of the light that passes through the sample. A simple example will be given in order to clarify the procedures that can be used. Rhodamine B is commonly used as an indicator due to the characteristic absorption in the visible region and the fluorescence emission depending on the form that is used. In order to obtain the transmitted spectra after passing through a liquid sample, a white light source and a spectrometer can be used placing the sample in between, see Figure 2.5. The transmission spectra of water and a solution of rhodamine B isothiocyanate (ITC) in sodium hydroxide (NaOH, 0.01 M) are depicted in Figure 2.6 as well as the respective calculated absorbance accordingly to Equation 2.3. Expected maximum absorption (λ_{max}) was at 555 nm.

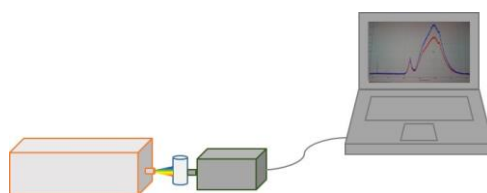


Figure 2.5 White light source, glass vial containing a liquid sample and spectrometer connected to a laptop - simple optical setup that can be used to obtain the transmitted spectrum of different liquid samples.

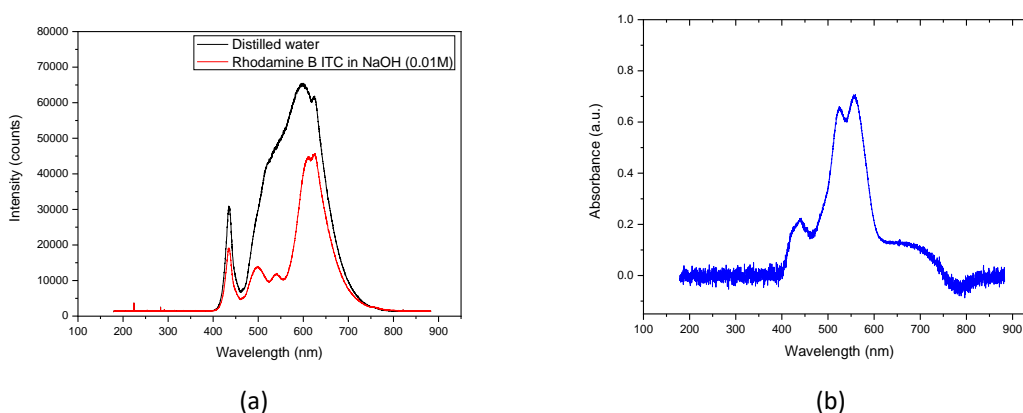


Figure 2.6 (a) Optical source transmission spectra - water and solution of rhodamine B isothiocyanate; (b) calculated absorbance of the rhodamine B solution (Equation 2.3 using the spectrum obtained with distilled water as a reference).

The absorption of light by an absorbing specie present in a medium is directly related to its concentration, higher the concentration higher will be the absorption of light, relation known as the Beer-Lambert law which can be expressed as:

$$A = \epsilon \cdot l \cdot c \quad \text{Equation 2.4}$$

where A is the Absorbance, ϵ is the molar absorptivity (dependent on the wavelength of the light and characteristic of the chemical specie), l is the distance that light travels in the medium (in cm)

and c is the molar concentration (mol/L) of the chemical specie in the medium. The Beer-Lambert law can be securely used when the light source is monochromatic (the molar absorptivity is wavelength dependent) and only compound of interest absorbs at the given wavelength (Swinehart, 1962). Furthermore, the Beer-Lambert law is adequate for measuring low concentrations (< 0.01 M) in clear solutions, otherwise electrostatic interactions and refractive index changes may occur as well as scattering due to the presence of particles in the sample. Furthermore, the sample and chemical species that are present should not be photoluminescent.

Fluorescence and phosphorescence are two examples of luminescence (emission of radiation), which can be visible or not and are a consequence of light absorption. A fluorescent specie emits light while absorbing light and the emission stops immediately as the source of light stops being present, as for example in the traffic signs or fluorescent clothes (lifetime in the range of ps or ns). On the contrary, a phosphorescent specie will maintain the emission of light even if the source of light is no longer present (lifetime greater than ms). Chemiluminescence occurs when the emission of light is a result of a chemical reaction and when present in glowing animals like jellyfish or some microorganisms is known as bioluminescence. When absorption of light occurs, the electrons that constitute the atoms and molecules will occupy higher energy states (excited state), after which they will decay again to the ground state (fundamental state) with the emission of light. Depending on the molecule and atoms, only discrete energy levels can be occupied by the electrons since the energy is quantized, which means only certain amounts can be absorbed and emitted. The necessary energy for excitation corresponds to the exact difference between the energy levels. The imaging of algae in the open sea is possible through the characteristic red fluorescence of chlorophyll.

Diffraction of the light that constitutes the visible part of the spectrum can be observed in a rainbow or when light hits the surface of a CD in a certain angle. Diffraction is also present in photonic crystals where colour changes due to the change of the periodicity of an ordered structure, for example as observed in butterflies, where the observed colour (known as structural colour) is due to the diffraction and interference of light. Diffraction and interference are also involved in the production and visualization of holograms, where, basically, a diffraction pattern is recorded in a photosensitive medium, and all the information about the object is recreated when light is incident in the same angle of recording. Bragg law can be used, the law of diffraction for constructive interference. The diffraction of light allows the development of optical sensors based in diffraction gratings and photonic crystals (Taylor, 1987)(Morey, Dunphy and Meltz, 1991)(Lukosz, 1995)(Asher and Holtz, 1997)(Asher *et al.*, 1998)(Homola, Koudela and Yee, 1999).

2.3 Polymeric Optical fibres (POFs) and light propagation

Polymeric optical fibres (POFs) are waveguides that allow the propagation of light through total internal reflection (TIR). The basic structure of a POF consist in concentric core and cladding sometimes covered by a protective jacket, see Figure 2.7.

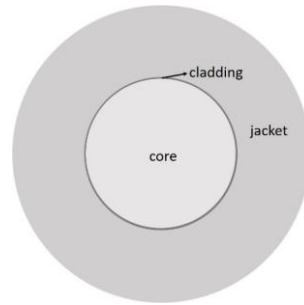


Figure 2.7 Cross section of a standard POF – schematic representation.

The first POF was produced by DuPont in early 1960s and improvements in the transparency and fabrication process have encouraged their use for optical fibre sensing (Koike and Koike, 2011).

In 1988, Christopher Emslie reported a review on polymer optical fibres, where he describes the historical background, production techniques, optical properties on light transmission and the market prospects – “There can be little doubt that the increased market acceptance which these fibres will warrant will stimulate further progress, both in fibre and allied systems technologies, and thus enable POFs to realize their latent potential” (Emslie, 1988). The historical evolution of POFs can be found in (Zubia and Arrue, 2001) and (Bhowmik and Peng, 2019).

Fibre optic sensors offer key advantages over other sensing technologies, including immunity to electromagnetic interference, lightweight, compactness, multiplexing capability and high sensitivity, among others (Oliveira *et al.*, 2018).

The advantages of POFs over glass optical fibres (GOFs) include high numerical aperture, low cost, high flexibility and ruggedness (Zhou, Tabacco and Rosenblum, 1991). Furthermore, they possess much higher elongation, lower Young’s modulus, higher thermo-optic coefficient and the common high diameters of POFs allow low-cost sensing systems through the use of LEDs and photodiode detectors. Polymers are also biocompatible materials and do not produce sharp edges if broken. Despite these inherent advantages of POFs, GOFs still possess lower attenuation and higher bandwidth, which are both important for data transmission.

The attenuation and losses are dependent on the light wavelength, material of the fibre and imperfections. Light absorption by the fibre material determined by its chemical composition and physical structure is considered intrinsic losses, whereas light absorption by contaminants is considered as extrinsic losses. Nevertheless, the surface properties of the POFs can be more easily manipulated compared to silica fibres, using simple and wide-ranging chemistry techniques to achieve the desired sensing application (Tow *et al.*, 2017).

The principle of optical signal transmission through an optical fibre starts with a transmitter, which converts an electrical signal into an optical signal, which propagates inside the POF (optical waveguide) and reaches a receiver, which will convert it back to an electrical signal that is analysed (according to Figure 2.1).

The propagation of the optical signal through the POF will depend on several factors such as: fibre diameter, core and cladding materials, fibre structure, incidence angle of the light rays, refractive index profile, surface morphology, etc.

2.3.1 Acceptance angle and numerical aperture

Light, when injected in one side of the fibre will propagate in the core through multiple reflections at the core-cladding interface, due to the difference between the refractive indices of the core (n_{co}) and cladding (n_{clad}), where $n_{co} > n_{clad}$. When the light reaches this interface between the two media part of the light will be reflected to the core and part will be refracted into the cladding, see Figure 2.8. Accordingly to the Snell's Law (Equation 2.2), the refracted light will travel parallel in the cladding (90° with the normal of the interface) when the incident angle reaches a certain value, known as the critical angle (φ_c , defined in Equation 2.5), after which the light will be totally reflected at the interface between the two media (when $\varphi > \varphi_c$). The acceptance cone illustrates the incident light rays that will undergo total reflection inside the fibre core.

$$\varphi_c = \sin^{-1} \left(\frac{n_{clad}}{n_{co}} \right) \quad \text{Equation 2.5}$$

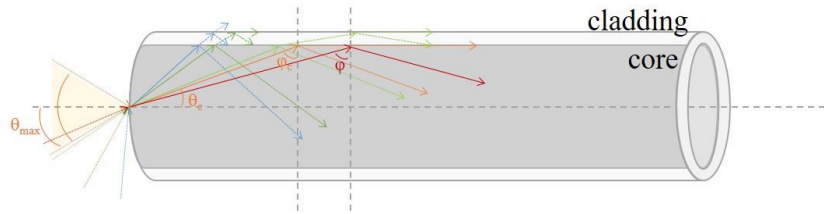


Figure 2.8 Schematic representation of light propagation in a step-index multimode POF.

The critical angle which is a characteristic of an optical fibre is the complementary angle of φ_c , defined as:

$$\cos \theta_c = \left(\frac{n_{clad}}{n_{co}} \right) \quad \text{Equation 2.6}$$

The acceptance angle, θ_{max} (maximum angle of the acceptance cone, depicted in Figure 2.8), will determine the quantity of light rays that will be totally propagated inside the fibre core and can be determined by:

$$n_{ext} \cdot \sin \theta_{max} = n_{co} \cdot \sin \theta_c \quad \text{Equation 2.7}$$

where n_{ext} is the refractive index of the external medium.

The numerical aperture, NA, is a measure of the quantity of light that can be received by an optical fibre and is defined as the sine of the acceptance angle, θ_{max} :

$$NA = \sin \theta_{max} \quad \text{Equation 2.8}$$

Taking into consideration Equation 2.5 and that $n_{ext} = 1$ (air):

$$\begin{aligned}
n_{ext} \cdot \sin \theta_{max} &= n_{co} \cdot \sin \theta_c \Leftrightarrow \\
\Leftrightarrow 1 \cdot \sin \theta_{max} &= n_{co} \cdot \sin(90 - \varphi_c) \Leftrightarrow \\
\Leftrightarrow \sin \theta_{max} &= n_{co} \cdot \cos(\varphi_c) \Leftrightarrow \\
\Leftrightarrow \sin \theta_{max} &= n_{co} \cdot \sqrt{1 - \sin^2(\varphi_c)} \Leftrightarrow \\
\Leftrightarrow \sin \theta_{max} &= n_{co} \cdot \sqrt{1 - \left(\frac{n_{clad}}{n_{co}}\right)^2} \Leftrightarrow \\
\Leftrightarrow \sin \theta_{max} &= \sqrt{n_{co}^2 - n_{clad}^2}
\end{aligned}$$

Which gives:

$$NA = \sin \theta_{max} = \sqrt{n_{co}^2 - n_{clad}^2} \quad \text{Equation 2.9}$$

The numerical aperture is thus determined by the difference between the refractive indices of the core and cladding. It should be taken into account when injecting light into an optical fibre and when coupling optical fibres together. Refractive index changes will determine the change in the numerical aperture, directly affecting the acceptance cone where the transmission of light in a low-loss regime is possible. (Weinert, 1999)

2.3.2 Types of fibres and refractive index profile

The propagation paths of the light rays in the core of an optical fibre may be determined by the solution of the wave equation. The number of possible propagation light rays (modes) decreases with decreasing fibre diameter, d . The number of modes is determined by the V-number, V_{number} , which is dependent on the fibre core radius, r_f , the wavelength of the light, λ , and the numerical aperture of the fibre (core and cladding refractive indices, according to Equation 2.9):

$$V_{number} = \frac{2\pi r_f NA}{\lambda} \quad \text{Equation 2.10}$$

If $V_{number} < 2.405$ only one mode can propagate (single mode fibre, SM), multimode fibres where several modes can propagate in the fibre core have higher values of V_{number} . The number of modes, M , can be calculated according to (Ziemann *et al.*, 2008):

$$M \sim \frac{V_{number}^2}{2} \quad (\text{step-index profile})$$

$$M \sim \frac{V_{number}^2}{4} \quad (\text{graded-index profile})$$

In the present work, a standard step-index (SI) POF with a fibre diameter of 1 mm was selected, with a core refractive index of 1.49 and a numerical aperture of 0.50. Therefore, an acceptance

angle (θ_{max}) of 30° and a critical angle (φ_c) $\sim 70^\circ$ is obtained. This fibre allows the propagation of 2.83×10^6 modes for a wavelength of 660 nm.

Schematic representations of the three basic types of optical fibres are represented in the following figure, according with the refractive index profiles:

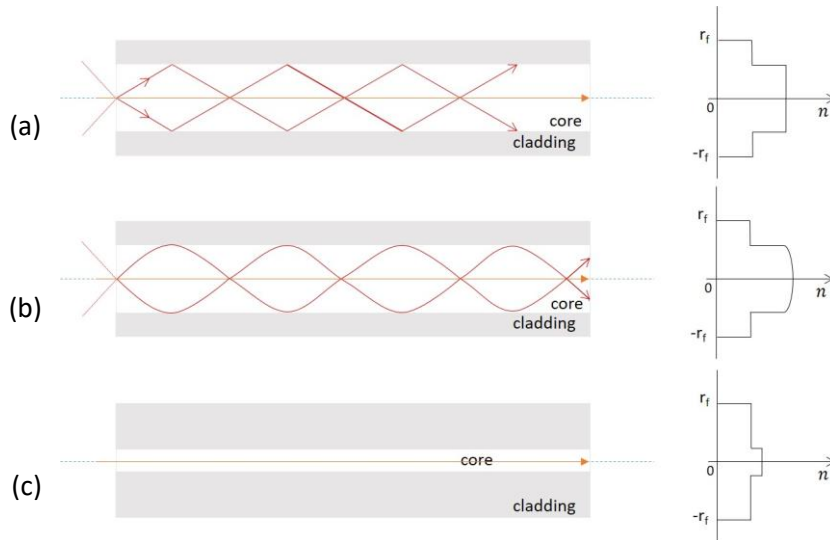


Figure 2.9 Schematic representation of fibres with different refractive index profiles: (a) step-index multimode fibre; (b) graded-index multimode fibre; (c) step-index single mode fibre. [The lower mode is represented in orange and the highest mode in red.]

When the refractive index (RI) of the core is constant, a fibre with a step-index (SI) profile is obtained and a step in RI occurs when passing to the cladding with lower RI, see Figure 2.9(a,c). Although traveling with the same phase velocity, the lower modes in a SI multimode fibre (Figure 2.9(a)) will travel faster across the fibre (lower path length, in orange) than the higher modes, which undergo higher number of reflections (in red). This will bring light dispersion and broadening of the signal.

A reduction in the modal dispersion of a step-index profile optical fibre can be achieved by decreasing the numerical aperture (till reaching a single mode profile fibre, Figure 2.9(c)) or by varying the core refractive index in such a way that the modes travel across the fibre at the same time – graded-index profile fibre, Figure 2.9(b). In this case, the RI decreases in the cross section of the core, allowing the higher modes to travel faster than the lower modes, and to decrease the time differences. With the appearance of the graded-index profile, the dispersion could be reduced in theory by 10^3 and in practice 10^2 in comparison with step-index profile optical fibres (Weinert, 1999).

The only way to completely avoid modal dispersion is by using a single mode fibre, which only allows one propagating mode. In this case, the numerical aperture must be around 0.1 and the typical core radius around $9 \mu\text{m}$ (Weinert, 1999). The ray-optics representation can be switched to the wave-optical representation and the propagation in the optical fibre is represented as a beam with Gaussian distribution in the transversal direction.

Furthermore, the number of modes propagating in an optical fibre is wavelength dependent, which means that a fibre only has a single mode profile until a cut-off wavelength. A multimode

(MM) SI POF system with a light emitting diode (LED) will have millions of fibre propagating modes and also several wavelengths (a source can be considered ideally monochromatic when the coherence time is large in relation to the arising differences in propagation time). (Weinert, 1999)

Dispersion is usually not a problem in POF sensors as short fibre cuts are used. Another advantage of POFs is that a large difference can be obtained between the refractive indices of the core and cladding, as polymers are available in a wide range of RIs varying from 1.32 (highly fluorinated acrylic based materials) to around 1.6 (some phenolic resins) (Emslie, 1988). Thus, high numerical apertures ranging from 0.2 to 0.7 can be achieved (Zubia and Arrue, 2001), permitting easy connectorization (Oliveira *et al.*, 2018).

2.3.3 POF's designation and materials

There are several ways of categorizing optical fibres as there are no general standard guidelines. POFs can be classified according to the constituent materials, diameter, numerical aperture, refractive index profile and attenuation, among others, see Table 2.1.

Table 2.1. Classification of optical fibres (adopted from (Ziemann *et al.*, 2008)).

| Parameter | Description | Examples |
|------------------------|--|---|
| Number of modes | Propagation of one mode or several modes | SM – single mode fibre MM – multimode fibre |
| Core material | Plastic or glass | POF – plastic optical fibre GOF – glass optical fibre |
| Special core materials | Doped materials or special polymers | PC-POF – polycarbonate POF PF-POF – perfluorinated POF |
| Cladding material | Special fibres, such as glass fibre with polymer cladding | PCS – polymer clad silica fibre |
| Index profile | There are several variants of the index profile | SI – step-index DSI – double step-index MSI – multi step-index GI – graded-index |
| Number of cores | Fibres can have one or several cores | MC-POF – multi-core POF |
| Polarization | Special fibres that can maintain the state of polarization or only one state of polarization can propagate (only in SM fibres) | PMF – polarization maintaining fibres |
| Microstructures | microstructures that extend along the length of the fibre | PCF – photonic crystal fibre mPOF – microstructured POF |

The most commonly used material for POF's cores is poly(methyl methacrylate) (PMMA), although materials such as polycarbonate (PC) or polystyrene (PS) are also used on POF's manufacturing, depending on the intended characteristics. For example, PS is very brittle but allows

low optical attenuation, while PC has high resistance to temperature but higher attenuation (Weinert, 1999).

The use of different materials allow to explore different characteristics presented by polymer materials such as humidity-sensitive (Zhang and Webb, 2014) or humidity-insensitive (Woyessa *et al.*, 2016), as well as the capability to resist to temperatures above 100 °C (Markos *et al.*, 2013)(Woyessa *et al.*, 2016). (Oliveira *et al.*, 2018)

The POF used in the present studies has a PMMA core and a perfluorinated cladding. The chemical structure of PMMA is depicted in the Figure 2.10 and the general characteristics of the POF made available by the manufacturer are listed in the Table 2.2.

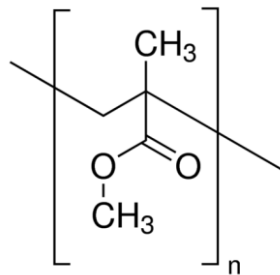


Figure 2.10 Chemical structure of PMMA.

Table 2.2. DB-1000 POF characteristics (Asahi Kasei, 2013).

| Item | Unit | Specifications |
|---|------|---------------------------|
| Core material | | PMMA |
| Clad material | | Fluorinated polymer* |
| Fibre diameter | µm | 1000 ± 60 |
| Numerical aperture (NA) | | 0.50 |
| Operating temperature (no deterioration in optical properties) - dry atmosphere - under 95 % RH conditions | °C | -55 ~ 70 60 max |
| Attenuation / transmission loss - 25°C 50% RH - operating temperature, 95% RH | dB/m | 0.16 max. ** Not rated |
| Tensile strength at break point | N | ≥ 75 |
| Minimum bending radius | mm | 20 |
| Sample conditions: - Temperature, T = 23 °C - Humidity, RH = 50 % - Storage time, t = 200h | | |

*Cladding specifications were not made available by the manufacturer; **@650 nm, collimated light.

PMMA is an amorphous acrylate polymer produced by free radical polymerization from the monomer methyl methacrylate (MMA). PMMA possess high flexibility, good resistance to alkalis, dilute acids and aqueous solutions of inorganic salts and UV-induced aging. It is a widely used

material in many industries under several different trade names such as Perspex, Plexiglas, Crylux, and Acrylite. (Bhowmik and Peng, 2019)

Several works reported optimization of cleaving methods for an optimum POF end face aiming at minimizing defects and improving connectorization (Oliveira *et al.*, 2018). End face quality is of extreme importance, especially when working with small diameter POFs, mPOFs or a splicing between a POF and a GOF, as fibre damage or even very small misalignment of the fibres' cores can induce high losses.

The POFs used in this work had a diameter of 1 mm and good quality end faces were achieved by cleaving with commercial POF cutter tools followed by polishing manually in an 'Figure ∞ ' pattern with humidified sandpapers of different grain sizes (5 – 3 – 1 – 0.3 μm , LFG5P, LFG3P, LFG1P, LFG03P, respectively, from Thorlabs Inc.), see Figure 2.11.

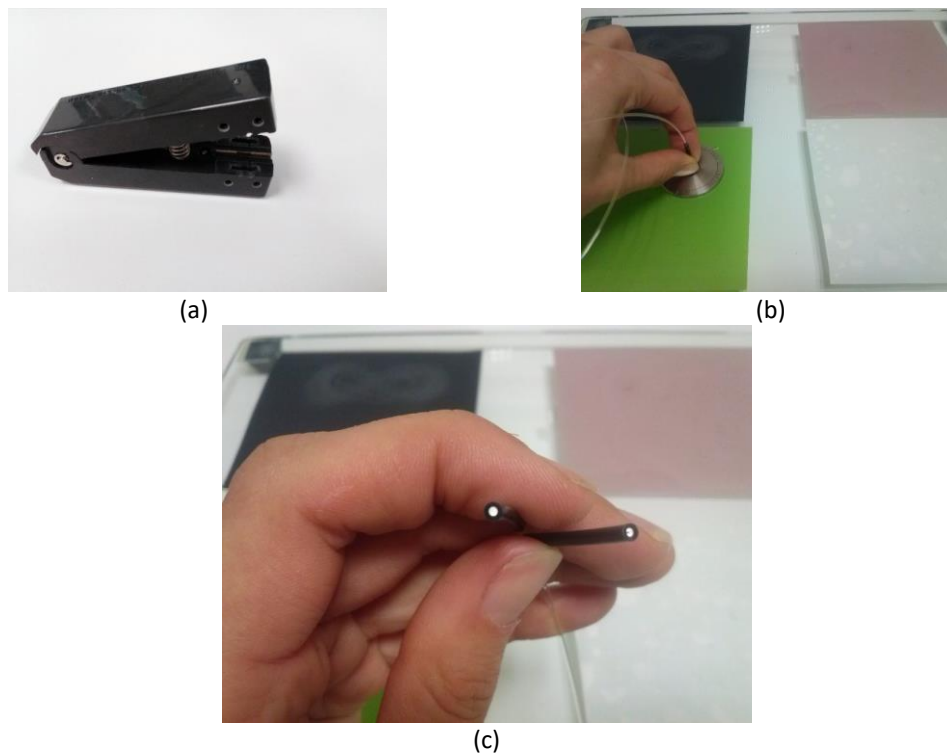


Figure 2.11 Preparation of POF's end faces: (a) example of a POF cutter tool; (b) manual polishing with sandpapers of different grain sizes (5 – 3 – 1 – 0.3 μm) and (c) obtained POF's end faces.

2.3.4 Optical attenuation

When light travels inside an optical fibre of length L , the optical power P will decay exponentially according with the equation:

$$P_L = P_0 \cdot 10^{-\alpha \frac{L}{10}} \quad \text{Equation 2.11}$$

where P_0 and P_L are the optical power at the beginning and end of the optical fibre, respectively.

Making the transition to a logarithmic notation, the attenuation A_t is specified in decibels (dB):

$$A_t = \alpha \cdot L = 10 \cdot \log\left(\frac{P_0}{P_L}\right) \quad \text{Equation 2.12}$$

Where $\alpha = \frac{A_t}{L}$ is the attenuation coefficient in dB/km. Decibel is not a unit of measurement but a ratio of two measurements (of power, intensity, voltage). If the output is higher than the input we say there is a gain (+), otherwise there is a loss (-).

The intensity relative to 1 mW has the unit dBm, corresponding to the following definition (P is the optical power in mW):

$$dBm = 10 \cdot \log\left(\frac{P}{1 \text{ mW}}\right) \quad \text{Equation 2.13}$$

The attenuation of an optical fibre is usually expressed as the attenuation coefficient, $\alpha(\lambda)$ in db/km, which is wavelength dependent. The power loss, the optical attenuation A_t in dB, can be determined by the difference between P_0 and P_L , both measured in dBm:

$$A_t = P_0 - P_L \quad \text{Equation 2.14}$$

Attenuation is caused by different processes: scattering (α_s), absorption (α_A) and radiation losses (α_L), see Figure 2.12 (Weinert, 1999). Due to the purity of PMMA used in POF's production, the intrinsic losses dominate and can be described with good approximation by the Rayleigh scattering law (Weinert, 1999):

$$\alpha_s \sim \frac{1}{\lambda^4} \quad \text{Equation 2.15}$$

The characteristic absorption of the CH groups present in PMMA fibres has a crucial effect on light attenuation. The radiation losses can be also related to fibre bending, fluctuation of the fibre diameter and defects in the core-cladding interface. (Weinert, 1999)

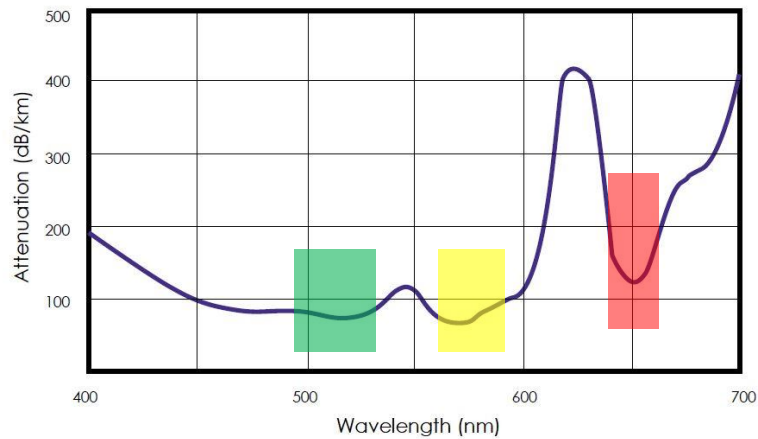


Figure 2.12 Graph of attenuation coefficient $\alpha(\lambda)$ of Luminous POFs (adapted from (Asahi Kasei, 2001)).

The ranges of wavelength where the attenuation reaches minimum values are called “optical windows” and usually light sources in this range are chosen, which for PMMA are around 530 nm, 570 nm and 650 nm, see Figure 2.12.

2.3.5 Mechanical and thermal properties

The mechanical properties of POFs namely high elastic strain limits, high fracture toughness, high flexibility in bending, high sensitivity to strain and potential negative thermo-optic coefficients promote their application for sensing development (Peters, 2011).

POFs have very low Young’s modulus compared to silica fibres, which is an advantage for strain-related sensing applications, as lower Young’s modulus means higher strain under a certain stress, and thus much higher sensitivity (Bhowmik and Peng, 2019). The thermo-optic coefficients of some polymers are negative which brings new possibilities for temperature compensation in strain sensors (Peters, 2011).

Annealing can remove POF’s internal stresses caused by the fabrication process (below the glass transition temperature, T_g). During drawing, the polymer molecules align in the longitudinal direction, creating anisotropy which affects the mechanical properties and reduces the transmission quality of POFs as well as leads to appearance of small cracks in the radial direction. (Peters, 2011)

Maximum operating temperatures for POFs are typically lying in the range between 80 – 100 °C and, above this limit (T_g) fibres start to lose their rigidity and transparency (Zubia and Arrue, 2001). However, elevated temperatures even below the maximum operating temperature can cause the POF to become brittle and disintegrate over time (Peters, 2011). Resistance of POFs to high temperatures also depends on the degree of moisture, as more attenuation can occur due to the strong OH⁻ absorption band in the visible range (Zubia and Arrue, 2001).

2.3.6 Chemical resistance

POFs have a good chemical resistance in aqueous solutions, diluted acids and alkali, and some organic solvents, including petrol and turpentine (Bhowmik and Peng, 2019).

The chemical resistance of POFs depends on the POF material and immersion conditions. Chemical resistance of some of the most common transparent polymers (PMMA, PC, ZEONEX®, TOPAS®, CYTOP®, and polyvinyl chloride (PVC)) to acids (hydrochloric, sulphuric and nitric acid), methyl ethyl ketone, gasoline, isopropyl alcohol, oils and alkalis classified as “usable”, “usable with care” or “not usable” can be found in (Oliveira, Bilro and Nogueira, 2019). Chemical resistance of PMMA to organic solvents, acids, bases and alcohols (classified as “not attacked”, “lightly attacked” and “strongly attacked” was reviewed in (Ali, Karim and Buang, 2015). PMMA has good resistance to many solvents except chlorinated and aromatic hydrocarbons, esters or ketones.

In 1999, Merchant et al. reported a simple and low-cost method to chemically remove the cladding of PMMA based POFs using organic solvents, which also can be used to create tapers of any profile. The exposed region becomes extremely susceptible to breakage as a result of preferential attack of stress induced microfissures. (Merchant, Scully and Schmitt, 1999)

Miller-Chou and Koenig presented a review on polymer dissolution in 2003. The dissolution of a polymer involves solvent diffusion and chain disentanglement. The solvent can diffuse into the polymer creating a gel-like swollen layer (plasticization of the polymer by the solvent) or polymer cracks with no gel layer being formed. Temperature is an important parameter in the dissolution process as the thickness of the gel-layer formed by solvent diffusion decreases with decreasing temperature (lower than T_g) and, at a certain temperature no gel layer is observed and the polymer cracks. The gel temperature, at which transition from normal dissolution to cracking occurs, was formally defined as the temperature at which the gel layer disappeared. Furthermore, the dissolution rate decreases with increased polymer molecular weight, which also affects the critical stress for crazing. (Miller-Chou and Koenig, 2003)

When cladding removal or chemical tapering are not necessary, the chemical resistance to organic solvents can be improved by coating the POFs with special protective layers.

The coating of a U-bent POF with a graphene oxide (GO) film allowed a significant enhancement on the chemical resistance of the POF. Divagar et al. measured in real-time the absorbance of U-bent POF probes dipped in acetone with and without graphene oxide (GO) coating. An abrupt drop in the intensity of light passing through the fibre probe is observed when the fibre breaks due to the solvent action. The GO U-bent POF probe was able to withstand acetone environment for longer, 30 min as opposed to only 10 min without the GO coating, demonstrating improvement in chemical resistance of the POFs. Furthermore, the GO-POF probes showed resistance to organic solvents such as methanol, ethanol and isopropyl alcohol for 12h, confirming the chemical stability and adhesion of the GO film to the POF probe. (Divagar *et al.*, 2018)

2.4 Optical fibre sensing principles

The development of POF sensors is based on the light interaction with matter and characteristics of light propagation in optical fibres as described in the sections 2.2 and 2.3. The variation of one or more properties of the light that is transmitted or collected by an optical fibre

can be related to the variation of the measurable parameter using optical interrogation schemes. Variations of the light intensity, wavelength shifts, changes in interferometric patterns and polarimetric changes are examples of physical principles that are used in POF sensors technology.

Below the general principles used in POF sensing will be described, with the focus on intensity based detection schemes as they were employed in the present work (section 2.4.1). Wavelength and interferometric based sensing will be described briefly. Since in this work (Chapter 5) the results obtained with an POF sensor based on surface plasmon resonance (SPR) were considered for the validation of the MIP sensitive layer, a brief description of this phenomenon will also be given in the following section (section 2.4.2).

Intensity based configurations can be implemented with low-cost experimental setups comprising LEDs and photodetectors. The same setups can be used for spectroscopic measurements with POFs as waveguides. While other sensing techniques normally allow to obtain sensors with higher sensitivities and resolution, they usually require more expensive and complex equipment.

Wavelength-based sensing relies on the variation of the light wavelength as a transduction mechanism, with the advantage of being independent of the stability of the light source's output power. However, its inherent disadvantage is higher costs of the optical sensing setup and instruments (from the POF sensor's manufacture to the interrogation of the optical signal). Common POF sensing techniques based on wavelength variation are surface plasmons (see section 2.4.2) (Al-Qazwini *et al.*, 2016) and Bragg gratings (Luo *et al.*, 2017)(Duarte, Nogueira and Bilro, 2019). Lossy mode resonance (LMR) is a relatively new physical optical phenomenon used for sensing (Wang and Zhao, 2018)(Rivero, Goicoechea and Arregui, 2018). Some applications of LMR in POF sensing have been already reported (Corres *et al.*, 2015).

Bragg gratings are based on periodic variations in the refractive index of the fibre core. Changes on the physical properties of the fibre causes a variation in this periodic pattern, causing variation in the properties of light that propagate in the fibre after the interaction with this periodic pattern (reflection, transmission or both). Examples of Bragg gratings in optical fibres are Fibre Bragg Gratings (FBGs) (Yuan *et al.*, 2011)(Nogueira *et al.*, 2015)(R. Oliveira, Bilro, *et al.*, 2016)(Oliveira *et al.*, 2017), Tilted Fibre Bragg Gratings (TFBGs) (Hu *et al.*, 2014) and Long Period Gratings (LPGs) (Min *et al.*, 2018)(Bundalo *et al.*, 2016). POF sensors based on Bragg gratings are commonly applied to fibres without any modification, or annealed fibres and chemically etched fibres for increased sensitivity, allowing to measure several physical parameters such as temperature, refractive index, humidity, strain and bending (Oliveira *et al.*, 2018).

POF sensors can also be based on the interference between two beams that propagate through different optical paths. If one of the beams interacts with a perturbation of the external medium, the interference pattern can be analysed in terms of wavelength, phase, intensity, frequency, etc. Examples of interferometric based sensing with POFs include Fabry–Pérot (FPI) (Ferreira *et al.*, 2017)(Theodosiou *et al.*, 2018)(Oliveira, Bilro and Nogueira, 2018) and Mach-Zehnder (MZI) (Silva-López *et al.*, 2005)(Jasim *et al.*, 2014) interferometers as well as multimode interference (MMI) (Kawa *et al.*, 2017)(Oliveira *et al.*, 2017). These types of fibre optic sensors are still mostly used as physical sensors (Tiwari and Uzun, 2017).

2.4.1 Intensity based sensing³

Intensity based sensing schemes allow the simplest and cost-effective POF based sensors. The key concept is based on the variation of the intensity of light that travels through or is collected by an optical fibre. Multimode (MM) fibres with large core diameters are of interest as they enable easier handling and installation as well as using low-cost connectors and components with less strict geometrical tolerances.

The experimental setup for intensity based detection schemes includes a light source (LED, OLED, halogen light, laser), the optical fibre, a light detector (photodetector or a spectrum analyser, like a spectrometer, oscilloscope or optical spectrum analyser (OSA)) and a data acquisition device / software (see Figure 2.13). LED's and photodetectors are interesting solutions for low-cost and miniaturized intensity based schemes. Yeh et al. reviewed the LED-based devices functioning in the UV, visible and IR range, 247 – 3800 nm, for chemical sensing applications, showing that they have become prominent light sources for chemical sensors which sensitivity improvement can be expected (Yeh *et al.*, 2017).



Figure 2.13 Schematic representation of intensity based optical fibre sensing setup.

2.4.1.1 Intrinsic and extrinsic sensors

Intensity based optical fibre sensors (OFSs) can be classified as intrinsic and extrinsic, depending if: (i) the light propagates in the fibre and interacts with the analysed medium (see Figure 2.14(a)) or (ii) the fibre is used only as a waveguide and the light interacts directly with the analysed environment (see Figure 2.14(b)), respectively. In Figure 2.14 is the schematic representation of intrinsic and extrinsic POF sensors, where “In” represents the input of light in the fibre and “Out” the output of the transmitted light.

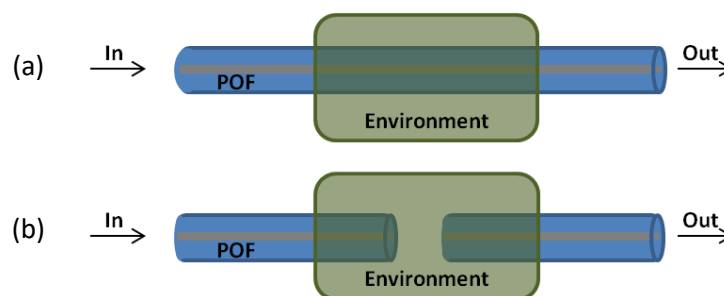


Figure 2.14 Schematic representation of (a) intrinsic and (b) extrinsic POF sensors.

³ (Oliveira *et al.*, 2018)

In the case of extrinsic sensors, the light interacts directly with the environment by leaking out and re-entering the optical fibre (in the same or in a different fibre). For intrinsic sensors, the optical fibre is modified to promote sensing capability, allowing to detect changes in the environment. The light propagates in the optical fibre and interacts with sensitive/selective layers or external medium, after which it can be transmitted to the other side (see Figure 2.15(a)) or reflected back (see Figure 2.15(b)). In transmission detection schemes the light source and detector are placed on opposite sides of the optical fibre while in reflection detection schemes both are placed on the same side.

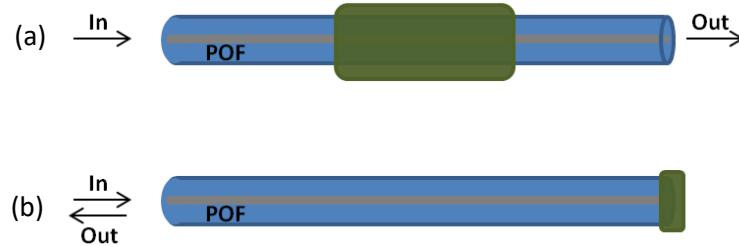


Figure 2.15 Schematic representation of intrinsic (a) transmission and (b) reflection POF sensors.

2.4.1.2 Transmission-based configurations

In extrinsic configurations, as depicted in Figure 2.14(b), two longitudinally aligned fibres can be used as sensing elements due to the intensity modulation of the optical signal as a function of the distance between the fibres or changes in the external medium (i.e. concentration, refractive index, intrinsic property of the analyte like absorption at a specific wavelength or fluorescence, etc.). When the distance between two fibres (l) is changed, the intensity of the signal that reaches the second fibre (I) will also change. The following relationship between the optical power (P) and the area (A_r) is valid if no light is absorbed or scattered by the medium: $P = I \times A_r$, see Figure 2.16. This principle can be used for detection of the thickness of cracks or small changes in the fibre position resulting in the misalignment of the fibres, which is widely used in the field of structural monitoring.

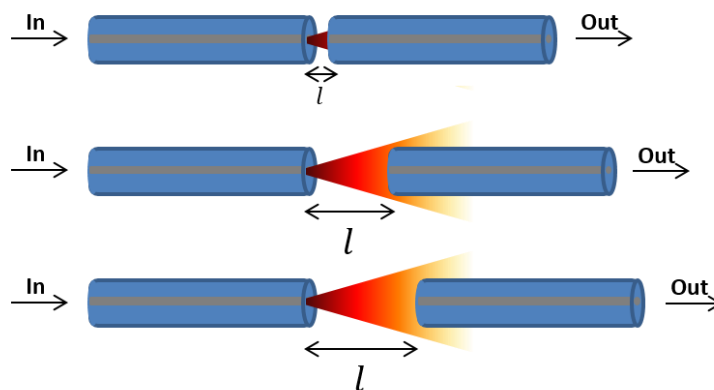


Figure 2.16 Schematic representation of extrinsic sensing in transmission configuration, with increasing distance (l) between the input and output fibres.

When an absorbing medium exists between the optical fibres, absorption of light will occur due to the interaction of light with the compounds that constitute the external medium and the concentration of a chemical specie can be monitored through the variation of the transmitted light, see Figure 2.17. This absorbance (A) can be related to the chemical concentration of a specie (c) by the Beer-Lambert law, as described by Equation 2.4, section 2.2. The Beer-Lambert law is not valid at high concentrations (> 0.01 M) due to electrostatic interactions or changes in refractive index, and in the presence of fluorescence or phosphorescence of the sample and scattering of light due to particulates.

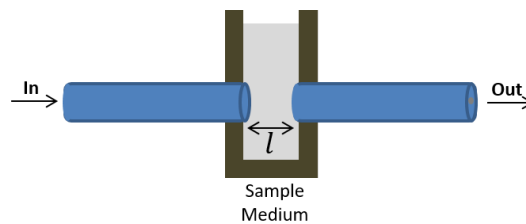


Figure 2.17 Schematic representation of extrinsic sensing in transmission configuration, where the concentration of a chemical specie (c) can vary in the external medium between the input and output fibres.

If a variation of the refractive index occurs in the external medium between the fibres, the irradiance will change, since the area of the light cone will decrease with increasing refractive index leading to an increase of the detected transmitted light, see Figure 2.18.

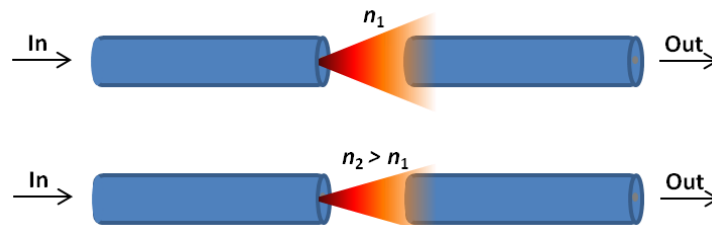


Figure 2.18 Schematic representation of extrinsic sensing in transmission configuration, with increasing refractive index (n) in the external medium between the input and output fibres.

2.4.1.3 Reflection-based configurations

The above-mentioned examples are also valid for reflection-based configurations. In that case, one single fibre can serve as transmitter and receptor or two independent fibres can work one as transmitter and another as a receiver. In Figure 2.19, schemes of two extrinsic reflection based sensors are depicted with one (Figure 2.19(a)) and two fibres (Figure 2.19(b)). In these configurations, any physical parameter that is responsible for the mirror displacement causes a variation in the path length and, consequently, a variation in the irradiance reaching the output fibre.

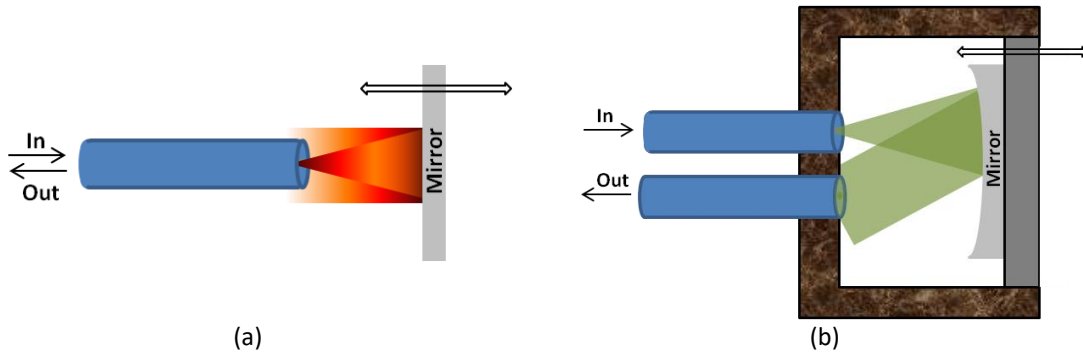


Figure 2.19 Schematic representation of extrinsic sensing in reflection configurations, with mirror displacement possibility.

These configurations are also valid when the distance between transmitter and target/receptor is constant but variations on the properties of the external medium occur, such as concentration or refractive index. Therefore, reflection based configurations can also be used to monitor absorption, fluorescence, light scattering and refractive index, on the same way as already explained for transmission-based configurations.

2.4.1.4 Enhancing optical fibre sensitivity

Interaction with the evanescent wave is another principle that can be employed in intrinsic sensors in order to monitor changes occurring at the surface of the fibre. The totally reflected light inside the optical fibre evanesces into the cladding with a penetration depth around the wavelength of the light, $\sim \lambda$ with the energy exponentially decaying with the distance from the core-cladding interface, see Figure 2.20. Sensing schemes based on this interaction between the light and this region of the fibre are known as evanescent field sensing.

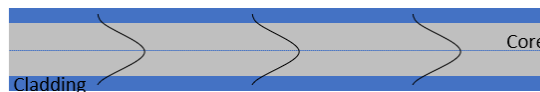


Figure 2.20 Schematic representation of the propagation wave in a standard optical fibre.

The penetration depth (d_p) of evanescent field is defined as the distance at which the amplitude of the electric field falls to $1/e$ of its initial value at the interface between core and cladding (or surrounding medium) and decreases with increasing refractive index contrast between these two mediums:

$$d_p = \frac{\lambda}{2\pi \sqrt{n_{co}^2 \cdot \sin^2 \varphi - n_{clad}^2}} \quad \text{Equation 2.16}$$

where n_{co} and n_{clad} are the core and cladding refractive indices, λ is the wavelength of the light and φ the incident angle at the core cladding interface (Gravina, Testa and Bernini, 2009) (Memon *et al.*, 2018). The lower the contrast between the refractive indices of the two mediums, the higher will be the evanescent field penetration depth leading to increased light interaction.

Interaction of the evanescent field with the external medium is negligible in straight configurations with standard POFs. To increase this interaction and monitor the changes occurring at the surface of the fibre, POF's can be easily manipulated by a wide range of simple physical and chemical techniques, depending on the desired sensing properties – tapering, etching, polishing and bending. POFs can be tapered by heating and stretching, see Figure 2.21(b), which decreases thickness of the core and cladding in a specific region creating a “waist”. After removing the fibre jacket (if it exists), one simple procedure is to partially or totally remove the cladding of the fibre exposing the core. The cladding can be removed either by mechanical polishing or chemical etching (see Figure 2.21(c)). Side-polishing allows removing the cladding and part of the core in one side of the fibre and a D-shaped fibre can be obtained, Figure 2.21(d).

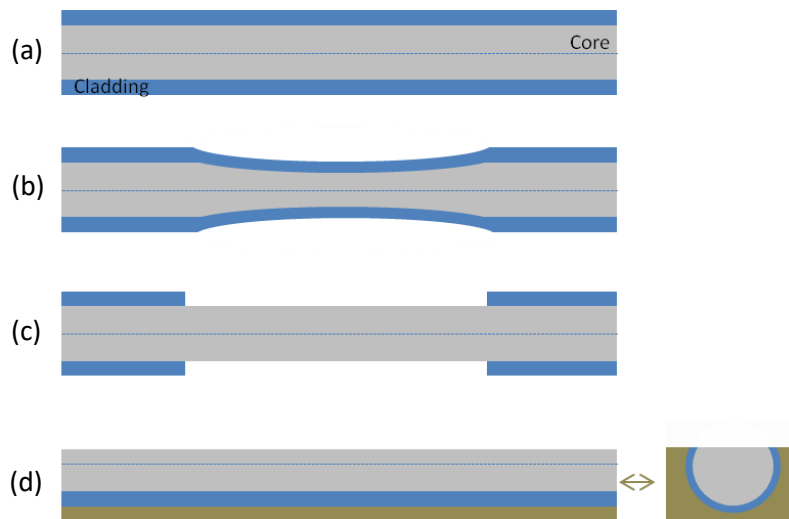


Figure 2.21 Schematic representation of (a) standard, (b) tapered, (c) etched and or polished and (d) D-shaped (side-polished) optical fibres.

Depending on the aim of the application, one can choose to remove only the cladding, partially or totally, or also part of the core. External medium acts as a substitute cladding in a fibre with an exposed core and the light that propagates in the fibre can interact with the external medium allowing changes to be monitored. In chemical sensing or biosensing, the sensitive layer will serve as a substitute cladding and the changes that occur in this layer will be used as analytical signal, e.g. variations of the sensitive layer refractive index as a function of binding or adsorption of the target analyte. The coating of a U-bent POF with a graphene oxide (GO) film, reported by Divagar *et al.* in 2018, allowed a significant enhancement of the RI sensitivity through reduction of the RI contrast

between the POF's core and deposited GO layer with consequent enhancement of evanescent field absorption. (Divagar *et al.*, 2018)

Another approach to increase optical intensity variation is using macrobending or points of strain and pressure. When a fibre goes from a straight configuration to a curved one, more radiation will leak out from the fibre, see Figure 2.22. This principle is employed in smart textiles, in which POFs are embedded for detection of several physical and chemical parameters.

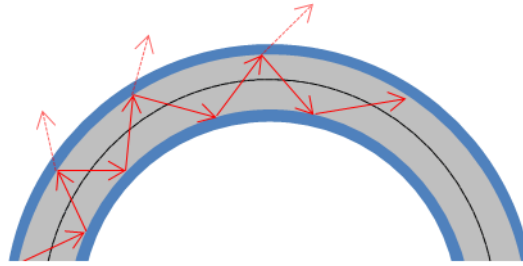


Figure 2.22 Schematic representation of a POF with macrobending configuration.

The morphology of the surface is of extreme importance on the sensing capability of POFs. Increase of both surface area and surface roughness can be related with increased sensitivity of POF sensors. Some authors explain the effect of surface roughness on sensitivity by the increase of surface area or accumulation of molecules on the “creases”, leading to higher localized variations of the refractive index (Qazi *et al.*, 2019). Roughness causes the scattering of light, leading to back-reflection or changes in the propagating conditions (Figure 2.3, section 2.2) therefore an increased light loss would be expected.

Zhong *et al.* reported in 2013 the theoretical and experimental study on the effect of surface roughness on the properties of fibre optic evanescent wave sensors using unclad graded-index multimode silica optical fibres. Increased roughness was created on the fibre's surface by chemical etching using hydrofluoric acid (HFA) solutions with different concentrations. Authors concluded that a higher sensitivity can be achieved by an appropriate increase in the roughness of the unclad (sensing) region and increased surface roughness causes increased light-scattering and refraction loss, decreased linearity and higher surface area. (Zhong *et al.*, 2013)

Qazi *et al.* presented in 2019 an experimental study on the influence of surface roughness on the sensitivity of single mode D-shaped optical fibre sensors (9/125 μm) using solutions with increasing RI (1.130 – 1.148). Surface roughness was estimated to be 343, 96, 25 and 9 nm obtained by polishing with 30, 9, 3 and 0.5 μm grit size aluminium oxide polishing films, respectively. The authors concluded that: i) roughness of the sensing region does not have significant effect on linear response of output signal and ii) a nonlinear increase on sensitivity was observed while increasing surface roughness. (Qazi *et al.*, 2019)

The influence of surface roughness on the performance of POF RI sensors will be discussed in the Chapter 4 on the example of transmission intensity based systems with POFs in D-shaped and straight configurations.

Fluctuation of the optical power signal can be a problem when dealing with intensity based sensors. Simple procedure to overcome this issue is to add a reference optical fibre into the experimental setup and use the normalized transmitted signal as output data, i.e. ratio between the transmitted signal from the sensor and the reference signal.

2.4.2 Surface plasmon resonance (SPR)

Surface plasmons are collective charge oscillations that occur at the interface between conductors and dielectrics, ranging from freely propagating electron density waves along metal surfaces (Surface Plasmon Resonance, SPR) to localized electron oscillations in metal nanoparticles (Localized Surface Plasmon Resonance, LSPR). SPR and LSPR are widely used as sensing principle in optical fibre technology for chemical and biochemical sensors. Sensitive layers can be either deposited on the optical fibre above a previously deposited metallic layer, or contain metal nanoparticles, see Figure 2.23(a,b) (Cennamo and Zeni, 2014)(Caucheteur, Guo and Albert, 2015)(Jin and Granville, 2016).

Light at a certain angle is not reflected but absorbed by the coated layer, and this angle depends on the refractive index of the coating. The excitation of surface plasmon occurs when the wave vector of the propagation constant of evanescent wave exactly matches that of the surface plasmon of similar frequency and state of polarization. This occurs at a particular angle of incidence (θ_{res}) and the corresponding resonance condition for surface plasmons is written as:

$$K_0 n \sin \theta_{res} = K_0 \sqrt{\frac{\epsilon_{mr} n_s^2}{\epsilon_{mr} + n_s^2}}, K_0 = \frac{2\pi}{\lambda} \quad \text{Equation 2.17}$$

where K_{inc} (term on the left) is the propagation constant of the evanescent wave generated as a result of Attenuated Total Reflection (ATR) of the light incident at an angle θ_{res} through a light coupling device with refractive index n , and K_{SP} (term on the right) is the surface plasmon wave propagation constant, ϵ_{mr} is the real part of the metal dielectric constant and n_s is the refractive index of the sensing (dielectric) layer (Cennamo and Zeni, 2014).

When a binding or adsorption is present between the target analyte and the sensitive layer, the refractive index at the interface changes giving rise to a detectable change in the resonance wavelength, which can be detected using appropriate interrogation systems, e.g. a common white light source and spectrometer(Figure 2.23(c)).

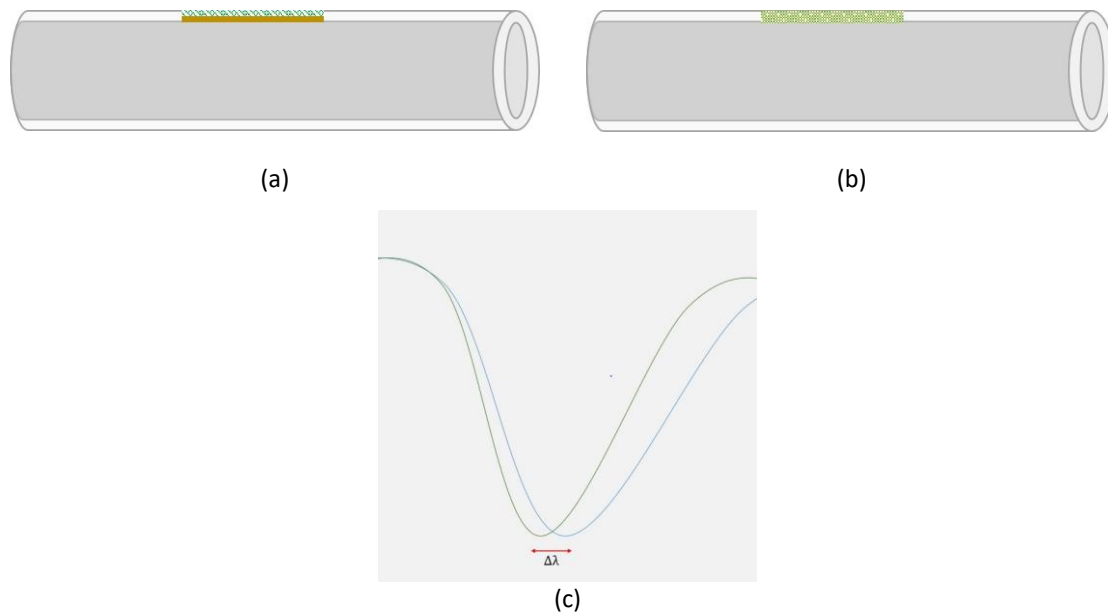


Figure 2.23 (a) POF with a selective layer deposited above a metallic layer (SPR); (b) POF with a selective layer with incorporated nanoparticles (LSPR); (c) schematic representation of a possible variation on the resonance wavelength due to refractive index changes.

Surface plasmons are highly sensitive to small variations in the refractive index at the close vicinity of the optical fibre's surface, however, their effective penetration length is less than a micron and usually in the range of several hundred nanometres (Tiwari and Uzun, 2017). Therefore, when applying sensitive layers for chemical sensing and biosensing based on SPR or LSPR, thin layers are used for increased sensor's sensitivity.

Cennamo *et al.* investigated the effect of the thickness of a gold layer deposited on a D-shaped POF and concluded that for SPR sensing a thickness of 60 nm is generally preferred (Cennamo *et al.*, 2016). Arcas *et al.* reported that 70 nm and 100 nm gold-coated bare U-bent POFs allow good performance for biosensing (Arcas *et al.*, 2018). Cennamo *et al.* investigated the influence of the buffer layer deposited prior to the metal layer as well as the buffer layer optimal thickness for increased sensitivity of POF-SPR-MIP sensors (Nunzio Cennamo, Pesavento, *et al.*, 2017)(Nunzio Cennamo, Maria, *et al.*, 2017).

The wavelength position of the LSPR absorption bands depend on several properties of the nanoparticles (NPs) such as shape (star, sphere, rods, hexagonal, etc.), size, inter-particle distance and aggregation state. Furthermore, silver nanoparticles (AgNPs) of different shapes, sizes and consequently with different colours (yellow, orange, red, violet, blue, green, brown) can be synthesized. As a result, location of the LSPR absorption bands in the UV-VIS spectra would depend on the AgNPs' colour (Rivero, Goicoechea and Arregui, 2018).

The sensitivity (S) of surface plasmon based sensors with spectral interrogation is obtained by calculating the shift in resonance wavelength (λ_{res}) per unit change in refractive index (n):

$$S = \frac{\delta\lambda_{res}}{\delta n} [nm. RIU^{-1}] \quad \text{Equation 2.18}$$

For biochemical optical sensors, the sensitivity is more conveniently defined as the shift in resonance wavelength (λ_{res}) per unit change in analyte concentration (c):

$$S = \frac{\delta\lambda_{res}}{\delta c} [nm. M^{-1}] \quad \text{Equation 2.19}$$

The resolution is then calculated as the minimum change in refractive index which can be determined as a function of the spectral resolution of the interrogation system (λ_{DR}):

$$\Delta n = \frac{1}{S} \delta\lambda_{DR} \quad \text{Equation 2.20}$$

Surface plasmon resonance can be applied in chemical sensing and biosensing using U-bent (Arcas *et al.*, 2018), etched (Al-Qazwini *et al.*, 2016), D-shaped (Gong *et al.*, 2019)(Nunzio Cennamo, D'Agostino, *et al.*, 2018)(Cennamo, Zeni, *et al.*, 2019) and tapered POFs (Cennamo *et al.*, 2014); furthermore, different coatings can be applied on the POF's surface making use of metal nanoparticles (LSPR) (N. Cennamo *et al.*, 2015).

Applications of SPR and LSPR based POF sensors combined with molecularly imprinted polymers (MIPs) for chemical sensing are described in section 2.6.4.

2.5 Chemical sensing and biosensing

Chemical sensors and biosensors can be developed using sensitive coatings on the POF's end face or lateral surface, imparting to it sensitivity and selectivity to specific analytes. In this case, the POF is the transducer, allowing to translate the chemical signal generated by analyte binding or recognition into an optical readable and quantifiable signal (Haupt and Mosbach, 2000). The sensitivity of the POF sensor platform to the external medium or changes in the sensing region should be evaluated prior to sensor development in order to guarantee that changes in interaction of light with the sensitive layer due to the presence of the analyte are detectable.

In 1991, Zhou *et al.* reported the development of POF chemical sensors by the combination of polymer sensing platforms with indicators covalently bonded to the polymer surface, allowing the detection of a variety of chemical species or the measurement of chemical parameters, in gaseous state or in solution, with high stability and sensitivity (Zhou, Tabacco and Rosenblum, 1991). The low-cost sensing setup comprised two wavelengths and allowed for online calibration.

Besides sensing capability of the POF platform, the selectivity to the analyte of interest is essential for the development of POF chemical sensors or biosensors in order to guarantee their viability in real samples.

2.5.1 Direct (label-free) and indirect (label-based) sensing methods

Optical sensors can be classified into two categories: label-free and label-based. A label-free detection is possible when interaction of analyte with sensitive layer generates measurable optical signal. Label-based sensing implies use of the label that does not interact with analyte but produces detectable optical signal that can be colorimetric or fluorescent, when interaction of analyte with sensitive layer takes place.

POFs can be easily employed for absorption measurements, as described in the section 2.2. The measurements can be performed using an extrinsic configuration, in which light passes through the sensing medium, see Figure 2.24(a), or based on intrinsic configuration where the light propagates in the POF and alteration of its characteristics are due to the analyte interaction with fibre surface, see Figure 2.24(b). For quantification, it is important to ensure that the concentration of the analyte is low, no other species absorbs at the same wavelength as analyte and solution is clear, so that changes in the medium's refractive index or turbidity do not interfere with the measurements.

More detailed information about detection based on absorbance can be found in section 2.2.

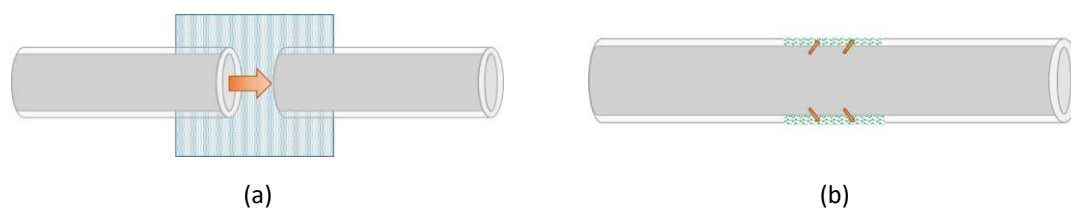


Figure 2.24 Schematic representation of absorbance-based optical fibre sensors in (a) extrinsic and (b) intrinsic configurations.

The same configurations can be used in fluorescence-based sensing. POFs can be doped with fluorescent dyes or modified with sensitive layers containing a fluorescent specie that binds to the target analyte or serve as fluorescent label. The monitoring of both absorption and fluorescence can be performed using simple and low-cost equipment such as LEDs and photodetectors or using a white light source and a spectrometer, which are more expensive but allow to obtain more detailed information about wavelength at which light is absorbed and/or emitted by the analyte.

Optical sensing can also use variation of the refractive index of the sensitive layer resulting from its interaction with the analyte. The variation of sensitive layer refractive index should therefore be correlated with the analyte concentration.

2.5.2 Sensitive layers

The sensitive layers deposited on the POF's surface are of paramount importance as it imparts sensitivity and selectivity to the sensor. Figure 2.25 depicts a schematic representation of a selective sensing layer deposited on a D-shaped POF (side-polished) and in an etched POF.

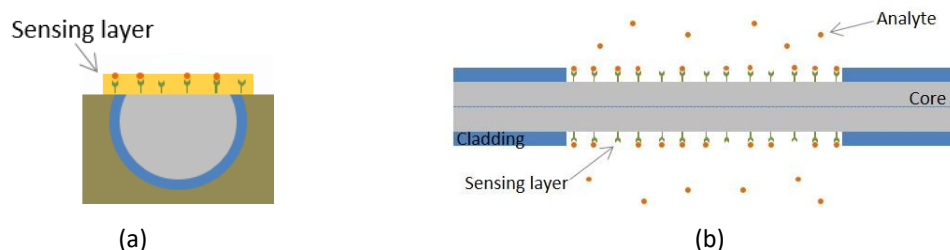
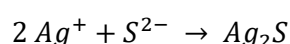


Figure 2.25 Schematic representation of a selective sensing layer deposited on (a) D-shaped POF (side-polished) and (b) etched POF.

There is a large variety of sensing materials that can be employed in optical sensing. Biological entities such as antibodies, enzymes, receptors, or whole cells are highly selective and thus very attractive as recognition elements. However, their poor chemical and physical stability prevent their use in harsh environments (Haupt and Mosbach, 2000). Aptamers are single-stranded DNA or RNA oligonucleotides with catalytic and receptor properties that have attracted a lot of attention as recognition elements of biosensors due to their high selectivity and versatility (Dehghani *et al.*, 2018)(Nunzio Cennamo, Pesavento, *et al.*, 2015).

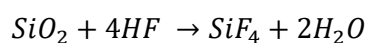
Receptor molecules can be directly immobilized on the POF's surface (Chu *et al.*, 2009)(Azkune *et al.*, 2018)(Maciak, Sufa and Stolarczyk, 2014)(Rivera *et al.*, 2009)(Rivera *et al.*, 2009). Functionalization of POFs can be done by grafting of receptors to the surface, or by deposition such as dip-coating, spin coating or drop casting.

Though interaction between sensitive layer of the sensor and analyte is expected to be reversible, functionalized coatings based on non-reversible chemical reactions can be used as well. Coating of POFs with silver (Ag) for the detection of hydrogen sulphide (H₂S) was reported in (Angelini *et al.*, 2010)(Grassini *et al.*, 2015)(Sultangazin *et al.*, 2017). Silver sulphide (Ag₂S), formed at the surface of POF, is less reflective material than Ag, which leads to decrease of light transmission:



POF sensors sputtered with Ag layer have been proposed for the measurement of the cumulative H₂S concentration indoors for cultural heritage (Grassini *et al.*, 2015) and environmental monitoring as handheld and low-cost sensor integrated into a smartphone (Sultangazin *et al.*, 2017).

Another example of non-reversible coatings is the POF sensor for the measurement of the cumulative concentration of hydrogen fluoride vapours (HF) using an unclad POF coated with glass layer (SiO₂) by plasma-enhanced chemical vapour deposition (PECVD). Detection is based on the variation in the transmitted light due to formation of silicon tetrafluoride (SiF₄) on the fibre surface:



This sensor has been developed for monitoring exposition to HF vapours inside the resistive plate chamber muon detector of the Compact Muon Solenoid (CMS) at CERN in Geneva, to prevent filter degradation and schedule their maintenance (Grassini *et al.*, 2015).

Polymers are another type of materials widely used in optical sensing (Rivero, Goicoechea and Arregui, 2018). Polymeric matrix can act as the sensitive layer itself or serve as the solid support for the immobilization of receptors or optical labels as metallic nanoparticles (gold, silver, copper), metal oxide nanoparticles (silica, titanium, caesium) and/or receptors.

A variety of synthetic receptors for optical sensing has been described in the literature including cyclodextrins, cyclophanes, crown-ethers and calixarenes (Liu, Nalluri and Stoddart, 2017). Synthetic organic receptors often need a label to be used in optical sensing, need to be designed specifically for each target molecule, for which a time-consuming multistep synthesis is necessary, and sometimes display low binding constants in aqueous environments (Wan, Wagner and Rurack, 2016).

Chemical sensors for molecule recognition are also developed using molecularly imprinting polymers (MIPs) (Chen *et al.*, 2016). MIPs have been used extensively as selective layers for optical fibre sensing. These synthetic polymers have highly selective recognition sites and the binding of the analyte to the MIP causes a variation in the polymer matrix that leads to the variation of the transmitted intensity or resonance wavelength allowing its optical detection. MIPs are attractive materials for sensor's development as they can be designed for the analyte of interest, although the process of optimization can be very time consuming.

2.5.3 Molecularly Imprinted Polymers (MIPs)

2.5.3.1 Working principle

Molecular imprinting of synthetic polymers is a process where functional and cross-linking monomers are co-polymerized in the presence of the target analyte (the imprint molecule). Initially the formation of a complex between the functional monomer and the imprint molecule occurs and, after polymerization, their functional groups are held in position by the highly cross-linked polymeric structure. Subsequent removal of the imprint molecule leaves behind binding sites that are complementary in size and shape to the analyte. Therefore, a molecular memory is introduced into the polymer which is now capable of rebinding the analyte with a very high specificity. (Haupt and Mosbach, 2000)

Molecular imprinting is basically performed in three steps (see Figure 2.26):

- complex formation of the template molecule with the functional monomers;
- co-polymerization with an excess of cross-linker agent in an (optional) inert solvent to form a rigid polymer;
- removal of the template molecule by hydrolysis or extraction.

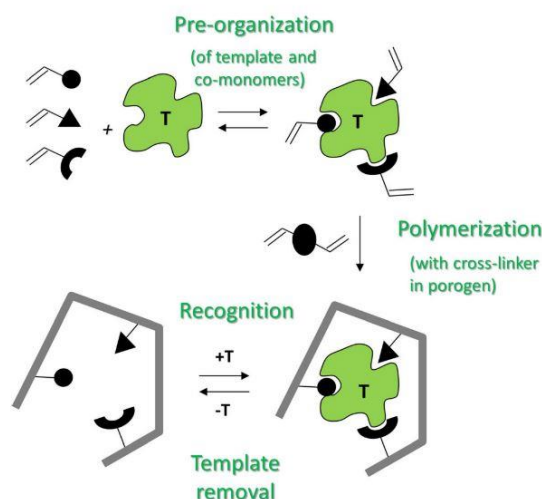


Figure 2.26 Schematic representation - steps involved in the assembly and operation of molecularly imprinted polymers (MIPs), where T is the template. (Wan, Wagner and Rurack, 2016)

The choice of the functional monomer is based on the ability to interact with the functional groups of the template. Molecular imprinting starts with the interaction between the template molecule and the functional monomer, creating a complex which can be based on two distinct interactions:

- monomers can be covalently coupled to the imprint molecule (reversible), therefore a polymerizable derivative of the imprint molecule is synthesized, which was firstly developed by Wulff (Wulff, 1995);

- a pre-polymerization complex between the imprint molecule and functional monomers can be formed via non-covalent interactions (i.e. hydrogen bonding, van der Waals' or ionic interactions), which has been pioneered by Mosbach and Ramström (Mosbach and Ramström, 1996).

A more homogeneous population of binding sites can be achieved with covalent imprinting, due to the high stability of covalent bonds, while the imprinting efficiency (binding sites relative to the amount of imprint molecule used) is higher with non-covalent imprinting. Nevertheless, the later allows more flexibility in the choice of functional monomers, target molecules and the use of imprinting materials (Haupt and Mosbach, 2000) while also leading to the formation of non-specific binding sites (Tiwari and Uzun, 2017).

The most commonly used functional monomers include carboxylic acids (methacrylic acid (MAA)) and hetero-aromatic bases with vinyl groups capable of non-covalent interactions (Tiwari and Uzun, 2017). For example, MAA, one of the most preferred monomers in MIP synthesis, can create hydrogen bonds with diverse functional groups of the template molecule and acts as a hydrogen donor and a hydrogen acceptor simultaneously (Yan and Row, 2006). Figure 2.27 depicts the most common functional monomers used in non-covalent molecular imprinting.

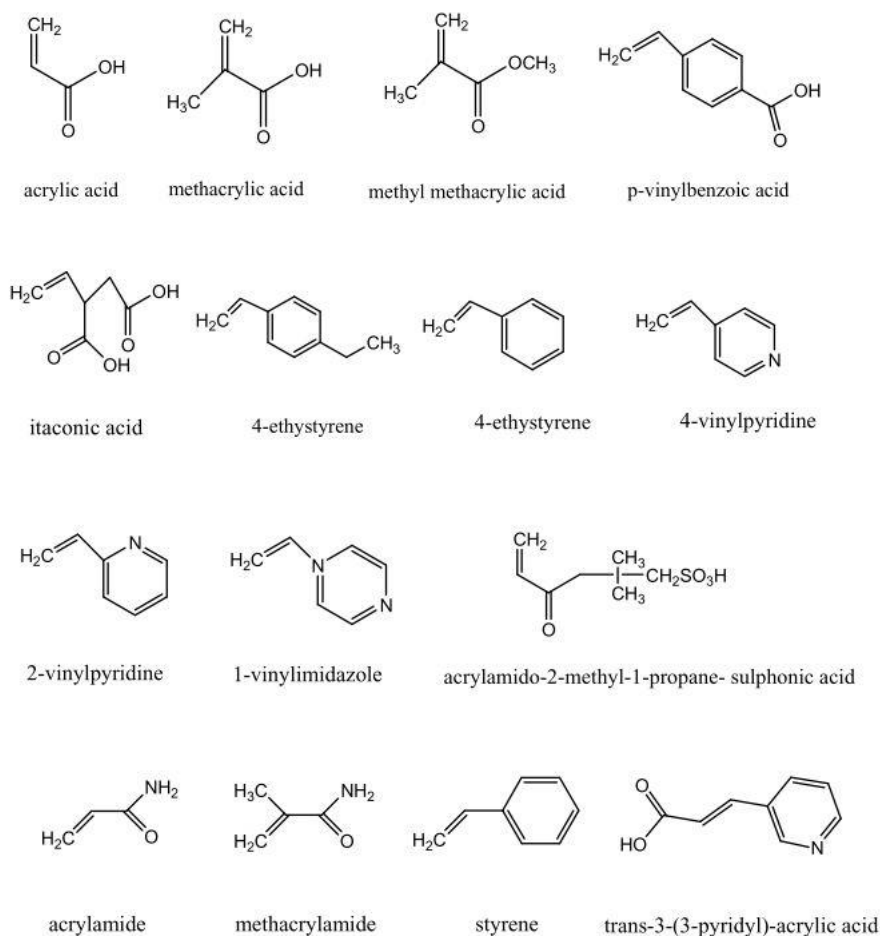


Figure 2.27 Chemical structure of common functional monomers used in non-covalent molecular imprinting (Yan and Row, 2006).

The role of the cross-linker is to ensure the stability of the cavity around the template molecule and prevent the collapse of the MIP after its extraction (Rico-Yuste and Carrasco, 2019). An excess of cross-linker in stoichiometric comparison with the functional monomer is usually added. Figure 2.28 depicts the most common cross-linkers used in non-covalent molecular imprinting procedures.

The characteristics of the cross-linker, such as type, length and fraction in the polymeric mixture have effect on the structure and specific binding interactions of the imprinted material - template recognition behaviour.

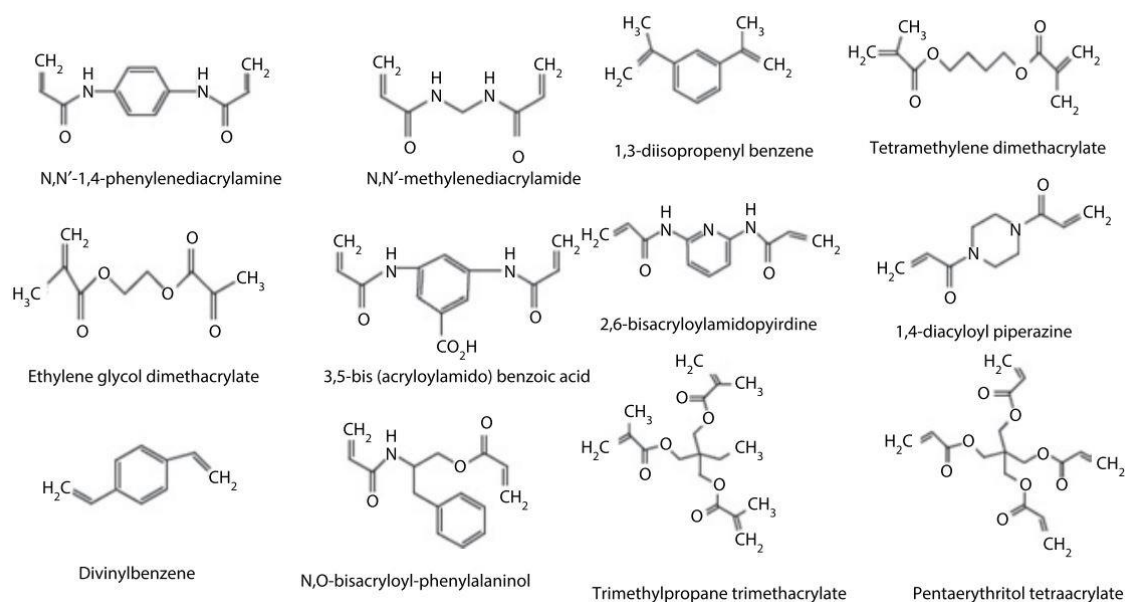


Figure 2.28 Chemical structure of common cross-linkers used in non-covalent molecular imprinting (Yan and Row, 2006).

Generally, an inert solvent called porogen is used for the preparation of the pre-polymeric mixture, which dissolves all the chemical species and generates a highly porous structure, allowing easier access to and out from the imprinted sites (Haupt and Mosbach, 2000). However, sometimes pre-polymeric mixtures are prepared without solvents (N. Cennamo *et al.*, 2013).

Morphology of MIPs are mostly determined by the cross-linker and solvent. On one side, the cavities' structure should be strong enough to maintain the conformation after template removal, which requires higher amount of cross-linker. On the other hand, an excess of cross-linker may lead to inhibition of the diffusion and removal of the template. Furthermore, higher selectivity is related with increased binding sites which are related with macro-porous structures and high cross-linker ratios (higher than 80%) (Tiwari and Uzun, 2017).

Polymerization usually takes place in the presence of initiators such as peroxides and azo-derivative compounds, that generate free radicals upon thermal or photo-chemical decomposition, or catalysts such as acids or bases that hydrolyse monomers and prompt their poly-condensation (Rico-Yuste and Carrasco, 2019). Figure 2.29 depicts the most common initiators used in non-covalent molecular imprinting.

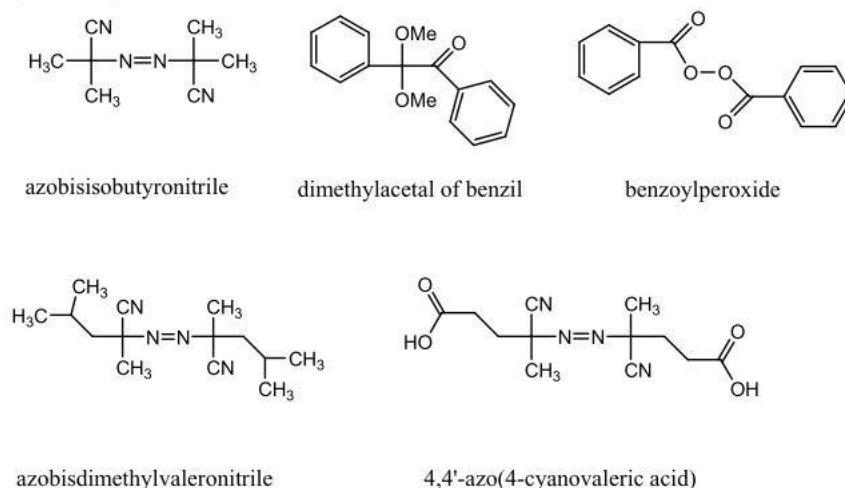


Figure 2.29 Chemical structure of common initiators used in non-covalent molecular imprinting (Yan and Row, 2006).

Synthesized MIP is usually washed to remove un-polymerized monomers and the template, leaving specific binding sites within the polymer matrix. It is expected that the target analyte will selectively rebind to the MIP while other species, even similar ones, will not be able to bind due to the differences in terms of size, shape or functional groups.

Typically two types of sites are present in MIPs: high-affinity sites that are the specific imprinted sites and low-affinity sites that are source of non-specific binding (Ton *et al.*, 2015). Usually a reference polymer matrix obtained in the same way as the MIP but in the absence of the template molecule, called a non-imprinted polymer (NIP), is studied along with the MIPs to evaluate the non-specific binding. However, several authors have stated some difficulties when obtaining the NIP, either because a different material is obtained due to the different reactivity of the monomers in the absence of template or the impossibility of obtaining a polymer due to changes in polymerization rates (Rico-Yuste and Carrasco, 2019).

2.5.3.2 MIP synthesis

MIPs can be synthesized in different forms including bulk, microspheres, nanoparticles and thin layers, which can influence selectivity and binding capacity of the polymer and consequently performance of optical fibre MIP-based sensors (Tiwari and Uzun, 2017).

Bulk polymerization is a very common procedure for MIP synthesis, which consists in polymerization of a solution containing all the reagents in the absence of oxygen producing bulk piece of solid polymer. The obtained MIP, in a solid state, is then grinded and particles with different shapes and sizes can be obtained. This process has some drawbacks, such as variation of the shape and size of the particles, the possibility of destruction of some of the binding sites and the fact that only binding sites at the surface are active. Bulk MIPs are not the most convenient form to use in MIP based optical fibre sensors, due to poor surface coverage and the irregular structures obtained, being mainly used in separation science for liquid chromatography, solid-phase extraction, etc.

(Tiwari and Uzun, 2017). For the development of MIP based optical fibre sensors other methods are more convenient, such as precipitation polymerization or surface grafting.

MIP micro and nanoparticles are prepared by precipitation polymerization, which affords particles of uniform shape and desired diameters and porosity by manipulating the polymerization reaction conditions such as temperature and radiation time (Tiwari and Uzun, 2017). Precipitation polymerization is very similar to bulk polymerization, although additional porogen is used and, when the polymer chains reach a critical length precipitation occurs in the form of small beads typically around 100 nm to 10 μm in diameter, which can be easily collected by centrifugation. No grinding is necessary in this case and relatively regular spherical beads are obtained.

In the work reported by (Ton *et al.*, 2015) MIP nanoparticles were synthesized by precipitation polymerization, dip coated on the POF and further polymerized by heating. MIPs synthesized by radical polymerization are attached to optical fibres simply by dip coating or spin coating methods followed by in situ polymerization using thermal or photochemical curing where the adhesion between the MIP layer and the substrate surface are based on non-covalent bonds (Tiwari and Uzun, 2017).

MIP microspheres were used for development of optical fibre sensors for the detection of enrofloxacin (ENRO), broadly used antibiotic (Carrasco *et al.*, 2015) and 6-mercaptopurine (6-MP) in human serum, an anti-cancer chemotherapy drug (Wang and Zhang, 2008). The work reported by Carrasco *et al.* in 2015 is the first applications of MIPs in fibre optic microarrays with multiple detection ability, where chemically etched fibre-bundle was used (50 000 individual 3.1 mm diameter fibre) (Carrasco *et al.*, 2015).

MIP nanoparticles combined with POFs have been reported in the literature, such as the work reported by (Ton *et al.*, 2015). Ton *et al.* reported the synthesis of MIP nanoparticles for the detection of herbicide 2,4-dichlorophenoxyacetic acid (average size ~ 300 nm) and mycotoxin citrinin (average size between 150 – 500 nm), coated on POFs obtaining disposable POF sensors (Ton *et al.*, 2015). Korposh *et al.* reported the coating of a single-mode LPG glass fibre with MIP nanoparticles with average size of ~ 280 nm for the selective detection of antibiotic vancomycin (Korposh *et al.*, 2014).

Graft polymerization is a process in which monomers are covalently bonded and polymerized as side chains onto the main polymer chain (the backbone). Graft polymerization can be initiated by chemical or photochemical treatment, ionizing radiation, photo-irradiation, plasma-induced techniques, enzymatic grafting, etc. (Sherazi, 2016).

The most efficient method for MIP deposition on optical fibre sensors is the “grafting from” polymerization, which implies the immobilization of the initiator directly on the surface of the fibre prior to the polymerization. This method is often preferred as enhance the sensing ability of the MIP layer. The initiator decomposition starts the polymerization reaction from the fibre’s surface, resulting in covalently attached MIP layers with thickness lower than 50 nm. (Tiwari and Uzun, 2017)

Thin-film MIP layers are the most common morphology used for POF platforms. They can be deposited by spin-coating (Nunzio Cennamo, D’Agostino, *et al.*, 2018), evanescent field polymerization (Ton *et al.*, 2015) or grafted on the fibre’s surface. POF sensor with an MIP layer

deposited on the fibre surface by in-situ polymerization using evanescent wave photopolymerization has been reported in (Ton *et al.*, 2015).

2.5.3.3 Deposition methods

Several deposition methods can be used for the coating of POFs with MIPs. The most common are dip-coating (Ton *et al.*, 2015), spin-coating (Nunzio Cennamo, D'Agostino, *et al.*, 2018), evanescent field photopolymerization (Ton *et al.*, 2015) and functionalization through chemical reactions or surface grafting. When modifications of the fibre's surface are made through surface grafting, the coating is chemically bound to the fibre resulting in high stability and good adhesion of the layer.

Dip coating consists in immersing the POF in the pre-polymeric mixture and pulling it out. Coating properties depend on the immersion time and its thickness on the viscosity of the mixture and the speed at which the POF is removed. Commonly, the fibre is left for some time in a proper holder for draining and solvent evaporation.

Spin coating is the acceleration and rotation at controlled speed of a small volume of the pre-polymeric mixture which is dropped on the surface of the substrate such as the flat section of the POF, usually D-shaped POFs. The thickness of the coating and its homogeneity depend on rotation time and speed, and the density and viscosity of the pre-polymerization mixture.

After deposition on the fibre either by spin coating or dip coating, pre-polymerization mixture is polymerized by heating (Ton *et al.*, 2015)(Foguel *et al.*, 2015)(N. Cennamo *et al.*, 2017) or photopolymerized with UV light (Ton *et al.*, 2015) to obtain the final MIP coating.

MIP deposition by evanescent field photopolymerization is performed by immersing a fibre in the pre-polymerization mixture and injecting UV light through it. Photopolymerization can also be performed by incident UV light on the POFs surface or tip.

2.5.3.4 MIP characterization

Different methods are used for characterization of MIPs (Tiwari and Uzun, 2017):

- batch rebinding studies for determination of binding affinity, heterogeneity index, total number of binding sites and imprinting factor;
- spectroscopy including ultraviolet (UV), infrared (IR), Raman and nuclear magnetic resonance (NMR), for investigation of the functional monomers-template interactions;
- isothermal titration calorimetry for investigation of the thermodynamics of imprinted polymer- template complex;
- light microscopy and scanning electron microscopy (SEM) for investigation of morphology of the imprinted polymers;
- Brunauer–Emmett–Teller analysis (BET) can be employed to measure the porosity of the polymer, providing information on the pore size and volume, average pore diameter and surface area of the polymers.

A detailed overview of the MIP's characterization methods can be found in (Tiwari and Uzun, 2017).

2.5.3.5 MIPs as sensing layers for chemical sensing

MIPs were applied as smart materials to separation, environmental and biomedical sciences and sensing (Tiwari and Uzun, 2017). MIPs are chemically stable, due to their highly cross-linked polymeric nature, facilitating their application in extreme environments (in the presence of acids or bases, organic solvents or at high temperatures and pressures). Clear advantages of MIPs over antibodies for sensing technology are that they can be stored dry at room temperature for long periods of time and are cheap to produce (Haupt and Mosbach, 2000). Sensitivity of MIP-based sensors is generally still lower compared to other receptors and, thus, some drawbacks still need to be worked out, such as more homogeneous binding site population, higher affinity for the target analyte and possibility to be used in aqueous solvents (Haupt and Mosbach, 2000).

Molecular imprinting technique allows the preparation of functionalized polymers with specific binding sites for a target molecule, presenting good chemical stability and selectivity. MIPs are usually synthesized by radical polymerization of a mixture of template (target molecule), radical initiator, cross-linker monomer(s), functional monomer(s) and optionally a solvent. MIPs can be grafted onto the POF's surface (or tip) or coated using techniques such as spin coating, dip coating or evanescent field photopolymerization. After polymerization, the target molecule is extracted leaving in the polymer formed binding sites, which can rebind target molecule selectively. (Sequeira, Nogueira and Bilro, 2019)

There's an increased interest in the combination of fibre optic sensors with MIPs due to their high selectivity, low-cost, mechanical and thermal stability, and ease of preparation (Tiwari and Uzun, 2017).

Application of MIPs as sensitive elements in chemical sensors requires their integration with the transducer. Intensity based detection schemes are commonly used when MIPs are grafted or coated directly on the POF's surface (Foguel *et al.*, 2015; Ton *et al.*, 2015; N. Cennamo *et al.*, 2017, 2018).

SPR or LSPR-based sensing requires MIPs deposition on top of a metallic layer or incorporation of metallic nanoparticles into it. The combination of D-shaped POFs and MIPs is an effective way to obtain highly selective and sensitive POF-SPR-MIP sensors, especially suitable for chemical sensing (Cennamo *et al.*, 2016). Cennamo *et al.* reported in 2018 the development of a D-shaped POF-SPR-MIP chemical sensor for the detection of perfluorinated alkylated substances (PFASs) in water (Nunzio Cennamo, D'Agostino, *et al.*, 2018) and a D-shaped POF-SPR biosensor based on a specific antibody for PFOA/PFOS (Nunzio Cennamo, Zeni, Tortora, *et al.*, 2018). MIP based sensor presented better stability compared to biosensor. Generally, in comparison with bio-receptors, MIPs are easier to prepare, have higher storage stability, mechanical strength and resistance to heat and pressure, making possible their implementation for remote sensing and in harsh environments (Yan and Row, 2006)(Tiwari and Uzun, 2017).

Besides all the described advantages, the development of POF chemical sensors with MIPs as selective layers is still a long and time-consuming process as development of highly efficient molecularly imprinted polymers entails the mastery of complex chemistry (Whitcombe, Kirsch and Nicholls, 2014)(Fu *et al.*, 2015)(Derazshamshir and Yavuz, 2017).

Batch binding studies of polymers are usually performed in order to evaluate the properties of the MIP, such as the selectivity, time of binding and specificity by comparison with the non-imprinted polymer (NIP), prepared in the same way but without the analyte.

MIPs can also be produced with fluorescent monomers, whose fluorescence intensity depends on the binding between the template molecule and the MIP (Ton *et al.*, 2015)(Foguel *et al.*, 2015). Fluorescent MIPs (fMIPs) binding with the target analyte may induce fluorescence quenching, enhancement or spectral shift. fMIPs can be also obtained by incorporating fluorescent dyes, probes, and NPs into the polymer (Tiwari and Uzun, 2017). The selection of the fluorophore is very important when designing a sensor and, generally, absorption and fluorescence in the visible range (or longer wavelength) are preferred to reduce absorption and scattering by the matrix (Wan, Wagner and Rurack, 2016).

In the literature several reviews can be found in molecular imprinting technology (Chen *et al.*, 2016)(Whitcombe, Kirsch and Nicholls, 2014)(Chen, Xu and Li, 2011), as well on MIP based sensors (Tiwari and Uzun, 2017)(Haupt and Mosbach, 2000)(Derazshamshir and Yavuz, 2017)(Henry, Cullen and Piletsky, 2005)(Cieplak and Kutner, 2016)(Uzun and Turner, 2016)(Ahmad *et al.*, 2018). Wan *et al.* reported a review in 2016 on fluorescent MIPs incorporating fluorescent monomers (Wan, Wagner and Rurack, 2016). In 2019, Rico-Yuste and Carrasco published a review on the development of new optical sensors based on MIPs including POF-MIP, focusing on the improvement of sensors' performance according to their limitations (Rico-Yuste and Carrasco, 2019).

2.6 Applications of intensity based POF sensors and POF-MIP based chemical sensing

Intensity based configurations are widely used for development of physical and chemical POF sensors. Efficiently sensitization of the optical fibre can be done using several techniques including tapering, etching, drilling, polishing, bending, laser patterning, coating with metal and/or special chemically engineered layers and nanoparticles.

Several reviews of POF technology and applications have been published lately, including review by Bilro *et al.* focusing on intensity variation schemes and low-cost solutions (Bilro *et al.*, 2012), and by Jin and Granville focusing on recent progress on intrinsic detection schemes (Jin and Granville, 2016).

2.6.1 Physical POF sensors

POF physical sensors have been developed for the detection of strain (A. Leal-Junior, Frizera, Lee, Mizuno, Nakamura, Paixão, *et al.*, 2018)(Ramani and Kuang, 2019), cracks (Luo *et al.*, 2016)(Yang *et al.*, 2017), curvature (A. Leal-Junior, Frizera, Lee, Mizuno, Nakamura, Leitão, *et al.*, 2018), ionizing radiation (Zhuang *et al.*, 2016), liquid level (R. Oliveira, Aristilde, *et al.*, 2016), turbidity (Bilro, Prats, *et al.*, 2010)(Boogert *et al.*, 2013)(N. Oliveira *et al.*, 2016), colour (N. Oliveira *et al.*, 2016)(Ferreira *et al.*, 2013)(Bilro *et al.*, 2013)(Pereira *et al.*, 2013), and monitoring of polymer curing (L. Bilro, Alberto, *et al.*, 2011). Application of POFs as wearable sensors have been demonstrated including monitoring of human gait (L. Bilro, Oliveira, *et al.*, 2011), joint functioning (Rezende *et al.*, 2018)(A. G. Leal-Junior, Frizera, *et al.*, 2018), foot functioning (A. G. Leal-Junior, Theodosiou, *et al.*, 2018)(Leal-Junior, Díaz, Marques, *et al.*, 2019) and respiratory movements (Leal-Junior, Díaz, Leitão, *et al.*, 2019)(Aitkulov and Tosi, 2019).

2.6.2 Refractive index sensing

Most refractive index POF sensors (RI-POF) operating in intensity based detection schemes employ light attenuation as sensing principle. The manufacturing of these sensors usually involves bending and/or the removal of the cladding and part of the core, called sensing region, rendering fibre sensitive to the refractive index of the external medium. Several parameters may affect sensor sensitivity including wavelength of the light source, waist diameter and total depth, length of the sensing region, macrobending and number of tapered/polished regions.

An example of an extrinsic reflection-based configuration is the displacement sensor proposed by Binu *et al.*, which allowed to measure the refractive index of a liquid (see as example Figure 2.19(b)). In the refractive index range between 1.3322–1.3617, obtained by varying glucose concentration from 0 to 250 gL⁻¹, a sensitivity of 0.0072 V/wt.% was observed (Binu *et al.*, 2009). In 2018, Cennamo *et al.* presented an extrinsic POF sensor based on a transmission configuration with two POFs and a slab waveguide (with and without a buffer layer). Proposed design allowed RI sensing with a removable chip and was suitable for thermo-stabilized flow cells (Cennamo, Mattiello and Zeni, 2019).

POF tapering is a common technique for sensitivity enhancement in intrinsic transmission-based configurations. Theoretical, numerical and experimental analysis of influence of POF tapering on its performance was reported by Xue *et al.* in 2007 (Xue *et al.*, 2007). Fabrication of POF tapers with different taper ratios by heat-and-pull method was reported in (Gravina, Testa and Bernini, 2009). Good manufacture repeatability was demonstrated. The tapered POF sensors allowed measurements by evanescent wave absorption of methylene blue solution and fluorescence of Cy5 dye. Feng *et al.* studied the influence of the wavelength (532 nm, 633 nm, and 780 nm) on evanescent field sensing with tapered POFs with different waist diameters. This work reported that the reduction of the diameter of a tapered POF (to 200 µm) and the increase of the number of tapered regions, using heat and pull method, improves the sensitivity and linearity of the sensor response. The best performance of the tapered POF RI sensors was achieved at 633 nm for RI ranging from 1.33 to 1.41, with a sensitivity of 950 µW/RIU (D. Feng *et al.*, 2014). In 2019, Teng *et al.* reported a POF sensor based on two twisted tapered POFs obtained by heating and drawing two fibres and twisting them around each other. Different fibre diameters and twisted region lengths were evaluated and a sensitivity of 1700 %/RIU and -3496 %/RIU in the RI ranges of 1.37–1.41 and 1.41–1.44 were obtained, respectively, for fibre diameters of 100 µm and 200 µm for the active and passive fibres, respectively, and a twisted region length of 18 mm (Teng *et al.*, 2019).

Zubia *et al.* presented a laterally polished SI POF with exposed core and slight curvature, that allowed to measure RI with a resolution of 5x10⁻³ refractive index units (RIU) in the refractive index range between 1.30–1.39 (Zubia, Garitaonandía and Arrúe, 2000). In 2011, Bilro *et al.* reported theoretical modelling of D-shaped POF responses with different macrobending and external RI, which was validated by experimental results (Lúcia Bilro *et al.*, 2011). The experimental study was

performed with macrobending for sensing regions with lengths of 1.3 cm, 1.5 cm, and 2.1 cm and a total depth of 550 μm , 640 μm , and 550 μm , respectively.

An optimization of depth and curvature radius of a D-shaped POF with 1 cm length, aiming to increase linearity range and sensitivity to RI (1.333–1.455) at 652 nm, was reported by Feng *et al.* The best results were obtained for a depth of 500 μm and a curvature radius of 5 cm (D.-J. Feng *et al.*, 2014). A further optimization scheme was reported by Liu and Feng, with the best results obtained for a D-shaped POF with 2 cm length and an excurvation structure, and the same bending radius and depth. However, sensitivity and resolution of the sensor were not specified (Liu and Feng, 2016).

U-bent POFs make use of the increased light losses and interaction with the evanescent field for the development of low-cost sensors. POF sensors can also combine bending with tapering, etching and/or polishing. Paz *et al.* presented in 2007 a U-bent POF sensor with a self-reference signal for wine monitoring in real-time, integrated in a portable detection system (Paz *et al.*, 2007). In 2010 a multi-point POF sensor for electrolyte density measurement in lead-acid batteries was presented using the same fibre setup but with optimized bending radius (between 0.1 and 1 cm). Sensitivity and resolution of the sensors were not reported (Cao-Paz *et al.*, 2010). A U-bent side-polished POF sensor was optimized by Jing *et al.* with respect to curvature radius (5 mm), polished depth (500 μm) and position (60°). Maximum sensitivity of 154 dB/RIU in the RI range of 1.33–1.44 was achieved (Jing *et al.*, 2015). In 2017, Teng *et al.* reported a U-bent side-polished POF-RI sensor in the range 1.33–1.44 with a resolution of 3.3×10^{-4} RIU. The sensitivity to refractive index variation was improved (864 %/RIU) by applying a curvature bending radius of 2 mm and a polished depth of 400 μm in a sensing region of 1 cm length (Teng *et al.*, 2017). The authors also concluded that straight polished POFs are not sensitive enough as RI sensing probes. The optimization of a U-bent unclad POF sensor was reported by Gowri and Sai in 2016, which displayed optimum sensitivity of $5.57 \Delta A_{560 \text{ nm}}/\Delta \text{RIU}$ with bending diameter (1.25 mm) and fibre diameter (500 μm core). The transmission of light decreased with the increase of the medium's refractive index in the range 1.33–1.37 and a resolution of 1 mRIU was obtained for measurements performed in terms of absorbance (Gowri and Sai, 2016). A U-bent unclad POF probe for determination of the content of fat milk (%) with a sensitivity of $0.15 \Delta A/\Delta \text{\%fat}$ (optical absorbance) was reported by Gowri *et al.* in 2019. The POF probe allows dip type sensing with response time less than 10 s and sample volume lower than 100 μL , and could be employed on-site for instantaneous milk quality monitoring due to a low-cost portable design of the optoelectronic device based on an LED and a photodetector (Gowri *et al.*, 2019).

In 2015, Liu *et al.* reported a side-hole polished POF as a low-cost RI sensor, with a sensitivity of 1862.1 $\mu\text{W}/\text{RIU}$, which depended on the hole diameter. An increase of the sensor's transmittance was observed with the increase of the RI from 1.34 to 1.475 (Liu *et al.*, 2015). In the same year, Shin and Park reported an POF sensor with a cascade in-line micro-drilled 3-hole structure with a sensitivity of 62.9 dB/RIU in 1.33–1.42 RI range (Shin and Park, 2015). In 2017, Mizuno *et al.* fabricated a quasi-extrinsic POF sensor by crushing the POF with a slotted screwdriver. Temperature independent (between 10–25 $^\circ\text{C}$) sensitivity of 173 dB/RIU in the RI range ~ 1.32 –1.43 was obtained (Mizuno *et al.*, 2017).

In 2017, Tiwari et al. reported a POF-RI sensor based on a spiral structure with ~ 1.2 cm length, 300 μm depth, and 3 mm pitch of the spiral channel. An increase in the output power was observed with the increase of the refractive index in the range 1.34–1.41. Sensitivity was found to depend on the spiral pitch and applied strain (Tiwari, Singh and Pandey, 2017).

A POF sensor with an inscribed long period grating (LPG), corrugated surface by a die press print method, was reported by Xue et al. in 2019. No difference on the resonant wavelengths (500 – 700 nm) was observed before and after the LPG inscription, although a loss of transmitted intensity occurred after the inscription process. The POF sensor with diameter of 0.25 mm, grating period of 100 μm , groove depth of 65 μm and tilted angle 20°, was characterized at 635 nm. A sensitivity of 2815 %/RIU with a resolution of 1.39×10^{-4} RIU was achieved for the refractive index range between 1.33–1.45 (Xue *et al.*, 2019).

There is a general concern to obtain sensing regions with smooth surfaces when producing POF sensors for RI sensing (D.-J. Feng *et al.*, 2014)(Teng *et al.*, 2017), while roughness of the surface is generally not considered. In 2018, Leal-Junior et al. reported a study where the roughness was included as an important parameter for the sensitivity of a POF curvature sensor based on intensity modulation, together with the length, depth and curvature radius of the sensing region (Leal-Junior, Frizera and José Pontes, 2018). This study concluded that the roughness of the sensing region obtained with sandpapers P400 or P600 would allow to obtain a POF curvature sensor with better performance in terms of sensitivity, hysteresis and linearity. Sensitivity enhancement resulted from the light attenuation due to the bending of the POF combined with the scattering losses due to the surface roughness.

Generally, reproducibility of the manufacturing process of the POF-RI sensors is not reported in the literature. Furthermore, the repeatability of the sensor's response with time is also rarely addressed.

2.6.3 Chemical sensing

POF chemical sensors are developed since 1989 - 1991 by combining polymer sensing platforms with a variety of indicators and sensitive layers (Sawada, Tanaka and Wakatsuki, 1989)(Zhou, Tabacco and Rosenblum, 1991).

In 1989, Sawada et al. reported an POF gas sensor for detection of ammonia (NH_3) and hydrogen chloride (HCl) at concentrations below 10 ppm. The POF with polycarbonate (PC) core and a PMMA/PVDF (polyvinylidene fluoride) cladding was doped with fluorescent materials enabling the conversion of white light into monochromatic light in less than 10 μs (Sawada, Tanaka and Wakatsuki, 1989). A tapered POF sensor for the detection of ammonia in the concentration range 0–50 ppm at room temperature was developed by Raj et al. in 2015, by coating of the POF's core with silver nanoparticles/PVP/PVA layer. Developed POF sensor showed high selectivity to ammonia in the presence of methanol and ethanol vapours, which increased with increase of silver

concentration (Raj et al., 2015). In 2016, Khalaf et al. coated a side polished POF with graphene/polyaniline nanocomposite also for ammonia sensing (0.25%-1%) at room temperature. Absorbance of sensitive layer in the range of 600–800 nm increased with the increase of ammonia concentration (Khalaf et al., 2016).

Chu et al. reported the detection of dissolved oxygen using an U-bent POF coated with sol-gel containing fluorescence indicator dichlorotris(1,10-phenanthroline) ruthenium (Chu et al., 2009). Another sensor for oxygen detection was prepared by deposition of a layer of fluorophore tris(2,2'-bipyridyl) dichlororuthenium(II) hexahydrate on the tapered POF (Pulido and Esteban, 2013). Detection in both cases was based on fluorescence quenching by oxygen.

A POF sensor for the detection of nitrogen dioxide (NO_2) concentration at temperatures below 50°C in a dry atmosphere was developed by Maciak et al. (Maciak, Sufa and Stolarczyk, 2014). The POF tip was firstly subjected to thermoforming after which it was coated with a functionalized polymer by dip-coating. The detection was performed using a reflection based setup. Adsorption of NO_2 by the selective layer caused a variation of the reflectance between 750 nm and 770 nm for NO_2 concentrations between 0-10 ppm. Authors refer sensitivities below 1 ppm of NO_2 , although sensor's reproducibility and selectivity needed to be improved (Maciak, Sufa and Stolarczyk, 2014).

Elias et al. reported in 2015 an early stage investigation towards the development of a sensor for detection of oral cancer. A simple transmission POF evanescent wave sensor was developed for the detection of nitrite (NO_2^-) in the concentration range $3\ \mu\text{M} - 100\ \mu\text{M}$ using Griess reaction, aiming at the future application in human saliva (Elias et al., 2015).

POF sensors based on non-reversible chemical reactions (see section 2.5.2), for the detection of the cumulative concentration of hydrogen sulphide (Angelini et al., 2010)(Grassini et al., 2015)(Sultangazin et al., 2017)(Aitkulov et al., 2018) and hydrogen fluoride vapours (Grassini et al., 2015) were reported.

In 2019, Zhong et al. reported the development of a highly selective photocatalytic POF sensor for phenol ($\text{C}_6\text{H}_5\text{OH}$) detection. The sensor was produced by removing the cladding and part of the core of a 2.5 cm POF and coating it with different layers – Canada balsam doped with GeO_2 (CBG, $150\ \mu\text{m}$), a UV-VIS light driven photocatalytic material, CdS sensitized $\text{Er}^{3+}:\text{YAlO}_3/\text{SiO}_2/\text{TiO}_2$ composite ($\sim 3\ \mu\text{m}$) and a phenol perm selective polymer membrane, which was insensitive to pH in the range from 2 to 14 (Zhong et al., 2019). The developed sensor, based on the variation of the transmitted light at the fixed temperature $30 \pm 2^\circ\text{C}$, showed good repeatability and selectivity in the presence of HNO_3 , KOH , CuCl_2 , carbamide, benzene, p-cresol, p-nitrophenol, 3-chlorophenol and 2,3-dichlorophenol.

An un-jacketed coiled POF dip coated with a fluorescent indicator (MEH-PPV, poly(2-methoxy-(2'-ethylhexloxy)-p-phenylene-vinylene)) was applied to the selective detection of TNT (2,4,6-Trinitrotoluene, a nitro aromatic explosive). Measuring setup comprised an LED centred at 470 nm and a photodiode with a sensitivity of 5 ng/ml (Chu and Yang, 2012). The binding of TNT caused irreversible quenching which can be a drawback of this sensor. At the same time, the irreversible change in colour can also allow for direct on/off detection of TNT in daylight and ambient conditions. The selectivity was verified in the presence of methanol, ethanol and chloroform (CHCl_3), which showed small interference.

A fluorescent dip-probe POF sensor based in an extrinsic reflection configuration was developed by Riviera et al. for the selective monitoring of lead ions (Pb^{2+}). The surface of the dip-

probe sensor was coated with a lead-selective plasticized PVC (polyvinyl chloride) membrane with commercial and synthesized ionophores. Sensor showed reversible response with a low detection limit (LOD) of 7×10^{-6} M (Rivera *et al.*, 2009).

Azkune *et al.* reported in 2018 a U-bent POF sensor with PMMA core functionalized with phenylboronic acid with Alizarin Red S for the selective detection of glucose by absorption variation at a specific wavelength using a transmission based configuration. Sensor displayed glucose response at different pHs showing potential for future development of low-cost glucose sensors. Nevertheless, sensitivity, resolution, LOD and response time of the sensor were not reported. The POF functionalization is a time-consuming process as at least three days were necessary for the development of the active surface. (Azkune *et al.*, 2018)

Several microstructured POF (mPOF) gas sensors with selective layers formed inside the holes were reported in the literature. Li and Wang reported mPOF sensors using Rhodamine 6G (Rh 6G) as a receptor for the detection of hydrogen peroxide and nitrites in acidic environment by fluorescence quenching (Li and Wang, 2010b)(Li and Wang, 2010a). Sensor for hydrogen peroxide (H_2O_2) detection used Rh 6G-doped titanium dioxide (TiO_2) gel film as a sensitive layer. Sensor displayed linear response between 1.6×10^{-7} mol/L to 9.6×10^{-5} mol/L in sulphuric acid solution of potassium iodide (KI) (Li and Wang, 2010b). Sensor for detection of nitrites (NO_2^-) was prepared using Rh 6G-doped cellulose acetate (CA) as a sensitive layer. This sensor displayed linear response for nitrite concentrations between 2.0×10^{-4} g/mL and 5.0×10^{-3} g/mL in the presence of sulphuric acid. Developed sensors were applied to the determination of H_2O_2 and NO_2^- in rain water and milk powder samples, respectively.

A carbon dioxide (CO_2) sensor was developed using a home-made 547-hole mPOF preform with a CO_2 -sensitive film, porous ethyl cellulose doped with phenol red, deposited on the surface. No changes in the light intensity were observed in the presence of NO_2 , N_2O_3 , CO, O_2 and Hg, although some acid gases such as HCl, SO_3 and SO_2 revealed to be interferents as they also react with the indicator (Wang and Wang, 2010).

An oxygen-selective optrode was fabricated by Yang *et al.* by immobilizing fluorophore ruthenium (II) dichloride on the inner walls of a mPOF using a sol-gel method. The sensor's response was reversible and reproducible, with a sensitivity of 10.8 (I_0/I_{100}) and response time of 50 ms.(Yang *et al.*, 2011)

An mPOF sensor for ammonia gas detection was developed by Peng *et al.* by modifying side-walls of mPOF holes by an eosin-doped cellulose acetate (CA) film with thickness of 150 nm. The detection was based on the fluorescence quenching with a linear response between 50 ppm and 400 ppm and a response time of 500 ms. (Peng *et al.*, 2011)

While numerous POF sensors have been described in the literature, their selectivity is rarely reported. Some sensors are known to be non-selective and their application is limited to specific well-defined samples. Few examples of non-selective will be given bellow.

Nagata *et al.* reported the detection of 1% methanol vapour using POF with a higher RI cladding polymer, which swelled in the presence of alcohol resulting in the decrease of the cladding RI to values lower than the core RI and consequent enhancement of the power output (Nagata *et al.*, 2007). The same principle of operation was applied by Fujii *et al.* for the detection of toluene dispersed in water. Detection of less than 1 wt% toluene in water with fast response time of ~ 1 s,

as well as the detection of pure toluene for amounts lower than 1 ml was demonstrated (Fujii *et al.*, 2007).

An unclad POF dip coated with sol-gel thin films with thickness of 20–22 nm was applied to the sensing of aerosol composition based on evanescent wave absorption. Two types of coatings, tetraethylorthosilane (TEOS) and TEOS doped with thymol blue (TB), were investigated for detection of black (elemental) carbon (BC) and ammonium sulphate ((NH₄)₂SO₄) aerosols. Measuring setup comprised different light sources (UV (340 nm), blue (440 nm), red (660 nm), and infrared (940 nm)) and a photodiode detector. This work demonstrated successful proof-of-concept of low-cost sensors for aerosol detection, however proposed sensors lacked sensitivity necessary for practical applications, thus, requiring further development. (Kulkarni *et al.*, 2010)

An POF with graphene layer deposited on the end face was applied to the detection of acetone vapour (44–352 ppm) in dehydrated air (Zhang *et al.*, 2011). The variation of the reflected light due to acetone adsorption on the graphene layer was related to the concentration of acetone. The same principle was applied to the fabrication of POF sensors for the detection of volatile organic compounds (VOCs) (Some *et al.*, 2013). Hydrophilic graphene oxide (GO) and hydrophobic reduced graphene oxide (rGO) were deposited on the POF end face, allowing to distinguish between tetrahydrofuran (THF) and dichloromethane.

A U-bent POF coated with a graphene oxide (GO) film was used for the sensing of organic solvents, methanol, ethanol and isopropyl alcohol. The U-bent POF was cladded by chemical etching using ethyl acetate, aminated and coated with GO by dip coating technique, see Figure 2.30:

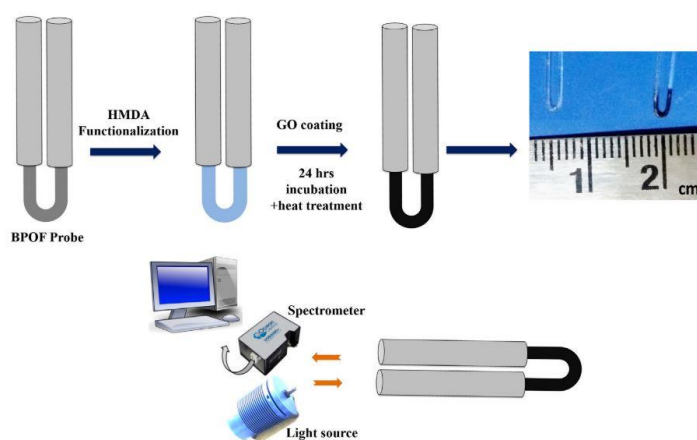


Figure 2.30 Schematic representation – preparation of the GO U-bent POF probe, optical setup and photographic image before and after the GO coating (Divagar *et al.*, 2018).

The sensitivity to organic solvents was evaluated by absorbance monitoring at 845 nm in real time. Modification with GO led to an increase of the RI sensitivity due to the ability of alcohols to effectively intercalate the GO layers increasing the layer refractive index. The sensitivity of the GO-POF probe to RI variation was not constant, depending on the alcohol and volume ratio. (Divagar *et al.*, 2018) This GO-POF probe lack of specificity as other organic compounds besides alcohols can interact with it, nevertheless this sensor can be used for the detection of organic solvents in a known matrix.

2.6.4 POF-MIP based sensing

POF-MIP sensors can be based on intensity modulation if the MIP is directly deposited on the POF's surface (POF-MIP sensors) and the variation of light transmission, absorption or fluorescence can be monitored at a specific wavelength. When the MIP is deposited over a metallic layer (POF-SPR-MIP) or with incorporated metal nanoparticles (POF-LSPR-MIP), the sensors characterization is usually wavelength-based.

Only few works reported optical fibre based MIP sensors (Tiwari and Uzun, 2017). The state of the art of POF-MIP based sensors is described below, mainly focusing on intensity based and wavelength-based configurations making use of surface plasmons.

POF-MIP sensors – intensity based sensing

Disposable evanescent wave POF sensors for the detection of the mycotoxin citrinin and the herbicide 2,4-dichlorophenoxyacetic acid (2,4-D) were developed by Ton et al. in 2015. MIP containing a fluorescent monomer (FIM) was deposited on a 4 cm polystyrene fibre. FIM was excited by the evanescent wave and the fluorescence intensity was proportional to the analyte concentration. The sensors showed LODs in the low nM range and exhibited high selectivity (Ton et al., 2015).

POF sensor coated with an MIP imprinted with the textile dye basic red 9 (BR9) was reported by Foguel et al. MIP was immobilized on the sensor surface by dip-coating the fibre in the suspension of polymer particles in polyvinyl alcohol (PVA). Detection was based on measuring characteristic absorption of BR9 at 545 nm, which increased upon binding between the analyte and the MIP. The detection in the range of the μM makes this sensor a very promising solution for the detection of this dye in the effluents. (Foguel *et al.*, 2015)

Cennamo et al. reported an POF-MIP sensor for the selective detection of dibenzyl disulphide (DBDS) in transformer oil, which is responsible for the oil corrosive properties. The sensor was based on two POFs optically coupled by drop coating with MIP in a trench milled between the two fibres. The variation on the MIP refractive index due to the binding of the DBDS was detected as a variation of the relative output signal, i.e. ratio between the transmitted signal of the two fibres. The sensor response was analysed at three wavelengths, 600 nm, 733 nm and 752 nm. Saturation of the signal was reached at a concentration of about 0.5 ppm (2×10^{-6} mol/L) and the LOD was about 0.013 ppm (5.3×10^{-8} mol/L) at 752 nm, at which the highest sensitivity at low concentrations was observed (N. Cennamo *et al.*, 2017). A halogen lamp and a spectrometer were used for the optical interrogation, while the substitution for an LED and a photodetector is aimed for industrial applications to decrease the cost of the detection system.

SPR-POF-MIP sensors – wavelength based sensing

Several works reported development of POF chemical sensors based on MIPs deposited on a metal surface that covers the sensing region of POFs. Making use of surface plasmon resonance (SPR) and a wavelength-based optical configuration such SPR-POF-MIP sensors usually show high sensitivity and low resolution values. However, expensive optical setup comprising white light source and a spectrometer is required for the measurements.

SPR-POF-MIP sensors are fabricated by the deposition of an MIP on a D-shaped POF with 1 cm length, which is previously covered with Microposit S1813 photoresist and a metal layer. The MIP is usually deposited by spin coating of the pre-polymeric mixture, followed by thermal polymerization, after which the template is extracted. In 2013, Cennamo *et al.* reported the detection and quantification of trinitrotoluene (TNT) in aqueous solutions with a sensitivity of 2.7×10^4 nm/M (N. Cennamo *et al.*, 2013). In 2014, the detection of L-nicotine was reported using a tapered D-shaped POF with taper ratio of 1.8, which displayed sensitivity of 1.3×10^4 nm/M (Cennamo *et al.*, 2014). In 2015, the detection of furfural (2-FAL) in the transformer oil was reported using SPR-POF-MIP platform. Sensor performance was tested in real oil samples collected from two ex-service current transformers (Nunzio Cennamo, De Maria, *et al.*, 2015). Simultaneous detection of DBDS and 2-FAL using two D-shaped POF sensors coated with respective MIPs over a Microposit S1813 photoresist and a thin gold layer was reported (Cennamo *et al.*, 2016). In 2017, Pesavento *et al.* presented two cascaded D-shaped sensors varying the thickness of the gold layer also for the simultaneous detection of DBDS and 2-FAL in power transformer oil (Pesavento *et al.*, 2017). In this case, the sensors were placed in-line, using the same POF platform with two D-shaped sensing regions. The sensors were characterized separately and simultaneously using a mineral oil for electrical transformer with and without analytes. Measurements at different resonance wavelengths, around 580 nm and 760 nm, allowed to detect both compounds simultaneously using one spectrometer. In 2018, a sensor for the detection of perfluorooctanoate (PFOA/PFO⁻) in water with a LOD of 0.13 ppb was reported (Nunzio Cennamo, D'Agostino, *et al.*, 2018). The sensor was characterized in individual aqueous solutions of PFOA as well as in a mixture of perfluorinated alkylated substances (PFASs), a certified reference material containing 11 different PFASs (C4–C11). The non-specific binding between the sensing layer and the analyte was evaluated using the non-imprinted polymer (NIP), prepared in the same way as the MIP without the target analyte.

Zeni *et al.* reported in 2018 the development of a slab waveguide (PMMA removable chip) coated with a gold layer and an MIP for the detection of 2-FAL in aqueous medium, using two POFs connected to the light source and spectrometer (Zeni *et al.*, 2018). Proposed sensor design had several advantages compared to a D-shaped-POF-SPR sensor with the same MIP, such as higher reproducibility between sensors can be achieved due to the better control of the thickness and roughness of the PMMA slab, lower number of steps required for the sensor preparation, and easy replacement of the chip (Zeni *et al.*, 2018). In the same year, Cennamo *et al.* reported a similar extrinsic POF sensor configuration, based on a PET (polyethylene terephthalate) substrate with a pattern of silver nanoparticles, printed by InkJet technology, and covered with an MIP for the detection of 2-FAL (Nunzio Cennamo, Zeni, Andò, *et al.*, 2018).

POF-MIP-LSPR sensors – wavelength based sensing

An POF-LSPR-MIP sensor based on MIP with incorporated metal nanoparticles, five-branched gold nanostars (GNS) was reported by Cennamo *et al.* in 2015. Sensor was used for the detection of 2,4,6-trinitrotoluene (TNT), a nitro-aromatic explosive. Pre-polymeric mixture containing the gold nanoparticles was deposited on the surface of the tapered and un-tapered D-shaped POFs (1 cm length) by spin coating and submitted to the thermal polymerization, see Figure 2.31.

Incorporation of nanoparticles in the MIP layer resulted in higher sensitivity compared to the SPR configuration with gold layer beneath MIP (reported in (N. Cennamo *et al.*, 2013)). Further improvement of sensitivity was achieved using a tapered D-shaped POF with LSPR configuration. (N. Cennamo *et al.*, 2015)

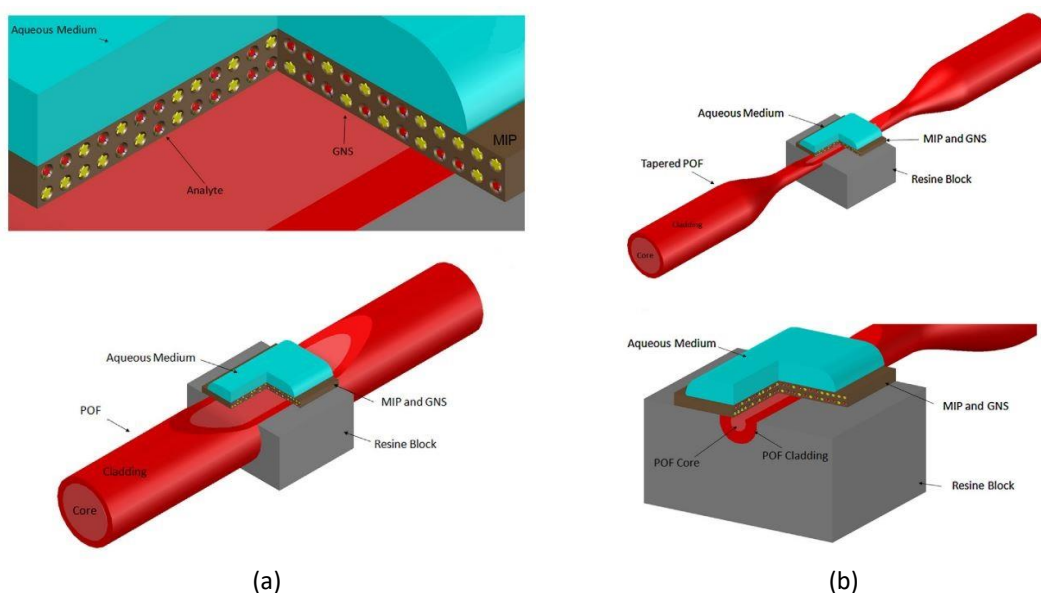


Figure 2.31 Schematic representation – MIP with incorporated gold nanostars (GNS) deposited on a D-shaped POF for the detection of 2,4,6-trinitrotoluene (TNT) in aqueous medium: (a) D-shaped POF; (b) tapered D-shaped POF. (N. Cennamo *et al.*, 2015)

2.6.5 POF biosensing

Biosensors rely on biological recognition elements that interact with the analytes (Wandemur *et al.*, 2014). Several optical fibre based biosensors have been described in the literature (Emiliyanov *et al.*, 2013).

The detection of glucose in aqueous solutions under harsh fermentation conditions was reported by Scully *et al.* Inorganic-organic coatings with oxygen sensitive ruthenium complexes (fluorophore) together with glucose oxidase (enzyme) were deposited on the unclad POF. As glucose is converted to gluconic acid by glucose oxidase, consumed oxygen is responsible for fluorescence quenching of the ruthenium complex. The sensor with the double-layer coating measured glucose in water over a range of 0.3–1.5 mmol/L. (Scully *et al.*, 2007)

In 2011, Beres *et al.* reported the development of a U-bent tapered POF biosensor for cell detection in aqueous medium. Tapered POF sensors were manufactured in U-bent and straight configurations with the waist diameter optimized for increased sensitivity to refractive index (between 0.40 mm and 0.50 mm). The sensor with the best performance, a U-bent tapered POF, was functionalized by three antibodies: anti-*E. coli*, anti-*Candida guilliermondii* and anti-erythrocytes. Sensor displayed different response in a saline solution containing 10^8 cells/mL of *E. coli*, *C. guilliermondii* and lamb erythrocytes. The sensor was only tested once in each cell solution, so no data on the repeatability of the sensor response was provided. The signal was not self-

referenced, which may lead to signal variations due to source fluctuations. The cells attachment to the POF sensor was confirmed by scanning electron microscopy (SEM). (Beres *et al.*, 2011)

In 2014, Wandermur *et al.* also presented U-bent POF sensors in three configurations, plain, unclad and tapered, capable to detect and monitor E-coli in less than 10 min. An intensity based low cost sensing system comprising an LED (880 nm) and a photodetector was used. Sensitivity of the U-bent POF RI sensors was evaluated in sucrose solutions using five fibres of each type (plain, unclad and tapered). The U-bent plain POF (MM SI) was functionalized with anti- E. coli antibody and tested in saline and saline bacterial suspensions with concentrations of 10^4 , 10^6 , and 10^8 colony forming units/ml (CFU/ml). (Wandemur *et al.*, 2014)

In 2018, Lopes *et al.* reported the development of a U-bent POF sensor (25 mm length and 9 mm bend diameter) for the detection of sulphate-reducing bacteria (SRB). Pieces of POF with 10 cm length were cut, their tips were polished and the sensing region was permanently bended, de-cladded and functionalized with anti-SRB antibody. The sensors were characterized with respect to the refractive index variation and tested in SBR suspensions with concentrations of 10^4 , 10^6 and 10^8 MPN/mL (most probably number per mL). The measuring setup consisted of a low-cost intensity based configuration with a self-referenced signal, comprising two LED's (880 nm) and two photodetectors connected to an Arduino Uno microcontroller. The U-bent POF sensors showed a sensitivity of around 6.1 au.RIU^{-1} with maximum uncertainty of 10.7×10^{-3} RIU. The immobilization of SRB antibodies was confirmed by the selective dye Alexa Fluor® 488. A saturation of the sensor's response was not observed after 40 min, and recovery and repeatability of the sensor response were not addressed. Authors refer the intention to improve the reproducibility on the sensor response. (Lopes *et al.*, 2018)

Emiliyanov *et al.* reported in 2013 the proof-of-concept of a mPOF biosensor for multi antibody detection based on fluorescence sensing. Sensitive layer fabrication included the following steps: AQ-Linker solution was flushed through the holes of the mPOF, made of TOPAS cyclic olefin copolymer, after which portion of the fibre was activated using UV light and antigen was immobilized. Then activation was repeated in another section of the fibre and the second antigen was immobilized. Two antigens, α -streptavidin and α -CRP labelled with fluorophores Cy3 and Cy5, respectively, were used. Fluorescent markers allowed simultaneous detection of both antibodies as they possess different maximum absorption and emission wavelengths, namely Cy3 at 550 nm and 570 nm, and Cy5 at 649 nm and 670 nm. The sensing setup comprised a 532 nm laser, which illuminated the mPOF from the side and a spectrum analyser connected to the fibre end. The emission wavelength from the first fluorophore (laser wavelength close the absorption line of the Cy3) allowed the excitation and emission of the second fluorophore (Cy5) validating the experimental setup. (Emiliyanov *et al.*, 2013)

2.7 Conclusions

POFs are promising transducers for sensors development and numerous POF sensors have been reported in the literature.

A variety of techniques can be used for the manipulation of POFs, allowing to change physical (diameter, waist, bending, shape, etching, polishing, tapering) and chemical properties of the waveguide (doping, surface immobilization and functionalization, etc.).

Several sensing techniques can be used. While wavelength or interference based techniques allow for better sensitivity and resolution, they require use of more expensive instruments restricting sensor applications to the laboratory facilities. On the other hand, portable low-cost sensing systems based on intensity based interrogation are experiencing a great development, although there is still the need to improve their performances (optimization orientated) and reproducibility.

POF based chemical sensors are still not as common as glass fibre chemical sensors, especially in intensity based sensing schemes, which may be explained by the variety of existing polymer fibres with differing characteristics such as water absorption which may directly influence sensor performance.

The work focused on intensity based detection schemes using simple and cheap procedures for POF's modification and functionalization aiming to develop low-cost POF chemical sensors. We hope to open the way for new sensing configurations, which would allow low-cost sensing of contaminants in water. Molecularly imprinted polymers were chosen as sensing material as they allow for selective detection with high reliability and fast response time.

Chapter 3 Preliminary study of POF-MIP based sensors

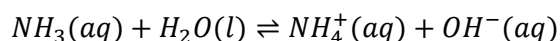
3.1 Introduction

These studies focused on the detection of ammonium ion in aqueous solutions using POFs combined with a molecular imprinted polymer (MIP) as sensitive layer.

Increased ammonium (NH_4^+) levels can promote eutrophication of the waterbodies making it a relevant compound for the evaluation of surface water quality. The monitoring of surface water status is of fundamental importance, since its chemical pollution presents a threat to human health and to the aquatic environment, however, the monitoring of relevant parameters is constrained by the availability and cost of commercial sensors.

Turbidity, pH and ammonia (NH_3) are important water quality indicators. Although ammonia is not toxic at concentrations generally found in water, its presence in raw water often indicates that the water is contaminated by sewage, by leaching from waste-disposal sites or by animal waste from agricultural activities (Thompson *et al.*, 2012)(Kurilić *et al.*, 2015). Natural levels of ammonia in ground waters are usually below 0.2 mgL^{-1} and, in drinking water the maximum ammonia concentration of 1.5 mgL^{-1} is recommended by the World Health Organization (WHO) to avoid changes of taste and odour of water (Tilaki and Kahe, 2012).

In aqueous solutions, ammonia exists in equilibrium with ammonium ion and hydroxide ion:



This equilibrium is pH dependent and an increase of pH will cause an increase of ammonia concentration. At the neutral pH, this equilibrium lies to the right, meaning the vast majority of nitrogen exists in the ammonium ion rather than the ammonia form.

Very few reports of optical sensors for detection of dissolved ammonia or ammonium ion can be found in the literature. Deng *et al.* presented a low-cost and portable optical sensor for the detection of dissolved ammonia up to 5 ppm. Sensor consisted of a two-layer structure comprising eosin, pH sensitive fluorescence dye, and a gas-permeable protection layer immobilized on glass microscope slides. (Deng *et al.*, 2016)

Fabrication of a POF based evanescent sensor for the detection of dissolved ammonia was reported, although the sensing of ammonia takes place in the vapour state (Jalal, Yu and Nnanna, 2012). The methods for sensor fabrication and ammonia detection were registered as a patent (Nnanna and Jalal, 2012). The sensor includes a sensing layer based on oxazine 170 perchlorate and a gas permeable membrane layer, allowing detection of ammonia with short response time ($\leq 10 \text{ s}$) with a LOD of 1.4 ppm, high sensitivity and reversibility over 99% (Jalal, Yu and Nnanna, 2012).

Khalaf *et al.* reported development of a highly sensitive side-polished POF coated with graphene/polyaniline nanocomposite for ammonia gas sensing at room temperature. Measurements of absorbance allowed to characterized the sensor and a sensitivity of 132.8 a.u./%

was obtained, with response and recovery times of 112 s and 185 s, respectively. (Khalaf *et al.*, 2017)

Most of works reported in the literature target ammonia detection in gaseous state, which is used to calculate equilibrium concentration of dissolved ammonia.

Several receptors or ionophores can be employed for the detection of ammonium ion such as nonactin (Späth *et al.*, 2010), or crown ethers (Späth *et al.*, 2010)(Lednev, Hester and Moore, 1997). Another approach, which was implemented in the present work, is synthesis of a polymer imprinted with ammonium.

In this work a molecularly imprinted polymer (MIP) was grafted on the surface of POFs as a sensitive layer for ammonium detection.

Preliminary studies (section 3.2) allowed to optimize the polymerization conditions and define the experimental procedures. Several difficulties were found with the development of the described studies. For that reason, the system design and procedures needed to be improved in order to overcome some difficulties observed (see section 3.2.5).

Further studies were performed using SI POFs with 1 mm (section 3.3.1). Several aspects were studied and evaluated, such as cladding removal, immobilization of the initiator on the surface of unclad POFs (section 3.4), NIP and MIP grafting on POFs surface (section 3.5) and stability of the unclad POFs by immersion in solvent (section 3.6).

POF-MIPs and modified POFs were optically characterized using a low-cost sensing optical setup based on intensity modulation (section 3.8) and sensors characterization can be found in section 3.9.

3.2 Preliminary studies⁴

Studies on the grafting of molecularly imprinted polymers (MIPs) on the surface of PMMA mPOFs was conducted targeting ammonium (NH_4^+) detection in water. Optimization of the surface grafting procedures, namely chemical reagents and solvents, their concentrations and polymerization time were carried out.

The POFs functionalization was done by surface grafting using thermal polymerization. Ammonium chloride (NH_4Cl) was used as template, methacrylic acid (MAA) and ethylene glycol dimethacrylate (EDMA) as functional and cross-linking monomers, respectively, mixture of ethanol/water (20/80%) as the solvent and 2,2'-Azobis(2-methylpropionamidine) dihydrochloride as an initiator. The polymerization conditions were studied for the non-imprinted polymer (NIP), based on the uniformity of the grafted polymer, and subsequently for the MIP layer.

The functionalized mPOFs were characterized using an intensity based experimental setup comprising a white light source and a spectrometer in solutions of increasing concentration of the target analyte (NH_4^+).

A summary of the obtained results as well as major conclusions will be presented below.

⁴ (Lopes, 2014)(Lopes *et al.*, 2015)(Sequeira *et al.*, 2014)

3.2.1 Optical fibres

Microstructured PMMA POFs, single-mode (SM) fibres with 320 μm diameter (8 μm core diameter) and multimode (MM) fibres with 150 μm diameter (50 μm core diameter), both from Kiriama Pty Ltd, were selected. The selected portion of the fibres was cut using a heated razor (60 $^{\circ}\text{C}$) against a glass slide. Prior to use, the POF samples were washed with 2-propanol at room temperature and cleaned with optical paper.

3.2.2 Chemical reagents

The chemical reagents used in these studies were: methacrylic acid (MAA) (Aldrich, 99%, STBB0035L9), 2,2'-Azobis(2-methylpropionamide) dihydrochloride (AAPH) (Aldrich, 97%, 101268336), ethylene glycol dimethacrylate (EDMA) (Aldrich, 98%, 3589PJ080), sodium hydroxide (NaOH) (Panreac, 98%, 131687.1211), ammonium chloride (NH_4Cl) (Merck, pa, 8564623), ethanol ($\text{C}_2\text{H}_5\text{OH}$) (Merck, pa, 1.00983.2511), 2-propanol ($(\text{CH}_3)_2\text{CHOH}$) (Merck, pa, 1.09634.2511) and boric acid (H_3BO_3) (Mayer Baker, pa).

All chemicals were analytical grade and used in the same form as received without any further purification. Aqueous solutions were prepared using distilled water.

3.2.3 MIP and NIP preparation and grafting

3.2.3.1 Solvent

The solvent was chosen taking into account fibre stability and solubility of the polymerization mixture compounds. Two solvents, acetonitrile, ethanol and its mixtures with water, were evaluated. The solubility of the PMMA fibres was evaluated through the variation of mass after immersion in the solvents for several hours (5h and 24h) at room temperature. Fibres were found to be stable in the mixtures of ethanol/water (20/80 % and 50/50 %), in which some increase of mass was observed meaning that the solvent was absorbed by the fibres.

3.2.3.2 Initiator

The initiator was selected considering the stability of the fibres in the solvent at the polymerization temperature. For the polymerization process two initiators were studied: 4,4'-Azobis(4-cyanovaleric acid) (ACVA) and 2,2'-Azobis(2-methylpropionamide) dihydrochloride (AAPH), see Figure 3.1, with maximum rate decomposition temperatures of 70 $^{\circ}\text{C}$ and 57 $^{\circ}\text{C}$, respectively.



Figure 3.1 Chemical structure of (a) 4,4'-Azobis(4-cyanovaleric acid) (ACVA); (b) 2,2'-Azobis(2-methylpropionamide) dihydrochloride (AAPH).

The fibres were immersed for 2h in mixtures of ethanol/water at those temperatures. No modification of the fibres was observed at 57 °C in the mixture of ethanol/water 20/80 %, therefore AAPH was chosen as initiator.

3.2.3.3 Synthesis

Molecularly imprinted polymer (MIP) and the non-imprinted polymer (NIP) were synthesized by radical polymerization and surface grafting with pre-polymeric mixtures of different concentrations of monomer (MAA) and cross-linker (EDMA). The difference between the MIP and the NIP is the presence or not of the template analyte, respectively.

Initially, the polymerization process was carried out without the use of the template. The quality of the resulting polymer allowed to define to optimum conditions for the MIP synthesis. Table 3.1 shows concentrations of tested polymerization solutions.

Table 3.1. Composition of polymerization solutions used for NIP's and MIP's preparation. (Lopes, 2014)

| | Solution | [MAA] / mM | [EDMA] /mM | [NH ₄ ⁺] / mM | Ratio $\left(\frac{[EDMA]}{[MAA]}\right)$ |
|-------|----------|------------|------------|--------------------------------------|---|
| NIP's | A | 6.3 | 22.5 | -- | 3.6 |
| | B | 4.3 | 15.4 | -- | 3.6 |
| | C | 4.3 | 7.7 | -- | 1.8 |
| MIP's | B | 4.3 | 15.4 | 0.614 | 3.6 |
| | C | 4.3 | 7.7 | 0.614 | 1.8 |
| | D | 2.1 | 7.7 | 0.300 | 3.6 |

After the inspection of the side and cross-section view of fibres by optical microscopy (Olympus BX51 Microscope), the quality of the polymerized fibres was evaluated. More uniform layers were obtained with the following solutions: NIP_C, MIP_C and MIP_D.

3.2.3.4 Immobilization of the initiator

For the immobilization of the azo initiator AAPH on the surface of PMMA fibres, see Figure 3.2, the POF samples were incubated in 10 % AAPH (w/v) solution in 100 mM borate buffer with pH 11.5, for 2h. The modified POF samples were rinsed with distilled water and remained immersed in distilled water in an ultrasonic bath for 10 minutes, after which they were allowed to dry overnight at room temperature.

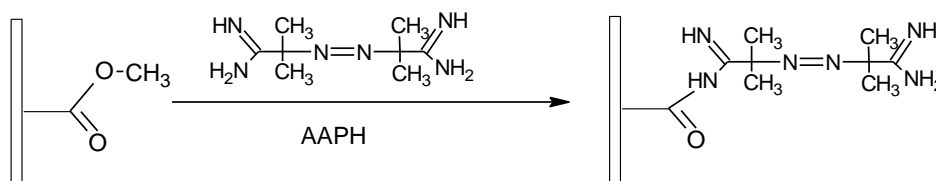


Figure 3.2 immobilization of AAPH on the PMMA. (Lopes, 2014)

3.2.3.5 MIP and NIP grafting

All reaction mixtures containing the functional monomer (MAA) and cross-linking monomer (EDMA), in the desired proportions, were prepared in a 20% ethanol aqueous solution and placed for 10 minutes in the ultrasonic bath. Polymerization was carried out in a reactor, containing the modified fibres and the polymerization solution, which was degassed with nitrogen for 15 minutes.

The reactor was transferred to a thermostated water bath (see Figure 3.3(b)), heated to 57°C, and polymerization was allowed to proceed for a predetermined time. See section 3.2.4. for more details.

After polymerization, the fibres were removed from the reactor, washed with distilled water and left to dry overnight at room temperature.

3.2.4 Optical characterization – mPOF-MIPs

3.2.4.1 Optical monitoring

The experimental setup is shown in Figure 3.3(a). The fibres were placed in a reactor (close up in Figure 3.3(b)) and connected to a Halogen light source (HL2000 from Ocean Optics, 400 – 1000 nm). The system was aligned through the injection and transmission of light through the modified fibres and connected to an Ocean Optics USB2000 spectrometer, the output of which is then displayed on a computer screen using SpectraSuite software.



Figure 3.3 (a) Experimental setup; (b) reactor with fibre inside the thermostated water bath.

Fibre transmission was measured in borate buffer and ethanol (20 v/v%)/water mixture with the MM fibres, and during the immobilization of the initiator and MIP/NIP grafting in real-time with both fibres (SM and MM). The obtained response was the integral of the normalized spectrum.

The characterization of MM polymerized fibres and one MM non-modified fibre using different concentrations of ammonium solutions was carried out in continuum.

3.2.4.2 Buffer solution vs initiator

Behaviour of the fibres differed in buffer and in the buffer solution of the initiator, see Figure 3.4.

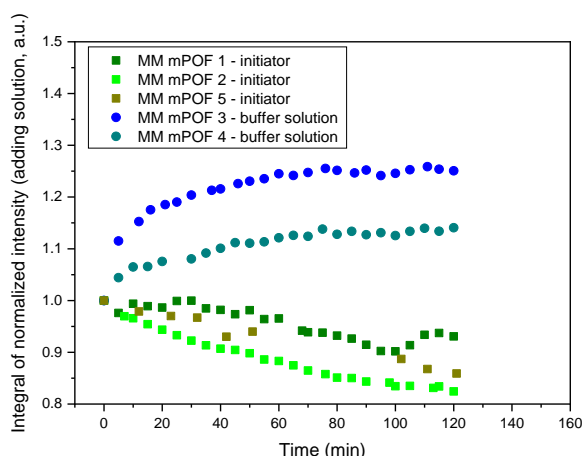


Figure 3.4 Integral of normalized intensity with time, normalized to the response when the initiator or buffer solutions were added to the reactor.

3.2.4.3 Solvent vs polymerization

The fibre transmission was monitored during polymerization and in ethanol (20 v/v%)/water mixture with the heating imitating polymerization conditions. Similar behaviour in relation with the time and temperature was observed in both cases, see Figure 3.5.

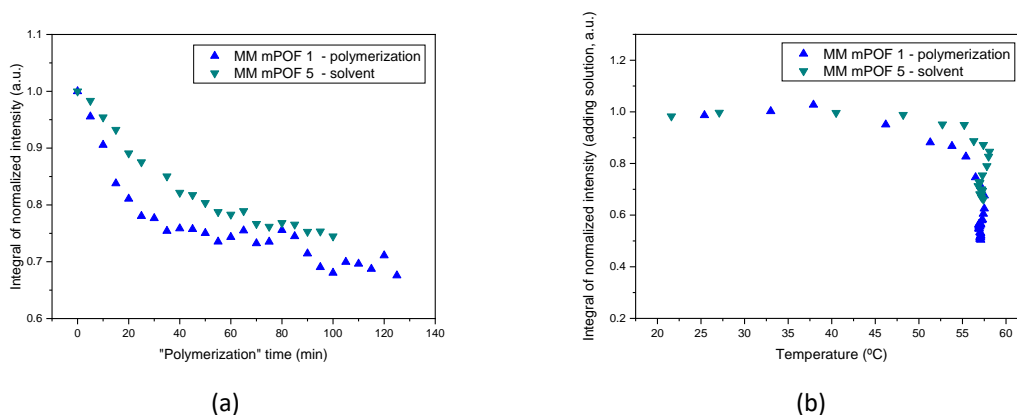


Figure 3.5 Integral of normalized intensity with (a) “polymerization” time, normalized to the response obtained when reaching ~56.5°C and (b) temperature, normalized to the response when the solution or solvent were added to the reactor.

3.2.4.4 Characterization with template solutions

Multimode polymerized fibres (with different polymerization times) were characterized with ammonium solutions of different concentrations: 0.001 M, 0.01 M, 0.09 M, and results were compared with the ones obtained for one unmodified fibre, see Figure 3.6.

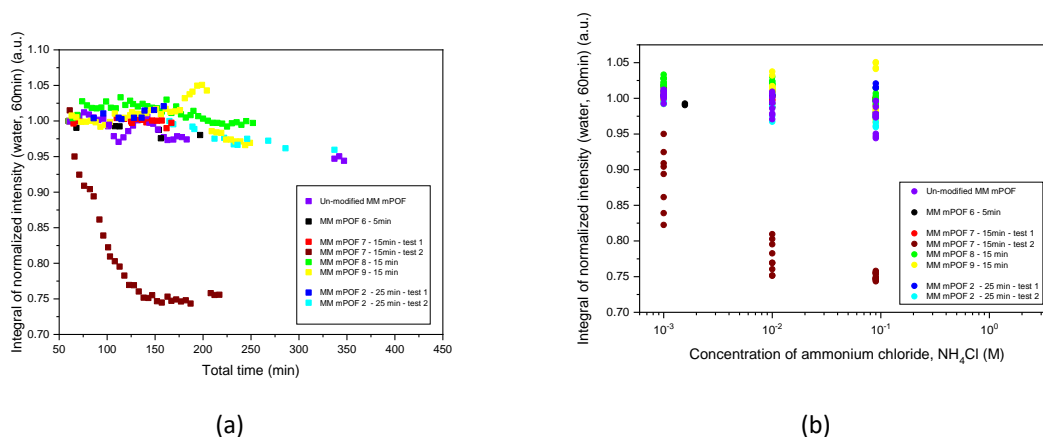


Figure 3.6 Characterization of polymerized MM fibres with ammonium solutions of different concentrations - integral of normalized intensity to water spectrum: (a) dependent on total time; (b) dependent on NH_4Cl concentration.

The obtained results showed a fluctuation of the signal output around $\pm 5\%$ for all MM polymerized fibres. Output intensity of MM fibre mPOF-7, polymerized for 15 min, decreased around 25%. This decrease in the transmitted light was continuous in time and did not depend on concentration. Nevertheless, a signal saturation seemed to occur between 0.01 M and 0.09 M.

3.2.5 Conclusions

Surface grafting was used for the POFs functionalization by thermal polymerization. MIP and NIP layers were covalently attached to the surface of mPOFs by surface grafting. Ammonium ion was used as a template for imprinting. More uniform layers of the imprinted polymer were obtained with solutions C and D as confirmed by optical microscopy.

Decrease in the transmitted light was observed for the functionalized fibre mPOF-7, polymerized in solution C for 15 min, in ammonium solutions. Other functionalized mPOFs did not respond to the variation of ammonium concentration.

During monitoring of the polymerization process, a similar behaviour was observed in ethanol (20 v/v%)/water mixture and during polymerization: a sharp decrease in the transmitted light after temperature reached $\sim 56.5^\circ\text{C}$. The modification with initiator also caused a decrease in the transmitted light through the mPOFs.

From this previous results several conclusions were taken:

- The system design and procedures needed to be improved in order to overcome some difficulties observed, namely the influence of the initiator solution and solvent on the light transmission capacity of POFs.
- These mPOF were not easy to handle and didn't allow high precision connectorization due to their small diameter. The alignment of the mPOFs with the light source and detector were performed in free space using a common index gel and micrometre screws (X,Y,Z), which could imply variation with time of the transmitted signal due to small misalignments.
- It was often to happen source fluctuations and small external variations.

New developments were performed in order to overcome these issues, namely the use of POFs with larger diameters (1 mm) that would allow easy and low-cost connectorization, and a reference branch was added to the experimental setup.

In addition, POFs should be sensitized to allow more interaction with the external medium/sensitive layer.

In the next sections the developments targeting POF chemical sensing using 1 mm SI POFs will be presented.

3.3 Materials and methods

3.3.1 Optical fibres

Initially two POFs were selected for these studies: a jacketed POF (J_x) from Mitsubishi Rayon CO. LTD. (GHCP4001, ESKATM) and an unjacketed POF (NJ_x) from Ahahi Kasei EMD Corporation. Both fibres have a total diameter around 1 mm, step-index profile, numerical aperture of 0.5, a (poly)methyl methacrylate core with a diameter around 980 μm and a refractive index of 1.49 (@650 nm) with a fluorinated polymer cladding. Jacketed (J_x) POFs also have a chlorinated polyethylene jacket with a total diameter of 2.2 mm. (Mitsubishi Chemical Co., 2000; Asahi Kasei, 2013)

Optimization of the polymerization conditions was performed by grafting of the non-imprinted polymer (NIP) on unclad POF samples using pre-polymeric mixtures of different concentrations. The inspection of the surface by optical microscopy and the evaluation of thickness variation allowed to optimize the polymerization conditions and select the POF to be used in further studies (see section 3.5.3).

The unjacketed POF (NJ_x) was selected for sensing development, the main characteristics are described in Table 2.2, Chapter 2.

Samples of POF were cut to the desired length (~4 cm or ~60 cm) using a commercial POF cutter (see Figure 2.11(a)). The POF sample end-faces were polished in a 'Figure ∞ ' pattern using polishing sheets from Thorlabs Inc. with different grain sizes: 5 μm , 3 μm , 1 μm and 0.3 μm (LFG5P, LFG3P, LFG1P, LFG03P, respectively), as described in section 2.3.3, Chapter 2.

3.3.2 Length of the sensing region

In order to increase the interaction of light travelling in the POF with the sensitive layer (MIP), the cladding was removed in the central region of the POF (sensing region) by chemical etching.

The maximum length of the POF sensing region, ~ 5 cm, was defined by size of the small glass reactors available in the laboratory (6.3 cm), see Figure 3.7. The smallest reactor (Figure 3.7 (a)) had a minimum volume of 3 mL and maximum of 5 mL and the biggest (Figure 3.7 (b)) a minimum volume of 7 mL and maximum of 10 mL.



Figure 3.7 Glass reactors used for POF's modification and functionalization.

Sultangazin et al. reported the experimental results (normalized intensity) obtained for two Ag-coated POF sensors for Hydrogen Sulphide (H_2S) detection, with 5.5 cm and 4.0 cm length of sensing region. According to the literature reports, higher length of sensing region is necessary to obtain higher sensitivity in the intensity based setups, although the sensitivity was also related with the quality of the sensing layer and the local quality of POF stripping (affecting the coating adhesion) (Sultangazin *et al.*, 2017).

3.3.3 Removal of the fluorinated cladding

In a selected portion of the fibre of ~ 5 cm length, the perfluorinated polymer cladding was removed by chemical etching using solutions of acetone and distilled water, adapted from (Merchant, Scully and Schmitt, 1999).

This process was optimized as the fibre needs to be gently handled to prevent it from breaking. Contact of the POF with pure acetone cannot last for longer than 10 seconds, otherwise POF breaks. It was suggested not to use pure acetone for more than 10 seconds or dilute the acetone in distilled water to prevent appearance of the micro-cracks on the fibre surface (Lopes *et al.*, 2018).

For cladding removal, the selected portion of the fibre was immersed in pure acetone during 5 seconds, followed by immersion in a solution of acetone and distilled water (50:50). At this point, the cladding starts to dissolve getting a milky aspect (see Figure 3.8(c)) and can be easily removed using lint free wipers (from Asahi Kasei, M-1). Finally the fibre was immersed in distilled water and cleaned with the lint free wipers, see Figure 3.8(d,e). This procedure was repeated several times until the portion of the fibre was considered clean, which was easily seen with the naked eye and possible to feel during the cleaning process, see Figure 3.8(f).

The unclad portion of the fibre (sensing region) was then washed thoroughly with distilled water and left to dry at room temperature.

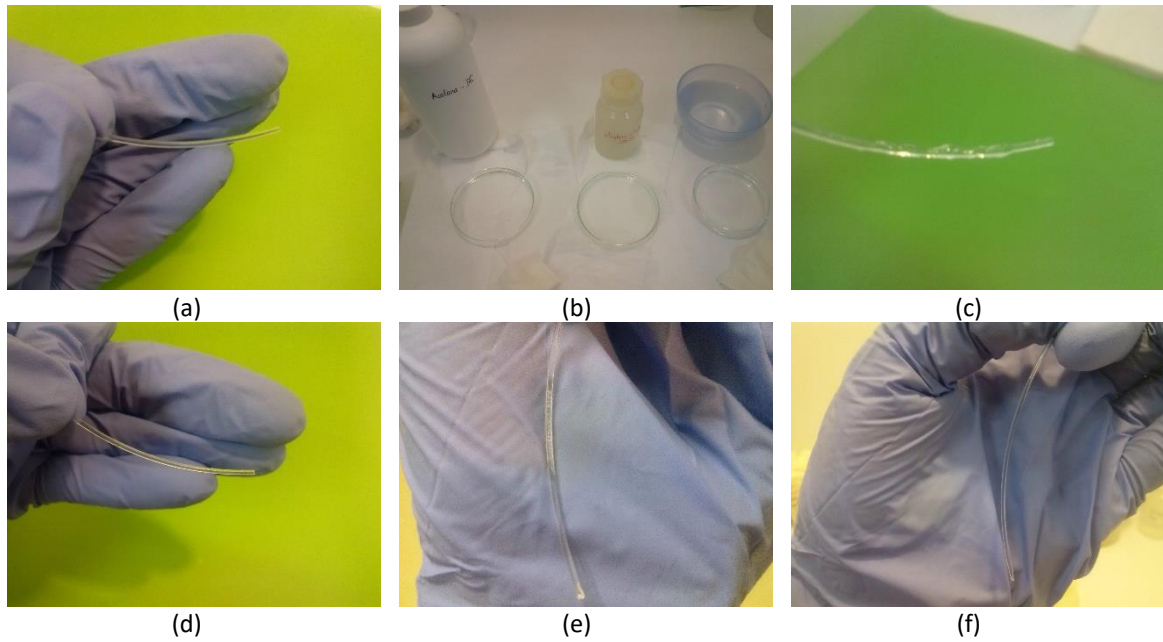


Figure 3.8 Procedures for cladding removal: (a) POF with cladding; (b) petri dishes and solutions of acetone and distilled water for POFs immersion; (c) cladding dissolution after immersion in acetone solutions - milky aspect; (d,e) intermediate states; (f) unclad POF.

A certain brittleness as well as micro-cracks on the surface were observed after the de-cladding process, see Figure 3.9 as example.

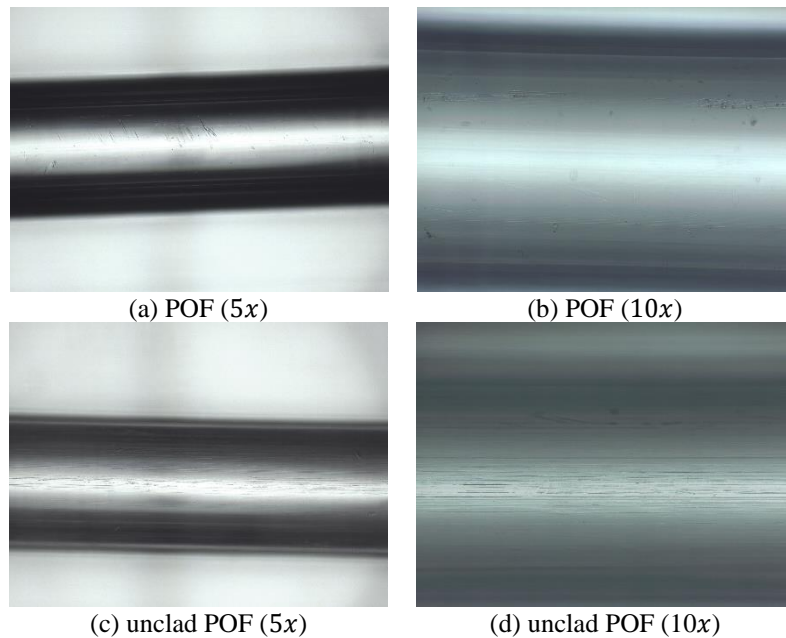


Figure 3.9 Images of optical microscopy before (a,b) and after (c,d) cladding removal (POF NJ3).

The interface between the clad and unclad regions is depicted in Figure 3.10 for the POF NJ9, where the transition between core and cladding is easily observed.

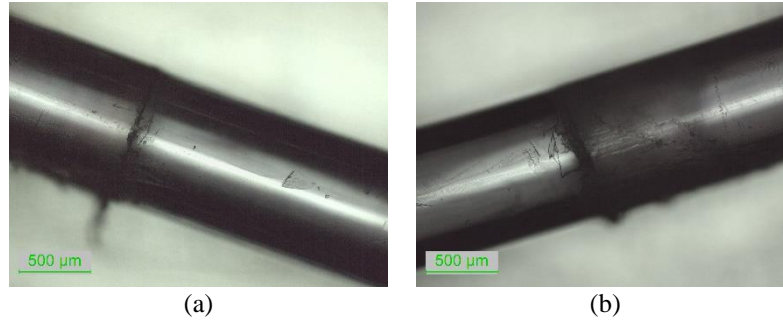


Figure 3.10 Images of optical microscopy (5x) of the interface between the claded and uncladed regions (POF NJ9).

3.3.4 Analyte solutions

3.3.4.1 Preparation of the analyte solutions

The prepared POF-MIP sensors were characterized with different solutions. First, solutions of ammonium chloride (NH_4Cl) were used for the characterization of POF-MIP sensors with the template analyte, NH_4^+ (see section 3.9.4). Cross-sensitivity was evaluated with solutions of sodium chloride (NaCl) and D-(+)-glucose (see section 3.9.5).

A solution of higher concentration of ammonium chloride was prepared with ultra-pure water by weighting the corresponding mass using the following equations:

$$c = \frac{n_{mol}}{V} \quad \text{Equation 3.1}$$

$$n_{mol} = \frac{m}{M} \quad \text{Equation 3.2}$$

where c is the concentration, n_{mol} the number of mol, m the mass and V the total volume of the solution. Solutions with lower concentration were prepared by dilution of the solution with higher concentration, using the following relation:

$$n_{mol_1} = n_{mol_2} \Leftrightarrow c_1 \cdot V_1 = c_2 \cdot V_2 \quad \text{Equation 3.3}$$

The refractive index of the prepared solutions was measured using a refractometer (Abbemat 200, Anton Paar) with a resolution of 10^{-4} RIU (n_D , 589 nm at 25 °C), see Table 3.2.

Solutions of sodium chloride and D-(+)-glucose were prepared to have the same refractive indices, to allow comparison between sensor responses, see Table 3.2.

Table 3.2. Prepared analyte solutions – concentration and refractive index (n_D , 25°C).

| Solution | Ammonium Chloride (NH ₄ Cl) | | D-(+)-Glucose (C ₆ H ₁₂ O ₆) | | Sodium Chloride (NaCl) | |
|----------|---|----------------|---|----------------|---------------------------|----------------|
| | [NH ₄ ⁺] (M) | $n(nD)$, 25°C | [D-(+)-Glucose] (M) | $n(nD)$, 25°C | [Na ⁺] (M) | $n(nD)$, 25°C |
| 1 | 0.00x10 ⁺⁰⁰ | 1.3325 | 0.00x10 ⁺⁰⁰ | 1.3325 | 0.00x10 ⁺⁰⁰ | 1.3325 |
| 2 | 1.01x10 ⁻⁰³ | 1.3325 | 1.03x10 ⁻⁰³ | 1.3326 | 4.21x10 ⁻⁰³ | 1.3325 |
| 3 | 1.02x10 ⁻⁰² | 1.3326 | 5.05x10 ⁻⁰³ | 1.3327 | 1.42x10 ⁻⁰² | 1.3327 |
| 4 | 1.00x10 ⁻⁰¹ | 1.3336 | 5.01x10 ⁻⁰² | 1.3338 | 9.97x10 ⁻⁰² | 1.3335 |
| 5 | 2.00x10 ⁻⁰¹ | 1.3346 | 7.52x10 ⁻⁰² | 1.3345 | 2.19x10 ⁻⁰¹ | 1.3347 |
| 6 | 4.00x10 ⁻⁰¹ | 1.3367 | 1.51x10 ⁻⁰¹ | 1.3364 | 4.27x10 ⁻⁰¹ | 1.3368 |
| 7 | 6.00x10 ⁻⁰¹ | 1.3387 | 2.51x10 ⁻⁰¹ | 1.3391 | 6.46x10 ⁻⁰¹ | 1.3389 |

POF-MIP sensors were also characterized with respect to the refractive index variation, between 1.33 – 1.41, using sucrose solutions of increasing refractive index. The sucrose solutions were prepared with ultra-pure water, through the dilution of a higher concentrated solution. The refractive index was measured using the Abbemat refractometer.

3.3.4.2 Characterization by UV-VIS spectroscopy

The analyte solutions, ammonium chloride, D-(+)-glucose and sodium chloride, were characterized by UV-VIS spectroscopy (EON microplate spectrophotometer, BioTek Instruments, USA).

Solutions with higher concentrations were also characterized by UV-VIS spectroscopy, see Table 3.3. UV-VIS characterization was performed using 300 μ L of each solution and the obtained spectra are depicted below (Figure 3.11).

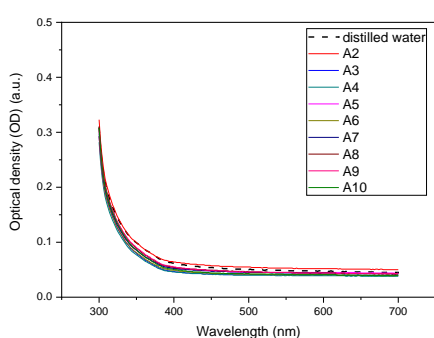
Sucrose solutions (1.33 – 1.45) were also analysed by UV-VIS spectroscopy. Concentration and refractive index of the prepared solutions can be found in Table 3.4.

Table 3.3. Concentration and refractive index of analyte solutions with higher concentration.

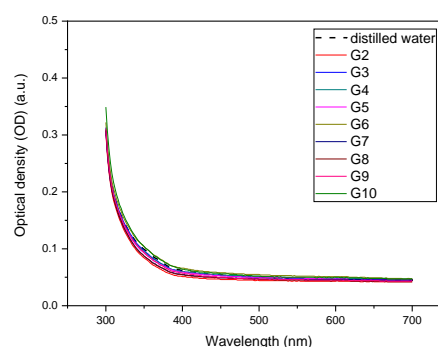
| Solution | Ammonium Chloride (NH ₄ Cl) | | D-(+)-Glucose (C ₆ H ₁₂ O ₆) | | Sodium Chloride (NaCl) | |
|----------|---|----------------|---|----------------|---------------------------|----------------|
| | [NH ₄ ⁺] (M) | $n(nD)$, 25°C | [D-(+)-Glucose] (M) | $n(nD)$, 25°C | [Na ⁺] (M) | $n(nD)$, 25°C |
| 8 | 0.10 | 1.3336 | 0.12 | 1.3357 | 0.50 | 1.3375 |
| 9 | 1.00 | 1.3427 | 0.25 | 1.3390 | 1.00 | 1.3423 |
| 10 | 2.50 | 1.3572 | 1.20 | 1.3629 | 3.00 | 1.3600 |

Table 3.4. Sucrose solutions – concentration and refractive index (n_D , 25°C).

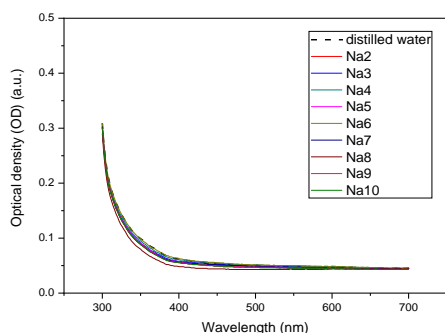
| Solution | [Sucrose] (M) | $n(n_D)$, 25°C | Solution | [Sucrose] (M) | $n(n_D)$, 25°C |
|----------|------------------------|-----------------|----------|------------------------|-----------------|
| 1 | $0.00 \times 10^{+00}$ | 1.3325 | 7 | 7.32×10^{-01} | 1.3678 |
| 2 | 2.89×10^{-02} | 1.3340 | 8 | 1.20 | 1.3905 |
| 3 | 5.88×10^{-02} | 1.3352 | 9 | 1.60 | 1.4005 |
| 4 | 8.86×10^{-02} | 1.3368 | 10 | 1.99 | 1.4202 |
| 5 | 1.19×10^{-01} | 1.3379 | 11 | 2.49 | 1.4518 |
| 6 | 3.67×10^{-01} | 1.3500 | | | |



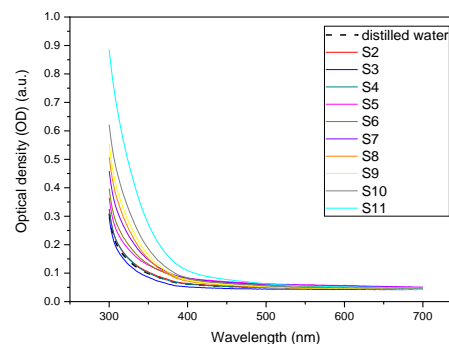
(a) ammonium chloride



(b) D-(+)-glucose



(c) sodium chloride



(d) sucrose

Figure 3.11 UV-VIS absorbance spectra: (a) ammonium chloride (A_x); (b) D-(+)-glucose (G_x); (c) sodium chloride (Na_x); (d) sucrose (S_x).

No absorbance occurs in any of the solutions between 600 – 700 nm in comparison with the spectra obtained for distilled water.

3.3.4.3 Refractive index (RI) characterization with temperature

3.3.4.3.1 Water RI with temperature

The refractive index (RI) of distilled water was measured using the *Abbat* refractometer for temperatures from 20°C to 40°C (*n_D*, 589 nm), see Figure 3.12.

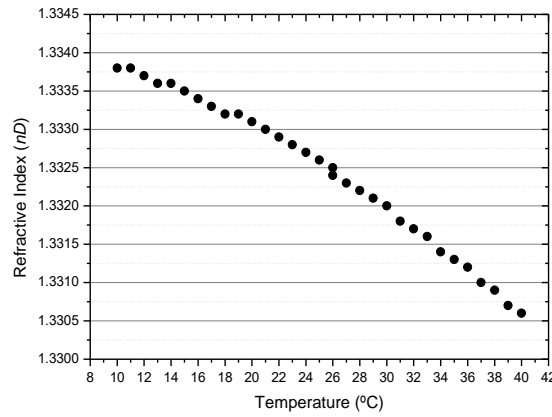


Figure 3.12 Refractive index of water with temperature, from 10°C to 40°C.

A 30 °C increase of the temperature, from 10°C to 40°C, leads to a decrease of refractive index of about 3.5×10^{-3} RIU. A linear fit was applied to the RI values in the range of temperature between 20°C and 30°C and a slope of -1.14×10^{-4} RIU/°C was obtained, see Figure 3.13. This means that a variation of temperature of 2 °C will result in a refractive index variation of 2.3×10^{-4} RIU.

$$\Delta RI = m \cdot \Delta T = 1.14 \times 10^{-4} \times 2.0 = 2.3 \times 10^{-4} \text{ RIU}$$

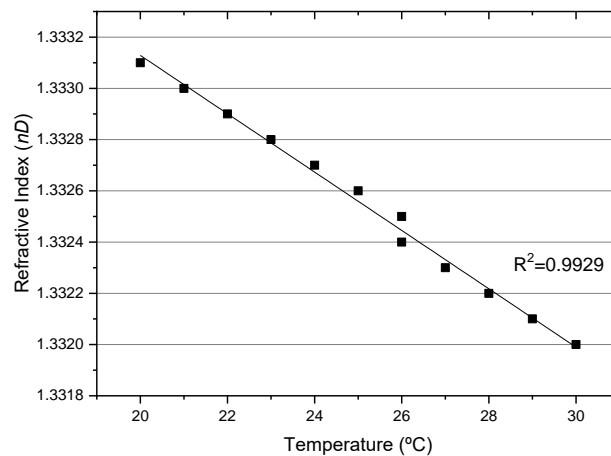


Figure 3.13 Refractive index of distilled water with temperature, between 20°C and 30°C, and linear fit applied.

If the temperature for the measurement of the refractive index in the refractometer is considered to be 25°C, the absolute measurement error should be less or equal to 6×10^{-4} RIU in

the temperature range between 18°C and 30°C (Figure 3.14), temperatures that are hardly reached in the laboratories.

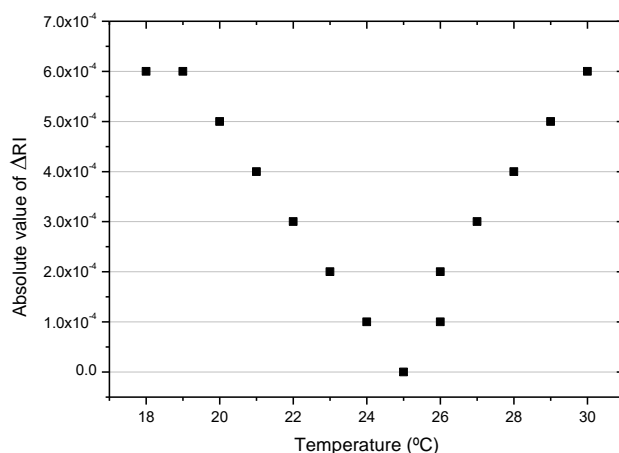


Figure 3.14 Absolute value of refractive index variation (ΔRI , between the real value and the value obtained at 25°C) with temperature varying from 18°C to 30°C.

This variation can be important, depending on the resolution of the optical acquisition system and also on the temperature variation during the sensor's characterizations.

3.3.4.3.2 Analyte solution's RI with temperature

Aqueous solutions of NH_4Cl , NaCl , D-(+)-glucose and sucrose were used for the characterization of modified POFs and POF-MIP sensors. Refractive index range in these solutions is between 1.33 and 1.41 RIU for sucrose and between 1.33 and 1.34 RIU for the remaining solutions.

The characterization of the sensors was analysed through the obtained values for the normalized output signal (to water), see section 3.8. In this case, the variation of refractive index is transduced by the POF and given by the variation of the normalized signal obtained.

The refractive index of each solution was measured at different temperatures using the *Abbemat* refractometer (1×10^{-4} RIU resolution) and the results are depicted in Figure 3.15.

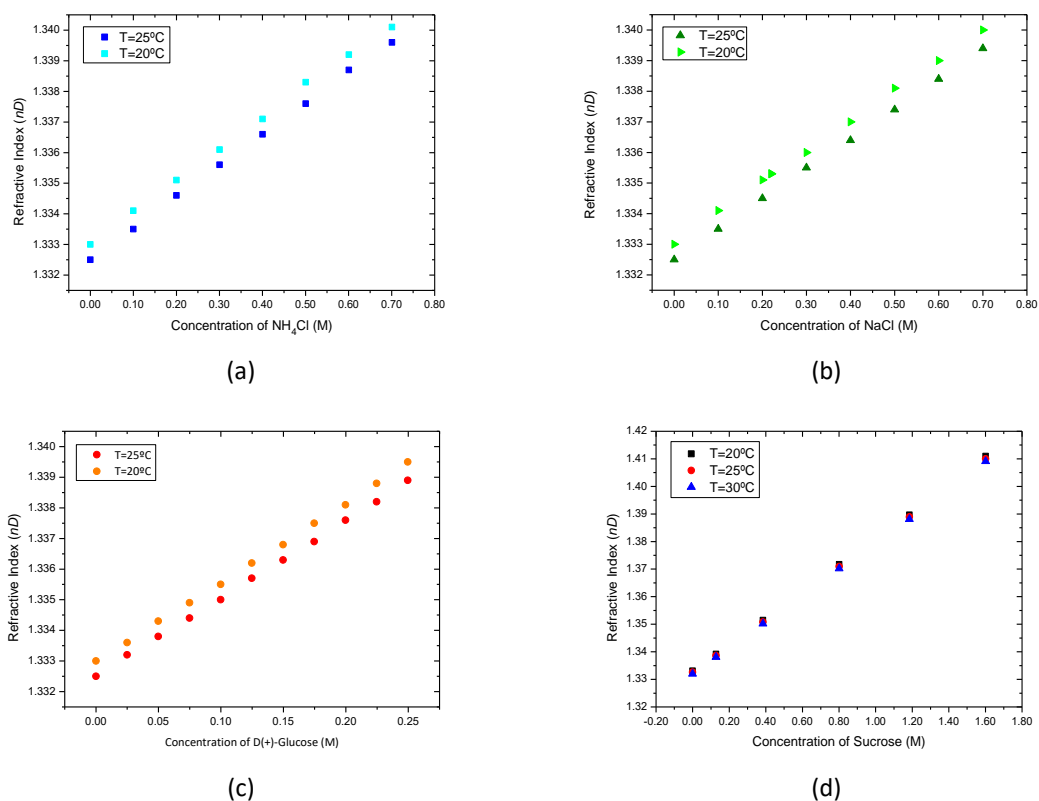


Figure 3.15 Dependence of refractive index with concentration for (a) ammonium chloride, (b) sodium chloride, (c) D(+)-glucose and (d) sucrose.

According to the obtained results, the variation of refractive index due to the variation of concentration did not depend on the temperature in the range from 20 °C to 30 °C. Parameters of the linear fit applied to the obtained results, for each temperature are shown in the Table 3.5.

Table 3.5. Linear fit obtained parameters – variation of the refractive index with concentration for ammonium chloride (NH₄Cl), sodium chloride (NaCl), D-(+)-glucose and sucrose, for different temperatures.

| | T (°C) | Intercept | SE | Slope | SE | Adj. R-square | Residual sum of squares |
|--------------------|--------|-----------|----|-----------------------|----------------------|---------------|-------------------------|
| NH ₄ Cl | 20 | 1.3330 | -- | 1.03x10 ⁻² | 3.6x10 ⁻⁵ | 1 | 5.05x10 ⁻⁸ |
| | 25 | 1.3325 | -- | 1.02x10 ⁻² | 2.4x10 ⁻⁵ | 1 | 2.20x10 ⁻⁸ |
| NaCl | 20 | 1.3330 | -- | 9.67x10 ⁻³ | 7.5x10 ⁻⁵ | 1 | 4.84x10 ⁻⁷ |
| | 25 | 1.3325 | -- | 9.55x10 ⁻³ | 6.3x10 ⁻⁵ | 1 | 3.46x10 ⁻⁷ |
| D-(+)-Glucose | 20 | 1.3330 | -- | 2.57x10 ⁻² | 8.8x10 ⁻⁵ | 1 | 1.85x10 ⁻⁸ |
| | 25 | 1.3325 | -- | 2.55x10 ⁻² | 7.2x10 ⁻⁵ | 1 | 1.24x10 ⁻⁸ |
| Sucrose | 20 | 1.3331 | -- | 4.83x10 ⁻² | 1.8x10 ⁻⁴ | 1 | 7.55x10 ⁻⁷ |
| | 25 | 1.3326 | -- | 4.80x10 ⁻² | 1.7x10 ⁻⁴ | 1 | 7.27x10 ⁻⁷ |
| | 30 | 1.3320 | -- | 4.78x10 ⁻² | 1.6x10 ⁻⁴ | 1 | 6.39x10 ⁻⁷ |

SE – standard error

Temperature is not an important parameter for the characterization of the sensors to refractive index variation as long as the temperature is constant during the characterizations performed. The characterization of the response of unclad POFs to temperature variation can be found in section 3.9.1.

3.4 Immobilization of the initiator on the unclad POF's surface

3.4.1 Chemical reagents

The chemical reagents used for the preparation of the initiator solution were: 2,2'-Azobis(2-methylpropionamidine) dihydrochloride (AAPH) (Aldrich, 97%, 101268336), sodium hydroxide (NaOH) (Panreac, 98%, 131687.1211) and boric acid (H_3BO_3) (Mayer Baker, pa).

All chemicals were analytical grade and used in the same form as received without any further purification. Aqueous solutions were prepared using ultrapure water.

3.4.2 Initiator immobilization

Immobilization of the azo initiator AAPH on the PMMA surface was done by incubating fibres in 10 % AAPH (w/v) solution in 100 mM borate buffer with pH 11.5, for a pre-determined time (Figure 3.2).

Aqueous solutions of boric acid (H_3BO_3) and sodium hydroxide (NaOH) were prepared by weighting the corresponding mass to prepare 20 mL of each solution with concentrations of 0.200 M and 0.216 M, respectively. The buffer solution was prepared by adding small amounts of sodium hydroxide to the boric acid solution until pH reached 11.5. The pH was measured at room temperature using a pH & Ion-meter (Crison; GLP 22+). The solution was placed inside a glass flask and ultrapure water was added until total volume reached 50 mL.

The solution of initiator was prepared by dissolving 1 g of AAPH in 5 mL of buffer solution and ultrapure water was added until the total volume reached 10 mL. The solutions of AAPH were freshly prepared prior to fibre modification.

The modified POF samples were washed with distilled water using magnetic stirring for 5 min, repeated five times, after which they were left to dry overnight at room temperature.

3.4.3 Characterization of AAPH immobilization on POF samples

3.4.3.1 Samples preparation

Unclad POF samples were prepared as previously described in section 3.3.3.

The immobilization of the initiator on the POF's surface was evaluated by FTIR-ATR, Raman spectroscopy (section 3.4.3.2) and by using UV-VIS spectrophotometry with Rhodamine B isothiocyanate (Rhodamine B ITC) as a label (section 3.4.3.3). Inconclusive results were obtained from FTIR-ATR spectroscopy (data not shown). Results obtained from Raman spectroscopy and spectrophotometry with rhodamine B ITC are presented below.

3.4.3.2 Raman spectroscopy

Three POF samples, two immersed in initiator solution overnight ($D_{INI_16h_1}$ and $D_{INI_16h_2}$) and the other one un-modified (D_2), were analysed by Raman spectroscopy. The Raman spectra were acquired by a Jobin Yvon (Horiba) HR800 instrument fitted with a 100x magnification lens (NA = 0.9) using the 442 nm laser line of a He:Cd laser (Kimmon). Appearance of a peak around 1550 – 1580 cm^{-1} characteristic of the functional group (N=N) present in the AAPH was expected.

The Raman spectra obtained for the three samples were very similar, and in accordance with the Raman spectrum expected for a PMMA POF (Thomas *et al.*, 2008), see Figure 3.16. For the samples immersed in initiator solution, no peak was observed at around 1550–1580 cm^{-1} .

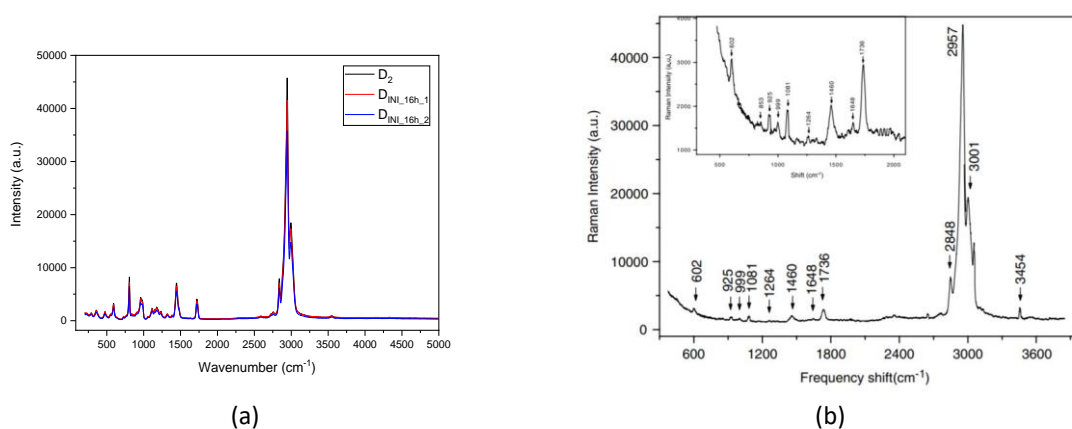


Figure 3.16 (a) Raman spectra obtained for POF samples immersed in initiator solution overnight ($D_{INI_16h_1}$ and $D_{INI_16h_2}$) and one unmodified unclad POF (D_2); (b) Raman spectrum of a PMMA POF, in (Thomas *et al.*, 2008).

3.4.3.3 Labelled AAPH - Rhodamine B ITC

Detection of the immobilized AAPH on the PMMA surface was attempted using a label with characteristic light absorption with maximum at 555 nm. Camli *et al.* reported the preparation of PMMA nanoparticles using MMA (methyl methacrylate), EDMA and AAPH and the presence of the AAPH initiator in the nanoparticles was confirmed using Rhodamine B ITC. Rhodamine B ITC was chosen since isothiocyanate (ITC) groups can covalently bind to amidine moieties. (Camli *et al.*, 2010)

Rhodamine B ITC (mixed isomers) was obtained from Sigma Aldrich, and used without any further purification (283924, CAS Number 36877-69-7), see Figure 3.17.

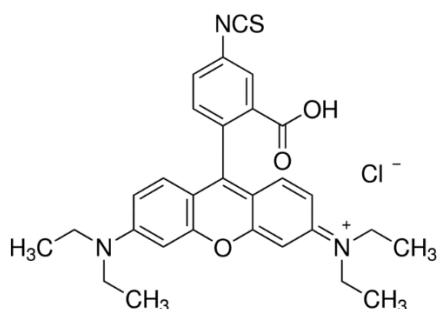


Figure 3.17 Structure of Rhodamine B isothiocyanate.

Experimental procedure was adapted from (Camli *et al.*, 2010). Twenty-five mg of rhodamine B ITC were dissolved in 5 mL of 0.01 mol/L solution of NaOH (pH 12).

The prepared solution was placed inside a glass cup and transmission spectra was measured using a Warm White Fibre-Coupled LED (MWWHF1) and a Fibre Optic Spectrometer (Ocean Optics USB4000) connected to a laptop, see Figure 3.18. The spectra were analysed using the SpectraSuite software (Ocean Optics).



Figure 3.18 Photographs of the experimental setup.

The transmission spectra of the rhodamine solution and distilled water are shown in the Figure 3.19(a). The absorbance of the rhodamine solution was calculated according to the Equation 2.3 (Chapter 2) and the maximum absorption was confirmed to be around 555 nm (Figure 3.19(b)):

$$A = -\log \frac{I_{\text{solution}}}{I_{\text{water}}}$$

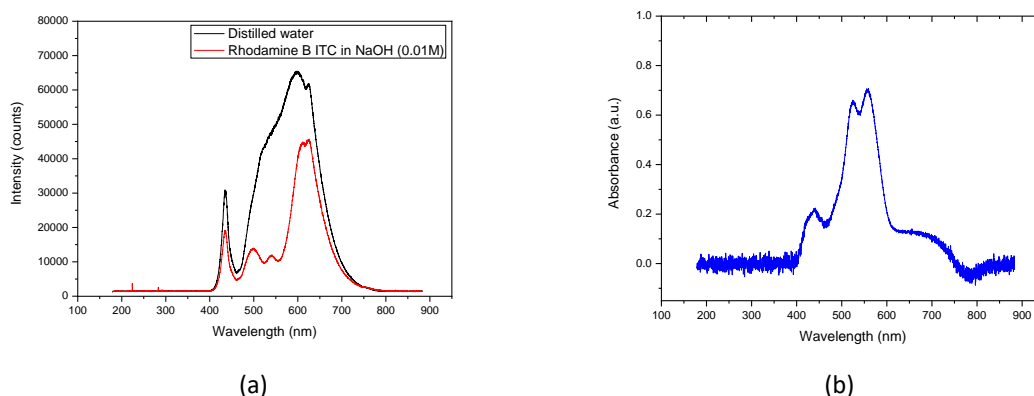


Figure 3.19 Transmission (a) and absorbance (b) spectra obtained with distilled water and Rhodamine B-ITC solution (in NaOH, 0.01 M).

The transmission spectra of the modified samples were analysed with the same experimental setup but with two bare fibre adapters (BARE-05-1000) to connect the POF samples directly to the light source and spectrometer, see Figure 3.20.



Figure 3.20 Experimental setup: (a) characterization of the modified POF samples; (b) close-up of the POF sample connected to both fibre adapters.

All fibres gained a pink colour after immersion in rhodamine solution, which disappeared after washing with isopropanol and distilled water, see Figure 3.21.



Figure 3.21 Photographs of control sample D2 after: (a) immersion in rhodamine solution overnight and (b) washing with squirts of isopropanol and cleaning with optical paper.

No significant changes were observed in the transmission spectra. Figure 3.22 depicts the spectra obtained for samples immersed in initiator solution overnight (16h) and unmodified control samples, after both have been immersed in rhodamine solution overnight (16h).

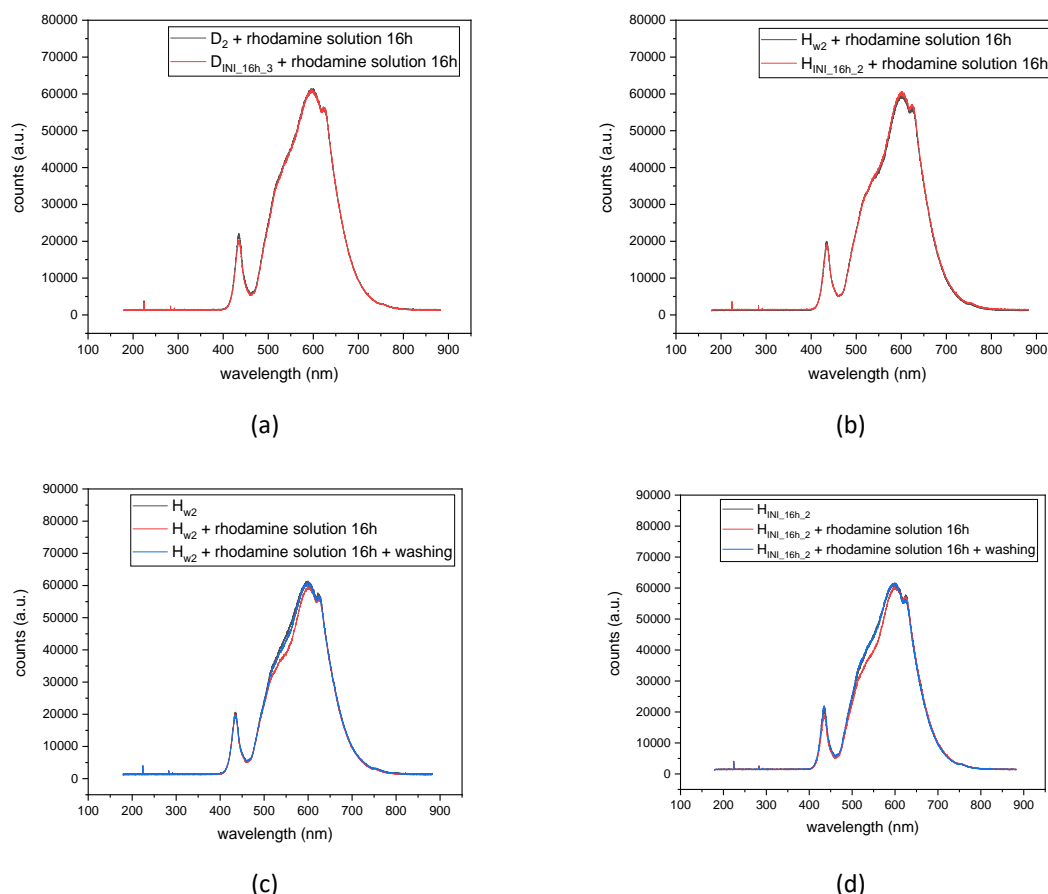


Figure 3.22 Transmission spectra of the modified POF samples after immersion in rhodamine solution overnight: (a) dry and (b) hydrated samples (control and initiator 16h); (c) control and (d) initiator 16h samples (hydrated) before and after the washing procedures.

3.4.3.4 Conclusions

Using techniques described above it was not possible to detect presence of initiator on the surface of POF after immersion in initiator solution, from 4h to 16h, at room temperature.

Spectra obtained by Raman spectroscopy for the modified samples did not reveal differences from the blank samples or samples only immersed in buffer solution. As AAPH is expected to form a monolayer on the POF's surface, sensitivity of the method can be not sufficient to detect it.

Immersion in rhodamine solutions also did not bring the validation of AAPH immobilization on the unclad POF's surface. All samples gained a pink colour, which disappeared with the washing procedures and no significant light absorption was observed by spectra analysis.

3.5 MIP & NIP grafting on POF's surface

3.5.1 Chemical reagents

The chemical reagents used for non-imprinted (NIPs) and molecular imprinted polymers (MIPs) grafting were: methacrylic acid (MAA) (Aldrich, 99%, STBB0035L9), ethylene glycol dimethacrylate (EDMA) (Aldrich, 98%, 3589PJ080), ammonium chloride (NH_4Cl) (Merck, pa, 8564623), ethanol ($\text{C}_2\text{H}_5\text{OH}$) (Merck, pa, 1.00983.2511).

All chemicals were analytical grade and used in the same form as received without any further purification. Aqueous solutions were prepared using ultrapure water.

3.5.2 Grafting procedures

Molecularly imprinted (MIPs) and non-imprinted polymers (NIPs) were synthesized by radical polymerization and by grafting at the surface of unclad PMMA POFs. The reaction mixtures for the NIP, containing the functional monomer (MAA) and cross-linking monomer (EDMA), were prepared in ethanolic solution and placed for 10 minutes in the ultrasonic bath. For the MIP preparation ammonium chloride (NH_4Cl) was added as template analyte.

Figure 3.23 depicts the grafting of the imprinted polymer with ammonium ion on the PMMA surface (Lopes, 2014).

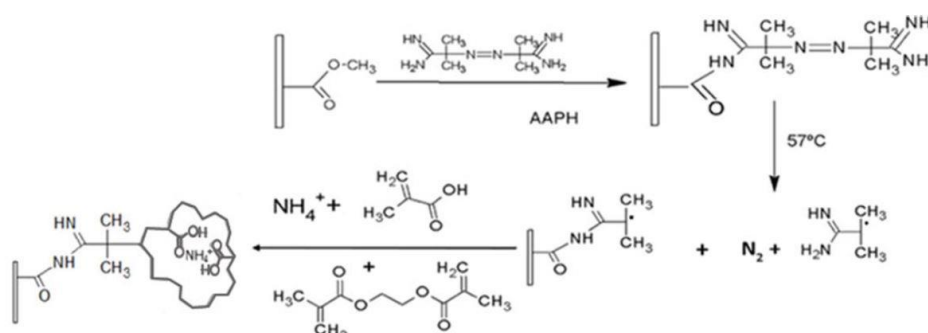


Figure 3.23 Grafting of the imprinted polymer with ammonium ion on the PMMA surface (Lopes, 2014).

Polymerization was carried out in a glass reactor, in which fibres modified with initiator were placed. After addition of the polymerization mixture, the reactor was closed and the mixture was degassed with nitrogen for 15 min using two needles, one for the gas inlet and one for outlet, see Figure 3.24(a). After 5 minutes, the gas inlet needle was pulled a bit up (no longer immersed in the reaction mixture).

After 15 minutes, the reactor was transferred to a thermostated water bath, heated to 57°C (10 h half-life temperature of the initiator) and polymerization was allowed to proceed for a pre-determined time, see Figure 3.24(b). The temperature of the water bath was controlled using C-MAG HS 4 digital with a PT1000 external temperature sensor, from IKA Works Inc.



Figure 3.24 (a) Glass reactor with POF and reaction mixture; (b) glass reactor placed inside the thermostated bath for the grafting procedure.

After polymerization, the functionalized POFs were removed from the reactor, washed with copious amounts of distilled water and magnetic stirring for 20 min, repeated five times, and were allowed to dry overnight at room temperature.

3.5.3 POF selection and NIP optimization

Effect of the polymerization conditions including cladding removal procedures, initiator immobilization time and polymerization time on the NIP deposition were assessed. Optimal polymerization conditions were selected using thickness of the grafted NIP layer on unclad POF samples and surface morphology as criteria. Deposition of the polymer was inspected using optical microscopy and measurements of the thickness were performed using a micrometre.

3.5.3.1 Experimental procedures

POF samples (J_x and NJ_x , ~4 cm) were prepared and the cladding was removed as described in Figure 2.11, section 2.3.3, and in section 3.3.3, respectively. In case of samples J_x , the protective jacket was previously removed by cutting with a razor blade.

Reaction mixtures with the concentration of 6.3 mmol/L MAA and 11.34 mmol/L EDMA in 20 % ethanolic solution were prepared. EDMA and MAA were first dissolved in pure ethanol. A solution of 1 mL of ethanol was prepared using 107 μ L MAA; 50 μ L of this solution was added to a glass flask containing 21.5 μ L EDMA and 2 mL ethanol. Distilled water was added to the glass flask until the volume of 10 mL was reached.



Figure 3.25 NIP grafting on POF samples: (a) POF samples immersed in the reaction mixture, inside the glass reactor; (b) close up of POF samples.

The experimental conditions used for the NIP grafting are described in Table 3.6, including the immersion time in the initiator solution, procedures of cladding removal (chemical etching, polishing), previous functionalization and polymerization time.

A previous functionalization of the surface was performed in six POF samples, based on (Varma *et al.*, 2003), to hydrolyse the surface ester groups to form $-\text{COOH}$ groups. Selected samples were immersed in a methanol solution of sodium hydroxide (NaOH, 5 %), for 10 min and 20 min.

Table 3.6. NIP grafting – experimental conditions.

| POF sample (J_x, NJ_x)* | Cladding removal | Previous fibre functionalization | Initiator (immersion time) | Polymerization time | |
|-----------------------------|------------------------------|--|----------------------------|---------------------|-----|
| J_1, NJ_1 | Chemical etching + polishing | PMMA 1 - NaOH (5%) in methanol, 10 min | 2h | 1 h | |
| J_2, NJ_2 | | | | 3 h | |
| J_3, NJ_3 | | PMMA 2 - NaOH (5%) in methanol, 20 min | | 3 h | |
| J_4, NJ_4 | | --- | | 1 h | |
| $J_{4.2}, NJ_{4.2}$ | | --- | | 3 h | |
| J_5, NJ_5 | | --- | | 4h | 3 h |
| J_6, NJ_6 | | --- | | 6h | 1 h |
| J_7, NJ_7 | --- | 3 h | | | |
| J_8, NJ_8 | Chemical etching | --- | 6h | 1 h | |
| J_9, NJ_9 | | | | 3 h | |

* J_x - GHCP4001 ESKA, Mitsubishi Rayon; NJ_x - DB-1000, Asahi Kasei.

3.5.3.2 Characterization of the POF-NIP samples

3.5.3.2.1 Optical microscopy

The surface of the POF samples was inspected by optical microscopy (Olympus BX51) before and after NIP grafting. Figure 3.26 depicts the top view of the fibre's end-faces for different modification conditions.

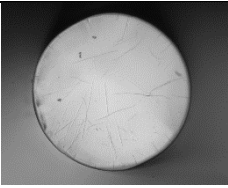
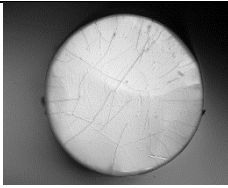
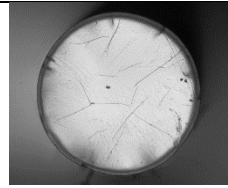
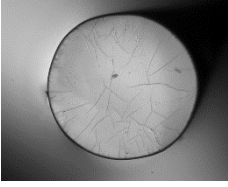
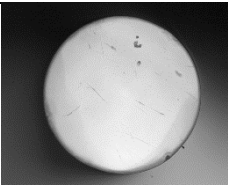
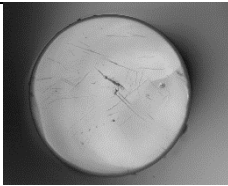
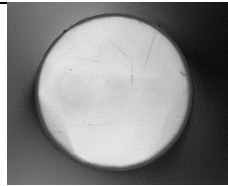
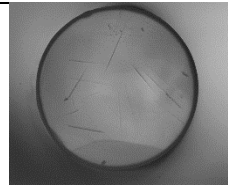
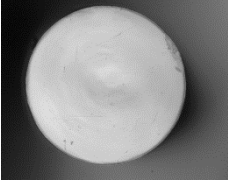
| Polymerization (1h) | | Polymerization (3h) | | Initiator |
|---|---|---|--|-----------|
| Chemical etching + polishing | | | | |
| Functionalization PMMA 1 - NaOH (5%) in methanol, 10 min | | | | |
|  |  |  |  | 2h |
| J ₁ | NJ ₁ | J ₂ | NJ ₂ | |
| Functionalization PMMA 2 - NaOH (5%) in methanol, 20 min | | | | |
| | |  |  | 2h |
| | | J ₃ | NJ ₃ | |
| Without previous functionalization | | | | |
|  |  |  |  | 2h |
| J ₄ | NJ ₄ | J _{4_2} | NJ _{4_2} | |
| | |  |  | 4h |
| | | J ₅ | NJ ₅ | |
|  |  |  |  | 6h |
| J ₆ | NJ ₆ | J ₇ | NJ ₇ | |
| Chemical etching | | | | |
|  |  |  |  | 6h |
| J ₈ | NJ ₈ | J ₉ | NJ ₉ | |

Figure 3.26 Images of optical microscopy of the modified POF samples, after the NIP grafting.

Cracks on the surface appeared on POF samples previously functionalized and POF samples immersed 2h in initiator solution and polymerized for 1h (J₄, NJ₄). These cracks are not observed when longer immersion time in the initiator solution or longer polymerization times were used.

3.5.3.2.2 Thickness variation

Thickness of the sensing region was measured before (D_{bP}) and after (D_{aP}) NIP deposition using a micrometre (Mitutoyo, Series 103-137, $\pm 2 \mu\text{m}$ accuracy, graduation of $\pm 10 \mu\text{m}$). Measurements were performed in several points along the length of the sensing region (30 \times) and the mean value and standard deviation were calculated, see Table 3.7. The variation of the sensing region thickness (ΔD) was calculated by the difference between the obtained values and the corresponding error ($\delta(\Delta D)$) was calculated by error propagation:

$$\Delta D = D_{aP} - D_{bP} \quad \text{Equation 3.4}$$

$$\delta(\Delta D) = \sqrt{\delta D_{aP}^2 + \delta D_{bP}^2} \quad \text{Equation 3.5}$$

Table 3.7. Thickness variation of the sensing region after polymerization (NIP).

| Initiator | POF preparation | Modification | Polymerization (1h) | | Polymerization (3h) | |
|-----------|------------------------------|------------------|---------------------|---------------------------|---------------------|---------------------------|
| | | | POF sample | Thickness variation (mm)* | POF sample | Thickness variation (mm)* |
| 2h | Chemical etching + polishing | PMMA 1** | J ₁ | 0.005 \pm 0.008 | J ₂ | 0.008 \pm 0.007 |
| | | | NJ ₁ | 0.007 \pm 0.010 | NJ ₂ | 0.007 \pm 0.008 |
| | | PMMA 2*** | - | - | J ₃ | 0.007 \pm 0.005 |
| | | | - | - | NJ ₃ | 0.007 \pm 0.006 |
| - | | J ₄ | 0.005 \pm 0.024 | J _{4_2} | 0.005 \pm 0.020 | |
| | | NJ ₄ | 0.001 \pm 0.007 | NJ _{4_2} | 0.012 \pm 0.008 | |
| 4h | | - | - | - | J ₅ | 0.008 \pm 0.004 |
| | | | - | - | NJ ₅ | 0.009 \pm 0.006 |
| 6h | - | - | J ₆ | 0.003 \pm 0.006 | J ₇ | 0.006 \pm 0.006 |
| | | | NJ ₆ | 0.002 \pm 0.004 | NJ ₇ | 0.006 \pm 0.006 |
| | | Chemical etching | J ₈ | 0.000 \pm 0.000 | J ₉ | 0.000 \pm 0.000 |
| | | | NJ ₈ | 0.000 \pm 0.002 | NJ ₉ | 0.010 \pm 0.002 |

Micrometre graduation of $\pm 10 \mu\text{m}$ (Series 103-137)*; NaOH (5%) in methanol, 10 min** and 20 min***.

POF samples previously treated with NaOH solution (PMMA 1 and PMMA 2) showed an increase on fibre diameter around $5 \mu\text{m} - 8 \mu\text{m}$, which is close to the readout error ($\pm 5 \mu\text{m}$).

Untreated samples polymerized for 1h didn't show significant variation on fibre diameter, taking into account the associated error, indicating that polymerization time should be increased.

POFs, which were chemically etched and polished, but not treated with alkali, and polymerized for 3h showed a decrease of thickness variation that was negatively correlated with the immersion time in the initiator solution: $12 \mu\text{m}$ NJ_{4_2} (2h) – $9 \mu\text{m}$ NJ₅ and $8 \mu\text{m}$ J₅ (4h) – $6 \mu\text{m}$ NJ₇ and J₇ (6h). Sample J_{4_2} was not considered (2h) due to a very high associated error ($\pm 20 \mu\text{m}$).

Chemically etched samples, immersed in initiator solution for 6h and polymerized for 3h, showed an increase of thickness of $10 \mu\text{m}$ (sample NJ₉) or no thickness variation (sample J₉).

Polishing the POF samples together with chemical etching for cladding removal caused higher associated errors of thickness measurements.

3.5.3.3 Conclusions

No advantages were found of treating fibres with alkali solution prior to the modification with the initiator (PMMA1 and PMMA2).

The immersion time on initiator solution should be equal or higher than 4h to prevent crack formation of the fibre surface. Polymerization should be longer than 1h.

Chemically etched POF samples showed a more regular thickness while etching and polishing caused higher variation of fibre thickness.

No advantages were obtained by using the jacketed POF (J_x). The jacket needs to be removed carefully to not damage the fibre, adding one more step to the fibre preparation. Therefore, the unjacketed POF (NJ_x) was selected for the development of POF-MIP grafting for ammonium detection.

3.5.4 **POF's functionalization by MIP grafting**

After optimization of the MIP grafting conditions, the selected POFs were functionalized with the MIP by adding the template molecule to the reaction mixture.

Furthermore, POFs were heated in the ethanolic solutions mimicking of polymerization conditions to evaluate effect of exposure to solvent at polymerization temperature on fibre.

Characterization of POF-MIP sensors will be presented on section 3.9.

3.5.4.1 Experimental procedures

NJ_x POF samples (~60 cm) were prepared and the cladding was removed as described in Figure 2.11, section 2.3.3, and section 3.3.3.

After the immobilization of the initiator on the sensing region (unclad POFs), the modified fibres were placed inside the glass reactor, taking care that the sensing region was placed in the central region inside the reactor.

The polymerization mixture was prepared as described in the section 3.5.3.1 with addition of 0.9 mmol/L NH_4Cl . The reaction mixtures containing the functional monomer (MAA), cross-linking monomer (EDMA) and ammonium chloride (NH_4Cl) as template, were prepared in a 30% ethanolic solution and placed for 10 minutes in the ultrasonic bath. When 20 % of ethanol was used as solvent in the preparation of the MIP, a milky solution was obtained even after placing in the ultrasonic bath. For this reason, 30 % of ethanol was used instead.

The experimental conditions used for the MIP grafting are described in Table 3.8, including the immersion time in the initiator solution, concentration of monomer, cross-linker and template, as well as polymerization time.

Some of the fibres were polymerized simultaneously with smaller pieces of POF (~ 4 cm length), as e.g. POF NJ2 and sample-NJ2, to have replicated samples.

The polymerization process (5h) was mimicked using only solvent and this process was monitored in real-time for two fibres (NJ8 and NJ9), see section 3.9.3. A POF sample was immersed at the same time and in the same conditions as POF NJ8, for comparison (sample-NJ8).

Table 3.8. MIP grafting – experimental conditions.

| POF | Initiator immersion time | [MAA] (mM) | [EDMA] (mM) | [NH ₄ Cl] (mM) | Polymerization time |
|---------------------------------|--------------------------|------------|-------------|---------------------------|---------------------|
| NJ1 | 4h | 6.3 | 11.34 | 0.9 | 2h |
| NJ2 Sample – NJ2* | | | | | 5h |
| NJ3 – hydrated Sample – NJ3* | | | | | |
| NJ4 | | 12h | | | |
| NJ5 – MIP _{1/2} | | | | | |
| NJ8 – solvent Sample – NJ8* | | 5h | - | - | - |
| NJ9 – solvent | - | | - | - | |

* POF samples (~4 cm length), sample-NJ2, sample-NJ3 and sample-NJ8, were modified in the exact same conditions in relation to POFs NJ2, NJ3 and NJ8 (solvent), respectively. [MIPs: 30 % ethanol; [EDMA]/[MAA] = 1.8; [MAA]/[NH₄⁺] = 7]

The functionalized POFs and POF samples were left to dry overnight at room temperature, except for POF NJ3 and sample-NJ3 that were kept hydrated by leaving them in distilled water.

The morphology of the functionalized fibre surface was evaluated by optical microscopy and measurements of the sensing region thickness performed before and after MIP deposition.

3.5.4.2 Thickness variation

Thickness of the sensing region was measured before and after the polymerization procedures using a Mitutoyo Micrometre with accuracy of $\pm 2 \mu\text{m}$ and readout error of $\pm 5 \mu\text{m}$. Measurements were performed as described in section 3.5.3.2.2 and the variation of the sensing region thickness ($\Delta D \pm \delta(\Delta D)$) was calculated according with Equation 3.4 and Equation 3.5, see Table 3.9.

Table 3.9. Thickness variation of the sensing region after polymerization.

| POF | Polymerization time | Thickness (mm) | | Thickness variation $\Delta D \pm \delta(\Delta D)$ (mm) |
|----------------------------|---------------------|--|---|--|
| | | before ($D_{bP} \pm \delta D_{bP}$) | after ($D_{aP} \pm \delta D_{aP}$) | |
| NJ1-MIP | 2h | 0.973 ± 0.004 | 0.980 ± 0.005 | 0.007 ± 0.006 |
| NJ2-MIP | 5h | 0.969 ± 0.003 | 0.980 ± 0.000 | 0.011 ± 0.003 |
| Sample-NJ2-MIP | | 0.955 ± 0.000 | 0.966 ± 0.002 | 0.011 ± 0.002 |
| NJ3 – hydrated-MIP | | 0.971 ± 0.003 | 0.971 ± 0.002 | 0.000 ± 0.004 |
| Sample-NJ3 –MIP | | 0.960 ± 0.002 | 0.969 ± 0.002 | 0.009 ± 0.003 |
| NJ4-MIP | 12h | 0.976 ± 0.003 | 0.983 ± 0.004 | 0.007 ± 0.005 |
| NJ5 – MIP _{1/2} * | | 0.966 ± 0.003 | 0.971 ± 0.003 | 0.005 ± 0.004 |
| NJ8-solvent | 5h | 0.990 ± 0.002 | 0.986 ± 0.003 | -0.004 ± 0.004 |
| Sample-NJ8-solvent | | 0.969 ± 0.003 | 0.979 ± 0.002 | 0.010 ± 0.004 |
| NJ9-solvent | | 0.965 ± 0.001 | 0.974 ± 0.001 | 0.009 ± 0.001 |

*MIP_{1/2} – see Table 3.8.

Only POF NJ2 (and sample-NJ2), polymerized for 5h, had an increase of thickness of 11 μm after MIP deposition. Inconsistent results were obtained for hydrated fibres (NJ3 and sample-NJ3) with an increase of 9 μm obtained for sample-NJ3 and no thickness variation for NJ3. The POFs polymerized for 2h (NJ1) and for 12h (NJ4) showed the same increase of sensing region thickness of 7 μm .

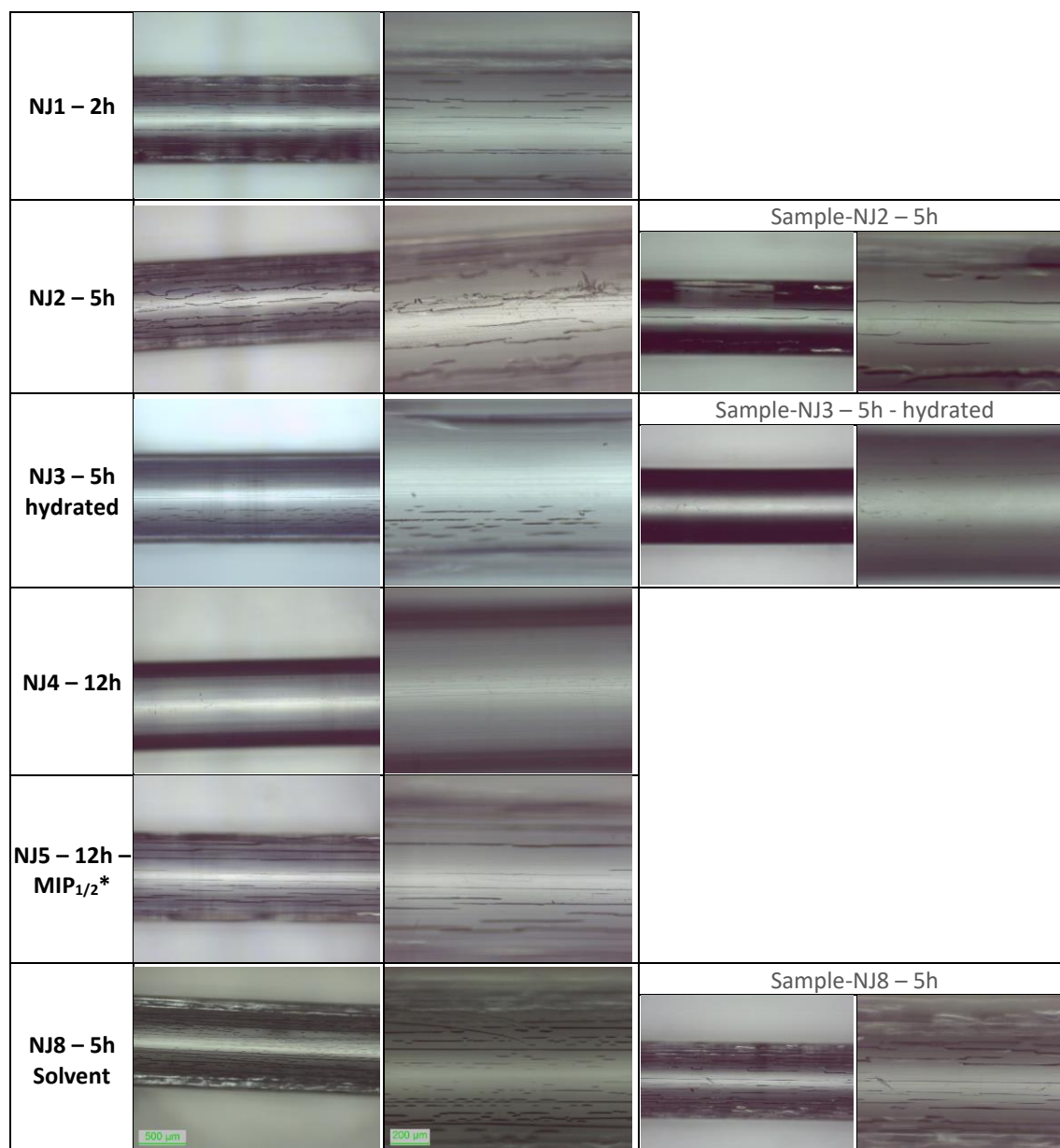
No significant variation in thickness was obtained when the concentration of reagents in the reaction mixture was twice lower (NJ5). The thickness variation was found to be equal to readout error, 5 μm .

Samples immersed in solvent, mimicking the polymerization conditions showed an increase of thickness of 10 μm (sample-NJ8-solvent) and 9 μm (NJ9-solvent), which is similar to the values obtained for fibres polymerized for the same time (5h). POF NJ8, also immersed in solvent in the same conditions did not show thickness variation.

Results suggest that increase of thickness can be related to solvent absorption by the unclad POFs. Further studies performed to evaluate solvent influence on fibre's stability are presented in the section 3.6. Longer polymerization time, using the same or lower concentration of the MIP leads to smaller variation of sensing region thickness.

3.5.4.3 Optical microscopy

The sensing region of grafted POFs was inspected by optical microscopy (LEICA DM750M), before and after polymerization procedures. Figure 3.27 shows obtained images after MIP grafting and polymerization mimicking with solvent for POF NJ8 and sample-NJ8, for comparison.



*MIP_{1/2} – see Table 3.8.

Figure 3.27 Images of optical microscopy (5x, 10x) of the sensing region after polymerization procedures and polymerization mimicking using only solvent solution.

Cracks are well visible on the sensing region’s surface for almost all POF samples.

Longer polymerization time using the same polymerization mixture concentration leads to a more homogeneous surface of POF-MIP NJ4 (12h), when comparing with POF-MIPs NJ1 and NJ2, polymerized for 2h and 5h, respectively. When lower concentrations of reagents were used (MIP_{1/2}), cracks were well visible on the surface even with polymerization time of 12h.

Hydrated fibres (NJ3 and sample-NJ3) had significantly less visible cracks on the surface in comparison with the dried POFs polymerized for the same time (5h), NJ2 and sample-NJ2.

POFs NJ8 and sample-NJ8, only immersed in solvent in the same conditions of time and temperature as POFs NJ2 and sample NJ2 (5h), showed similar surface morphology.

Top view of the POF samples polymerized for 5h and immersed in solvent in the same conditions, are shown in the Figure 3.28. Surface of sample-NJ8, immersed in solvent, seems much more damaged than fibres that were immersed in polymerization solution.

The POF-MIP samples were cut in the middle region, the tip was polished and new images were registered (middle region), see Figure 3.28. These images suggest that maintaining fibres hydrated during all modification process, from immobilization of initiator to polymer deposition (sample-NJ3) prevents surface damage along the fibre length.

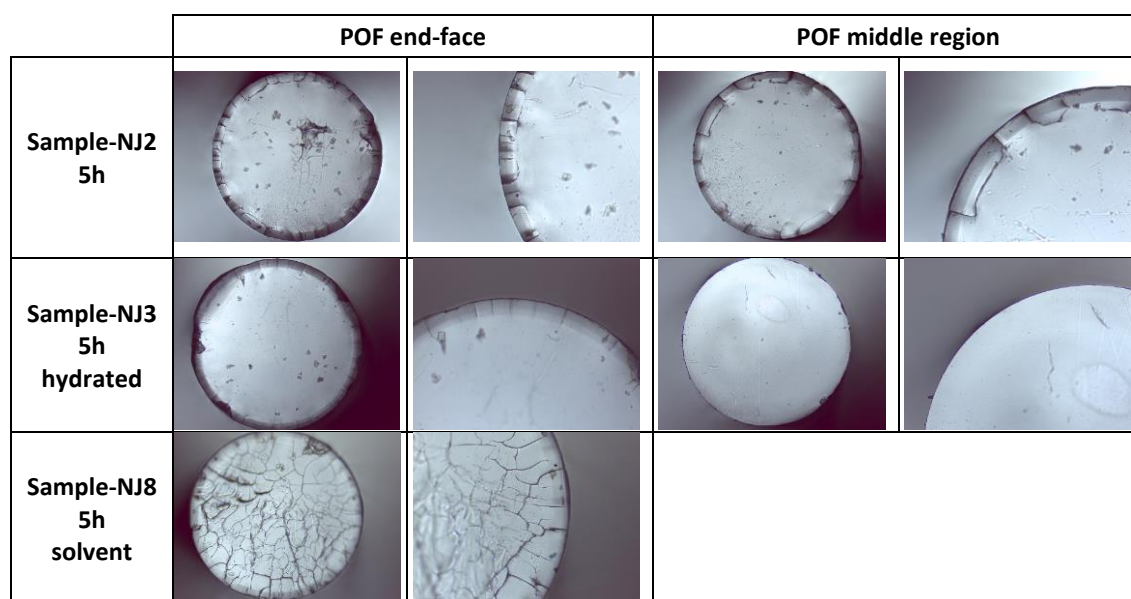


Figure 3.28 Images of optical microscopy (10x, 20x) - top view of the POF's end-face and middle region.

3.6 Stability of unclad POF samples immersed in solvent

POF samples immersed in solvent solution at polymerization conditions revealed cracks on the surface and thickness variation (see section 3.5.4).

Evaluation of the stability of unclad POF samples in solvent was performed for dry and hydrated fibres varying immersion time (1h – 5h) and temperature (room temperature and at 57 °C).

Surface morphology, thickness and mass of the POFs were evaluated before and after the modification procedures.

3.6.1 General procedures

POF samples prepared as described in the section 3.3.3 and section 2.3.3, Chapter 2.

The unclad POF samples were washed with distilled water, cleaned with optical paper and placed in identified Eppendorf's – dry samples (D_n) and hydrated samples (H_n). The hydrated samples were left in distilled water for 3 days for complete water absorption.

The immersion conditions are described in Table 3.10. The dry (D_n) and hydrated (H_n) POF samples were placed in the solvent solution (30 % ethanol in distilled water), from 1h to 5h. Stability was evaluated at two different temperatures: room temperature and temperature at which polymerization was performed (57 °C). Climatic Chamber (CH340, Angelantoni Industrie) was used for temperature control.

After immersion on the solvent solution, the samples were washed with distilled water and cleaned with optical paper, procedure repeated five times. The hydrated fibres were kept in water prior to measurements.

Table 3.10. Experimental conditions – immersion of unclad POF samples in solvent solution.

| Immersion time | Sample condition | POF sample | |
|----------------|------------------|-----------------------|--------------------------|
| | | Room temperature (RT) | Temperature of 57 °C (T) |
| 1h | dry | RT_D ₁ | T_D ₁ |
| 2h | | RT_D ₂ | T_D ₂ |
| 3h | | RT_D ₃ | T_D ₃ |
| 4h | | RT_D ₄ | T_D ₄ |
| 5h | | RT_D ₅ | |
| | | | T_D _{5_2} |
| | | | T_D _{5_3} |
| 1h | hydrated | RT_H ₁ | T_H ₁ |
| 2h | | RT_H ₂ | T_H ₂ |
| 3h | | RT_H ₃ | T_H ₃ |
| 4h | | RT_H ₄ | T_H ₄ |
| 5h | | RT_H ₅ | |
| | | | T_H _{5_2} |
| | | | T_H _{5_3} |

The surface of the unclad POF samples was inspected by optical microscopy and the thickness and mass were evaluated before and after immersion in solvent.

3.6.2 Optical microscopy

No changes on the surface morphology were observed by optical microscopy for the fibres kept in the solvent at room temperature. As an example, images of optical microscopy (Olympus BX51) are shown in Table 3.11 and Table 3.12 for dry and hydrated fibres, respectively, with immersion times of 1h and 5h.

Table 3.11. Images of optical microscopy – dry POF samples at room temperature (RT), before and after immersion in solvent (1h and 5h).

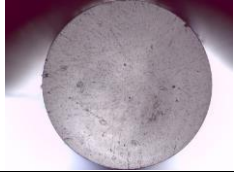
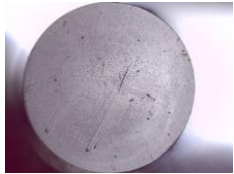
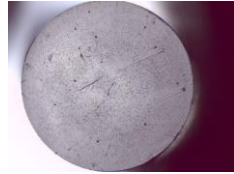
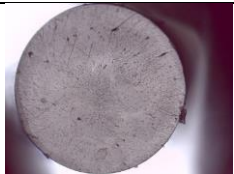
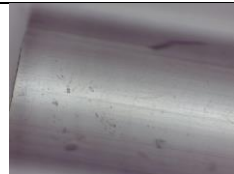
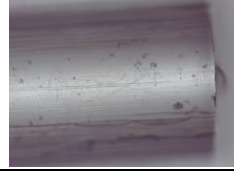
| POF sample | Before immersion | | After immersion | |
|------------------------------|---|---|--|---|
| RT_D ₁ Dry, 1h |  |  |  |  |
| RT_D ₅ Dry, 5h |  |  |  |  |

Table 3.12. Images of optical microscopy – hydrated POF samples at room temperature (RT), before and after immersion in solvent (1h and 5h).

| POF sample | Before immersion | | After immersion | |
|--------------------------------------|---|---|--|---|
| RT_H ₁ Hydrated, 1h |  |  |  |  |
| RT_H ₅ Hydrated, 5h |  |  |  |  |

Variation of the surface morphology was observed for the unclad POF samples that were immersed in solvent at 57°C. Cracks appeared on the surface for all samples, except for the hydrated sample immersed during 1 h (T_H₁).

As an example, images of optical microscopy are shown in Table 3.13 and Table 3.14 for dry (1h,3h,5h) and hydrated (2h,3h,5h) samples.

Table 3.13. Images of optical microscopy – dry POF samples at 57°C (T), before and after immersion in solvent (1h, 3h and 5h).

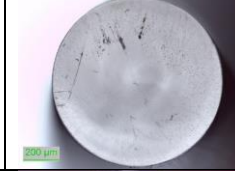
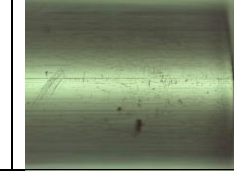
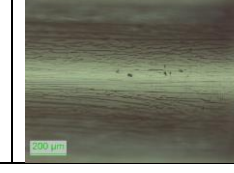
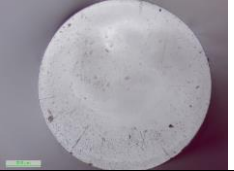
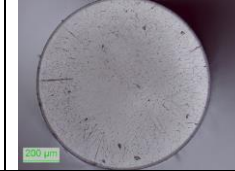
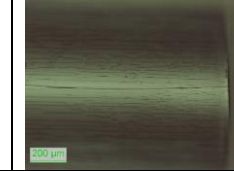
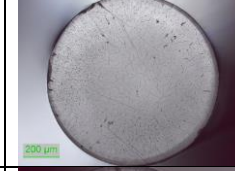
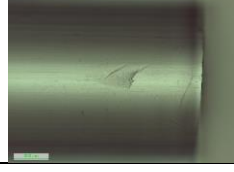
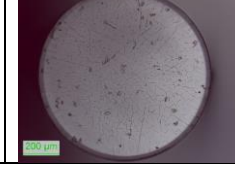
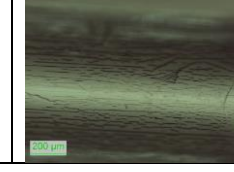
| POF sample | Before immersion | | After immersion | |
|-------------------|---|---|--|---|
| T_D1 Dry, 1h |  |  |  |  |
| T_D3 Dry, 3h |  |  |  |  |
| T_D5_3 Dry, 5h |  |  |  |  |

Table 3.14. Images of optical microscopy – hydrated POF samples at 57°C (T), before and after immersion in solvent (2h, 3h and 5h).

| POF sample | Before immersion | | After immersion | |
|------------------------|---|---|--|---|
| T_H2 Hydrated, 2h |  |  |  |  |
| T_H3 Hydrated, 3h |  |  |  |  |
| T_H5_3 Hydrated, 5h |  |  |  |  |

3.6.3 Thickness variation

Thickness of the fibres was measured as described in section 3.5.3.2.2. Results are presented in the Table 3.15.

Measurements of thickness for POF samples immersed at room temperature were performed using a micrometre with graduation of $\pm 10 \mu\text{m}$ (Series 103-137), while for POF samples immersed at 57 °C were measured with a micrometre with graduation of $\pm 1 \mu\text{m}$ (Series 103-129).

No significant variation of the POF thickness could be detected for the samples kept in the solvent at room temperature from 1h to 5h, both dry and hydrated (see Table 3.15). The observed thickness differences were within readout error of the micrometre (Series 103-137).

Thickness of fibres kept in the solvent at 57°C increased up to 6 µm for dry samples concomitantly with the increase of immersion time (see Table 3.15). Thickness of hydrated samples increased between 4 µm and 8 µm. These fibres were measured using micrometre with graduation of ±1 µm (Series 103-129).

Table 3.15. Thickness variation by immersion in solvent (30 % ethanol) at different temperatures.

| Immersion time | Sample condition | Room temperature | | T=57 °C | |
|----------------|------------------|-------------------|----------------------------|--------------------|-----------------------------|
| | | POF sample | Thickness variation (mm) * | POF sample | Thickness variation (mm) ** |
| 1h | dry | RT_D ₁ | -0.001 ± 0.004 | T_D ₁ | 0.000 ± 0.002 |
| 2h | | RT_D ₂ | 0.000 ± 0.005 | T_D ₂ | 0.002 ± 0.002 |
| 3h | | RT_D ₃ | 0.000 ± 0.003 | T_D ₃ | 0.003 ± 0.001 |
| 4h | | RT_D ₄ | -0.001 ± 0.002 | T_D ₄ | 0.004 ± 0.002 |
| 5h | | RT_D ₅ | 0.000 ± 0.003 | T_D _{5_1} | 0.004 ± 0.001 |
| | | | | T_D _{5_2} | 0.006 ± 0.001 |
| | | | | T_D _{5_3} | 0.005 ± 0.002 |
| 1h | hydrated | RT_H ₁ | -0.005 ± 0.005 | T_H ₁ | 0.005 ± 0.003 |
| 2h | | RT_H ₂ | 0.001 ± 0.002 | T_H ₂ | 0.004 ± 0.002 |
| 3h | | RT_H ₃ | -0.004 ± 0.004 | T_H ₃ | 0.005 ± 0.003 |
| 4h | | RT_H ₄ | -0.004 ± 0.004 | T_H ₄ | 0.006 ± 0.002 |
| 5h | | RT_H ₅ | -0.002 ± 0.004 | T_H _{5_1} | 0.005 ± 0.003 |
| | | | | T_H _{5_2} | 0.008 ± 0.002 |
| | | | | T_H _{5_3} | 0.006 ± 0.001 |

*micrometre graduation of ±10 µm (Series 103-137); **micrometre graduation of ±1 µm (Series 103-129).

Smaller thickness variations were obtained in this case compared to the previous experiment with dry fibres immersed in solvent at 57°C: 4 – 6 µm for dry samples and 5 – 8 µm for hydrated samples vs. 4 - 10 µm obtained previously.

Results show that absorption of solvent by the POF samples is favoured at increased temperature and longer immersion time in case of dry samples.

3.6.4 Mass variation

POF samples immersed in solvent solution at 57 °C showed variation of the surface morphology and thickness of the sensing region. Mass variation was evaluated for these samples using Sartorius micro balance (XM 1000P, resolution of 0.001 mg). Samples were dried in an oven, overnight at 30 °C prior to measurements.

Three replicated measurements were performed and the mass variation ($\Delta m \pm \delta(\Delta m)$) was calculated in the same way as described in section 3.5.3.2.2. The obtained mass variation can be found in Table 3.16.

Table 3.16. Mass variation – POF samples immersed in solvent (30 % ethanol) at 57 °C.

| Immersion time | Sample condition | T=57 °C | |
|----------------|------------------|--------------------|---------------------|
| | | POF sample | Mass variation (mg) |
| 1h | dry | T_D ₁ | -0.020 ± 0.001 |
| 2h | | T_D ₂ | 0.002 ± 0.001 |
| 3h | | T_D ₃ | 0.012 ± 0.003 |
| 4h | | T_D ₄ | 0.025 ± 0.003 |
| 5h | | T_D _{5_1} | 0.038 ± 0.003 |
| | | T_D _{5_2} | 0.036 ± 0.004 |
| | | T_D _{5_3} | 0.036 ± 0.002 |

A decrease of mass of 20 µg was obtained for sample T_D₁, immersed during 1h in solvent. For other samples, the mass increased with immersion time. Samples immersed for 5h showed mass increase between 36 µg and 38 µg.

3.6.5 Conclusions

No changes on the surface nor thickness variation were observed for dry and hydrated unclad POFs that were immersed in solvent during 1h to 5h at room temperature.

Alterations of the surface morphology, thickness of the sensing region and mass of the dry samples occurred when POF samples were immersed in solvent at 57 °C.

Mass increased with immersion time for dry samples, reaching 36 – 38 µg for 5h of immersion time, showing solvent absorption by the polymer with increased immersion time.

The thickness of the sensing region also increased with immersion time for dry samples, with a maximum of 4 µm – 6 µm. For hydrated samples, the thickness variation (maximum of 5 µm – 8 µm) was not related with immersion time.

At 57 °C, cracks appeared on the surface for all samples, except for the hydrated sample immersed during 1h in solvent (T_H₁).

The influence of solvent on the transmission capacity of POFs will be further evaluated. The monitoring in real time during immersion will be presented, and the sensitivity of the fibres to the refractive index variation will be evaluated, see section 3.9.3 and 3.9.6.

3.7 MIP grafting on PMMA slabs

Assessment of the MIP grafting using another PMMA platform was carried out. Two PMMA slabs (1 cm × 5 cm) were functionalized using the same procedures as described for the POF NJ2 (4h immersion in initiator solution and 5h of polymerization time), see section 3.5.4.1. Figure 3.29 depicts the adapted experimental setup used for the modification with initiator, simultaneous polymerization of the PMMA slabs and washing procedures.

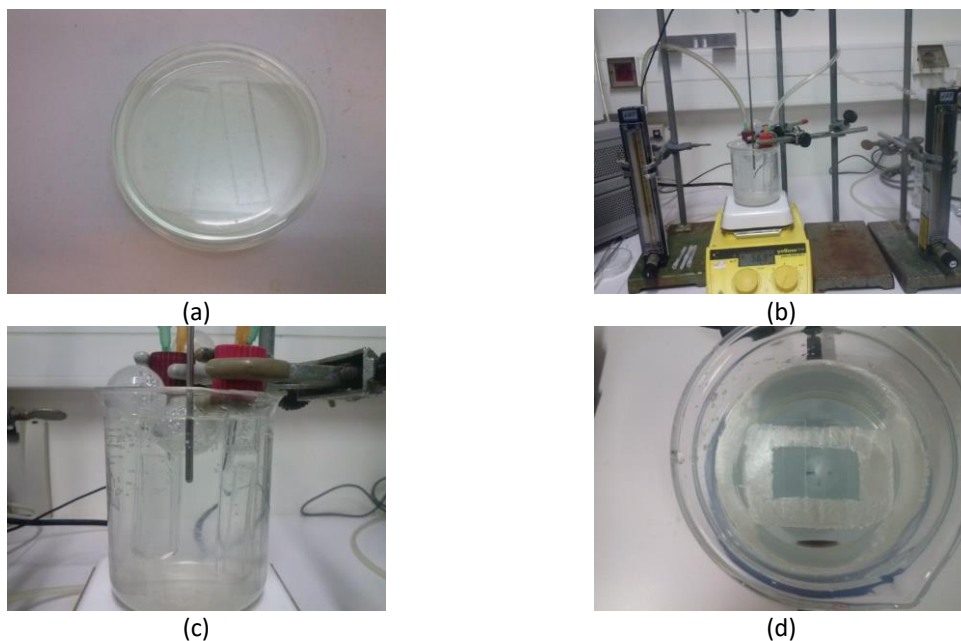


Figure 3.29 Adapted experimental setup: (a) immersion in the initiator solution; (b,c) simultaneous polymerization of the PMMA slabs; (d) washing procedures with distilled water and magnetic stirring.

The PMMA slabs stopped being transparent and became opaque after the MIP grafting (Figure 3.30) and their surface became grainy (Figure 3.31). Cracks were not observed on the surface of the functionalized slabs.

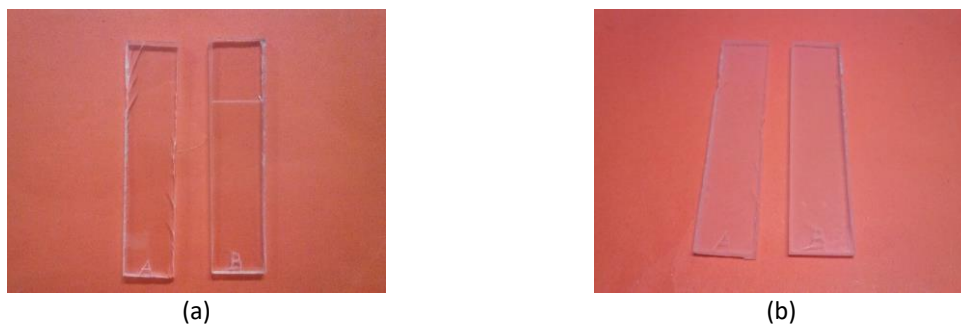


Figure 3.30 Photographs of the PMMA slabs before (a) and after (b) the MIP grafting procedures (4h immersion in initiator solution and 5h of polymerization time).

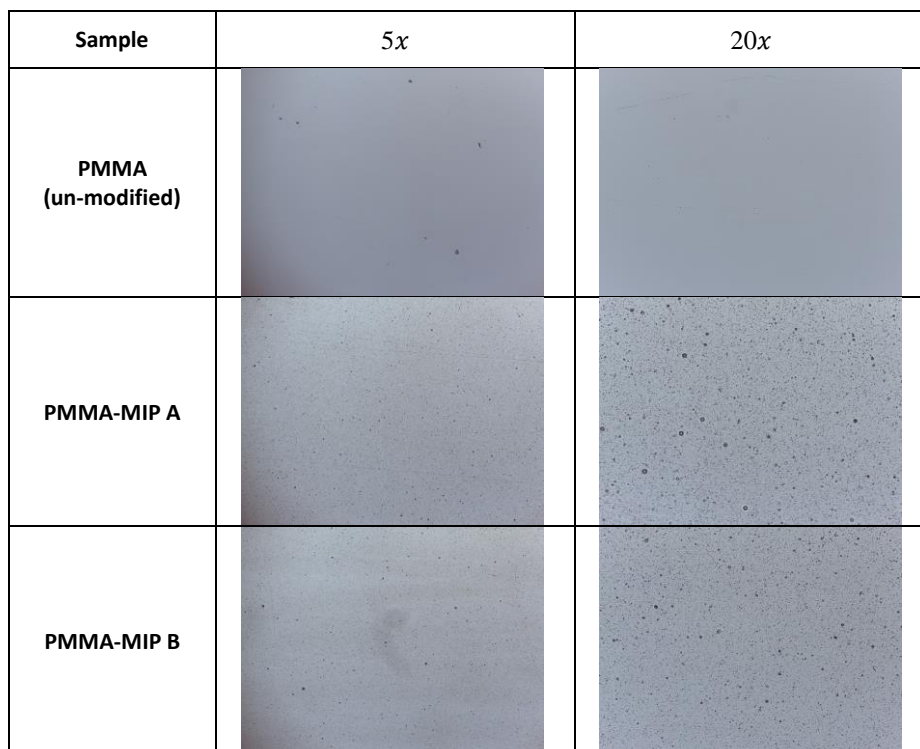


Figure 3.31 Images of optical microscopy (5x, 20x) – functionalized PMMA slabs (PMMA-MIP), after the MIP grafting procedures, and comparison with an unmodified PMMA sample.

Thickness was measured before and after the polymerization procedures using a Mitutoyo Micrometre with accuracy of $\pm 2 \mu\text{m}$ (graduation of $\pm 10 \mu\text{m}$). Measurements were performed as described in section 3.5.3.2.2 and the variation of the sensing region thickness ($\Delta D \pm \delta(\Delta D)$) was calculated according with Equation 3.4 and Equation 3.5, see Table 3.17. The thickness of the PMMA slabs increased between $10 \mu\text{m}$ and $15 \mu\text{m}$, which is consistent with the values of the thickness variation obtained for the POF-MIP NJ2 samples ($11 \mu\text{m}$), polymerized in the same conditions.

Table 3.17. Thickness variation of the PMMA slabs after MIP grafting procedures.

| Sample | Thickness (mm) | | Thickness variation $\Delta D \pm \delta(\Delta D)$ (mm) |
|------------|--|---|--|
| | before ($D_{bP} \pm \delta D_{bP}$) | after ($D_{aP} \pm \delta D_{aP}$) | |
| PMMA-MIP A | 2.047 ± 0.003 | 2.062 ± 0.003 | 0.015 ± 0.004 |
| PMMA-MIP B | 2.050 ± 0.006 | 2.060 ± 0.002 | 0.010 ± 0.010 |

Smaller pieces of the PMMA slabs were cut ($0.7 \text{ cm} \times 0.7 \text{ cm}$) and the refractive index was measured using the Abbemat refractometer with 1×10^{-4} resolution. The obtained values of refractive index were: 1.4903 (PMMA), 1.4908 (PMMA-MIP A) and 1.4911 (PMMA-MIP A), average value and standard deviation of several measurements performed.

3.8 Optical sensing setup and data processing

The data acquisition system was previously developed aiming at a portable, wearable and low-cost optical sensing system for gait monitoring with POF (Bilro, 2011). Later, this optical sensing system was used for sediments monitoring in water samples (Ferreira *et al.*, 2013)(Sequeira *et al.*, 2013).

The intensity based transmission system comprised an LED (IF-E96, wavelength centred at 660 nm), a POF coupler (90:10, IF-542) and two photodiode detectors (IF-D91), one connected to the POF sensor and the other to the reference POF, see Figure 3.32(a,b). The POF sensor was placed inside a glass reactor, above a magnetic stirrer, see Figure 3.32(c).

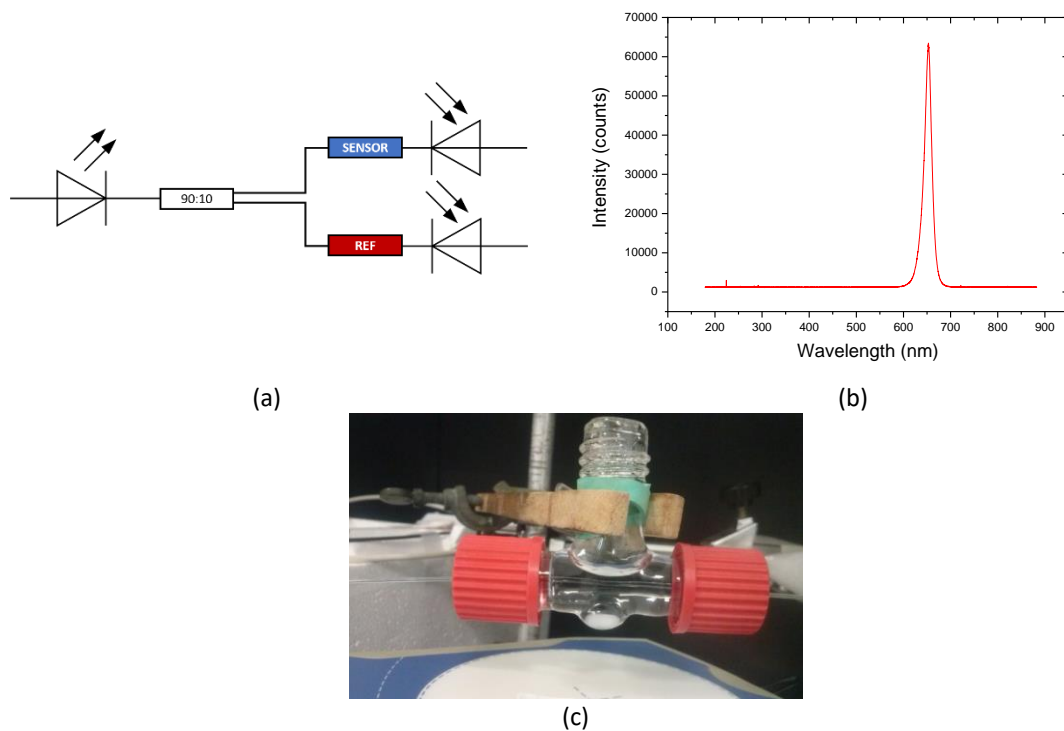


Figure 3.32 (a) Schematic representation of the optical sensing setup; (b) LED spectrum; (c) close-up of the POF sensor inside the glass reactor.

The data acquisition system, depicted in Figure 3.33, contained an electronic board that controlled the LED and the two photodiodes, a micro-processing unit that managed the data acquisition, a Bluetooth data transmitter and a battery.

The LED and the photodetectors were placed inside a black paper box made manually to prevent from possible light fluctuations due to the external environment. The data acquisition system was placed inside a plastic box and the battery was completely charged overnight prior to the measurements.

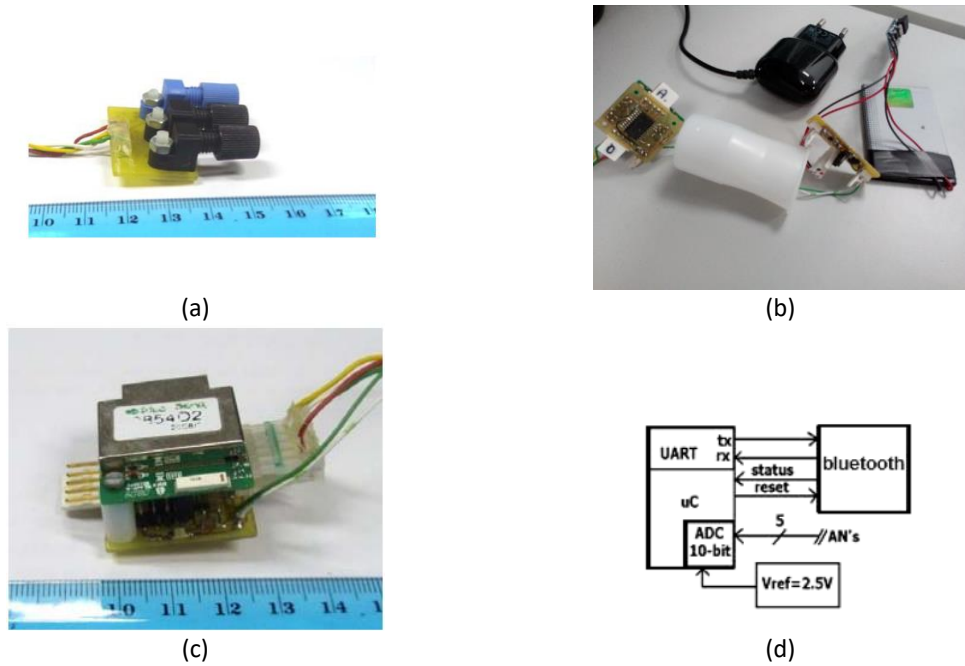


Figure 3.33 (a) LED and photodetectors; (b) data acquisition system; controller board with the wireless module ESD110, photograph (c) and schematic representation (d). [(a,c,d) in (Bilro, 2011)]

The graphical interface, a LabVIEW application, allowed to choose the active virtual serial port, start and stop data acquisition, save the output data as text file and with a graphical visualization of the signal output in real-time monitoring, see Figure 3.34.

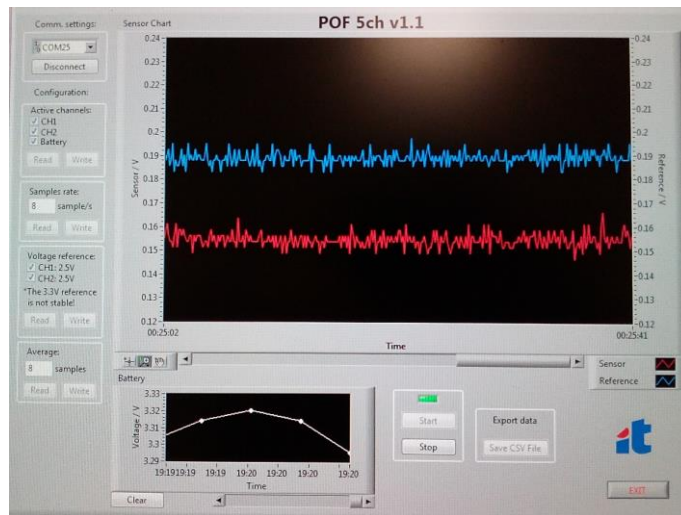


Figure 3.34 Graphical interface available for the user.

The output data, time and the output voltages of the reference and sensor signals, V_{ref} and V_{sensor} respectively (in V), were monitored in real time with the LabVIEW application. The optical power (P) detected at each photodetector is given by:

$$P = \frac{V}{R \times R_{\lambda} \times G} \quad \text{Equation 3.6}$$

where R is the resistance of the photodetector, R_{λ} the responsivity and G the optical gain. The self-referenced transmitted signal (k), ratio between the optical power obtained in each photodetector, was used to correct source fluctuations and variations due to external conditions. The values of responsivity and gain are the same for both photodetectors, thus we obtain:

$$k = \text{smooth} \left(\frac{P_{\text{sensor}}}{P_{\text{ref}}} \right) = \text{smooth} \left(\frac{V_{\text{sensor}} \times R_{\text{PDref}}}{R_{\text{PDsensor}} \times V_{\text{ref}}} \right) \quad \text{Equation 3.7}$$

A smoothing using a 1st order Savitzky-Golay filter was applied using MATLAB software and the average value and standard deviation ($k \pm \delta k$) of 5 min monitoring were calculated. The Savitzky-Golay filter can be understood as a weighted moving average filter that allows the smoothing of continuous physical experiments.

Measurements usually started with distilled water, and the normalized transmitted signal and respective error ($k_{\text{norm}} \pm \delta k_{\text{norm}}$) were calculated as follows:

$$k_{\text{norm}} = \frac{k}{k_{\text{water}}} \quad \text{Equation 3.8}$$

$$\delta k_{\text{norm}} = \sqrt{\left(\frac{1}{k_{\text{water}}} \times \delta k \right)^2 + \left(\frac{-k}{k_{\text{water}}^2} \times \delta k_{\text{water}} \right)^2} \quad \text{Equation 3.9}$$

The normalized transmitted signal was calculated as the ratio with the first measurements performed after signal stabilization for monitoring modification procedures such as initiator immobilization or POF stability in solvent.

Prior to the sensor characterization, the stability of the sensor response was verified with variations below 0.5% for sensor responses being considered acceptable.

At least three replicated measurements were performed with sensor in analyte solutions. The average value and respective standard deviation of the replicated measurements ($k_{\text{avg}} \pm \delta k_{\text{avg}}$) were calculated.

The reproducibility of the results, related to the consistency and agreement among independent measurements can be analysed by calculating the relative error:

$$\text{relative error } (k_{\text{avg}}) = \frac{\delta k_{\text{avgmax}}}{k_{\text{avgmax}}} \times 100 \quad \text{Equation 3.10}$$

where δk_{avgmax} is the maximum value of standard deviation (δk_{avg}) obtained.

The sensitivity (S) of the sensor's response is defined by:

$$S = \left| \frac{\partial k_{avg}}{\partial c} \right| \quad \text{or} \quad S = \left| \frac{\partial k_{avg}}{\partial n_{ext}} \right| \quad \text{Equation 3.11}$$

expressed in terms of concentration (c) or refractive index (n_{ext}) of the external medium.

The resolution (Δn) is defined as the minimum amount of change in concentration or refractive index that can be detected and can be defined as:

$$\Delta n = \frac{1}{S} \cdot \delta k_{norm_{max}} \quad \text{Equation 3.12}$$

where $\delta k_{norm_{max}}$ is the maximum value of standard deviation obtained in all characterizations performed.

3.9 Sensors characterization

The response of the modified fibres was monitored in real-time using the experimental setup described in section 3.8. Modified POFs and functionalized POF-MIP sensors were also characterized with solutions of different analytes.

3.9.1 Response of unclad POFs with temperature variation

The influence of the temperature in the output signal (k) was evaluated for one unclad POF (NJ8). The stability of the response in water at room temperature was previously verified by monitoring the output signal for 1h.

The transmitted signal was normalized using response of an unclad POF immersed in distilled water at room temperature. After 15 min, the water was removed with a syringe and cold water (ca. 4 °) was added to the reactor. The output signal was monitored during 3h - 4h until distilled water in the reactor reached again the room temperature.

The temperature of the external medium (distilled water) was measured each 5 min using a digital thermometer.

Three replicated measurements were performed in order to verify the reproducibility of the response given by the unclad POF.

Figure 3.35 shows changes of self-referenced transmitted signal (k) in real time and normalized transmitted signal ($k_{norm} \pm \delta k_{norm}$) with temperature for one experimental run. Figure 3.36 depicts the data obtained for three replicated measurements.

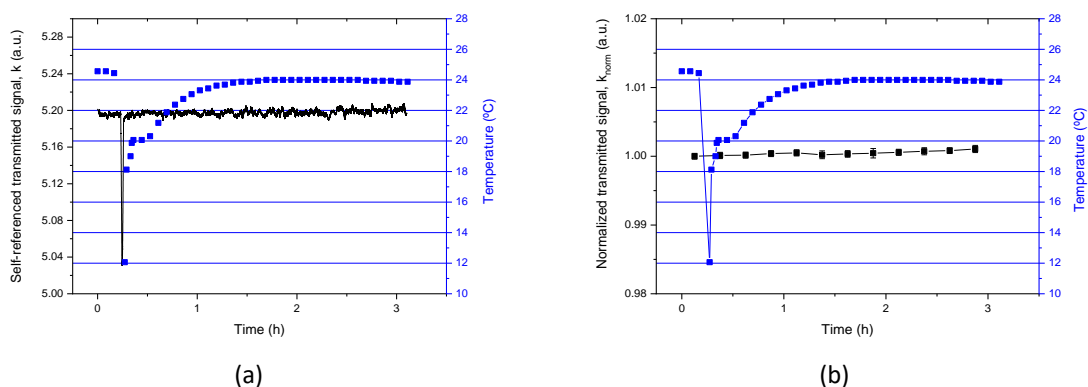


Figure 3.35 Response of the unclad POF NJ8 with temperature variation: (a) self-referenced transmitted signal (k) and (b) normalized output signal ($k_{norm} \pm \delta k_{norm}$).

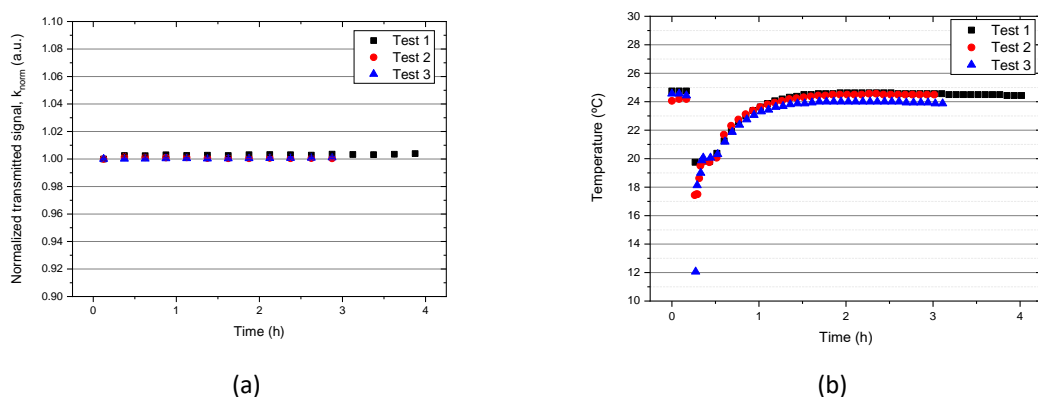


Figure 3.36 Three replicated characterizations – response of the unclad POF NJ8 to the variation of temperature: (a) normalized output signal ($k_{norm} \pm \delta k_{norm}$); (b) temperature variation.

No change of the sensor response (variation < 0.5%) was observed for temperature variation between 12°C and 25°C (Figure 3.35 and Figure 3.36). The drastic variation on the sensor response at 15 min is due to the removal and addition of distilled water to the glass reactor (Figure 3.35).

3.9.2 Initiator immobilization and MIP's grafting on PMMA surface

The immobilization of the initiator and the MIP grafting on the PMMA surface was monitored in real-time for sensor NJ2, see Figure 3.37.

Firstly, stability of the transmitted signal in air (variation < 0.5%) was verified, after which the initiator solution was added to the reactor and the output signal was monitored as previously described (section 3.8). After 4h the initiator was removed from the reactor with a syringe and the sensor was washed with distilled water and left to dry till the next day at room temperature.

The polymerization was monitored in real-time during 5h, after the stability of the sensor response was verified in distilled water.

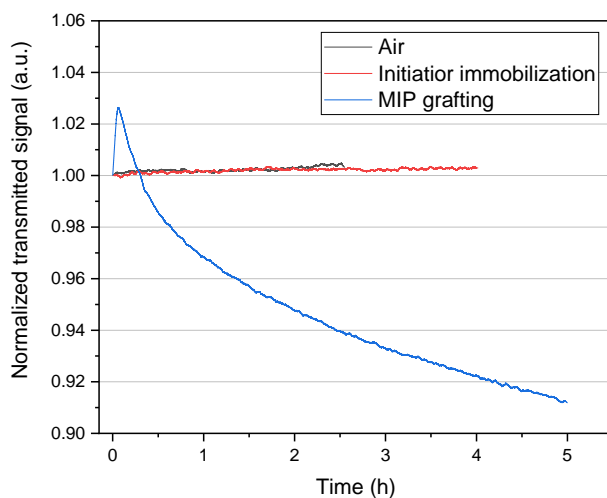


Figure 3.37 Sensor NJ2 – normalized transmitted signal with time in air, with the immobilization of the initiator on the unclad POF's surface and the MIP grafting procedures.

Immobilization of initiator does not affect transmission as no significant variation of the response was observed (below 0.5%). The MIP grafting, on the contrary, causes a $\sim 11\%$ decrease of the transmitted signal.

This decrease in the transmitted signal can be related to surface modification occurring during polymerization, such as cracks formation, which increases the light loss. The grafting of a MIP with higher refractive index than the fibre core also could cause increased light loss, nevertheless, from the results presented in section 3.7, no significant differences on RI were obtained.

Monitoring of the response of unclad POFs using only the solvent solution and mimicking the polymerization conditions is discussed in the next section.

3.9.3 Effect of solvent at polymerization conditions

The polymerization process was mimicked using only the solvent solution (30% of ethanol in distilled water). This experiment aimed at assessing the influence of the solvent on the transmission capacity of unclad POFs and on the sensitivity of the sensors to concentration of template solutions and external refractive index.

C-MAG HS7, an IKA Magnetic Stirrer with a heating plate was used with the accessory ETS-D5, an electronic contact thermometer which allows the measurement of temperature with 0.1 K resolution and ± 0.2 K accuracy. Figure 3.38 depicts the experimental setup.

The responses for the unclad POFs NJ8 and NJ9 are depicted in Figure 3.39.

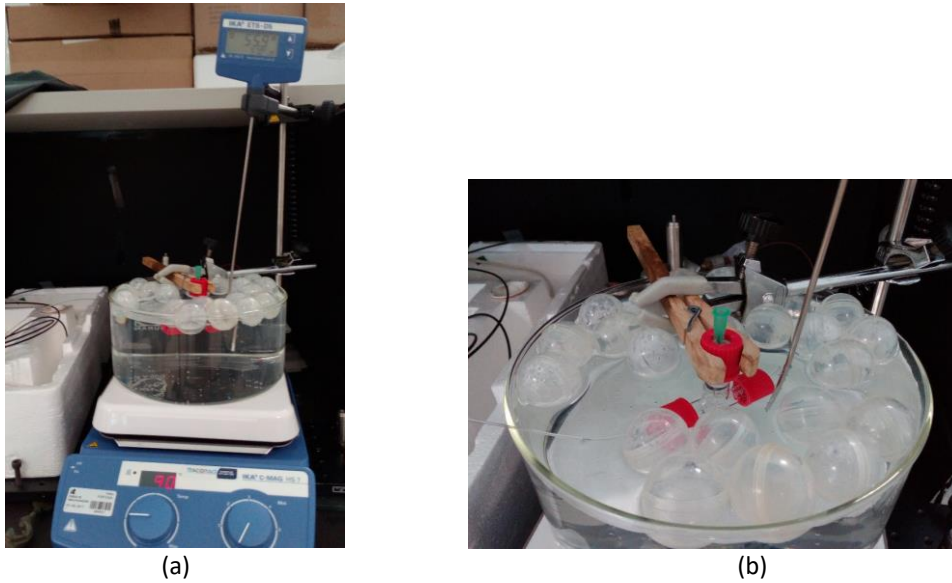


Figure 3.38 Experimental setup for the monitoring of unclad POF's response in solvent mimicking polymerization conditions.

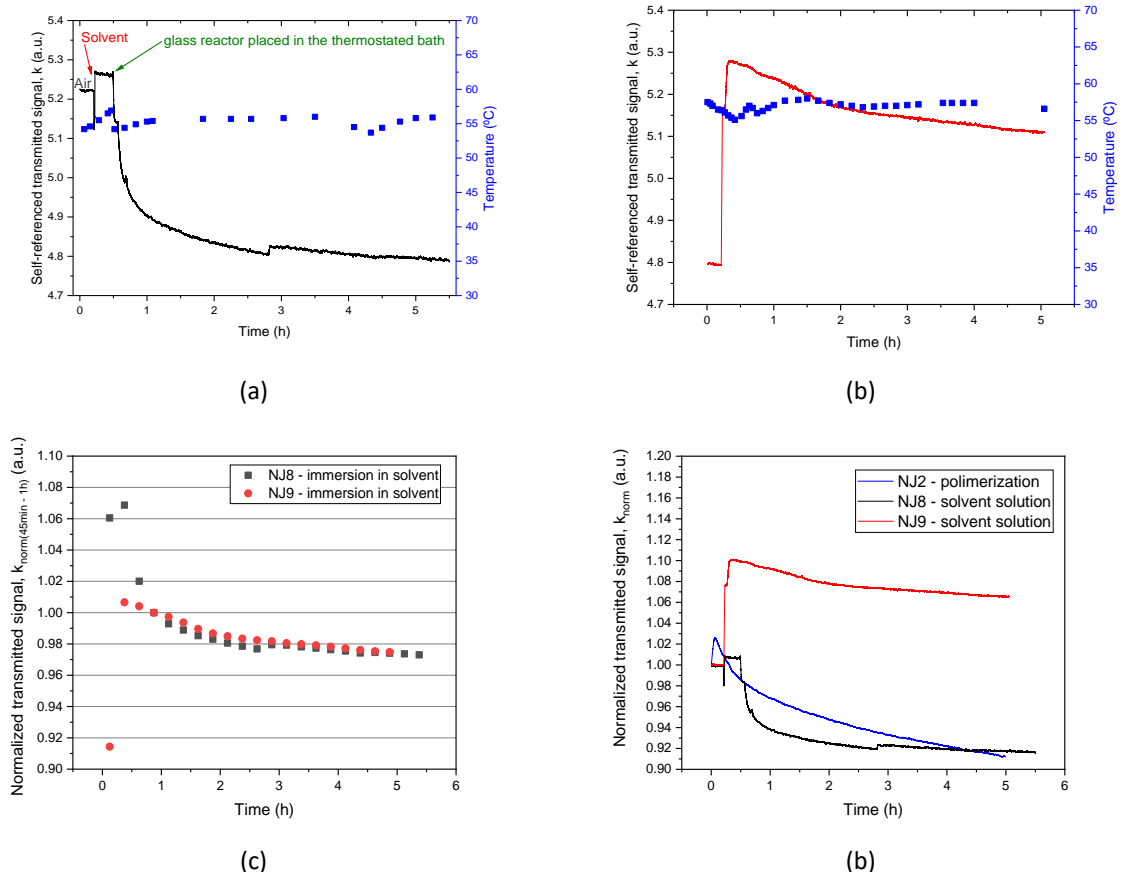


Figure 3.39 Unclad POF's response by immersion in solvent mimicking the polymerization conditions (time and temperature): self-referenced transmitted signal (a) NJ8 and (b) NJ9; (c) normalized transmitted signal with ratio to the value of k obtained between 45 min and 1h; (d) comparison between polymerization (NJ2) and immersion in solvent solution (NJ8, NJ9) in the same conditions.

The total light loss after 5h exposure to the polymerization solution or solvent was very similar (POFs NJ8 and NJ2,) though trajectories of the decrease were different.

Therefore, we can conclude that the transmission loss observed during polymerization is probably associated with the action of solvent. Further studies are needed to understand the influence of the solvent on the sensitivity to variations on the external medium.

3.9.4 Response to the template analyte (NH_4^+)

The MIP grafted fibres (POF-MIP) were characterized in the ammonium chloride solutions (NH_4Cl) (see section 3.3.4). A certain volume of previously prepared NH_4Cl solutions of different concentrations was added to the reactor each 15 min. The final concentrations were: 0 M, 1×10^{-3} M, 1×10^{-2} M, 1×10^{-1} M, 2×10^{-1} M, 4×10^{-1} M and 6×10^{-1} M, corresponding to a refractive index range 1.3325 – 1.3387. The refractive index of NH_4Cl solutions was measured using the Abbemat refractometer with 1×10^{-4} resolution.

The stability of the transmitted signal was first evaluated in distilled water. The sensor response was considered stable when the variation was below 0.5%.

POF-MIP's characterization was performed with constant stirring, the sensor response was expressed as the normalized transmitted signal to water, $(k_{norm} \pm \delta k_{norm})$ (see section 3.8). After each calibration, fibres were washed with distilled water. Figure 3.40 depicts the real-time response (k) of the sensor NJ2 in NH_4^+ solutions followed by three washing steps with distilled water.

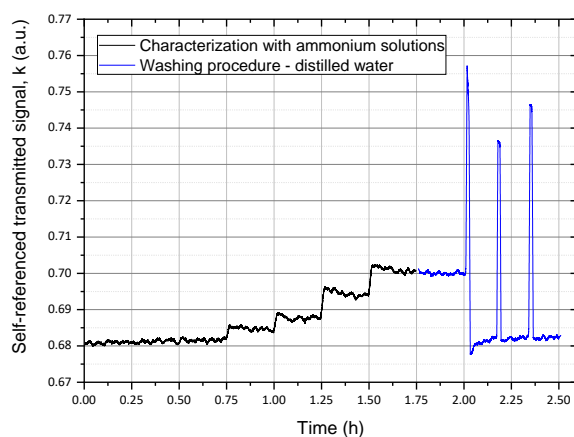


Figure 3.40 POF-MIP NJ2 – real-time characterization with ammonium solutions of increased concentration, followed by washing distilled water.

After addition of 1×10^{-3} mol/L and 1×10^{-2} mol/L of ammonium chloride (between 0.25h – 0.50h and 0.50h – 0.75h), which had RI of 1.3325 and 1.3326, respectively, no change of the self-referenced transmitted signal (k) was observed. In the solutions with concentrations of 1×10^{-1} mol/L with RI of 1.3336 or higher, the sensor response is very clear and fast, less than 1 minute. The recovery of the signal was obtained after washing with distilled water (see Figure 3.40).

At least three replicated measurements were performed for each functionalized fibre with the aim to verify the reproducibility on the response ($k_{norm} \pm \delta k_{norm}$). Generally, the first calibration was not considered as smaller values for the transmitted signal were obtained, a common behaviour observed with chemical sensors (see Figure 3.41).

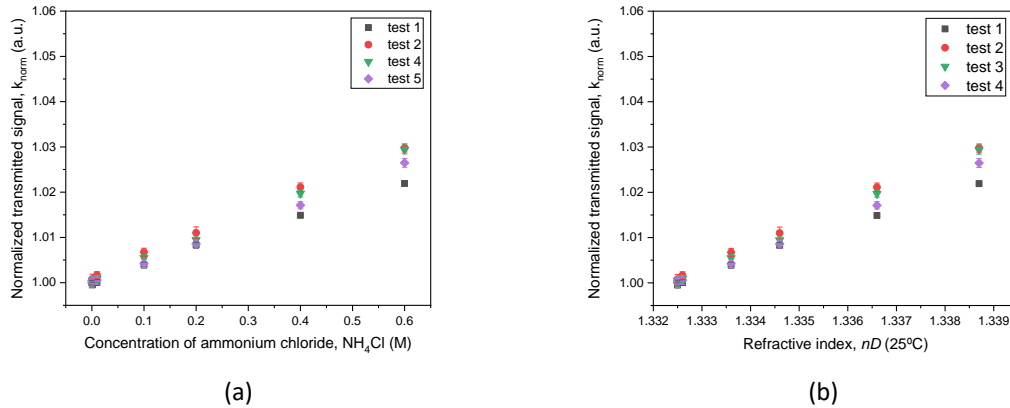


Figure 3.41 POF-MIP NJ2 response ($k_{norm} \pm \delta k_{norm}$) in solutions with increasing concentration of ammonium (NH_4^+) plotted vs.: (a) concentration; (b) refractive index.

The mean sensor response ($k_{avg} \pm \delta k_{avg}$) was calculated as described in section 3.8. As an example, Figure 3.42 depicts the mean response obtained for the functionalized POF-MIP NJ2.

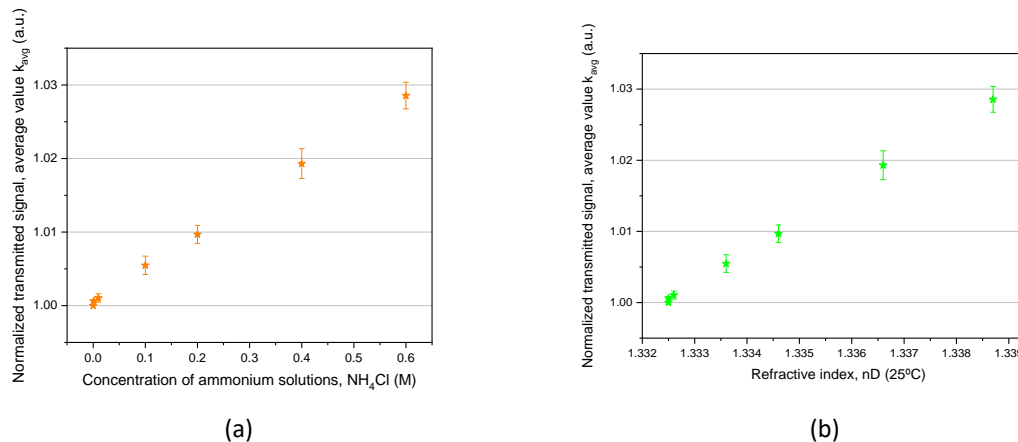


Figure 3.42 POF-MIP NJ2 mean response ($k_{avg} \pm \delta k_{avg}$) in the solutions with increasing concentration of ammonium (NH_4^+) plotted vs.: (a) concentration; (b) refractive index.

The mean responses obtained for several functionalized POF-MIPs (NJ1 – NJ4) are depicted in Figure 3.43(a) and were compared with the response of the unmodified unclad fibres, Figure 3.43(b). POF-MIPs were functionalized using the same reaction mixture (MIP) with different polymerization times. POF-MIP NJ3 was kept hydrated.

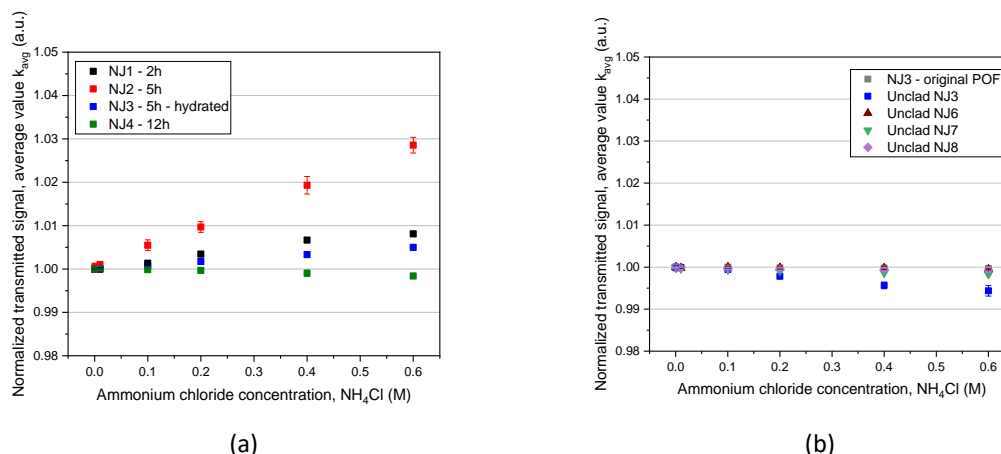


Figure 3.43 Response ($k_{avg} \pm \delta k_{avg}$) of the POF-MIP functionalized fibres (a), unmodified and unclad POFs (b) in the solutions with increasing concentration of ammonium (NH_4^+).

Unmodified fibre and unclad POFs do not respond to the variation of analyte (NH_4^+) concentration (Figure 3.43(b)). The same behaviour was observed for the fibre polymerized for 12h (NJ4).

POF-MIP NJ1 (polymerized for 2h) and POF-MIP NJ3 (polymerized for 5h and kept hydrated) showed an increase of the sensor response below 1%. POF-MIP NJ2 (polymerized for 5h) showed the highest increase of the transmitted signal, almost 3%.

The maximum response and maximum error can be found in Table 3.18. The results can be considered reproducible as the relative error was below 0.20% for all measurements.

Table 3.18. Response of functionalized POF-MIPs in the solutions with increasing concentration of ammonium: maximum response ($k_{avg,max}$), maximum error between experiments ($\delta k_{avg,max}$) and relative error calculated by Equation 3.10.

| POF-MIP | Maximum response $k_{avg,max}$ (a.u.) | Maximum error $\delta k_{avg,max}$ (a.u.) | Relative error (%) |
|-----------|--|--|--------------------|
| NJ1 – 2h | 1.008 | 0.4×10^{-3} | 0.04 |
| NJ2 – 5h | 1.028 | 2.0×10^{-3} | 0.19 |
| NJ3 – 5h | 1.005 | 0.3×10^{-3} | 0.03 |
| NJ4 – 12h | 0.998 | 0.7×10^{-3} | 0.07 |

A linear fit was applied to the obtained results (see Figure 3.44) and the fitting parameters together with the maximum error of all measurements are presented in the Table 3.19.

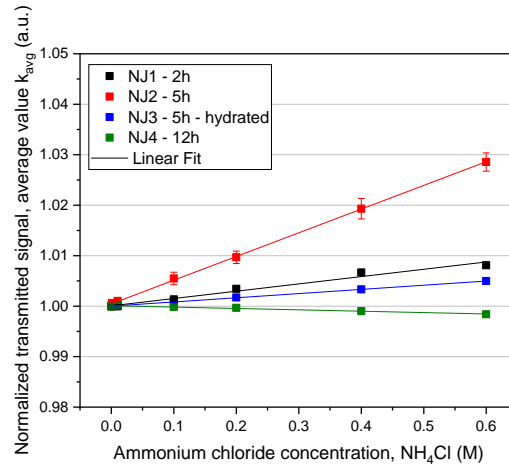


Figure 3.44 Response ($k_{avg} \pm \delta k_{avg}$) of the POF-MIP functionalized fibres in the solutions with increasing concentration of ammonium (NH_4^+) and linear fit applied.

Table 3.19. Response of functionalized POF-MIPs in the solutions with increasing concentration of ammonium: maximum error of all measurements ($\delta k_{norm_{max}}$) and the linear fit parameters.

| POF-MIP | $\delta k_{norm_{max}}$ (a.u.) | m | b | Adj. R^2 |
|------------------|-----------------------------------|-----------------------------------|----------------------------------|------------|
| NJ1 – 2h | 4.91×10^{-4} | $0.0145 \pm 9.4 \times 10^{-04}$ | $1.0001 \pm 2.7 \times 10^{-04}$ | 0.9750 |
| NJ2 – 5h | 9.75×10^{-4} | $0.0470 \pm 4.8 \times 10^{-04}$ | $1.0004 \pm 1.4 \times 10^{-04}$ | 0.9994 |
| NJ3 – 5h | 5.49×10^{-4} | $0.0083 \pm 0.9 \times 10^{-04}$ | $1.0000 \pm 0.3 \times 10^{-04}$ | 0.9992 |
| NJ4 – 12h | 7.29×10^{-4} | $-0.0027 \pm 1.7 \times 10^{-04}$ | $1.0001 \pm 0.5 \times 10^{-04}$ | 0.9762 |

The sensitivity (S) and resolution (Δn) of the POF-MIPs to the variation of ammonium concentration as well as the linear fitting of experimental data were calculated according to the Equation 3.11 and Equation 3.12, respectively (see Table 3.20):

$$S = \left| \frac{\partial k_{avg}}{\partial c} \right| = |m| \quad \text{and} \quad \Delta n = \frac{1}{S} \cdot \delta k_{norm_{max}} = \frac{1}{|m|} \cdot \delta k_{norm_{max}}$$

Table 3.20. Sensitivity and resolution of POF-MIP sensors in ammonium solutions calculated using Equation 3.11 and Equation 3.12.

| POF-MIP | S (a.u.M ⁻¹) | Δn (M) |
|------------------|----------------------------|------------------------|
| NJ1 – 2h | 1.45×10^{-2} | 3.39×10^{-2} |
| NJ2 – 5h | 4.70×10^{-2} | 2.07×10^{-2} |
| NJ3 – 5h | 0.83×10^{-2} | 6.61×10^{-2} |
| NJ4 – 12h | 0.27×10^{-2} | 27.00×10^{-2} |

It was found that only ammonium concentrations above 0.1 mol/L lead to the detectable signal variation. Although calculated resolution for POF-MIPs NJ1, NJ2 and NJ3 are lower, the minimum concentration that could be detected is about 0.1 mol/L for POF-MIP NJ2. For other POF-MIPs the total response variation was lower than 1%.

The POFs subjected to heating in solvent (NJ8 and NJ9) mimicking the polymerization conditions were also characterized in solutions of ammonium chloride. Their response is depicted in Figure 3.45.

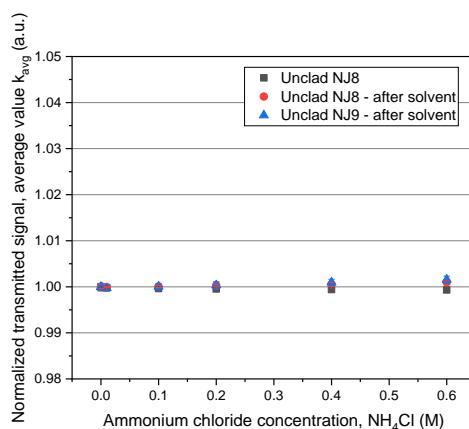


Figure 3.45 Response ($k_{avg} \pm \delta k_{avg}$) of unclad POFs before (NJ8) and after (NJ8, NJ9) heating in solvent at polymerization conditions, in ammonium solutions with increasing concentrations.

Fibres that were heated in solvent mimicking polymerization conditions for 5h displayed no response to ammonium. Therefore, sensitivity of the POF-MIP NJ2 sensor is not due to alterations of the fibre surface caused by the exposure to ethanol/water mixture at 57 °C.

3.9.5 POF-MIP sensor response to interferences – NaCl and D-(+)-glucose

The response of the POF-MIPs was evaluated in the solutions of sodium chloride (NaCl) and D-(+)-glucose. The solutions were prepared to have the same refractive index as the solutions of template analyte (ammonium chloride) previously used for sensor characterization, see section 3.3.4.

Sodium chloride was chosen due to the similarity of the sodium ion (Na⁺) with ammonium ion (NH₄⁺). Both are positively charged ions, with ionic radii of 1.02 Å and 1.43 Å, respectively (Gómez *et al.*, 2011)(Buurman *et al.*, 1989). Therefore, sodium is a likely interferent that could also bind to MIP imprinted with ammonium ions. D-(+)-glucose is a molecule with bigger size and molecular weight. This experiment aimed to elucidate if POF-MIP sensor could discriminate between different compounds or responded solely to the changes of the external medium, RI.

The response ($k_{avg} \pm \delta k_{avg}$) of the POF-MIP NJ2 to all three compounds is shown in Figure 3.46. The mean response was calculated as described in section 3.8.

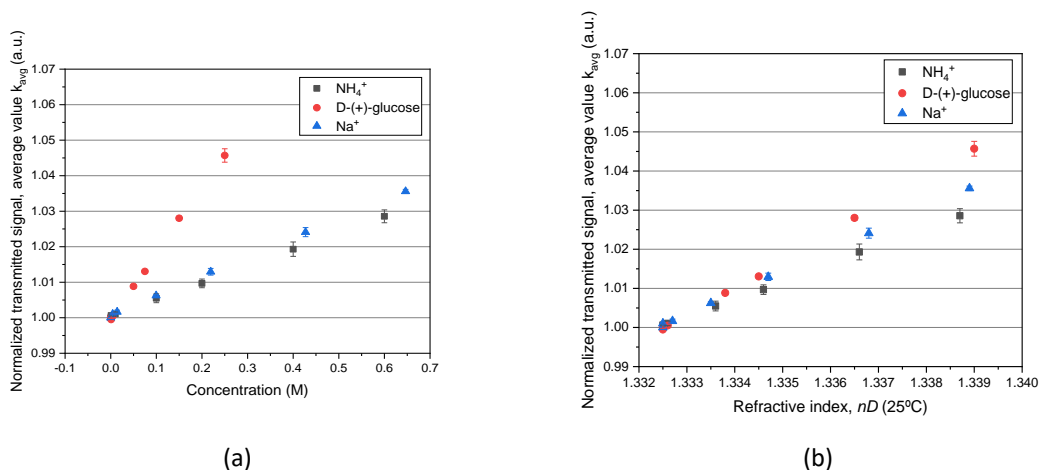


Figure 3.46 Response ($k_{avg} \pm \delta k_{avg}$) of the POF-MIP NJ2 (5h) in the solutions of ammonium chloride, D-(+)-glucose and sodium chloride plotted vs.: (a) concentration and (b) refractive index.

The sensor response was very different in terms of concentration of the analyte particularly to the response obtained with D-(+)-glucose. However, sensor response with respect to RI was similar in the solutions of three compounds, suggesting that the POF-MIP NJ2 is responding to changes on the refractive index of the external medium.

Measurements with POF-MIP sensor were made in mixed solutions of these analytes and the obtained responses are depicted in Figure 3.47. Mixed solutions were prepared with the constant concentration of one of the analytes and varying the concentration of the other. The responses obtained in the individual solutions of each of the analytes is also depicted for comparison.

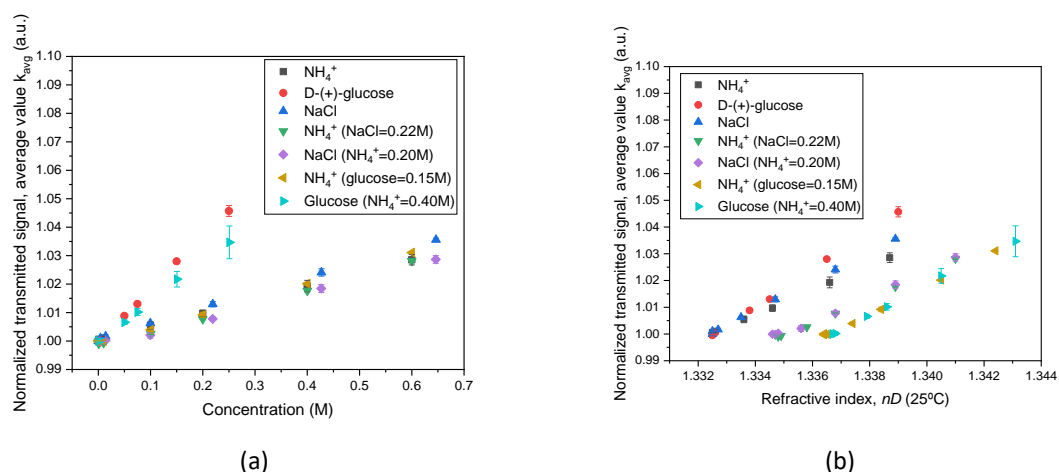


Figure 3.47 Response ($k_{avg} \pm \delta k_{avg}$) of the POF-MIP NJ2 (5h) in the mixed solutions of ammonium chloride, D-(+)-glucose and sodium chloride plotted vs.: (a) concentration and (b) refractive index.

Measurements in mixed solutions revealed POF-MIP selectivity towards the ammonium ion. No interference was observed at glucose or sodium concentrations of 0.15 mol/L and 0.22 mol/L, respectively. Despite the large responses to glucose it was attenuated in the presence of 0.4 mol/L of ammonium.

In terms of refractive index, Figure 3.47(b), a similar increase in the response was obtained with the increase of refractive index, independently of the analyte which concentration is increasing.

3.9.6 Sensitivity to refractive index variation

The response of the POF-MIPs to refractive index variation from 1.33 to 1.41 was evaluated in solutions of sucrose. The experimental procedures and data processing are described in section 3.8.

Sucrose stock solution was prepared in distilled water and used to prepare solutions of lower concentration by dilution (section 3.3.4.1 and Equation 3.3). The refractive index of the sucrose solutions was measured using Abbemat refractometer (resolution of 10^{-4} RIU).

Prior to the RI measurements, the POF-MIPs response in distilled water was monitored until it stabilized ($<0.5\%$ variation). The response ($k_{norm} \pm \delta k_{norm}$) in distilled water is depicted in Figure 3.48(a).

Response to RI was measured in sucrose solutions with increasing concentrations. After each addition of sucrose solutions, sensor was left to stabilize for 15 min with magnetic stirring. Solutions' RI was measured right after being removed from the reactor with the Abbemat refractometer. Before addition of each solution, the reactor was washed with it to remove any residues of the previous solution. After calibration measurements were completed, the reactor was washed twice with distilled water, which allowed to verify the recovery of the transmitted signal and wash the sensor and reactor. Three replicated measurements were carried, see Figure 3.48(b).

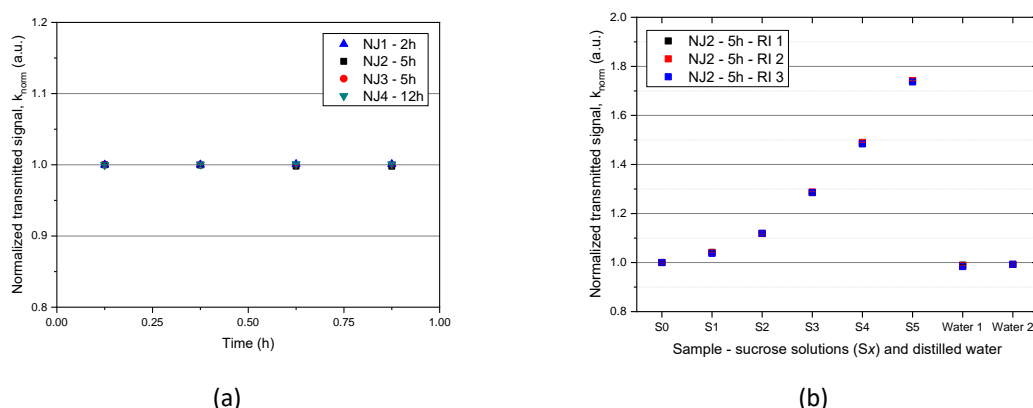


Figure 3.48 Response ($k_{norm} \pm \delta k_{norm}$) of the (a) POF-MIPs in distilled water; (b) NJ2 (5h) to RI in sucrose solutions (samples S0 – S5) and recovery of the transmitted signal in distilled water (water 1 , water 2).

The average value obtained for the three characterizations and respective standard deviation were calculated ($k_{avg} \pm \delta k_{avg}$). The error of k_{avg} (δk_{avg}) is only representative of the repeatability of the obtained results, while the error of k_{norm} (δk_{norm}) is related to the signal fluctuation during 5 min monitoring.

The response of the POF-MIPs in sucrose solutions is depicted in Figure 3.49(a). POFs heated in solvent mimicking polymerization conditions were also characterized in sucrose solutions. Obtained responses are depicted in Figure 3.49(b).

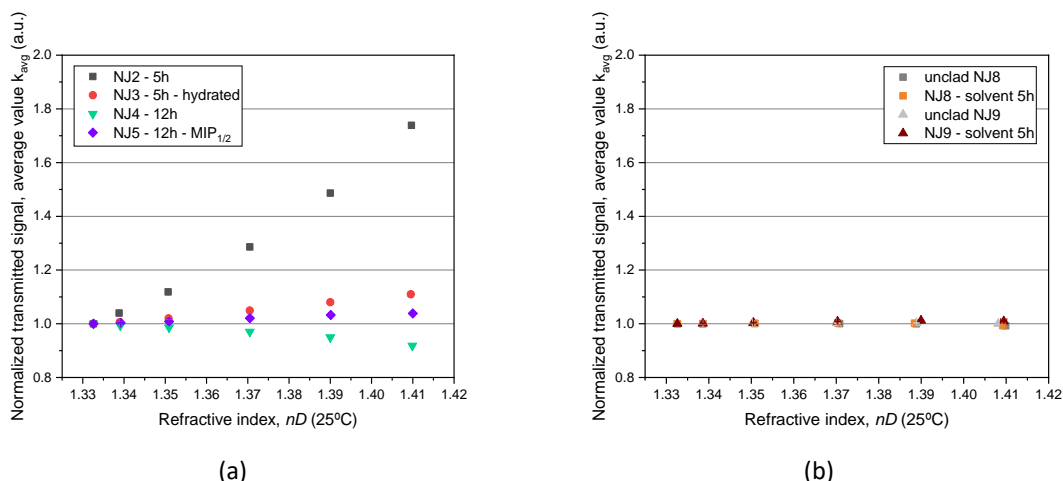


Figure 3.49 Response ($k_{avg} \pm \delta k_{avg}$) to the refractive index variation in sucrose solutions: (a) POF-MIPs; (b) POFs before and after heating in solvent at polymerization conditions (5h).

POFs submitted to heating in solvent at polymerization conditions (5h) do not respond to the refractive index variation.

The highest sensitivity was observed for POF-MIP NJ2 (5h) with an increase of 74% of the transmitted signal with RI increase from 1.33 to 1.41. The POF-MIP polymerized in the same conditions but kept hydrated (NJ3) only showed an increase of 11% and NJ4, polymerized for 12h, showed an increase of 4%. These POF-MIPs also presented less cracks on the surface (section 3.5.4.3).

The POF-MIP NJ5, polymerized in the polymerization mixture with lower concentration (MIP_{1/2}), showed a decrease of the transmitted signal of 8%.

The POF-MIPs sensitivity to external medium variations seems to be related to the damage of the POF's surface, such as cracks, but also to polymerization conditions such as concentration of the reagents and polymerization time. Fibres heated in solvent (NJ8, NJ9) and POF-MIP NJ5 (12h, MIP_{1/2}) also revealed cracks on the surface but no response to the refractive index variation.

The maximum response and maximum error between experiments can be found in Table 3.21. The results can be considered reproducible as the relative error was below 0.80% for all POF-MIP measurements.

Table 3.21. POF-MIPs – response to RI: maximum response ($k_{avg_{max}}$), maximum error between experiments ($\delta k_{avg_{max}}$) and relative error calculated by Equation 3.10.

| POF-MIP | Maximum response $k_{avg_{max}}$ (a.u.) | Maximum error $\delta k_{avg_{max}}$ (a.u.) | Relative error (%) |
|--------------------------------------|--|--|--------------------|
| NJ2 – 5h | 1.739 | 3.2×10^{-3} | 0.18 |
| NJ3 – 5h | 1.110 | 8.0×10^{-3} | 0.72 |
| NJ4 – 12h | 0.918 | 1.8×10^{-3} | 0.20 |
| NJ5 – 12h – MIP_{1/2} | 1.038 | 3.1×10^{-3} | 0.30 |

An exponential fit was applied to the obtained data (see Figure 3.50) and the fitting parameters together with the maximum error are presented in the Table 3.22.

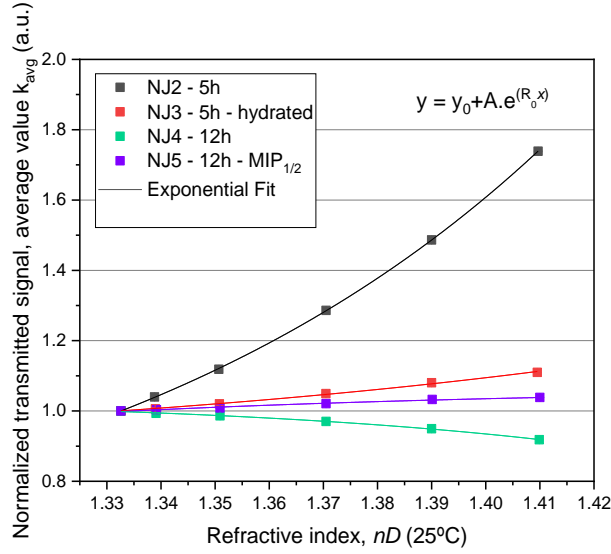


Figure 3.50 POF-MIPs' response ($k_{avg} \pm \delta k_{avg}$) to refractive index in sucrose solutions and exponential fit of the data.

Table 3.22. POF-MIPs response to RI: maximum error for the series of calibrations ($\delta k_{norm_{max}}$) and parameters of the exponential fit.

| POF-MIP | $\delta k_{norm_{max}}$ (a.u.) | R_0 | A | Adj. R^2 |
|--------------------------------|-----------------------------------|-----------------------------------|--|------------|
| NJ2 – 5h | 2.7×10^{-3} | $11.20 \pm 8.72 \times 10^{-15}$ | $1.77 \times 10^{-07} \pm 2.26 \times 10^{-21}$ | 1.0000 |
| NJ3 – 5h | 7.0×10^{-4} | $7.90 \pm 1.01 \times 10^{-14}$ | $3.56 \times 10^{-06} \pm 5.42 \times 10^{-20}$ | 1.0000 |
| NJ4 – 12h | 6.0×10^{-4} | $-10.74 \pm 1.96 \times 10^{-14}$ | $-1.16 \times 10^{+05} \pm 2.90 \times 10^{-09}$ | 1.0000 |
| NJ5 – 12h – MIP _{1/2} | 4.4×10^{-4} | $14.69 \pm 1.14 \times 10^{-14}$ | $-1.18 \times 10^{-10} \pm 1.94 \times 10^{-24}$ | 1.0000 |

The sensitivity (S) and resolution (Δn) to refractive index variation were calculated using Equation 3.11 and Equation 3.12. Exponential fit was applied to the obtained results:

$$S = \left| \frac{\partial k_{avg}}{\partial n_{ext}} \right| = |R_0 \cdot A \cdot e^{R_0 \cdot n_{ext}}| \quad \text{Equation 3.13}$$

$$\Delta n = \frac{1}{S} \times \delta k_{norm_{max}} = \frac{1}{|R_0 \cdot A \cdot e^{R_0 \cdot n_{ext}}|} \times \delta k_{norm_{max}} \quad \text{Equation 3.14}$$

where $\delta k_{norm_{max}}$ is the maximum value of standard deviation of all the tests performed, for each sensor, see Table 3.22. The sensitivity and resolution are depicted in Figure 3.51.

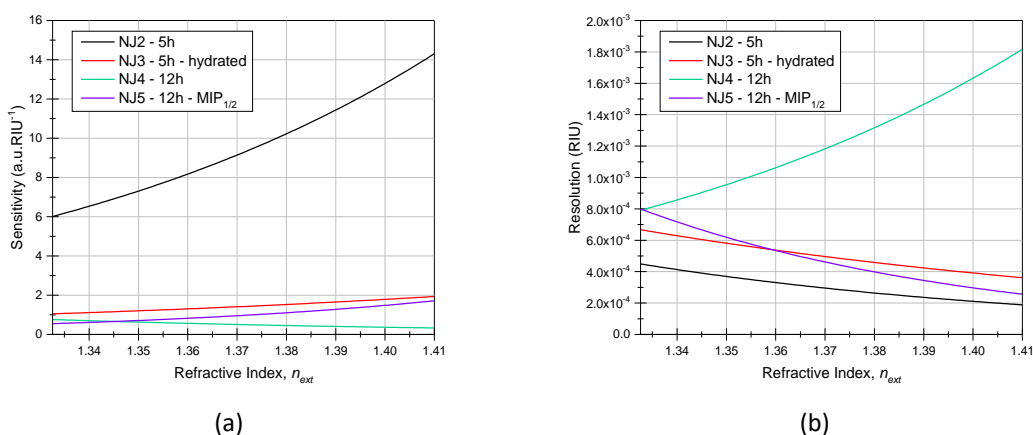


Figure 3.51 POF-MIPs sensitivity and resolution to refractive index variation (RI: 1.3326 – 1.41).

POF-MIP NJ2 (5h) displayed sensitivity to refractive index variation between 6 – 14 au.RIU⁻¹ and a resolution below 5×10^{-4} RIU in the studied refractive index range. Sensitivity obtained for the other POF-MIPs (NJ3 and NJ4) was very low (< 2 au.RIU⁻¹) and resolutions lower than 7.0×10^{-4} RIU and 1.8×10^{-3} RIU were obtained for POF-MIPs NJ3 and NJ4, respectively.

3.10 Conclusions and future developments

Several aspects of MIP grafting procedures on PMMA based POFs were evaluated with these studies.

A successful procedure for cladding removal was optimized using solutions of acetone and distilled water. Even so, unclad POF samples did not respond to refractive index variation (1.33 – 1.41), therefore the fibre should be further sensitized for sensing applications.

Different surface morphologies were obtained after MIP grafting to PMMA slabs and unclad POF using the same polymerization conditions. This can suggest that removing the cladding with acetone solutions can inhibit the immobilization of the initiator on the POF's surface.

Detection of initiator AAPH on the unclad fibre surface was not possible by FTIR-ATR and Raman spectroscopy, or labelling with rhodamine B ICT.

Immobilization of the initiator on the fibre surface did not affect light transmission as no significant variation of the response was observed (lower than 0.5%). The MIP grafting, on the contrary, caused a decrease in the transmitted signal of ~11%, also observed after unclad POFs were heated in solvent mimicking polymerization conditions.

Heating in solvent at polymerization conditions caused increase of mass and thickness as well as the appearance of cracks on the POF's surface. Nevertheless, these alterations did not render fibres sensitive to external medium refractive index, including sucrose solutions with refractive index varying between 1.33 to 1.41.

POF-MIPs in general showed very low sensitivity to variations of external medium RI, with sensitivity below 2 au.RIU⁻¹ for a refractive index variation between 1.33 and 1.41 and a maximum response below 1% with solutions of the template analyte (0 – 0.6 mol/L, NH₄Cl).

Only sensor NJ2, polymerized for 5h, responded to concentration variation of the different analytes, with a sensitivity of around 0.05 a.u.M^{-1} to ammonium anion, the template analyte (maximum response of 2.8%). Some selectivity towards ammonium ion was observed in mixed solutions. Nevertheless, higher response was obtained in solutions of D-(+)-glucose and sodium chloride (maximum responses of 3.6% and 4.6%, respectively) compared to ammonium chloride.

POF-MIP NJ2 displayed sensitivity between $6 - 14 \text{ au.RIU}^{-1}$ and a resolution below $5 \times 10^{-4} \text{ RIU}$ in solutions of sucrose with refractive index varying from 1.33 to 1.41.

Low specificity was obtained to the template analyte, while highly sensitive response was observed to refractive index variation. These results indicate that sensors responded to both binding of the analyte by the imprinted sites and external medium RI.

Several explanations can be put forward for the obtained results. Polymerization process can damage polymeric fibre, increasing light loss and interaction between the light that propagates in the fibre and the external medium. At the same time, longer polymerization time did not impart higher sensitivity to the fibres, on the contrary, it appears that polymer growth diminished the fibre sensitivity to the variations of external medium RI.

Several improvements of the optical setup were made. A low-cost sensing setup based on intensity modulation was implemented. The signal was self-referenced by adding a reference POF and the stability of the transmitted signal was improved.

Used washings procedures were sufficient to ensure reproducibility of the sensor responses and signal recovery. Sensor responses to the changes of the concentration or external medium RI were immediate, revealing promising possibilities for POF sensor development.

This chapter highlighted the difficulties inherent to the development of POF chemical sensors using MIPs as sensitive layers, which allowed the understanding and optimization of different techniques and was the basis of questioning responsible for further developments.

To conclude, new studies were needed which paved the way to the work developed and reported in the subsequent chapters:

- optimization of the POF's sensitivity to variations on the external medium;
- development of new POF sensor's geometries;
- ensure the sensing characteristics of the sensitive layer, including specificity to the target analyte, prior to deposition on the POF's surface;
- combine POF's with sensitive layers using other deposition methods or polymerization procedures;
- assessment of the sensitive layer deposition on POF's surface by optical characterization (i.e. through the use of specific labels).

Chapter 4 Intensity based POF refractive index sensors – performance and optimization

4.1 Introduction

This chapter presents the studies performed aiming the development of low-cost POF refractive index (RI) sensors. Two intensity based sensing platforms were developed and characterized. One based on D-shaped POF's (section 4.2) and the other in modified straight POFs (section 4.3). Studies related with the performance optimization of the D-shaped POF sensors with the variation of length and roughness of the sensing region were performed. The performance of the straight POF sensors was analysed and optimized with the variation of the roughness and curvature of the sensing region. POFs with 1 mm diameter from Asahi Kasei were selected for these studies.

4.2 D-shaped POF RI sensors

D-shaped POF sensors for refractive index sensing were developed and optimized. Sensing principles were based in intensity based modulation, allowing easy and low-cost implementation that could replace or be complementary to plasmonic sensing with POF in chemical sensing applications. First, the suitability of this sensing platform was evaluated and optimized for RI sensing.

4.2.1 General manufacturing procedures

The commercially available POFs from Asahi Kasei, DB-1000, with 1 mm diameter (d) were selected for this study (characteristics described in Table 2.2, Chapter 2. The POFs were cut to the desired length with a POF cutter and embedded in grooves in planar supports.

The D-shaped sensors were obtained by polishing the fibres in the planar support with polishing papers of different grain sizes and with “Figure ∞ ” pattern. Higher grit size polishing paper, e.g. 5 μm , was used to remove the cladding and part of the core until the surface of the planar supports was reached and a grey line was seen at naked eye. Lower grit sizes, e.g. 3 μm and/or 1 μm were used to obtain smoother surfaces. In this process the cladding and part of the core were removed, as depicted in Figure 4.1.

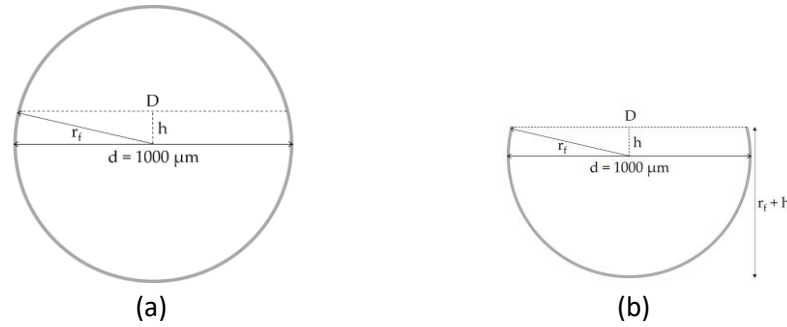


Figure 4.1 Schematic representation of the POF before (a) and after (b) the polishing procedures.

The total height of the produced sensors ($r_f + h$) can therefore be calculated by the Pythagorean theorem:

$$r_f^2 = h^2 + \left(\frac{D}{2}\right)^2 \quad \text{Equation 4.1}$$

where r_f is the POF radius and D is the thickness of the sensing region.

4.2.2 Preliminary results

4.2.2.1 Length of the sensing region

Preliminary studies on the influence of the sensing region length on the performance of D-shaped POF sensors for refractive index sensing were conducted.

4.2.2.1.1 Experimental setup

Three D-shaped POF sensors with different lengths were prepared according to the procedures described in section 4.2.1 (length around 21 cm). The D-shaped POF sensors were obtained by polishing the fibres in the planar support (resin block, PROLAB45, Axson Italie) with polishing papers of 5 μm (LFG5P), 3 μm (LFG3P) and 1 μm (LFG1P) grit size with “Figure ∞ ” pattern. D-shaped POF sensors with a sensing region length of 1 cm (D1), 3 cm (D2) and 5 cm (D3) were manufactured as depicted in Figure 4.2.

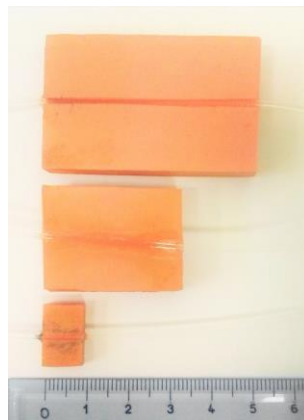


Figure 4.2 D-shaped POF sensors with 1 cm, 3 cm and 5 cm length.

The variation of the external refractive index (n_{ext}) will cause a variation in the light that reaches the photodetector after being transmitted through the D-shaped sensors and can be monitored by an intensity based detection scheme.

The experimental setup, as shown in Figure 4.3 (a,c,d), comprised a stabilized power supply (ELIND 32DP32), an LED (Avago SFH757V, wavelength centered at 650 nm, see Figure 4.3 (b)), a 50:50 POF coupler (Luccat, Splitter 1x2, SI POF 50/50, Class 5 product N°S51-01), two photodetectors (Avago SFH250V) and a Picoscope (PicoScope 6) connected to a laptop.

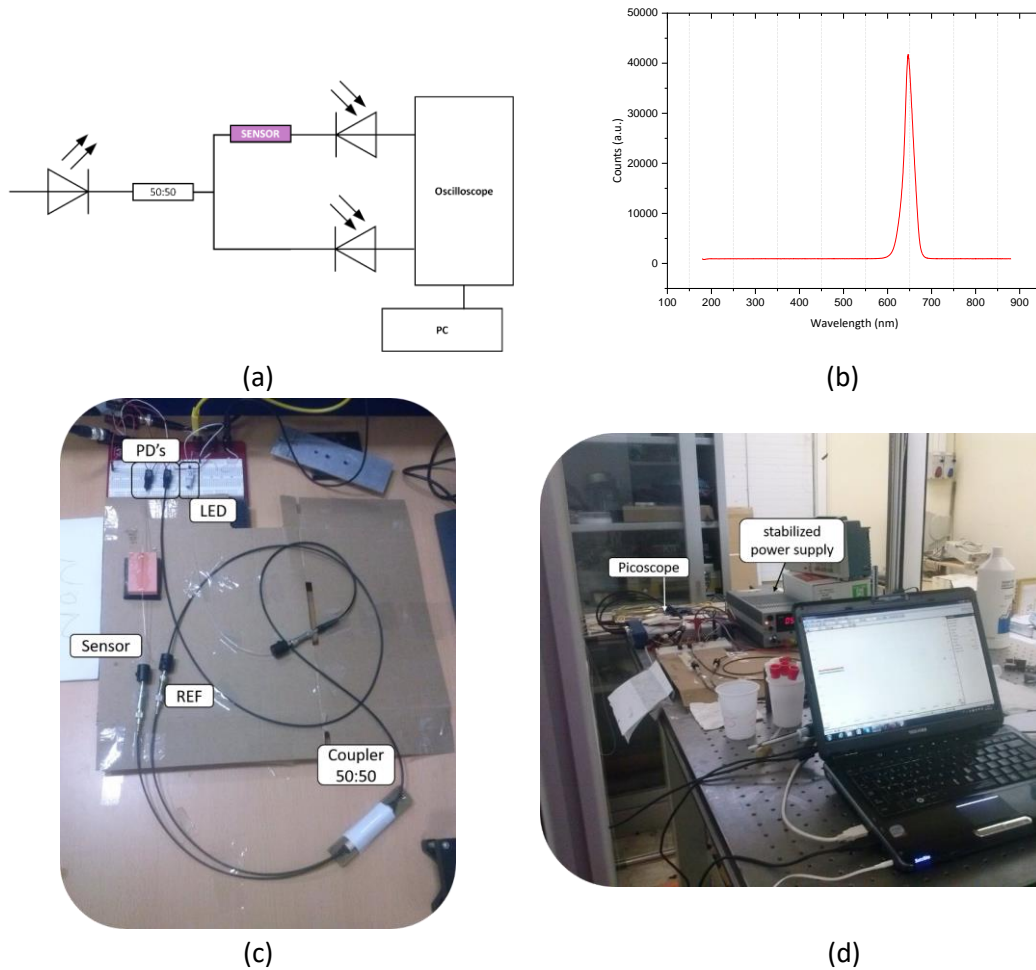


Figure 4.3 (a) Outline of the experimental setup; (b) LED spectrum; (c,d) experimental apparatus.

The data acquisition protocol consisted on obtaining reference and sensor signals, V_{ref} and V_{sensor} respectively which were logged into a laptop by means of Picoscope's software.

The parameter self-referenced transmitted signal (k) was used to correct source fluctuations and variations due to external conditions, as described in section 3.8, Chapter 3.

4.2.2.1.2 Refractive index characterization

The response of the D-shaped POF sensors to refractive index variation was studied by placing water-glycerin solutions with different refractive indices on the sensing area. The solutions of glycerin were prepared with distilled water and the refractive index was measured with an Abbe

refractometer (Model RMI, from *Exacta* and *Optech Labcenter*). The glycerin was purchased from Carlo Erba Reagenti. The refractive index of the solutions varied from 1.332 to 1.385.

After placing each solution on the sensing region of the D-shaped sensor, the transmitted signal was monitored for 5 min and the average value and respective error were calculated ($k \pm \delta k$), see section 3.8. The self-referenced transmitted signal in water (k_{water} , RI=1.332) was used for normalization as described in section 3.8, Equation 3.8 and Equation 3.9, obtaining ($k_{norm} \pm \delta k_{norm}$).

Between measurements the surface of the D-shape POF sensors was washed two times with the next solution in order to clean the surface and eliminate any residues from the previous solution.

The results of the RI characterization of sensors D1, D2, and D3 are depicted in Figure 4.4. For the sensor D1, with 1 cm of sensing region's length, there was no significant variation in the transmitted signal with refractive index variation. For the sensors with 3 cm and 5 cm of sensing length, D2 and D3 respectively, an increase in the transmitted signal was obtained with the increase of the external refractive index.

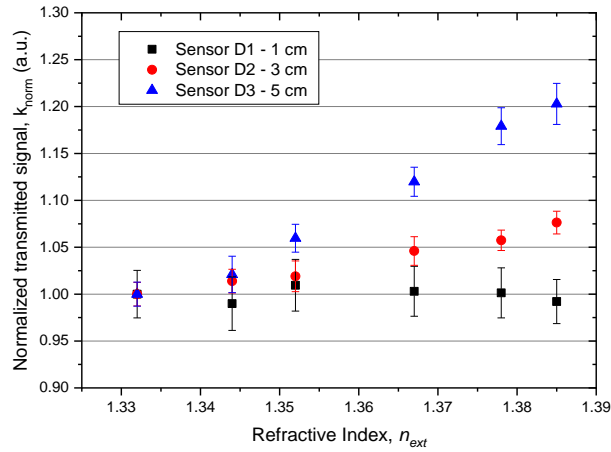


Figure 4.4 Response ($k_{norm} \pm \delta k_{norm}$) of the D-shaped POF sensors (D1 - D3) with glycerin solutions of increasing refractive index.

The obtained sensitivity (S_{PSL}) and resolution (Δn) for the D-shaped POF sensors to RI variation was strongly dependent on the length of the sensing region and were calculated as follows, based on section 3.8 and Equation 3.11 and Equation 3.12:

$$S_{PSL} = \left| \frac{\partial k_{norm}}{\partial n_{ext}} \right| \approx \frac{\Delta k_{norm}}{\Delta n_{ext}} \quad \text{Equation 4.2}$$

$$\Delta n = \frac{1}{S} \times \delta k_{norm_{max}} \quad \text{Equation 4.3}$$

The resolution can be defined as the minimum change in refractive index that can be detected, where $\delta k_{norm_{max}}$ is the maximum calculated error (see Equation 3.9) for each sensor in the range

of refractive index studied. The obtained values for the sensitivity and resolution of the characterized sensors are in Table 4.1, as well as the maximum calculated error.

Table 4.1. D-shaped POF sensors (D1 – D3): length of the sensing region, maximum calculated error, sensitivity and resolution (Equation 4.2 and Equation 4.3).

| Sensor | Length (cm) | $\delta k_{norm_{max}}$ (a.u.) | Sensitivity (au.RIU ⁻¹) | Resolution (RIU) |
|--------|-------------|-----------------------------------|--|----------------------|
| D1 | 1 | 1.51×10^{-2} | 0.15 | 1.0×10^{-1} |
| D2 | 3 | 0.94×10^{-2} | 1.44 | 6.5×10^{-3} |
| D3 | 5 | 1.87×10^{-2} | 3.83 | 4.9×10^{-3} |

The sensitivity and resolution of the D-shaped POF sensors are strongly dependent on the length of the sensing region. For the D-shaped sensor with 3 cm of sensing length the sensitivity is low, only an increase of 7.6% was obtained in the transmitted signal for an increase in the refractive index of 0.053 with a resolution of 6.5×10^{-3} RIU. The highest sensitivity was obtained for the D-shaped sensor D3, with a sensing region with 5 cm length. An increase of 20% in the transmitted signal was obtained with a resolution of 4.9×10^{-3} RIU, revealing promising developments for chemical and biochemical sensing.

4.2.2.2 Roughness of the sensing region

The performance of D-shaped POF RI sensors with the variation of the sensing region's roughness were preliminarily performed and the results will be presented.

4.2.2.2.1 Experimental Setup

Two D-shaped POF sensors were manufactured similarly to the procedures described in the previous section (length 20 cm), only changing the final polishing procedure. 3D printed planar supports had 6 cm length.

Sensor D10 was obtained by polishing the surface of the POF embedded in the planar support with a sandpaper of 5 μm (LFG5P), with a "Figure ∞ " pattern, in order to remove the cladding and part of the core. Sensor D9 was obtained with additional polishing using sandpapers of 3 μm and 1 μm grit size. The D-shaped regions were inspected by scanning electron microscopy (SEM), see Figure 4.5.

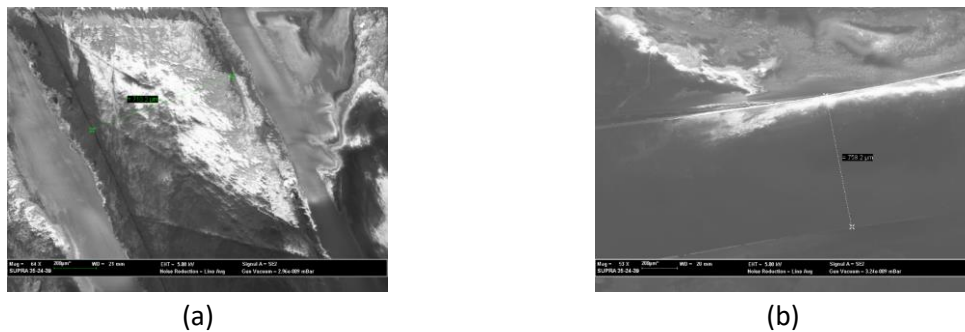


Figure 4.5 SEM images - sensing region of the D-shaped POF sensors after polishing with sandpapers of (a) 5 μm grit size (Sensor D10); (b) 5 – 3 – 1 μm grit size (Sensor D9).

The experimental setup (see Figure 4.3) comprised a stabilized power supply, an LED (centred at 650 nm), a POF coupler 50:50, two photodiode detectors and a picoscope connected to a laptop.

4.2.2.2.2 Refractive index characterization

Refractive index characterization was performed with solutions of glycerin with increasing refractive index, from 1.332 to 1.471. The refractive index of these solutions was measured at each experiment with the Abbe Refractometer (Model RMI, from Exacta and Optech Labcenter).

As already described, the response of the D-shaped sensors to RI variation was normalized to the response in water, 5 min monitoring ($k_{norm} \pm \delta k_{norm}$). Additionally, three replicated measurements were performed and the average value and standard deviation were calculated ($k_{avg} \pm \delta k_{avg}$).

Figure 4.6(a) depicts the response obtained for sensors D9 and D10. Results show that the response of the D-shaped POF sensors is enhanced for higher roughness of the sensing region. A fitting was applied to the obtained results in the refractive index range between 1.33 and 1.39. A linear fitting was applied to the response given by the sensor D9 and for the D10 an exponential fitting, see Figure 4.6(b). Table 4.2 contains the fitting parameters obtained for both sensors as well as the maximum error obtained in the set of experiments performed ($\delta k_{norm_{max}}$) and the relative error (see Equation 3.10).

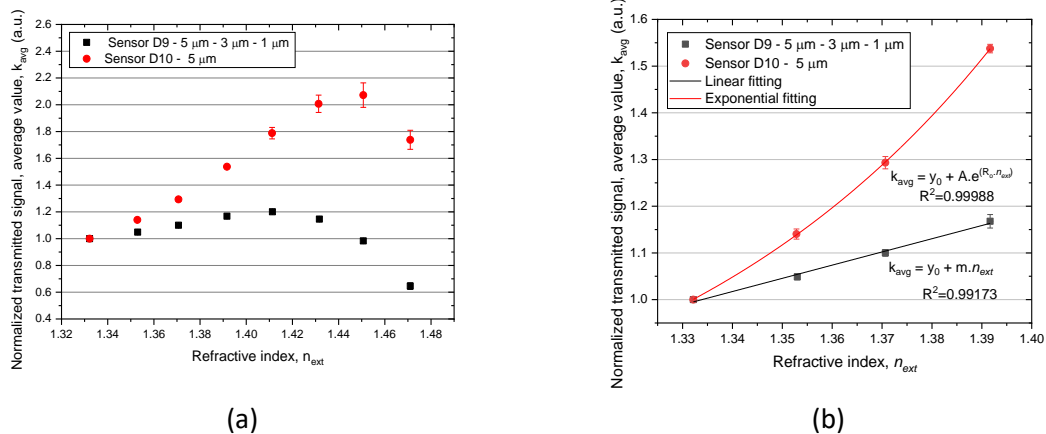


Figure 4.6 Response of the D-shaped POF sensors (D9, D10) with external refractive index: (a) RI: 1332 – 1.471; (b) RI: 1332 – 1.392, with the linear and exponential fittings.

Table 4.2. D-shaped POF sensors (RI 1.332 – 1.392): length, grit size of the sandpaper's used for polishing the surface, obtained parameters from the linear (m) and exponential (R_0, A) fitting, maximum calculated error (Equation 3.9) and relative error considering all the refractive index range (Equation 3.10).

| Sensor | Length (cm) | Grit size (μm) | m | R_0 | A | $\delta k_{norm_{max}}$ (a.u.) | relative error k_{avg} (%) |
|--------|-------------|-----------------------------|--------|-------|-----------------------|--------------------------------|------------------------------|
| D9 | 6 | 5 - 3 - 1 | 2.8271 | - | - | 0.0111 | 2.07 |
| D10 | | 5 | - | 14.17 | 2.56×10^{-9} | 0.1624 | 4.42 |

Considering all the refractive index range, the relative error obtained for the sensor D10 is higher than twice the value obtained for sensor D9, meaning that higher sensing region’s roughness can lead to lower reproducibility of the obtained results. It would be important to perform more studies in order to better understand if this aspect is consistent. In case of the RI range 1.332 – 1.392, the relative error is 0.86% for sensor D10 and 1.23% for sensor D9, showing higher reproducibility of the sensor’s response in this refractive index range.

The sensitivity and resolution of the sensors were calculated for the RI range 1.332 – 1.390 according with Equation 3.11 and Equation 3.12, and are depicted in Figure 4.7. Sensitivity of sensor D9 is equal to the slope of the linear fitting (m) while for the sensor D10 will be dependent of the external refractive index (n_{ext}) and the fitting parameters (R_0, A):

$$S_{D9 (RI:1.332 - 1.390)} = \left| \frac{\partial k_{avg}}{\partial n_{ext}} \right| = m \quad \text{Equation 4.4}$$

$$S_{D10 (RI:1.332 - 1.390)} = \left| \frac{\partial k_{avg}}{\partial n_{ext}} \right| = R_0 \cdot A \cdot e^{R_0 \cdot n_{ext}} \quad \text{Equation 4.5}$$

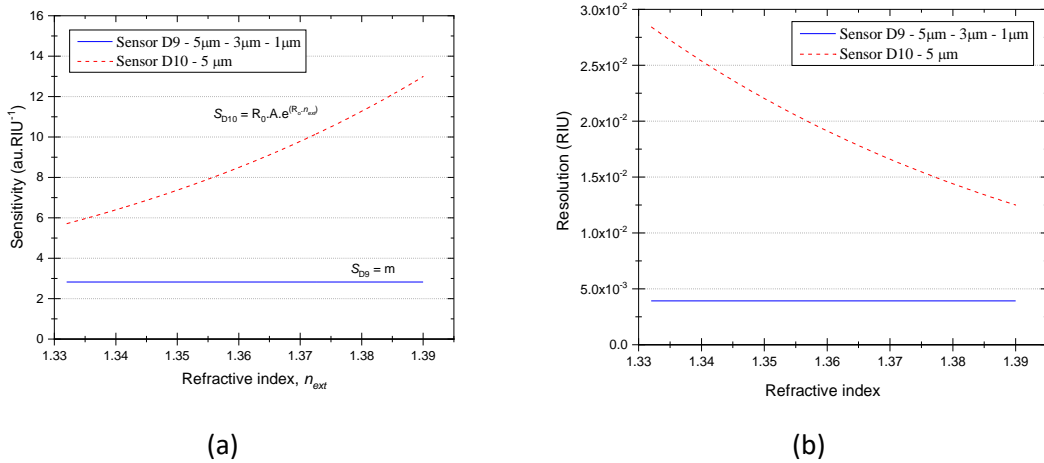


Figure 4.7 (a) Sensitivity and (b) resolution of the D-shaped POF sensors D9 and D10 in the refractive index range 1332 – 1.390.

These results show that sensor D10, with coarser surface, has higher sensitivity for RI sensing than sensor D9 with smoother surface, in the RI range 1.332 - 1.390. Furthermore, for sensor D10 sensitivity depends on the external refractive index.

The resolution obtained for sensor D10 was much higher ($\sim 10^{-2}$ RIU) than the resolution obtained for sensor D9 (3.93×10^{-3} RIU), showing that polishing the surface with sandpapers of higher grit size can lead to lower sensor’s resolution, due to higher fluctuation in the sensor’s response.

4.2.2.3 Conclusions

The developed D-shaped POF sensors were easy to produce by a fast and low cost procedure.

The performance of the D-shaped POF sensors is strongly dependent on the length of the sensing region, higher length resulted in sensors with higher sensitivity and lower resolution value for the same refractive index range. Considering the three sensors characterized under these preliminary tests, the lowest resolution was 4.9×10^{-3} RIU.

With respect to the study targeting roughness dependence, the D-shaped POF sensor with higher surface roughness showed higher sensitivity but also higher resolution value, dependent on the external refractive index.

More detailed studies were conducted in order to understand the variation of the sensor's performance (sensitivity and resolution) with the variation of the sensing region's length and roughness and will be presented in the next section 4.2.3.

4.2.3 Optimization

4.2.3.1 Length of the sensing region

A more detailed study was performed related with the influence of the sensing region's length on the performance of D-shaped POF RI sensors.

4.2.3.1.1 *Sensors' preparation*

Six samples of POF were prepared (length of 20 cm) and embedded in grooves on planar supports with different lengths, as already described in the previous section. After gluing the fibres in the planar supports with an instant glue gel, standard 3 step-polishing procedure was applied (5 μm , 3 μm and 1 μm). Six D-shaped POF sensors were therefore manufactured with a sensing region length varying from 1 cm to 6 cm - sensors D4, D5, D6, D7, D8 and D9, depicted in Figure 4.8.

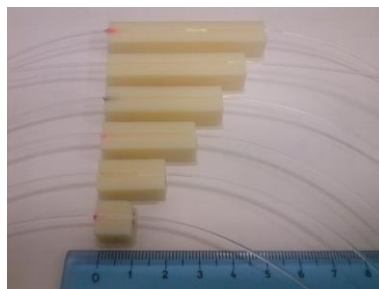


Figure 4.8 (a) Produced D-shaped sensors (D4 – D9) with sensing region lengths from 1 cm (Sensor D4) to 6 cm (Sensor D9).

The sensing region of the D-shaped POF sensors was observed by scanning electron microscopy (SEM, model Zeiss SUPRA35), see Figure 4.9. The sensing region's thickness was measured directly as before.

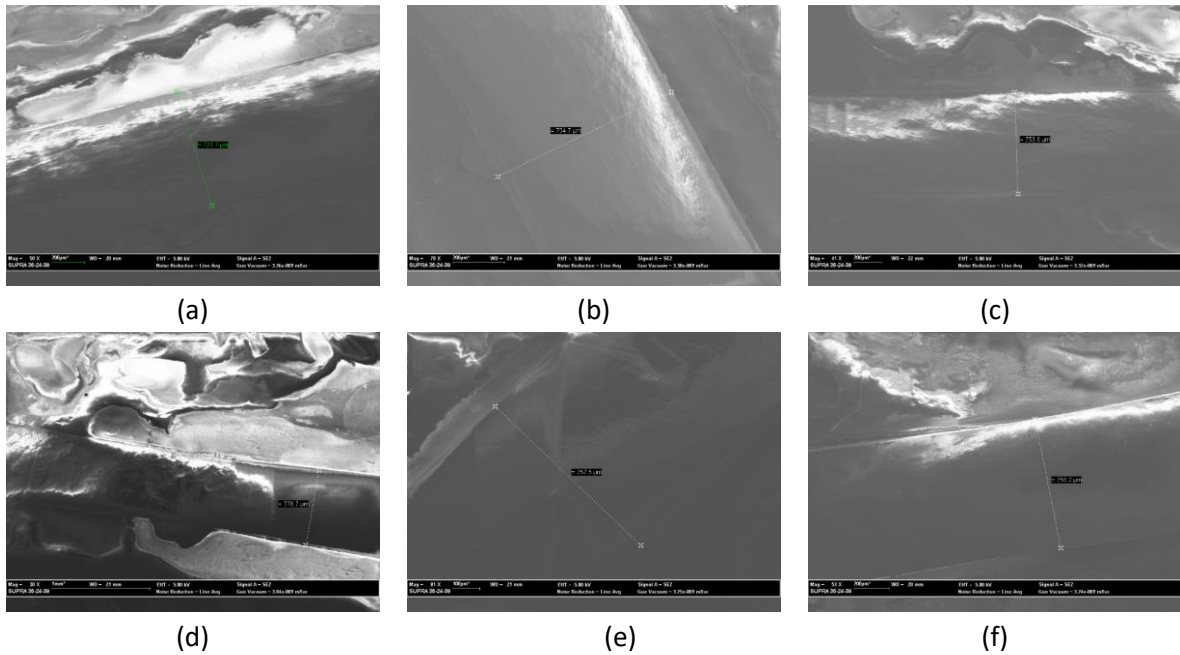


Figure 4.9 D-shaped POF sensors – SEM images of the sensing region: (a) Sensor D4 ; (b) Sensor D5; (c) Sensor D6; (d) Sensor D7; (e) Sensor D8; (f) Sensor D9.

For a more accurate analysis of the sensing region thickness, the SEM images were inspected with the NI Vision Builder for Automated Inspection software. This program allows to determine the thickness of the sensing region (D) considering the visible lines of the fibre in the whole image. In these measurements the scale is taken into account as well as the contrast between two different areas, allowing to calculate the sensing region's thickness. Several measurements were performed for each sensor and the thickness of the sensing region was obtained through the average value and standard deviation, see Table 4.3.

Table 4.3. D-shaped POF sensors – thickness of the sensing region (D).

| Sensor | Length (cm) | D (μm) | Measurements |
|--------|-------------|-----------------------|--------------|
| D4 | 1 | 738 ± 8 | 8 |
| D5 | 2 | 758 ± 5 | 9 |
| D6 | 3 | 738 ± 15 | 9 |
| D7 | 4 | 766 ± 28 | 12 |
| D8 | 5 | 777 ± 29 | 9 |
| D9 | 6 | 779 ± 23 | 12 |

The average thickness of $761 \pm 26 \mu\text{m}$ was obtained considering the measurements performed for all the sensors. The total height of the produced sensors, $808 \mu\text{m} < (r_f + h) < 839 \mu\text{m}$ was obtained using Equation 4.1.

4.2.3.1.2 Experimental setup

The D-shaped POF sensors were characterized in transmission with the intensity based setup already described (depicted in Figure 4.3). The stability of the transmitted light through the D-shaped POF sensors with time, when water was placed in the sensing region, was confirmed prior to the sensors' characterization with increasing RI. The sensor's response was considered stable when the variation of the normalized transmitted signal $\sim 1\%$.

4.2.3.1.3 Refractive index characterization

All D-shaped POF sensors were characterized to refractive index variation using glycerin solutions with increasing refractive index from 1.332 to 1.471. In each performed test, the refractive index of the glycerin solutions was measured with the Abbe Refractometer.

Response of the sensors ($k_{norm} \pm \delta k_{norm}$) was calculated in agreement with the already described before. Three replicated measurements with refractive index variation were performed to validate the obtained results and verify the reproducibility of the sensor's responses ($k_{avg} \pm \delta k_{avg}$).

As shown in Figure 4.10, the response of the D-shaped POF sensors to refractive index is dependent on the length of the sensing region and on the refractive index of the external medium. The sensor D4, D-shaped POF sensor with 1 cm of sensing region, revealed almost no variation on the transmitted signal until the refractive index reached 1.37 and an exponential decrease was observed in the refractive index range between 1.37 – 1.47.

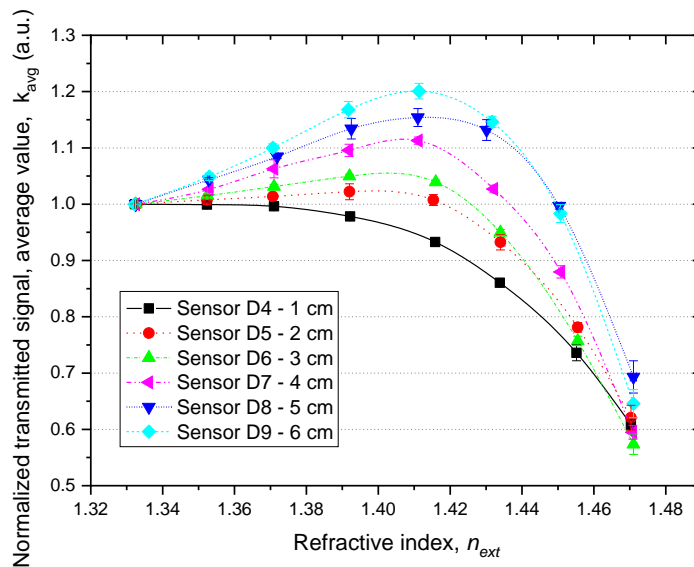


Figure 4.10 Sensor's response ($k_{avg} \pm \delta k_{avg}$) with increasing refractive index, with the length of the sensing region.

For all the others sensors two different responses were observed and are depicted in Figure 4.11. In the refractive index range between 1.33 – 1.39 a linear increase in the transmitted signal

was observed with increasing refractive index and between 1.41 – 1.47 an exponential decrease was observed with increasing RI.

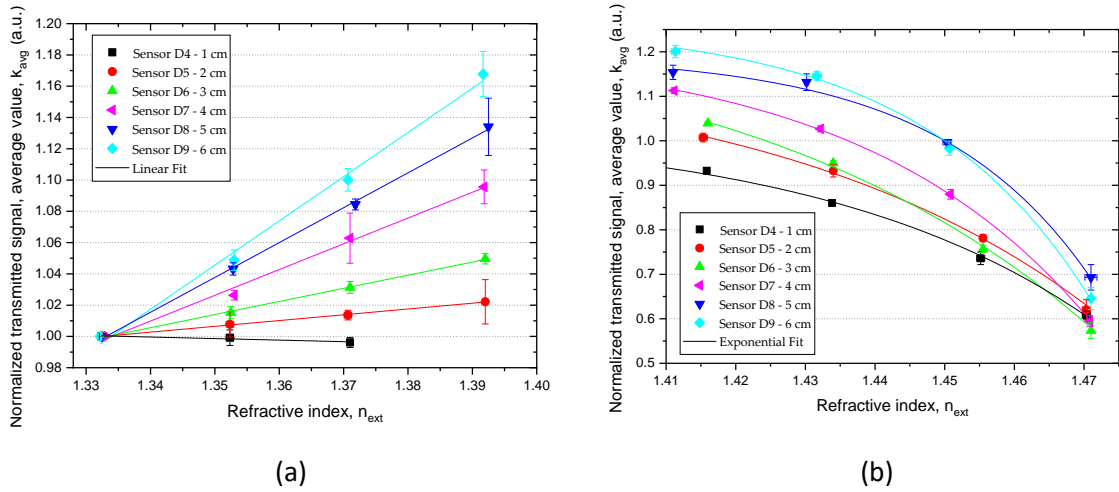


Figure 4.11 Response ($k_{avg} \pm \delta k_{avg}$) of the D-shaped POF sensors with increasing refractive index: (a) RI: 1.33 – 1.39, linear fitting; (b) RI: 1.41 - 1.47, exponential fitting. For the sensor D4 consider RI: 1.33 – 1.37 RIU, linear fitting and RI: 1.37 – 1.47 RIU, exponential fitting.

In the Table 4.4 are the maximum values obtained for the calculated error ($\delta k_{norm_{max}}$) in each refractive index range, as well as the relative error of the set of experiments performed for each sensor, calculated using Equation 3.10.

Table 4.4. D-shaped POF sensors – length, maximum value obtained for the calculated error (Equation 3.9) for the different refractive index ranges and the relative error (Equation 3.10).

| Sensor | Length (cm) | $\delta k_{norm_{max}}$ (a.u) | RI | $\delta k_{norm_{max}}$ (a.u.) | RI | relative error (k_{avg}) (%) |
|-----------|-------------|-------------------------------|-------------|--------------------------------|-------------|----------------------------------|
| Sensor D4 | 1 | 0.0059 | 1.33 - 1.37 | 0.0275 | 1.37 - 1.47 | 1.40 |
| Sensor D5 | 2 | 0.0076 | | 0.0143 | | 2.16 |
| Sensor D6 | 3 | 0.0039 | | 0.0118 | | 1.71 |
| Sensor D7 | 4 | 0.0062 | 1.33 - 1.39 | 0.0168 | 1.41 - 1.47 | 1.44 |
| Sensor D8 | 5 | 0.0176 | | 0.0210 | | 2.48 |
| Sensor D9 | 6 | 0.0111 | | 0.0137 | | 2.07 |

When the external refractive index is higher, higher variation in the obtained response of each experiment is generally observed, given by $\delta k_{norm_{max}}$. Furthermore, for higher values of refractive index also higher variation was observed between experiments, translated in higher relative error. In this study, the maximum relative error was obtained for the sensor D8, equal to 2.48%, which validates the reproducibility of the obtained results.

Sensitivity and resolution were calculated according to Equation 3.11 and Equation 3.12. In the refractive index range from 1.33 to 1.39 the sensor’s response increases linearly with the increase of the external refractive index, therefore, the sensitivity is equal to the slope of the linear fitting.

The values obtained for the sensitivity, resolution and maximum calculated error ($\delta k_{norm_{max}}$) are in Table 4.5. Sensitivity and resolution for this refractive index range are depicted in Figure 4.12.

Table 4.5. Sensitivity and resolution (Equation 3.11 and Equation 3.12) of the D-shaped sensors, RI: 1.33 - 1.39 and maximum calculated error ($\delta k_{norm_{max}}$).

| Sensor | Length (cm) | Sensitivity (au.RIU ⁻¹) | $\delta k_{norm_{max}}$ (a.u.) | Resolution (RIU) | R ² | RI Range |
|-----------|-------------|-------------------------------------|--------------------------------|-----------------------|----------------|-----------|
| Sensor D4 | 1 | 0.099 | 0.0059 | 5.98×10^{-2} | 0.7787 | 1.33–1.37 |
| Sensor D5 | 2 | 0.370 | 0.0076 | 2.05×10^{-2} | 0.9978 | |
| Sensor D6 | 3 | 0.839 | 0.0039 | 4.65×10^{-3} | 0.9982 | 1.33–1.39 |
| Sensor D7 | 4 | 1.647 | 0.0062 | 3.76×10^{-3} | 0.9902 | |
| Sensor D8 | 5 | 2.229 | 0.0176 | 7.90×10^{-3} | 0.9986 | |
| Sensor D9 | 6 | 2.827 | 0.0111 | 3.93×10^{-3} | 0.9917 | |

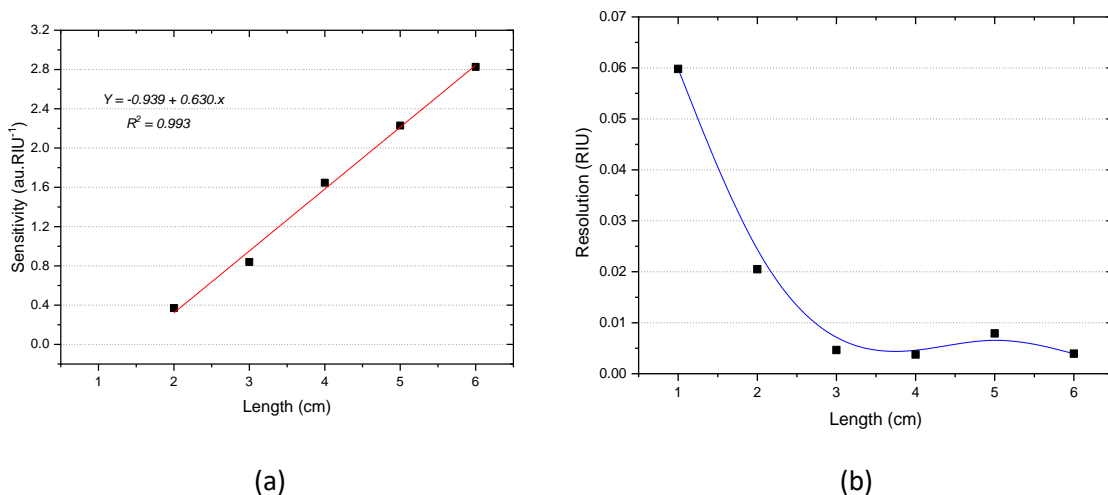


Figure 4.12 RI: 1.33 - 1.39: sensitivity (a) and resolution (b) of the D-shaped POF sensors with the length of the sensing region. For the Sensor D4 the resolution was calculated in the RI range 1.33 – 1.37.

As concluded before, in this refractive index range, the sensitivity and resolution of the D-shaped POF sensors were strongly dependent on the length of the sensing region. Higher the length higher the sensor’s performance, which means higher sensitivity and lower resolution value. The best results — sensitivity of 2.83 au.RIU⁻¹ and resolution of 3.93×10^{-3} RIU — were obtained for the Sensor D9 with 6 cm of sensing region’s length.

On the other side, D-shaped POF sensors with sensing region’s length equal or higher than 3 cm allowed to obtain a resolution lower than 8×10^{-3} RIU, although with lower sensitivities (0.84 – 2.23 au.RIU⁻¹).

In the range of refractive index between 1.41–1.47, the normalized transmitted signal decreased exponentially with the increase of the external refractive index. The sensitivity and resolution were calculated (Equation 3.11 and Equation 3.12) for this refractive index range, depicted in Figure 4.13, and the obtained parameters are in Table 4.6.

Table 4.6. RI: 1.41 - 1.47 – obtained parameters from the exponential fitting, and maximum calculated error ($\delta k_{norm_{max}}$)

| Sensor | Length (cm) | R_0 | A | $\delta k_{norm_{max}}$ (a.u.) | R^2 | RI Range |
|-----------|-------------|-------|-------------------------|--------------------------------|--------|-----------|
| Sensor D4 | 1 | 25.25 | -3.19×10^{-17} | 0.0275 | 0.9980 | 1.37–1.47 |
| Sensor D5 | 2 | 21.31 | -1.36×10^{-14} | 0.0143 | 0.9968 | |
| Sensor D6 | 3 | 19.52 | -2.38×10^{-13} | 0.0118 | 0.9917 | |
| Sensor D7 | 4 | 30.30 | -2.76×10^{-20} | 0.0168 | 0.9995 | 1.41–1.47 |
| Sensor D8 | 5 | 45.41 | -4.91×10^{-30} | 0.0210 | 0.9882 | |
| Sensor D9 | 6 | 40.91 | -4.52×10^{-27} | 0.0137 | 0.9916 | |

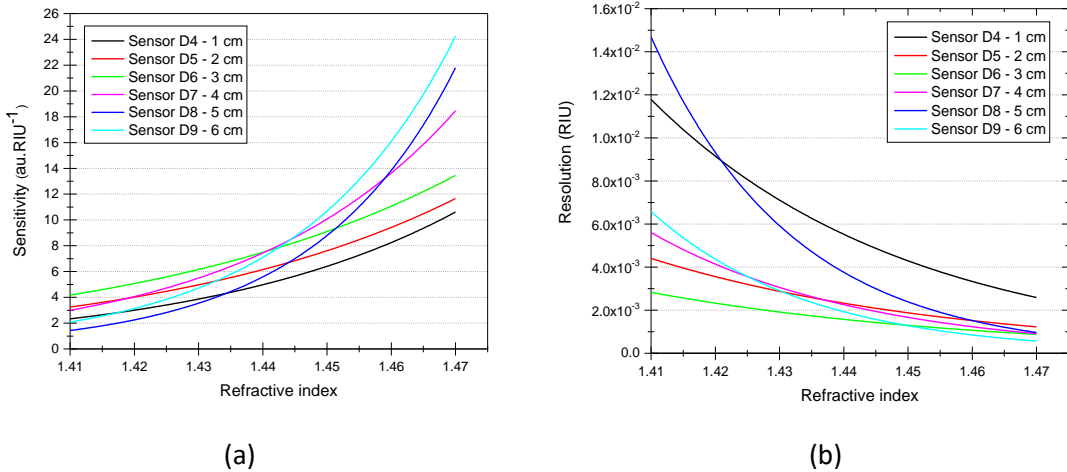


Figure 4.13 RI: 1.41 - 1.47 – performance of the D-shaped POF sensors with the length of the sensing region: (a) sensitivity; (b) resolution.

In this range of refractive index (RI: 1.41 – 1.47) the performance of the D-shaped sensors is dependent on the external refractive index – higher the external RI higher was the obtained sensitivity and lower the resolution for all the sensors. Moreover, the length of the sensing region was no longer a critical parameter to obtain the best performance. A resolution of 10^{-3} RIU was obtained for all the sensors when the external RI was equal or higher than 1.42 and sensor D9 showed a resolution of 10^{-4} RIU for RI higher than 1.46 RIU. For example, for sensor D6 with 3 cm of sensing region’s length was obtained a resolution of 2.83×10^{-3} RIU for 1.41 RIU and 8.77×10^{-4} RIU for 1.47 RIU, with a sensitivity of 4.17 au.RIU^{-1} and $13.46 \text{ au.RIU}^{-1}$, respectively – much higher than the values obtained in the RI range from 1.33 to 1.39.

4.2.3.1.4 Conclusions

A more detailed study was performed with D-shaped POF sensors with different lengths of sensing region, from 1 cm to 6 cm. The refractive index range is very important in the choice of the length of the sensing region in D-shaped POF sensors, in order to achieve the best performance for RI sensing.

In the refractive index range between 1.33 and 1.39, the performance of the D-shaped sensors was independent of the external RI. In this case, the best results were achieved with sensor D9 with 6 cm of sensing region's length, namely a sensitivity of 2.83 au.RIU^{-1} and resolution of $3.93 \times 10^{-3} \text{ RIU}$.

In the refractive index range from 1.41 to 1.47, the performance of the sensors was dependent on the external refractive index. In this case, the external RI should be considered in order to choose the length of the sensing region that will allow to obtain the highest sensing performance (higher sensitivity and lower resolution value).

A resolution of $10^{-3} - 10^{-4} \text{ RIU}$ was achieved using very simple and low-cost methods, dependent on the external refractive index. The obtained resolution is still higher than the one obtained for a D-shaped POF-SPR platform ($6 \times 10^{-4} \text{ RIU}$) (Cennamo *et al.*, 2011), nevertheless, suggests that further investigations in chemical sensing can be fruitful, which will be addressed in the Chapter 5.

4.2.3.2 Roughness of the sensing region

A more detailed study was performed in order to deepen the comprehension of the influence of surface roughness on the performance of D-shaped POF RI sensors.

The transmission losses due to the polishing procedures were evaluated, the morphology of the sensing region was analysed with optical microscopy and the D-shaped POF sensors were characterized with sucrose solutions of increasing refractive index.

4.2.3.2.1 Sensors' preparation

Five samples of POF (20 cm length) were cut with a POF cutter and the end faces were polished in "Figure ∞ " pattern with sandpapers of different grain sizes (5 - 3 - 1 - $0.3 \mu\text{m}$), see Figure 2.11, section 2.3.3, Chapter 2. The prepared samples were cleaned several times using distilled water and optical paper.

The POF samples were embedded in grooves on 3D printed planar supports with 6 cm length, as depicted in Figure 4.14(a), using an instant glue gel (SuperTite[®], SUPERTITE SAM, S.A.).

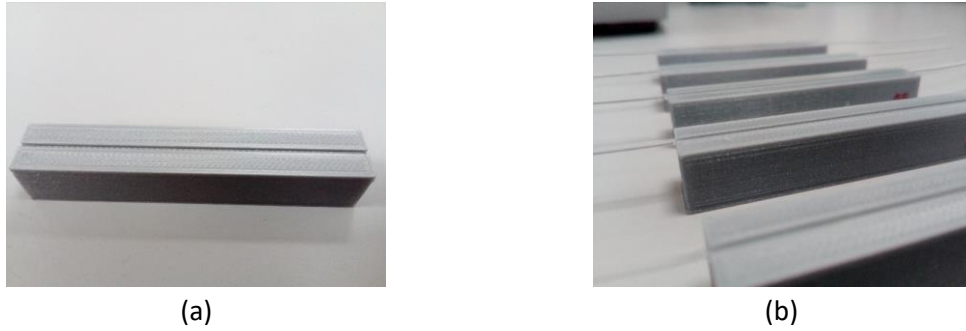


Figure 4.14 (a) Platform used for embedding the prepared fibres (groove's dimensions: 6.0 cm, 1.1 mm, 0.7 mm); (b) produced D-shaped POF sensors.

The polishing procedure was modified regarding to previous sections. The first polishing procedure (Polishing 1) was performed manually, around 60 times, until the platform was reached with sandpaper P320 (~46 μm grit size) in "Figure ∞ " pattern. The produced D-shaped sensors (D11, D12, D13, D14 and D15), see Figure 4.14(b), were washed several times with distilled water and cleaned with optical paper prior to RI characterization.

The roughness of the sensing region was decreased by polishing with sandpapers of lower grit size: P600 (~26 μm grit size, Polishing 2), 12 μm (Polishing 3) and 5 μm (Polishing 4).

All the polishing steps were performed manually, with circular movements along the length of the sensors' sensing region. After each polishing procedure the D-shaped POF sensors were washed with distilled water and their performance for RI sensing was evaluated through the characterization with sucrose solutions of increasing refractive index.

4.2.3.2.2 Losses due to the polishing procedures

The transmission characteristics of the D-shaped POF sensors was evaluated in different steps of sensors' preparation. The end faces of the POFs were connected to an LED (IF-E96) and a photodiode detector (IF-D91), which were then connected to a TTI bench power supply ($V_{source} = 1.50\text{ V}$ and $I_{source} = 1\text{ mA}$) and a digital multimeter, see Figure 4.15.

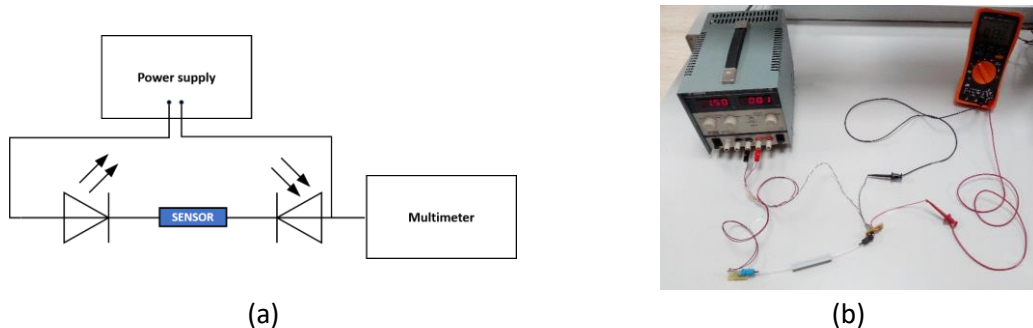


Figure 4.15 Evaluation of the transmission losses due to the manufacturing procedures: (a) schematic representation; (b) photography.

The output voltage ($V_{multimeter}$) was measured with the digital multimeter before and after embedding the POF samples in the planar support, after the first polishing procedure (Polishing 1, P320) and after all the polishing procedures and sensor’s characterization to RI variation. These measurements were performed consecutively for all the prepared sensors, with air as external medium (no liquid present in the POF sensing region).

The transmission losses were calculated in relation to the obtained output voltage for the unpolished POF sample (before embedding the POF in the planar support, V_0), accordingly with the following equation:

$$Light\ loss\ (\%) = \frac{V_0 - V_{multimeter}}{V_0} \times 100 \quad \text{Equation 4.6}$$

Table 4.7. D-shaped POF sensors - calculated light losses (%) in different production stages (relative to the unpolished POF sample).

| Sensors | Light loss (%) | | | |
|---------|-------------------------|------------------------------------|------|---------------|
| | Unpolished POF embedded | D-shaped POF (polished, grit size) | | |
| | | P320 | P600 | 12 μm |
| D11 | | 93.8 | 93.3 | |
| D12 | | 93.3 | - | (88.8 - 88.2) |
| D13 | < -0.1 | 94.4 | - | (87.1 - 86.6) |
| D14 | | 90.5 | - | (86.0 - 85.4) |
| D15 | | (93.3 - 92.7) | 92.2 | |

The obtained results show that the transmission capacity of the POFs was not affected by the embedding process in the planar platform ($light\ loss < -0.1\%$), although losses of light around 90% to 94% were obtained after the first polishing procedure with sandpaper P320 (see Table 4.7).

The results obtained after all the polishing procedures performed for each sensor showed that the transmission of light through the POF can be increased even though more polishing was performed (see Table 4.7).

After the Polishing 2 (sandpaper P600) only a slight increase in the obtained output power was observed (light loss of around 92% - 93%). After the Polishing 3 (12 μm grit size) the light loss was around 88% - 89% and after the Polishing 4 (5 μm grit size) was around 85% - 87%.

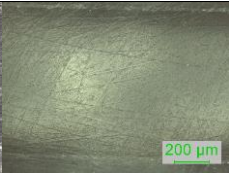
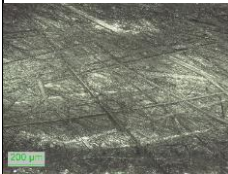
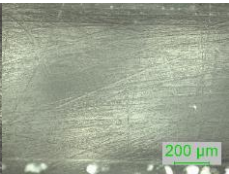
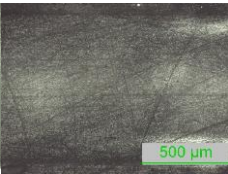
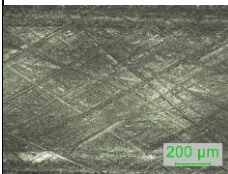
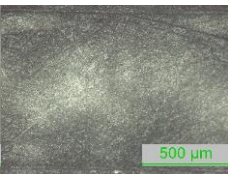
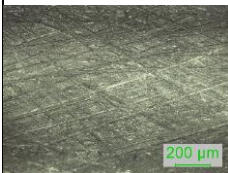
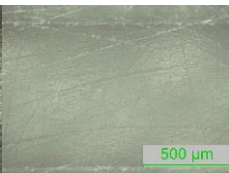
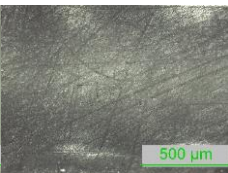
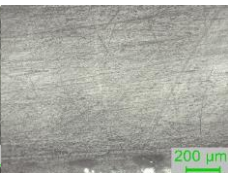
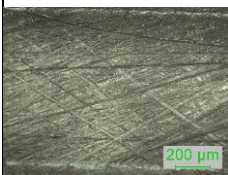
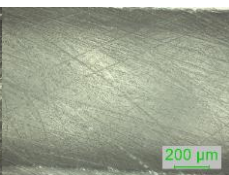
These results show that roughness of the sensing region is an important parameter in the transmission capacities of POFs. Furthermore, by decreasing the roughness of the sensing region (by polishing with sandpapers of decreasing grit size) the transmission of light through the POF increases because the scattering on the sensitive region decreases.

Although a small variation was obtained between the measured output voltages for different sensors after each polishing procedure (from 1% to 4%) this can probably be related to the manual manufacturing process. Before the polishing procedures, the measured output voltage was the same for all the samples.

4.2.3.2.3 Morphology of the sensing region

The sensing region of the D-shaped POF sensors was observed by optical microscopy after each polishing procedure, see Table 4.8. The surface was observed using different magnifications and the thickness of the sensing region was calculated using the microscope’s software.

Table 4.8. D-shaped POF sensors: sensing region after each polishing procedure - images of optical microscopy (in reflection, with 10x objective lens).

| Sensors | Polishing procedures (sandpaper, grit size) | | | |
|---------|---|---|--|---|
| | P320 (~46 μm) | P600 (~26 μm) | 12 μm | 5 μm |
| D11 |  |  | | |
| D12 |  |  |  | |
| D13 |  |  |  |  |
| D14 |  |  |  |  |
| D15 |  |  | | |

Observation of the sensing region by optical microscopy allowed to confirm the decrease of surface roughness by polishing the sensing region with sandpapers of lower grit size.

In the interface between the sensing region and the unpolished POF, the roughness did not change in a well-defined way, revealing the difficulty to obtain a clear interface between these two areas, see Figure 4.16.

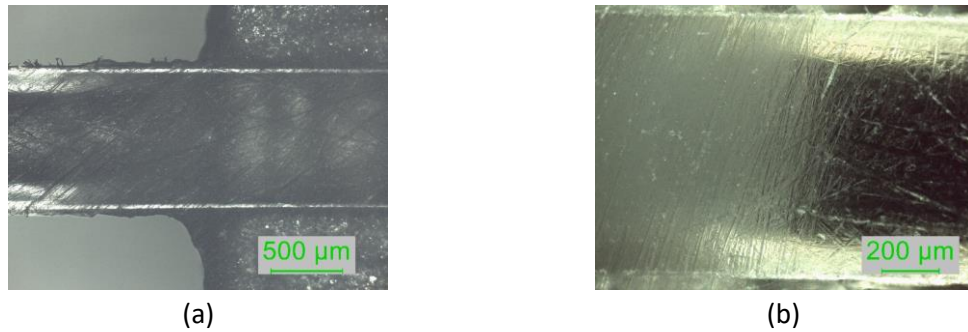


Figure 4.16 Interface between the sensing region and the unpolished POF – images of optical microscopy: (a) sensor D13 (P320, P600, 12 μm grit size); (b) close-up of sensor D11 (P320 and P600).

Light losses occur in the interface between the sensing region and the unpolished POF. Below are two photographs of a D-shaped sensor with distilled water covering the sensing region where the red light from the LED is easily observed, Figure 4.17.

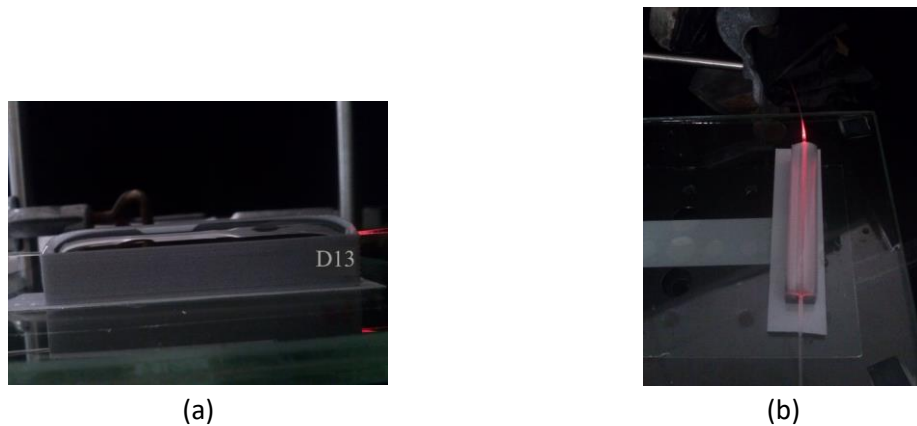


Figure 4.17 D-shaped POF sensor covered by distilled water – visible light losses in the interface between the sensing region and the unpolished POF.

This aspect should be improved in future developments, as the sensing region should be limited to the zone immediately above the planar support. Outside of this region the POF should be unpolished in order to prevent light losses that do not contribute to the sensing capabilities of the sensors. Furthermore, this aspect can be relevant for the sensor's reproducibility, i.e. achieve the same sensitivity for sensors prepared in a similar way. In future developments the planar support should be optimized in order to prevent light losses that do not contribute for the sensing capabilities of the D-shaped POF sensors. One possibility is to create a very smooth macro bending in the limits of the sensing region making the unpolished POF enter in the planar support.

The thickness of the sensing region (D) was calculated as the average value and standard deviation of several measurements performed at different points of the surface, obtained from different images of optical microscopy. The obtained thickness can be found at Table 4.9. Only images obtained with 5x objective lens were used, as only this magnification allows to view completely the fibre diameter. As an example, in Figure 4.18 are depicted two images of optical microscopy with several performed measurements.

After polishing with sandpaper P320 it was very difficult to obtain clear images where the limits of the sensing region could be easily identified. For this reason, measurements were mostly not performed.

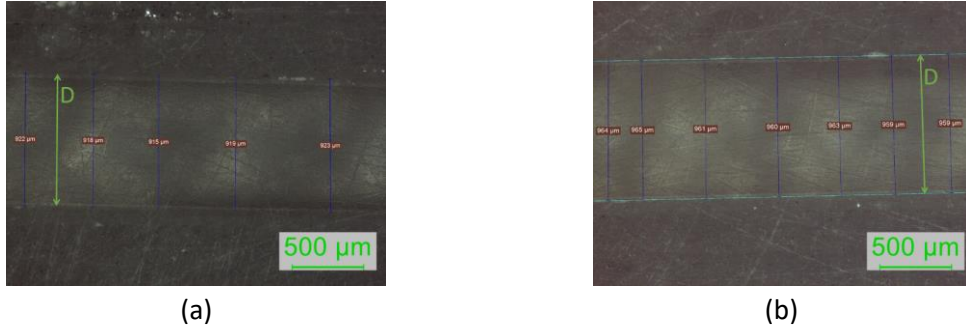


Figure 4.18 Images of optical microscopy (in reflection, with 5x objective lens): sensor D12 (a) and sensor D13 (b) - measurements of the sensing region’s thickness after Polishing 2 (P600).

Table 4.9. D-shaped POF sensors: thickness of the sensing region after the polishing procedures, average value and standard deviation (n is the number of measurements performed).

| Sensor | Thickness of the sensing region (D , μm) | | | |
|--------|---|---------------------------|---------------------------|---------------------------|
| | P320 | P600 | 12 μm | 5 μm |
| D11 | x | 875 ± 12 ($n = 33$) | -- | -- |
| D12 | x | 912 ± 07 ($n = 29$) | 896 ± 05 ($n = 14$) | -- |
| D13 | 934 ± 08 ($n = 13$) | 952 ± 10 ($n = 14$) | 947 ± 10 ($n = 11$) | 944 ± 06 ($n = 12$) |
| D14 | x | 888 ± 08 ($n = 13$) | 893 ± 11 ($n = 14$) | 868 ± 06 ($n = 20$) |
| D15 | x | 936 ± 19 ($n = 13$) | -- | -- |

After polishing the sensing region of different sensors with the same polishing paper, slight differences in the thickness were obtained. This can be related with the manual process involved, nevertheless, the selected POF has a diameter error of $60 \mu\text{m}$ (manufacturer data), higher than the variation of thickness obtained. Furthermore, the length used for the measurements (microscope images) is only representative of the sensing region total length.

From the obtained thickness (D) the total height of the D-shaped sensors was calculated, $653 \mu\text{m} < (r + h) < 748 \mu\text{m}$, as determined by the Pythagorean theorem and considering the maximum thickness, d , as $1000 \mu\text{m}$, see Figure 4.1 and Equation 4.1.

The total height obtained for the produced D-shaped POF sensors is in accordance with the groove’s depth on the planar supports ($700 \mu\text{m}$) with variations of around $50 \mu\text{m}$.

4.2.3.2.4 Experimental setup

The D-shaped-POF sensors were characterized with the battery powered Bluetooth based optical setup described in the section 3.8, Chapter 3.

For simplicity, the optical setup is briefly described. The intensity based transmission system comprised an LED (IF-E96, wavelength centred at 660 nm), a POF coupler (90:10, IF-542) and two

photodiode detectors (IF-D91), one connected to the D-shaped POF sensor and the other to the reference POF, see Figure 4.19.

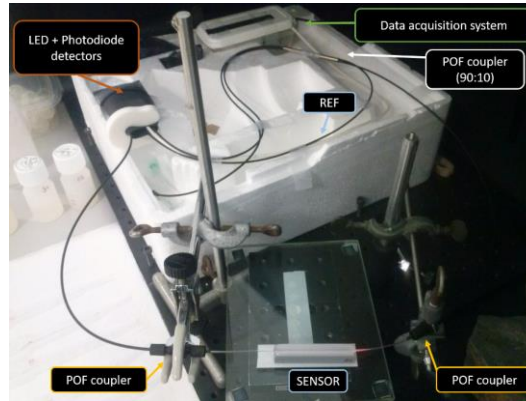


Figure 4.19 Optical sensing setup used for the characterization of the D-shaped POF sensors with increasing RI and variation of the surface roughness.

4.2.3.2.5 Refractive index characterization

The performance of the D-shaped POF sensors for refractive index (RI) sensing was evaluated through the characterization with sucrose solutions prepared in distilled water with RI varying from around 1.3326 (water) to 1.4118. In this study, the refractive index of the prepared solutions (nD at 25°) was measured with a commercial refractometer (Abbemat 200, Anton Paar) with 1×10^{-4} resolution.

The response of the D-shaped POF sensors to the variation of RI was monitored in continuum. First, the stability of the sensor's response when water was placed in the D-shaped region was evaluated and, when considered stable, the RI characterizations were performed. The response of the sensors was considered stable when the variation of the sensor's response was $\sim 1\%$.

The sensor's response was firstly recorded in distilled water ($k_{water} \pm \delta k_{water}$), after which the distilled water was removed and the next solution was added ($k_{solution} \pm \delta k_{solution}$), see Figure 4.20(a). The sensing region was washed twice between measurements with the new solution in order to clean the fibre and platform from residues of the previous solution. The solutions were added and removed each 15 min using plastic pipettes, see Figure 4.20(b,c). Three replicated experiments (RI characterizations) were performed.

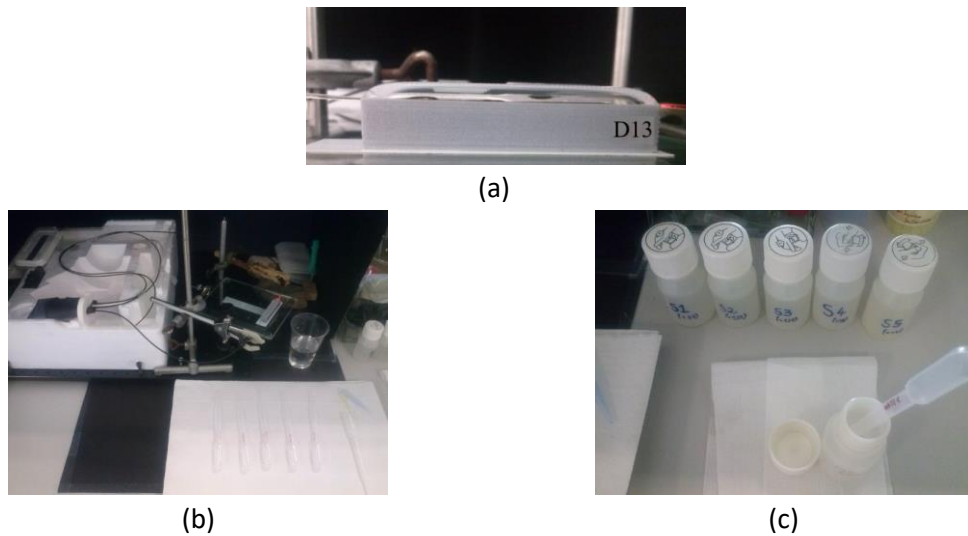


Figure 4.20 (a) D-shaped POF sensor D13 with the sensing region covered by water; (b) experimental setup and plastic pipettes (used to add and remove the sucrose solutions to/from the sensor’s surface); (c) sucrose solutions used for the D-shaped POF sensors characterization to RI variation.

The transmitted signal normalized to water ($k_{norm} \pm \delta k_{norm}$) was calculated according with Equation 3.8 and Equation 3.9. The average value of the replicated measurements and respective standard deviation ($k_{avg} \pm \delta k_{avg}$) were calculated.

The results obtained for ($k_{avg} \pm \delta k_{avg}$) were plotted against the average value and standard deviation of the measured RI of each solution ($n_{ext} \pm \delta n_{ext}$), performed immediately after their removal from the sensors’ surface (measured with the commercial refractometer).

As an example, the results obtained for three experiments with the sensor D12 after being polished with sandpapers P320 and P600 are depicted in Figure 4.21.

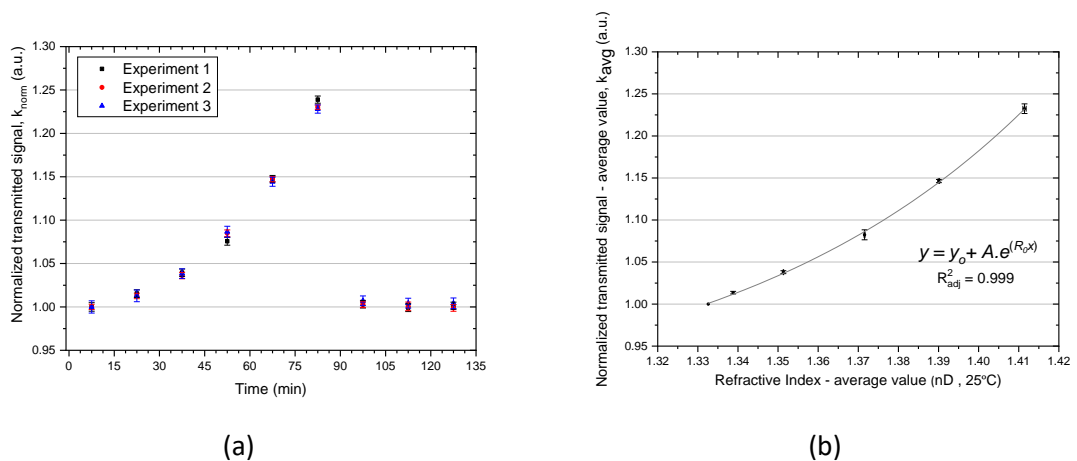


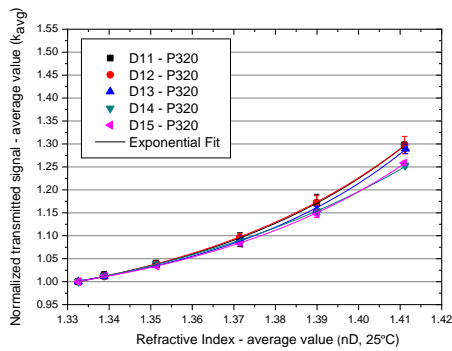
Figure 4.21 Response of the D-shaped POF sensor D12 when in contact with solutions of different refractive indices after polishing 2 (P600): (a) normalized transmitted signal ($k_{norm} \pm \delta k_{norm}$) with time; (b) average value of the three replicated measurements ($k_{avg} \pm \delta k_{avg}$) and exponential fitting.

Figure 4.21(a) shows the normalized transmitted signal ($k_{norm} \pm \delta k_{norm}$) obtained with sucrose solutions of increasing RI (1.3326 – 1.411) and three washing steps with distilled water, showing the reversibility of the sensors' response. The average values and standard deviation were calculated and are depicted in Figure 4.21(b). For sensor D12 the relative error was 0.48%, see Equation 3.10 and Table 4.10.

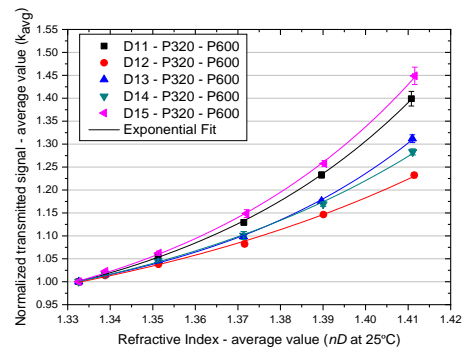
The best fitting applied to the obtained results is a nonlinear curve with an exponential model, as depicted in Figure 4.21(b), no weighting:

$$y = y_0 + A \cdot e^{R_0 \cdot x} \tag{Equation 4.7}$$

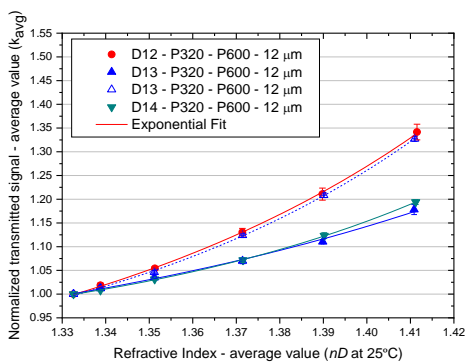
The sensor's responses to RI variation after each polishing procedure are depicted in Figure 4.22 together with the exponential fitting of the data. The error bars are the standard deviation of the set of measurements with each sensor and are related with the repeatability of the experiments as already mentioned (δk_{avg}). The relative error was calculated for all the sensor's characterizations after each polishing procedure, see Table 4.10. The fitting parameters as well as the maximum error obtained for each sensor ($\delta k_{norm,max}$) are listed in Table 4.11.



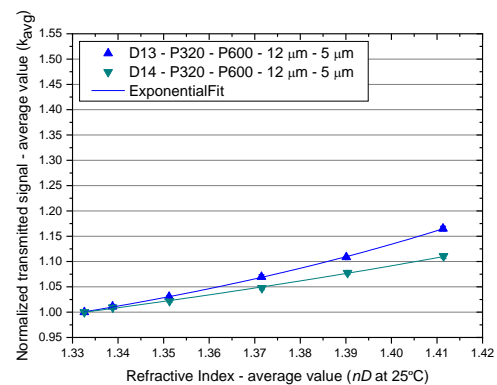
(a) Polishing 1 (P320 ~ 46 μm)



(b) Polishing 2 (P600 ~ 26 μm)



(c) Polishing 3 (12 μm grit size)



(d) Polishing 4 (5 μm grit size)

Figure 4.22 Response of the D-shaped POF sensors with increasing refractive index after each polishing procedure.

Table 4.10. Relative error obtained from the RI characterizations after each polishing procedure (calculated using Equation 3.10).

| Sensor | Relative error (%) | | | |
|--------|--------------------|------|----------------------------|---------------------------|
| | P320 | P600 | 12 μm grit size | 5 μm grit size |
| D11 | 1.50 | 1.14 | - | - |
| D12 | 1.92 | 0.48 | 1.23 | - |
| D13 | 0.79 | 0.65 | 0.89 / 0.41 | 0.39 |
| D14 | 0.62 | 0.68 | 0.51 | 0.43 |
| D15 | 0.66 | 1.31 | - | - |

A relative error lower than 2% was obtained for all the sensors in all RI characterizations showing the reproducibility on the sensor's responses. A relative error lower than 1% was obtained for sensors D13 and D14 in all RI characterizations and for sensor D12 after polishing with sandpaper P600 and sensor D15 after polishing with sandpaper P320. These results show that the relative error is not dependent on the grit size of the sandpaper used for the polishing procedure.

 Table 4.11. D-shaped POF sensors – maximum error obtained from the RI characterizations ($\delta k_{norm_{max}}$) and obtained parameters from the exponential fit.

| Sensor | $\delta k_{norm_{max}}$ (a.u.) | R_0 | A | Reduced χ^2 | Adj. R^2 |
|---|-----------------------------------|------------------|-----------------------------------|--------------------------|------------|
| Polishing 1 - P320 (~46 μm) | | | | | |
| D11 | 5.67×10^{-3} | 19.74 ± 0.92 | $(3.01 \pm 3.96) \times 10^{-13}$ | 5.7387×10^{-6} | 0.99956 |
| D12 | 5.67×10^{-3} | 17.67 ± 0.96 | $(5.80 \pm 7.96) \times 10^{-12}$ | 6.2849×10^{-6} | 0.99951 |
| D13 | 5.23×10^{-3} | 20.87 ± 1.33 | $(0.57 \pm 1.09) \times 10^{-13}$ | 1.1250×10^{-5} | 0.99908 |
| D14 | 3.86×10^{-3} | 15.59 ± 0.63 | $(9.93 \pm 9.05) \times 10^{-11}$ | 2.0756×10^{-6} | 0.99978 |
| D15 | 7.54×10^{-3} | 19.19 ± 0.70 | $(5.74 \pm 5.72) \times 10^{-13}$ | 2.5028×10^{-6} | 0.99974 |
| Polishing 2 - P320 (~46 μm) - P600 (~26 μm) | | | | | |
| D11 | 4.61×10^{-3} | 18.13 ± 0.63 | $(4.09 \pm 3.68) \times 10^{-12}$ | 4.9376×10^{-6} | 0.99979 |
| D12 | 7.07×10^{-3} | 12.97 ± 1.32 | $(4.08 \pm 7.84) \times 10^{-09}$ | 8.0058×10^{-6} | 0.99900 |
| D13 | 5.94×10^{-3} | 19.52 ± 1.27 | $(4.28 \pm 7.80) \times 10^{-13}$ | 1.1990×10^{-5} | 0.99915 |
| D14 | 3.72×10^{-3} | 15.44 ± 1.18 | $(1.38 \pm 2.35) \times 10^{-10}$ | 8.9359×10^{-6} | 0.99923 |
| D15 | 4.25×10^{-3} | 18.45 ± 0.84 | $(2.76 \pm 3.32) \times 10^{-12}$ | 1.1189×10^{-5} | 0.99962 |
| Polishing 3 - P320 (~46 μm) - P600 (~26 μm) - 12 μm | | | | | |
| D12 | 3.44×10^{-3} | 12.16 ± 0.67 | $(1.92 \pm 1.88) \times 10^{-08}$ | 4.4856×10^{-06} | 0.99974 |
| D13 | 6.48×10^{-3} | 8.20 ± 3.06 | $(0.35 \pm 1.58) \times 10^{-05}$ | 2.4399×10^{-05} | 0.99461 |
| | 7.32×10^{-3} | 12.03 ± 0.97 | $(2.29 \pm 3.23) \times 10^{-08}$ | 8.6735×10^{-06} | 0.99947 |
| D14 | 3.77×10^{-3} | 12.33 ± 0.68 | $(8.68 \pm 8.67) \times 10^{-09}$ | 1.5171×10^{-06} | 0.99973 |
| Polishing 4 - P320 (~46 μm) - P600 (~26 μm) - 12 μm - 5 μm | | | | | |
| D13 | 3.19×10^{-3} | 8.09 ± 0.68 | $(3.85 \pm 3.93) \times 10^{-06}$ | 1.1013×10^{-06} | 0.99973 |
| D14 | 3.19×10^{-3} | 4.06 ± 1.88 | $(1.29 \pm 3.93) \times 10^{-03}$ | 3.7801×10^{-06} | 0.99794 |

An increase in the transmitted signal through the D-shaped POF sensors was obtained with the increase of the external refractive index. After polishing with sandpaper P320, an increase of

around 25% to 30% in the light transmitted through the POF sensor's was observed, see Figure 4.22(a). The response of the sensors was very similar until the refractive index reached around 1.37. With further increase of the external refractive index, the sensors D11, D12 and D13 showed higher response.

After Polishing 2 (P600), depicted in Figure 4.22(b), higher variation in the transmitted light (23% to 45%) with the same variation in refractive index was generally obtained. Contrary to the others sensors, sensor D12 showed a lower response ($k_{avg} \sim 1.23 \text{ a.u.}$ instead of $\sim 1.29 \text{ a.u.}$) and initial transmitted light in water ($k_{water} = 0.174 \text{ a.u.}$ instead of 0.179 a.u.). This can mean that this polishing procedure was not enough to change the guiding properties of the sensor D12 as the obtained results were very similar.

The D-shaped POF sensors D12, D13 and D14 were further polished with a sandpaper of lower grit size ($12 \mu\text{m}$) and generally showed a lower response (19% to 34% variation), see Figure 4.22(c). Two sets of experiments were performed with the sensor D13 and different responses were obtained. It was verified that higher the initial transmitted signal in water (k_{water}) higher response was obtained, revealing the importance of the connectorization between the POF sensor, the LED and the photodiode. Higher transmitted signal was expected with the decrease of the sensing region roughness as discussed in the section 4.2.3.2.2. The lower transmitted signal firstly obtained for the sensor D13 can be related with a mismatch in the POF connectorization or dust in the fibre tip and, when the experiments were repeated higher values were obtained. Nevertheless, after this polishing procedure, lower or similar response was obtained even with higher initial transmitted light in water.

After Polishing 4 ($5 \mu\text{m}$ grit size) the variation in the transmitted light decreased with increasing RI for both sensors (variation from around 11% to 17%), depicted in Figure 4.22(d).

In order to better understand the influence of the initial transmitted light in water (k_{water}) and surface roughness in the variation of the sensor's response (maximum value of k_{avg}), all the data was analysed together and is depicted in Figure 4.23.

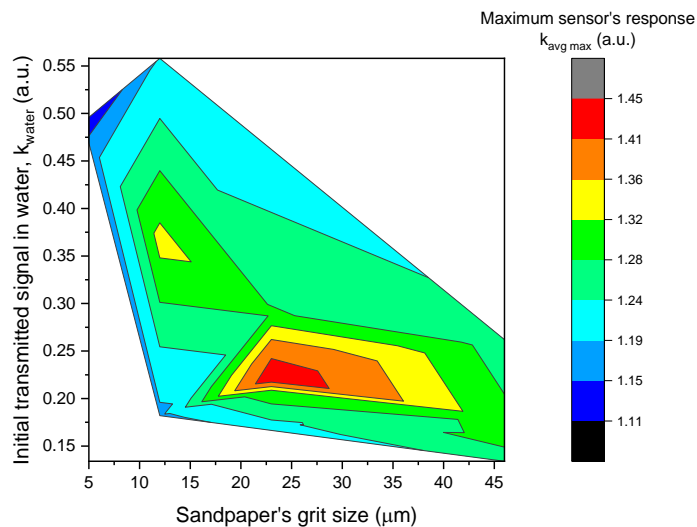


Figure 4.23 Combined data - maximum response of the D-shaped POF sensors ($k_{avg_{max}}$), initial transmitted signal in water (k_{water}) and grit size of the polishing paper.

From the analysis of the light losses in the D-shaped POF sensors with the polishing procedures (section 4.2.3.2.2) it was observed that by polishing the sensing region with a sandpaper of lower grit size (leading to lower surface roughness) the scattering of the light decreases, increasing the transmitted light through the POF sensor (higher output voltage measured in the photodiode).

Figure 4.23 shows that lower surface roughness (obtained after polishing with finer sandpaper with grit sizes of 12 μm or 5 μm) generally resulted in higher light transmission but lower sensor's response with RI variation. By polishing with coarser sandpapers, e.g. P320 with grit size of $\sim 46 \mu\text{m}$, the response of the sensors is similar to when the sandpaper of 12 μm grit size was used, even if a decrease in the initial transmitted signal in water was obtained. In summary, the best sensor's performance was achieved when the balance between roughness (enhancing the interaction of light with the external medium) and transmission losses due to polishing was obtained. Results show that this balance was achieved when the sensors were polished with sandpaper P600 ($\sim 26 \mu\text{m}$ grit size).

It was also observed more linearity on the sensor's responses after polishing with sandpapers of lower grit size (lower values of R_0). For that reason, sensor's responses were also fitted using linear regression and the obtained adjusted R square are listed in Table 4.12.

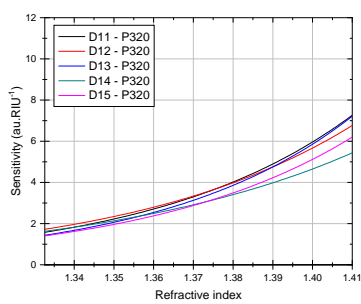
Table 4.12. Linear regression – obtained adjusted R-Square after the different polishing procedures.

| Sensor | Sandpaper | | | |
|--------|--------------------------------|--------------------------------|----------------------------|---------------------------|
| | P320 ($\sim 46 \mu\text{m}$) | P600 ($\sim 26 \mu\text{m}$) | 12 μm grit size | 5 μm grit size |
| D11 | 0.94575 | 0.95417 | - | - |
| D12 | 0.95513 | 0.97251 | 0.97823 | - |
| D13 | 0.94009 | 0.94718 | 0.97839 - 0.97865 | 0.99037 |
| D14 | 0.96572 | 0.96648 | 0.97791 | 0.99368 |
| D15 | 0.94895 | 0.95200 | - | - |

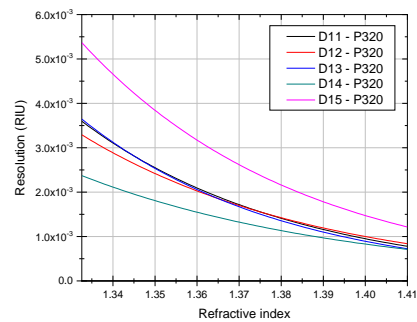
Clearly, the linearity on the response of the D-shaped POF sensors increases with the decreasing roughness of the sensing region and the consequently decrease of scattering at the sensitive region. Nevertheless, linearity is not mandatory in sensing – the sensors can be characterized and calibrated as they give a repeatable and recoverable response.

The sensitivity (S) and resolution (Δn) of the D-shaped POF sensors (D11-D15), depicted in Figure 4.24, were also calculated using Equation 3.11 and Equation 3.12, respectively, together with Equation 4.7.

The performance of the sensors is not only dependent on the increase of the transmitted light with refractive index (sensitivity) but also on the maximum error obtained for each sensor in the set of experiments performed ($\delta k_{norm,max}$), which was used to calculate the resolution of the sensors.

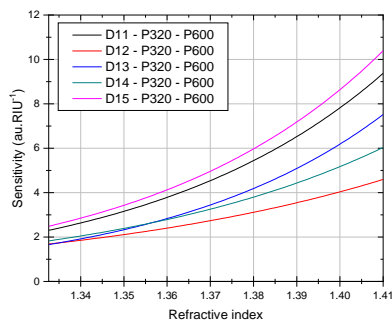


(a)

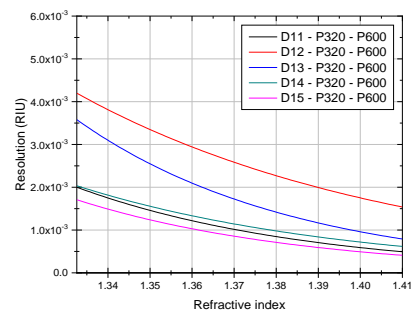


(b)

Polishing 1 - P320 (~46 μm)

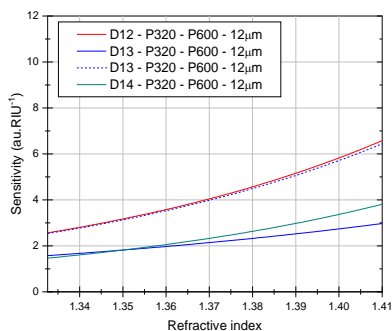


(c)

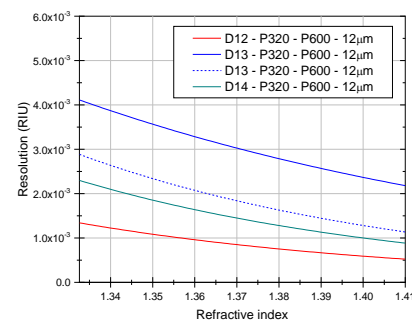


(d)

Polishing 2 - P320 (~46 μm) - P600 (~26 μm)

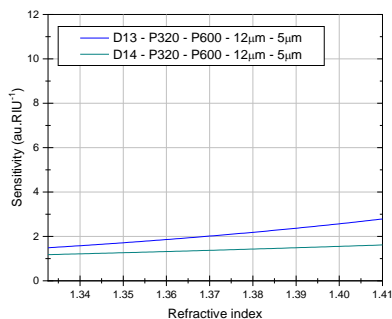


(e)

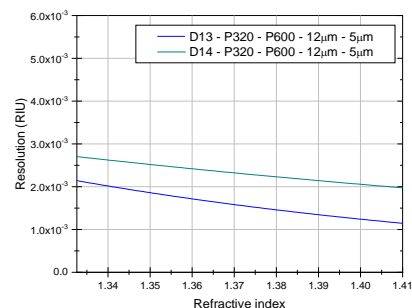


(f)

Polishing 3 - P320 (~46 μm) - P600 (~26 μm) - 12 μm



(g)



(h)

Polishing 4 - P320 (~46 μm) - P600 (~26 μm) - 12 μm - 5 μm

Figure 4.24 D-shaped POF sensors D11 – D15: sensitivity (a,c,e,g) and resolution (b,d,f,h) after each polishing procedure.

The sensitivity and resolution of the D-shaped POF sensors are dependent on the external RI: higher the refractive index of the external medium, higher was the sensitivity and lower the resolution of the sensors, as previously verified. The sensors' performance is also dependent on the roughness of the sensing region. To have an overview of the obtained results, all data were combined in a contour – colour fill plot and depicted in Figure 4.25.

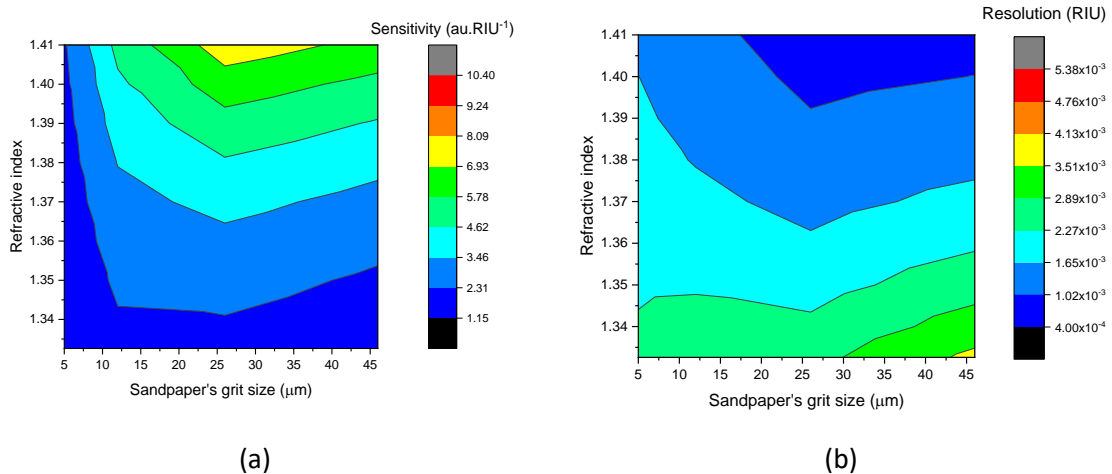


Figure 4.25 Sensitivity (a) and resolution (b) of the D-shaped POF sensors (D11 – D15).

In general, the D-shaped POF sensors showed higher sensitivities and lower resolution values after Polishing 2 (P600 ~ 26 μm) (see Figure 4.25). A resolution of 10⁻⁴ RIU was achieved for values of RI higher than 1.36 for sensor D15, 1.37 for sensor D11, 1.38 for sensor D14, and 1.40 for sensor D13 after polishing with sandpaper P600; for the sensor D12, a resolution of 10⁻⁴ RIU was obtained for RI higher than 1.36 after Polishing 3 (12 μm grit size).

Polishing with coarser sandpaper leads to higher roughness of the sensing region and, consequently, higher scattering of the light and less light transmission through the fibre, as already discussed and validated. With the increase of the external medium's refractive index an increase in the transmitted light through the POF was observed, independently of the roughness of the sensing region. Considering the external medium as a substitute cladding, a decrease in the transmitted light would be expected with the increase of the refractive index, as at higher external RI, the angle needed for the total internal reflection (TIR) to occur also would be higher (see section 2.3.1, Chapter 2). According to Snell's law of refraction, for the RI variation from 1.3326 (distilled water) to 1.41, the critical angle would increase from around 63° to 71° (see Equation 2.5), which means that fewer light rays would satisfy the condition for TIR, and, consequently, more light would be refracted and less light would be totally transmitted, reaching the detector. However, this is true considering smooth flat surfaces, while for rough surfaces scattering will play an important role. As the obtained results show, an increase in the medium refractive index leads to a decrease in the scattering losses caused by the roughness of the sensing region, as a higher refractive index will allow for the surface to appear smoother to the light ray that travels in the POF, resulting in the observed increase in transmitted light.

Lower surface roughness means lower scattering and higher transmitted light; however, at the same time, it also means that less light will interact with the external medium and the same variation in the refractive index will cause a lower variation in the transmitted signal, resulting in

the increasingly linear response with decreasing surface roughness. In opposition, rough surfaces mean higher scattering and less light transmitted through the POF but also higher interaction with the external medium with an exponential response to RI variations. Therefore, a balance in surface roughness is needed in order to optimize the sensor's performance.

In the studies reported in the literature, P600 was found to be the polishing paper that allowed better sensor performance (Leal-Junior, Frizera and José Pontes, 2018). In this case, an increase in linearity was not observed after polishing with this sandpaper. On the contrary, it was observed that smoother surfaces allow for more linearity in the sensor's response. Furthermore, when several polishing papers are used in the sensor's manufacture, care should be taken as the previous polishing procedure can affect and influence the sensor's response if the surface roughness is not properly changed by the new polishing procedure, as reported in (Cennamo, Pesavento, *et al.*, 2019).

4.2.3.2.6 Conclusions

The roughness of the sensing region is an important parameter for the transmission capacities of POFs and, consequently, for their sensing performance. Smoother surfaces allow for more light being transmitted, whereas rougher surfaces lead to more scattering losses and, therefore, less light transmission through the POF. At the same time, correct adjustment of the surface roughness allows to increase the sensor's response to changes in the external medium properties, such as refractive index variations.

Despite the manual manufacturing process of these sensors, it was verified that the thickness of the sensing region and the consequent height of the D-shaped sensors were very similar, with a variation smaller than the thickness variation given by the POF manufacturer. Also, the roughness of the sensing region can be directly controlled by using sandpaper with specific grit sizes.

In general, the best performances were achieved after polishing the sensing region with sandpaper P600, and by smoothing the surface lower sensitivity and higher resolution value were obtained. Smoother surfaces allow higher linearity on the sensor's response, although this is not an important request as sensors with nonlinear response can be used as long as their response is repeatable and reversible. A resolution of 10^{-3} – 10^{-4} RIU was obtained, dependent on the value of the external refractive index.

The reproducibility on the sensor's response was verified after the first polishing procedure (P320) as a similar response was obtained with increasing RI. Less reproducible behaviour was observed after the following polishing procedures, which can be related to the manual manufacturing process resulting in an irregular interface between the unpolished POF and the sensing region. This aspect should be improved in the future in order to obtain higher reproducibility of the sensor's manufacture and to avoid scattering losses that do not contribute to the sensing capabilities of the sensors. Furthermore, the connectorization between the POFs and the LED and photodiodes is also an important parameter that can affect the reproducibility in the sensor's responses.

The lack of normalization in the calculation of the performance of POF-RI sensors makes it difficult to compare the obtained results with those reported in the literature. Nevertheless, the obtained resolution was similar to that reported in (Gowri and Sai, 2016) (1 mRIU), although it was dependent on the external refractive index (10^{-3} – 10^{-4} RIU).

The surface roughness of the sensing region is of extreme importance when developing POF chemical sensors, as the variation in the refractive index that occurs in the selective receptor layer through the binding of the target analyte will allow for chemical detection.

4.2.4 Conclusions and future work

D-shaped POF sensors were developed and their performance was characterized and optimized for RI sensing. These sensors are easy to produce by simple, fast and low cost procedures. The performance of the D-shaped POF sensors is strongly dependent on the length, roughness of the sensing region and external refractive index.

Higher length of the sensing region resulted in higher sensitivity (2.83 au.RIU^{-1}) and lower resolution value ($3.93 \times 10^{-3} \text{ RIU}$) in the refractive index range between 1.33 – 1.39 when the sensing region was polished with sandpapers of 5 – 3 – 1 μm grit size. In the refractive index range between 1.41 – 1.47 the performance was dependent on the external refractive index and resolutions between 10^{-2} – 10^{-4} RIU were obtained. For RI higher than 1.42 the resolution is lower than 10^{-3} RIU for all sensors and only sensor D9, with a 6 cm of sensing region's length, allowed to obtain a resolution of 10^{-4} RIU ($8.5 \times 10^{-4} \text{ RIU}$) at RI equal or higher than 1.46. In this refractive index range the external RI must be taken into account in order to choose the length of sensing region that allows to obtain higher performances.

With increased surface roughness, by polishing with coarser sandpapers, the response of the sensors to RI variation becomes less linear and an exponential behaviour was observed in the RI range between 1.33 – 1.41. The preliminary studies revealed that by polishing the sensing region with a sandpaper of 5 μm grit size sensitivities between 5.7 – 12.9 au.RIU^{-1} could be obtained although with resolution of 10^{-2} RIU .

Further studies showed that a balance in the roughness of the sensing region allows to achieve the best sensor's performance. On one side, higher surface roughness means higher scattering and higher transmission losses. On the other side, also means higher interaction with the external medium and variations of refractive index led to higher sensor's response – higher increase in the transmitted light. In general, higher performances were obtained after polishing the sensing surface with sandpaper P600 and resolutions of 10^{-3} – 10^{-4} RIU were obtained.

Less reproducible behaviour (between the sensor's responses) was observed after the second and following polishing procedures. Furthermore, it was reported by Cennamo et al. (Cennamo, Pesavento, *et al.*, 2019) that previous polishing procedures can influence the sensor's response if the surface roughness is not properly changed by the new polishing procedure. Therefore, in further developments and in order to obtain higher reproducibility, the sensing region should be polished only using one polishing paper.

Other aspects can be also improved in order to increase the reproducibility of the sensor's manufacture, which can also increase the reproducibility of the sensor's response. These aspects are related with the interface between the sensing region and the unpolished POF. As already discussed, in further developments the planar support to which the POFs are embedded should be optimized in order to prevent light losses that do not contribute to the sensing capabilities of the D-shaped POF sensors. One possibility is to create a very smooth macro bending in the limits of the

sensing region making the unpolished POF enter the planar support, preventing its polishing. In that case, the D-shaped region could be defined easier and be limited to the sensing region.

As higher surface roughness allows for higher sensing performances, probably the length of the sensing region can be decreased still allowing for chemical detection. The proper length of the sensing region can be optimized depending on the refractive index of the selective layer which will be deposited on the D-shaped POF.

The developed sensors allow for low-volume sampling through the use of an appropriate flow cell or the sensors can be directly immersed in the matrix to be analysed. As it is, a volume of 1.6 mL is needed to cover completely the sensing region's surface (for 6 cm of sensing length).

D-shaped POF chemical sensors were developed through the deposition of a molecularly imprinted polymer (MIP) on the sensor's surface. The results will be presented in Chapter 5.

4.3 Straight POF RI sensors

POF sensors with a straight configuration were manufactured and characterized with sucrose solutions of increasing refractive index. Based on the results presented in Chapter 3 and presented in the previous section, namely the lack of sensitivity to RI variation when using unclad straight POFs and the enhancement of sensitivity with roughness adjustment using D-shaped POFs, there was the need to undergo in a deeper study about the possibility of sensitivity enhancement using an optical platform based on a straight POF configuration.

The performance (sensitivity and resolution) of the straight POF sensors for RI sensing was analysed and optimized by varying the roughness (section 4.3.1) and the curvature (section 4.3.2) of the sensing region. The length was fixed on 5 cm in accordance with the previous studies performed (section 3.3.2).

4.3.1 Roughness of the sensing region

From the studies performed and presented in Chapter 3 (section 3.9.6), unclad POFs do not respond to variations of refractive index, in the RI range between 1.33 – 1.41.

Preliminary studies related with the variation of surface roughness were performed. Two sensors were prepared by polishing the sensing region with a sandpaper of 12 μm grit size. These sensors were characterized to RI variation and their performance was compared with the one obtained for an unclad POF sensor. The obtained results confirmed that higher surface roughness allowed to increase the sensor's performance.

A more detailed study was carried out by manufacturing straight POF sensors with different sensing region's roughness, by polishing the sensing region with sandpapers of different grit sizes.

4.3.1.1 Sensors' preparation

The selected POF (DB-1000, from Asahi Kasei) has 1 mm diameter and 0.5 numerical aperture, step-index profile with a PMMA core and a perfluorinated polymer cladding (characteristics described in Table 2.2, Chapter 2).

Samples of POF were cut to the desired length using a POF cutter (45 cm and 60 cm) and the end faces were polished (5 μm , 3 μm , 1 μm and 0.3 μm) in a "Figure ∞ " pattern (see Figure 2.11).

The fluorinated polymer cladding was removed in the central region of the POF, using solutions of acetone (see section 3.3.3). In this process the fibre needs to be handled carefully to prevent from breaking. The length of the sensing region was fixed in 5 cm. After cladding removal, the fibres were washed with distilled water several times and left to dry.

The roughness of the sensing region was modified by polishing with sandpapers of different grit sizes – P320 (~ 46 μm), P600 (~ 26 μm), 12 μm , 5 μm and 1 μm . The polishing procedures were performed manually and intended to increase the roughness of the sensing region without significantly changing its thickness. All the polishing procedures were performed softly. The modified POF sensors were washed with distilled water several times and left to dry.

The sensing region's surface was observed by optical microscopy and the thickness was measured with a Mitutoyo Micrometer, see section 4.3.1.2.

Two sensors were prepared for each grit size, see Table 4.13.

Table 4.13. Straight POF sensors - sandpaper grit sizes used for the sensor's manufacture.

| Sandpaper grit size | Straight POF sensors | | | | | | | | | |
|------------------------|----------------------|----|----|----|----|----|----|----|----|-----|
| | S1 | S2 | S3 | S4 | S5 | S6 | S7 | S8 | S9 | S10 |
| P320 | x | x | | | | | | | | |
| P600 | | | x | x | | | | | | |
| 12 μm | | | | | x | x | | | | |
| 5 μm | | | | | | | x | x | | |
| 1 μm | | | | | | | | | x | x |

4.3.1.2 Morphology of the sensing region

The sensing regions were observed by optical microscopy (LEICA DM750M), see Figure 4.26. From the obtained images was possible to confirm the increase of the sensing region roughness due to the polishing procedures. Furthermore, polishing with coarser polishing papers lead to rougher surfaces. It was also possible to verify that the roughness did not change uniformly along the sensing region, which can probably lead to irreproducibility in sensor's responses.

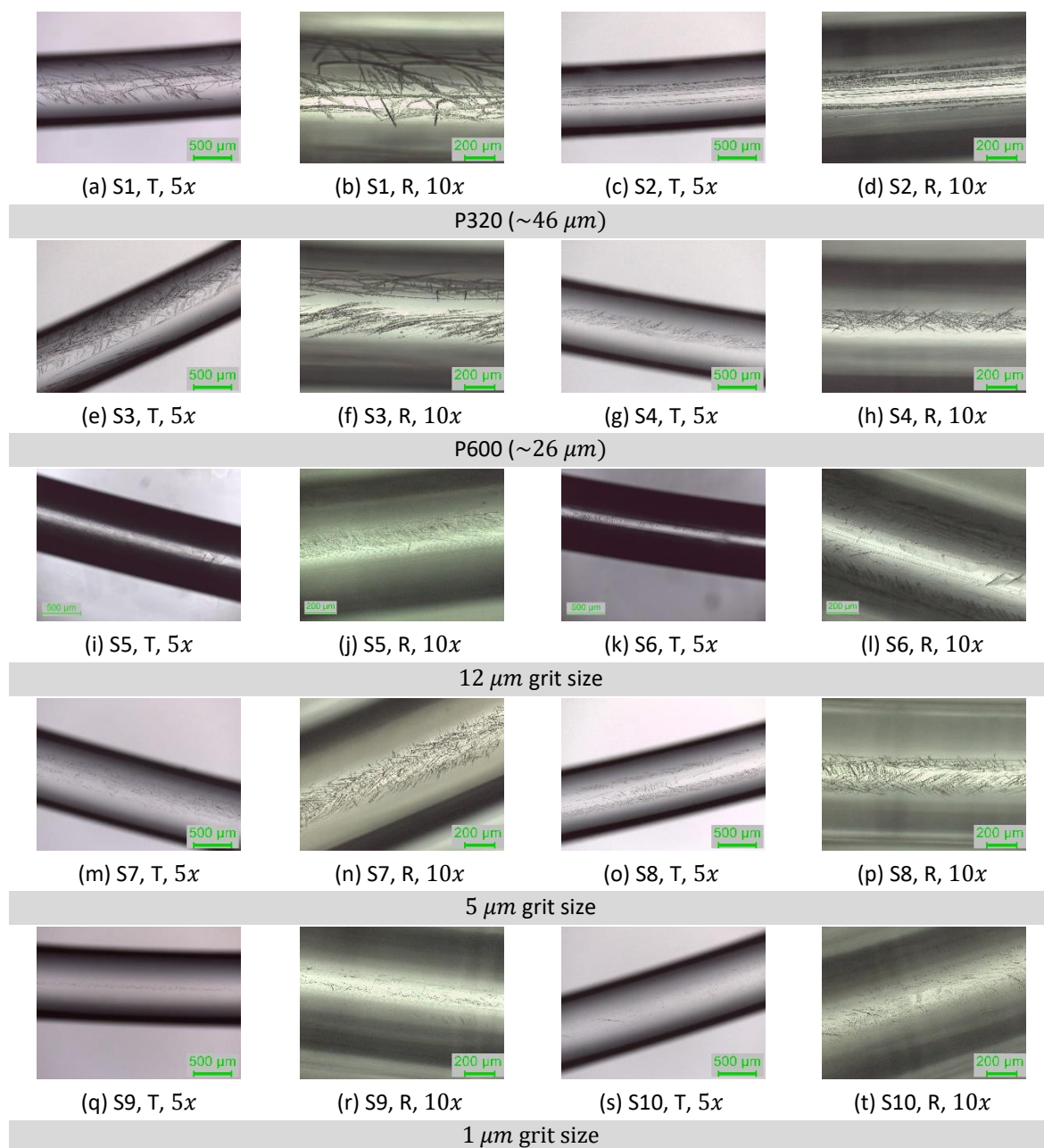


Figure 4.26 Straight POF sensors - microscope images of the sensing region, in transmission (T) and in reflection (R), using different magnifications (5x and 10x).

The thickness of the sensing region was measured before and after the polishing procedure and calculated by the average value and standard deviation of 30 measurements performed at different points of the sensing region. The measurements were performed using a Mitutoyo Micrometer (graduation of 1 μm and accuracy of $\pm 2 \mu\text{m}$), see Figure 4.27.



Figure 4.27 Thickness of the sensing region - measurements performed along the length of the sensing region with a Mitutoyo Micrometer.

The results are summarized on Table 4.14. As expected, a decrease in thickness of around $26 \mu\text{m}$ was obtained by removing the POF's cladding (cladding thickness is $\sim 10 \mu\text{m}$), with a standard deviation between $1 \mu\text{m}$ and $6 \mu\text{m}$, see Table 4.14. After polishing, no relevant thickness variation was obtained in the POF's sensing region. The obtained variation due to soft polishing was between $0.0 \pm 0.9 \mu\text{m}$ for sensor S4 and $1.2 \pm 6.4 \mu\text{m}$ for sensor S5.

Table 4.14. Straight POF sensors: thickness of the sensing region in different steps of production.

| Sensor | Thickness (μm) | | | | |
|--------|-----------------------------|-----------------|--------------------|-----------------|-----------------------|
| | Original POF | Unclad POF | Variation - unclad | Polished POF | Variation - polishing |
| S1 | - | 981.0 ± 2.1 | - | 980.8 ± 2.0 | 0.2 ± 2.9 |
| S2 | - | 958.4 ± 1.4 | - | 958.8 ± 1.5 | -0.3 ± 2.0 |
| S3 | - | 977.8 ± 1.0 | - | 977.3 ± 1.0 | 0.4 ± 1.4 |
| S4 | - | 971.1 ± 0.7 | - | 971.1 ± 0.6 | 0.0 ± 0.9 |
| S5 | 998.9 ± 4.5 | 972.9 ± 4.1 | 26.0 ± 6.1 | 971.6 ± 5.0 | 1.2 ± 6.4 |
| S6 | 998.4 ± 1.0 | 972.8 ± 1.1 | 25.7 ± 1.5 | 972.0 ± 0.9 | 0.7 ± 1.4 |
| S7 | - | 991.4 ± 0.5 | - | 991.0 ± 0.2 | 0.4 ± 0.5 |
| S8 | - | 962.1 ± 1.3 | - | 961.7 ± 0.9 | 0.4 ± 1.6 |
| S9 | - | 983.2 ± 1.4 | - | 983.1 ± 1.0 | 0.1 ± 1.7 |
| S10 | - | 982.3 ± 0.9 | - | 982.0 ± 1.1 | 0.2 ± 1.4 |

These results show that: (i) it is possible to change the roughness of the sensing region without significantly change its thickness when soft polishing is applied; (ii) the variation of thickness obtained is also related with the sensors' preparation conditions (see standard deviations obtained for the original POF sensors S5, S6).

4.3.1.3 Refractive Index Characterization

The polished straight POF sensors were characterized with the variation of refractive index using the battery powered Bluetooth based optical setup described in the section 3.8 and section 4.2.3.2.4.

The sensors were placed inside a glass reactor (see Figure 4.28) and characterized with the intensity based transmission system which comprised an LED (centred at 660 nm), a POF coupler

(90:10), two photodiode detectors and the data acquisition system (see Figure 4.19 and Figure 3.33). From Figure 4.28 is possible to see the scattered light from the POF's sensing region, due to the polishing procedure after removing the fibre's cladding.

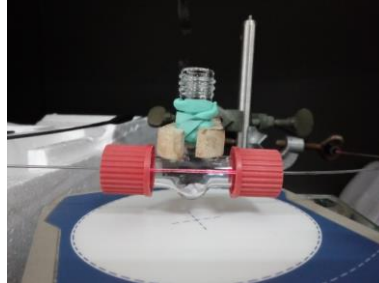


Figure 4.28 Sensing region of sensor S1, polished with sandpaper P320, inside the glass reactor.

The sensors were characterized using sucrose solutions prepared in distilled water with refractive index varying from 1.3326 (distilled water) to around 1.41. The refractive index of the solutions (n_D at 25°C) was measured using the Abbemat refractometer with 1×10^{-4} resolution.

The response of the sensors with air as the external medium was monitored during 15 min ($k_{air} \pm \delta k_{air}$) and then distilled water was added to the reactor ($k_{water} \pm \delta k_{water}$), see Figure 4.29(a).

The sensor's response was monitored for 5h and was normalized to the response obtained in air ($k_{norm_air} \pm \delta k_{norm_air}$), see Figure 4.29(b). The average values and standard deviations of the central 5 min were calculated for each 15 min monitoring (according with Equation 3.8 and Equation 3.9):

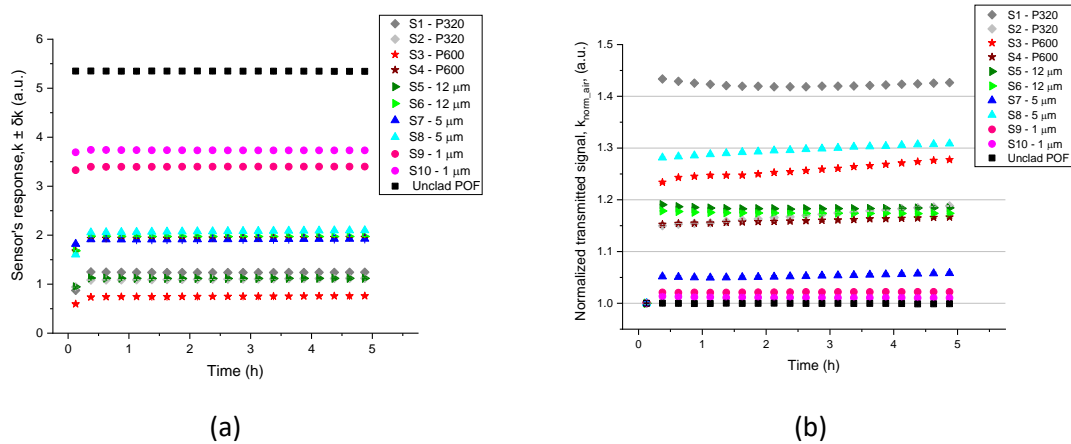


Figure 4.29 (a) Sensor's response ($k \pm \delta k$) with time; (b) normalized transmitted signal with time ($k_{norm_air} \pm \delta k_{norm_air}$). Water was added to the reactor at $t = 15$ min.

Results show that an increase of 1.35% for sensor S10 and 43.36% for sensor S1 in the transmitted signal occurs when distilled water was added. Sensors S9 and S10 (1 μm grit size)

presented higher transmitted signal and lower signal variation, similar to the unclad POF (sensor NJ8). Sensor's polished with sandpapers of 5 μm grit size or more showed lower transmitted signal (higher light losses) and higher signal variation with the transition air – water. This variation was not the same for sensors polished with the same sandpaper showing the irreproducibility of the sensor's manufacture.

After 5h, no significant variation was observed on the sensor's response for sensors S1, S5, S6, S7, S9, S10 (lower than 1%). An increase of the transmitted signal lower than 5% was obtained for sensors S4 (1.4%), S8 (2.7%), S2 (3.8%) and S3 (4.4%). This can be explained by water absorption mechanism of PMMA (Oliveira, Bilro and Nogueira, 2019).

The straight POF sensors were left in the glass reactor with the sensing region immersed in distilled water, until the variation of the transmitted signal was lower than 1% and the signal was considered stable.

The response of the straight POF sensors to the variation of refractive index was monitored in continuum. The sensors response was first recorded in distilled water ($k_{water} \pm \delta k_{water}$) for 15 min with constant stirring, after which the distilled water was removed and the next solution was added ($k_{solution} \pm \delta k_{solution}$). The average value and standard deviation of the sensor's responses were calculated for each solution, for the central 5 min monitoring. One washing was made with the next solution in order to clean the glass reactor and the POF sensing surface. This procedure was repeated for all the sucrose solutions.

The transmitted signal normalized to the response obtained with water ($k_{norm} \pm \delta k_{norm}$) was calculated according to Equation 3.8 and Equation 3.9.

At the end of each RI characterization, several washing steps with distilled water were performed in order to clean the reactor and the fibre's surface, which also allowed to verify the reversibility on the sensor's response. At least, three replicated measurements with increasing RI were performed for each sensor in order to verify the repeatability of the sensor's response and validate the obtained results.

The solutions were added using plastic pipettes and removed with a syringe. When the solutions were removed from the reactor, their refractive index was measured immediately using the commercial refractometer (1×10^{-4} resolution).

Prior to the sensors characterization with solutions of increasing refractive index, the stability of the sensor's response in water was verified before each RI characterization. This means that variations below 1% for all the sensor's responses were obtained.

As an example, Figure 4.30 depicts the obtained response in water in comparison with the response obtained with solutions of increasing RI, for sensor S3 and sensor S6.

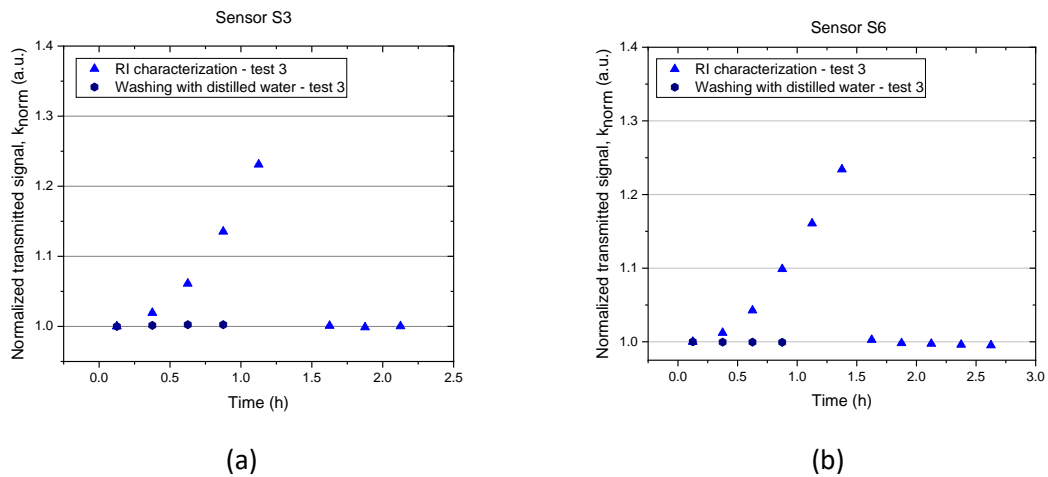


Figure 4.30 Straight POF sensors – water stability and RI characterization with time: (a) S3; (b) S6.

For each sensor, the considered replicated measurements were used to calculate the average value and standard deviation of the normalized transmitted signal ($k_{avg} \pm \delta k_{avg}$) related with the average value and standard deviation of the measured refractive index of the sucrose solutions ($n_{ext} \pm \delta n_{ext}$), see Figure 4.31 as an example. Outliers were not considered.

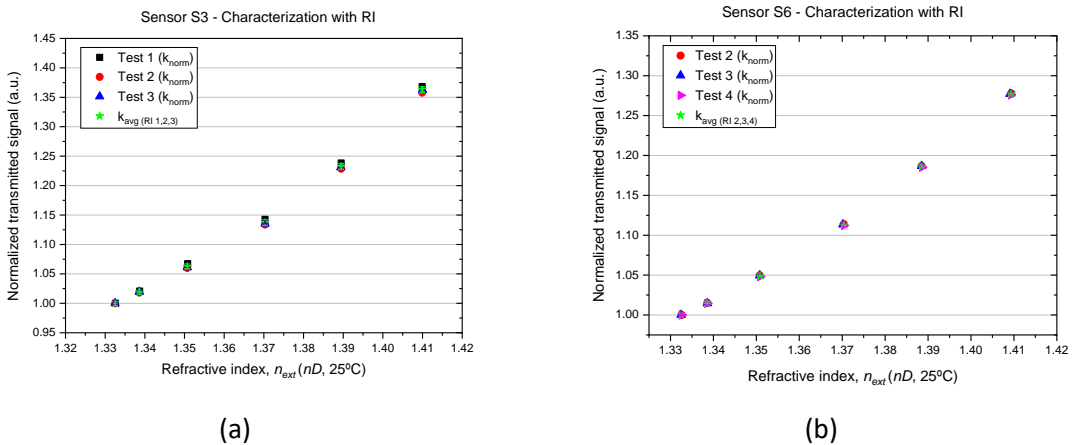


Figure 4.31 Straight POF sensors – obtained response with increasing refractive index: (a) S3; (b) S6.

The obtained responses with increasing refractive index for all the modified POF sensors ($k_{avg} \pm \delta k_{avg}$) are depicted in Figure 4.32, and were compared with the response given by an unclad POF (NJ8). The relative errors obtained for each sensor in the set of experiments performed were calculated, according with Equation 3.10, see Table 4.15. A relative error lower than 1% (0.08 – 0.51 %) was obtained for all straight POF sensors, showing the reproducibility on the sensor's responses.

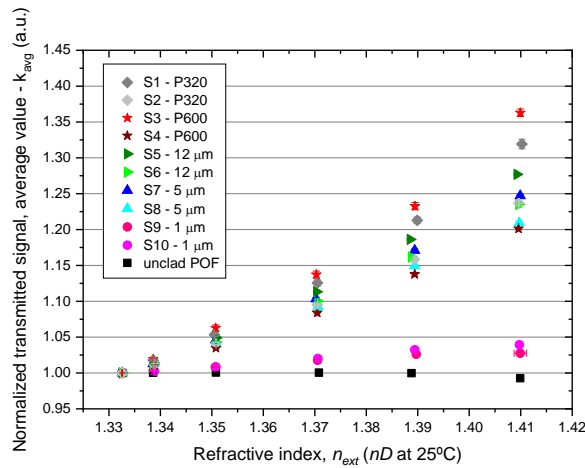


Figure 4.32 Straight POF sensors - response with increasing refractive index after polishing procedures and comparison with an unclad POF (NJ8).

Table 4.15. Straight POF sensors (S1 – S10) – characterization to RI variation: maximum sensor's response ($k_{avg_{max}}$), maximum error between experiments ($\delta k_{avg_{max}}$) and relative error calculated by Equation 3.10.

| Sensor | Sandpaper's grit size (μm) | Maximum response $k_{avg_{max}}$ (a.u.) | Maximum error $\delta k_{avg_{max}}$ (a.u.) | Relative error (%) |
|--------|---|---|---|--------------------|
| S1 | P320 ($\sim 46 \mu\text{m}$) | 1.319 | 6.7×10^{-3} | 0.51 |
| S2 | | 1.237 | 3.1×10^{-3} | 0.25 |
| S3 | P600 ($\sim 26 \mu\text{m}$) | 1.363 | 5.2×10^{-3} | 0.38 |
| S4 | | 1.201 | 2.7×10^{-3} | 0.22 |
| S5 | 12 μm | 1.277 | 1.0×10^{-3} | 0.08 |
| S6 | | 1.235 | 3.5×10^{-3} | 0.28 |
| S7 | 5 μm | 1.247 | 3.7×10^{-3} | 0.30 |
| S8 | | 1.209 | 2.1×10^{-3} | 0.17 |
| S9 | 1 μm | 1.028 | 2.0×10^{-3} | 0.19 |
| S10 | | 1.039 | 3.5×10^{-3} | 0.34 |

For the unclad POF (NJ8), as already shown in section 3.9.6, no variation in the sensor's response was observed with the increase of the external refractive index between 1.33 – 1.41. When the sensing region was polished with sandpapers of different grit sizes, an increase in the transmitted signal was observed for all sensors with increasing RI, as already verified for the D-shaped POF sensors. These results confirm the influence of surface roughness on sensor's response due to the increased light interaction with external medium.

For the sensors S9 and S10, polished with sandpaper of 1 μm grit size, the variation in the sensor's response is only of around 2.8% and 3.9%, respectively, for an RI range between 1.3326 and 1.41. For the sensors polished with sandpapers of 5 μm grit size or higher, was observed an increase of the transmitted signal between 20.1% and 36.3%. The response of the sensors polished with sandpaper of 5 μm grit size (20.9% - 24.7%) was much higher than the response obtained with

the sensors polished with sandpaper of 1 μm grit size. These results show the importance of surface roughness in the sensitivity of straight POF - RI sensors.

No reproducibility was obtained in the manufacture of these sensors as different sensors polished with the same sandpaper showed different responses with RI variation. Only sensors polished with sandpaper of 1 μm grit size showed similar responses. Sensors polished with sandpapers of 5 μm and 12 μm grit sizes showed a difference lower than 5 % between the maximum responses obtained for the different sensors (S7 and S8, 3.8 %; S5 and S6, 4.2 %). In future developments the POF's sensing region should be polished by a mechanical process in order to increase the reproducibility of the manufacturing process.

An exponential fit was applied to the obtained results, see Equation 4.7 and Figure 4.33. The fitting parameters as well as the maximum error obtained for each sensor ($\delta k_{norm_{max}}$) are listed in Table 4.16.

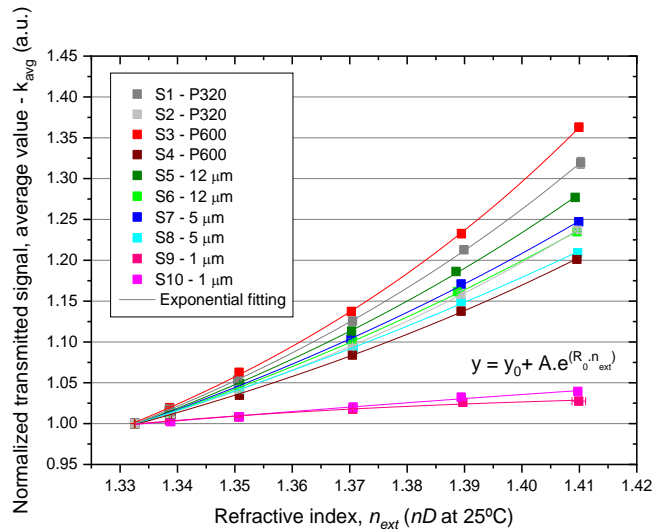


Figure 4.33 Straight POF sensors - response with increasing refractive index and exponential fitting.

Table 4.16. Straight POF sensors – sandpaper's grit size, maximum error obtained from the RI characterizations ($\delta k_{norm_{max}}$) and obtained parameters from the exponential fit.

| Sensor | Sandpaper's grit size | $\delta k_{norm_{max}}$ (a.u.) | R_0 | A | Reduced χ^2 | Adj. R^2 |
|--------|-----------------------|--------------------------------|-------------------|------------------------------------|------------------------|------------|
| S1 | P320 | 1.42×10^{-3} | 9.70 ± 0.38 | $(6.89 \pm 3.83) \times 10^{-07}$ | 1.21×10^{-06} | 0.99992 |
| S2 | (~46 μm) | 1.12×10^{-3} | 9.04 ± 0.39 | $(1.38 \pm 0.81) \times 10^{-06}$ | 7.26×10^{-07} | 0.99992 |
| S3 | P600 | 1.25×10^{-3} | 11.54 ± 0.63 | $(5.21 \pm 4.83) \times 10^{-08}$ | 4.31×10^{-06} | 0.99978 |
| S4 | (~26 μm) | 0.93×10^{-3} | 7.75 ± 0.77 | $(8.16 \pm 9.50) \times 10^{-06}$ | 2.05×10^{-06} | 0.99967 |
| S5 | 12 μm | 0.98×10^{-3} | 8.29 ± 0.66 | $(5.01 \pm 4.96) \times 10^{-06}$ | 2.86×10^{-06} | 0.99976 |
| S6 | | 0.68×10^{-3} | 6.34 ± 0.84 | $(0.81 \pm 1.05) \times 10^{-04}$ | 3.40×10^{-06} | 0.99960 |
| S7 | 5 μm | 1.05×10^{-3} | 6.56 ± 0.71 | $(6.03 \pm 6.56) \times 10^{-05}$ | 2.67×10^{-06} | 0.99972 |
| S8 | | 0.89×10^{-3} | 4.95 ± 1.15 | $(0.62 \pm 1.12) \times 10^{-03}$ | 4.95×10^{-06} | 0.99927 |
| S9 | 1 μm | 0.83×10^{-3} | -14.78 ± 6.55 | $(-1.55 \pm 13.11) \times 10^{07}$ | 2.67×10^{-06} | 0.98048 |
| S10 | | 0.70×10^{-3} | -2.96 ± 4.28 | -10.42 ± 45.99 | 2.59×10^{-06} | 0.99023 |

In order to better understand the influence of surface roughness on sensor’s performance, all data was analysed together by plotting contour – colour fill plots, see Figure 4.34, including the sandpaper’s grit size, transmitted signal in air (k_{air}) before water was added to the glass reactor, transmitted signal in water (k_{water}) after signal stabilization (average value of the obtained values in each RI test) and maximum sensor’s response with RI variation (k_{avgmax}).

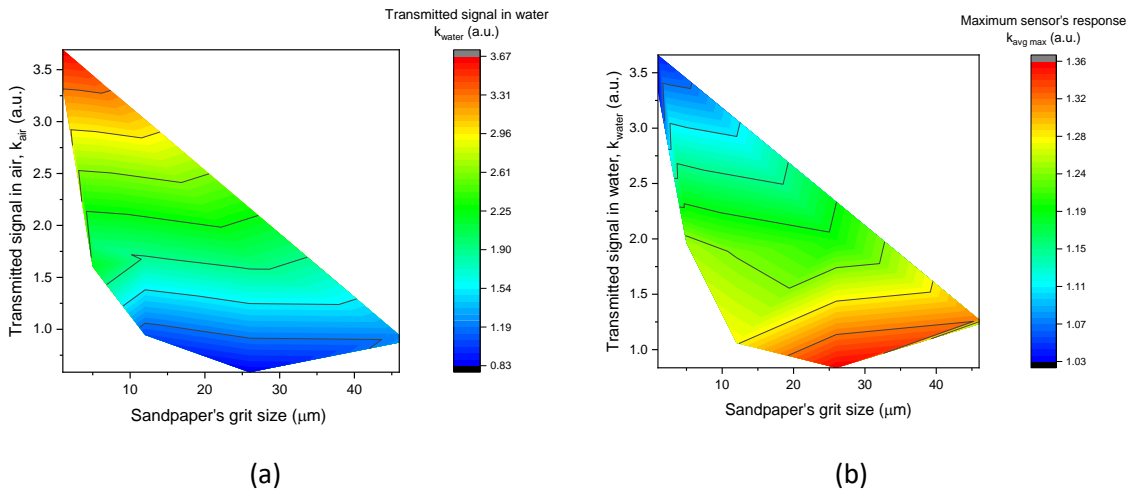


Figure 4.34 Combined data - grit size of the polishing papers, sensor’s response in air (k_{air}), transmitted signal in water (k_{water}) and maximum sensor’s response (k_{avgmax}).

Generally, lower the grit size of the sandpaper used for the polishing procedure, higher the transmitted signal in air before water was added to reactor (k_{air}) and consequently higher was the transmitted signal in water (k_{water}), see Figure 4.34(a). Moreover, lower the grit size of the sandpaper lower the maximum sensor’s response and the best results were achieved when sandpaper P600 (~26 μm grit size) was used for the polishing procedure, see Figure 4.34(b).

4.3.1.3.1 Sensitivity and resolution

The sensitivity (S) and resolution (Δn) of the straight POF sensors (S1-S10) were calculated using Equation 3.11 and Equation 3.12, respectively, as well as the exponential fitting applied to the obtained results (Equation 4.7). The obtained sensitivity and resolution are depicted in Figure 4.35.

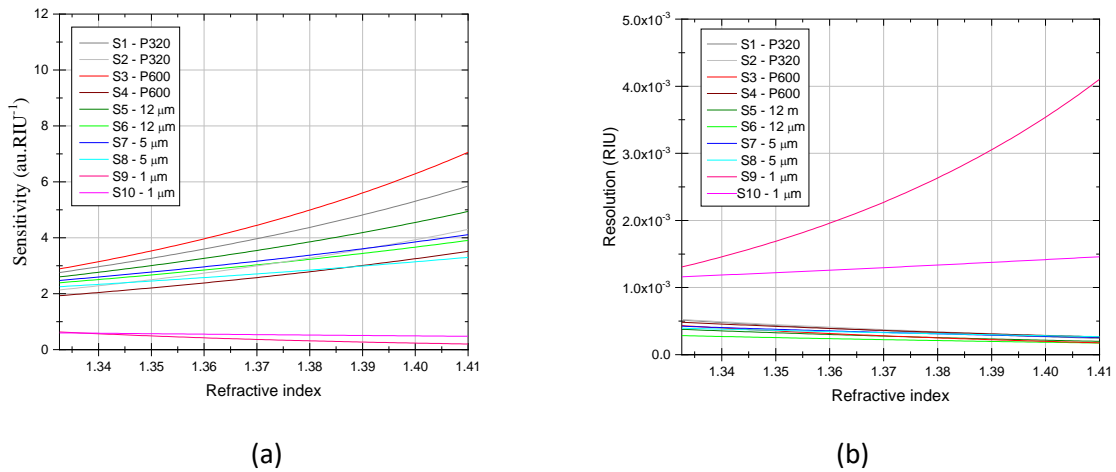


Figure 4.35 Sensitivity (a) and resolution (b) of the straight POF sensors.

The obtained sensitivity and resolution are dependent on the refractive index of the external medium. The sensors S9 and S10 (1 μm grit size) show a sensitivity lower than 1 au.RIU^{-1} and resolution higher than 1×10^{-3} RIU, for all the refractive index range. The sensors polished with sandpapers of 5 μm grit size or higher show sensitivities between $1.9 - 7.1 \text{ au.RIU}^{-1}$ and resolutions bellow 5.25×10^{-4} RIU, confirming the viability of these sensors for future developments on chemical sensing.

All data from the sensors polished with sandpaper of 5 μm grit size or higher was combined into a contour – colour fill plot and the results are depicted in Figure 4.36.

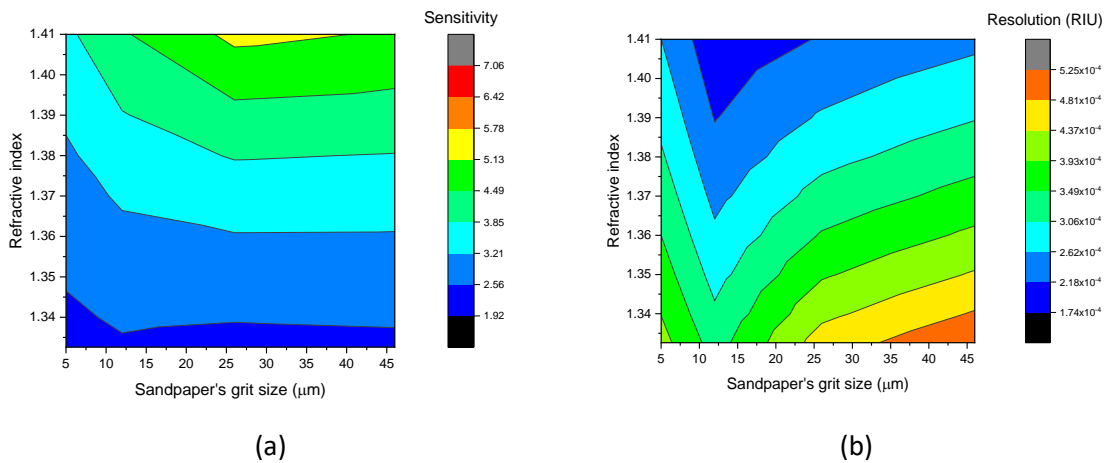


Figure 4.36 Combined data – sandpaper’s grit size, refractive index, sensitivity and resolution of the straight POF sensors.

From Figure 4.36, higher sensitivities were generally obtained for a grit size of 26 μm (P600) for RI equal or higher than 1.36. Lower resolution values were obtained for a grit size of 12 μm for RI equal or higher than 1.343. Nevertheless, because all sensors (S1 – S8) show a resolution below 4×10^{-4} RIU for RI higher than 1.36, P600 was the sandpaper which allowed the best balance between sensitivity and resolution obtained.

4.3.1.4 Conclusions

POF-RI sensors with a straight configuration were developed by simple and fast methods, only by changing the roughness of the sensing region with sandpapers of known grit size.

The soft polishing procedure applied allowed to change the roughness of the sensing region without significantly change the obtained thickness. The variation of roughness was confirmed by optical microscopy, although it was also verified the non-homogeneity of this process. The modification procedures by polishing should be further improved, in order to increase the reproducibility of the sensor's manufacture and consequently of the sensor's responses.

All sensors gave a repeatable response, as a relative error $\leq 0.51\%$ was obtained for all the straight POF sensors and the recovery on the sensor's response was verified with distilled water.

Sensor's produced by polishing the sensing region with a sandpaper of 1 μm grit size didn't show significant improvement in the performance, namely in terms of sensitivity and resolution.

Sensor's performance improved significantly when the sensing region was polished with sandpapers of 5 μm grit size or higher. The best sensor's performance was generally achieved by polishing the sensing region with sandpaper P600, nevertheless all sensors showed a resolution lower than 5.25×10^{-4} RIU, for all the refractive index range.

The straight POF sensors show much lower resolution values than the D-shaped POF sensors for RI sensing and, in this case, the resolution is on the same order of magnitude as the one obtained by SPR sensing with POF (6×10^{-4} RIU, (Cennamo *et al.*, 2011)), revealing promising results in chemical sensing with POFs.

4.3.2 Curvature of the sensing region - straight vs U-bent configurations

There are several POF sensors reported in the literature making use of bending for sensitivity enhancement (see section 2.6.2, Chapter 2). In order to understand the influence of curvature combined with roughness on the sensing capabilities of POFs, two sensors were again characterized with increasing RI by changing the curvature of the sensing region, one unclad POF (NJ9) and one unclad polished POF (S2, polished with sandpaper P320).

The same optical setup was used for the RI characterization with curvature (section 3.8 and section 4.2.3.2.4) and the bending radius (r_c) of the sensing region was varied between 6 cm and 2 cm, see Figure 4.37. Sensor's performance for bending radius below 2 cm was not evaluated, as advised by the manufacturer (Asahi Kasei, 2013).

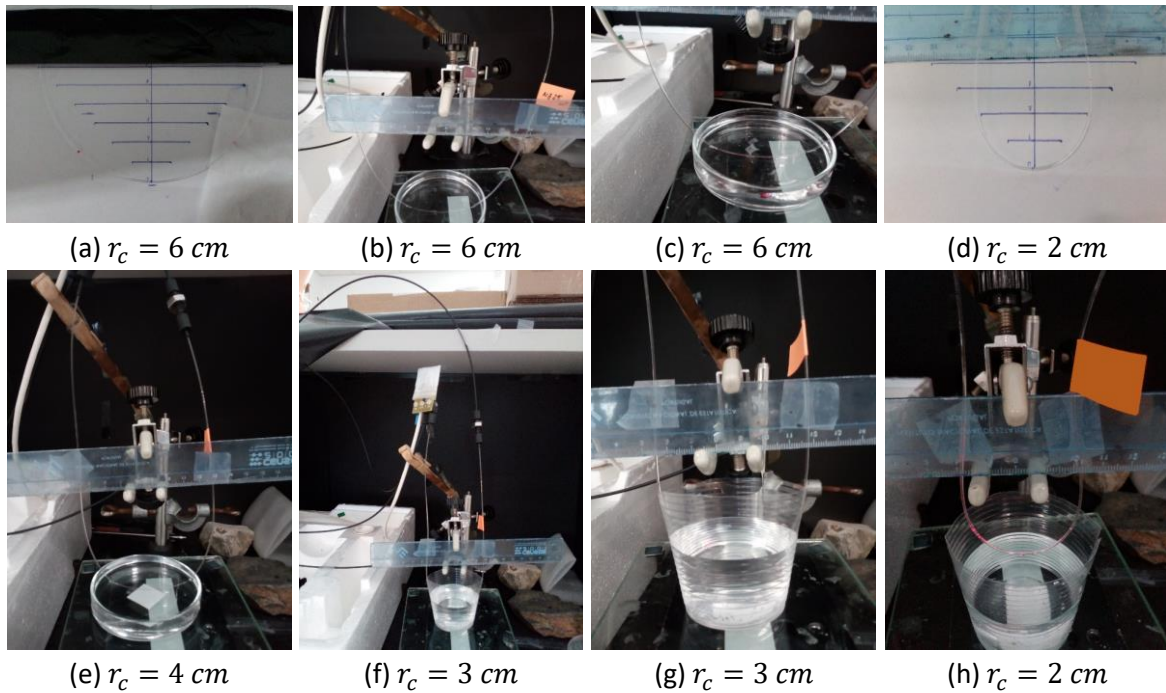


Figure 4.37 Images of the experimental setup for the RI characterization with curvature, for bending radius (r_c) between 6 cm and 2 cm.

Only one RI characterization was performed for each curvature radius. The POF's sensing region was totally immersed in sucrose solutions of different refractive indices, from 1.3326 to 1.41, and the sensor's response was monitored and recorded for 5 min, average value and standard deviation ($k \pm \delta k$). The normalized transmitted signal ($k_{norm} \pm \delta k_{norm}$) was calculated according to Equation 3.8 and Equation 3.9.

Two measurements in water were performed after RI characterization, for each curvature, to verify the recovery of the sensor's response, see Figure 4.38. The results for the straight configuration are the average values obtained ($k_{avg} \pm \delta k_{avg}$) for the RI characterizations described in section 3.9.6 (NJ9) and 4.3.1.3 (S2, P320).

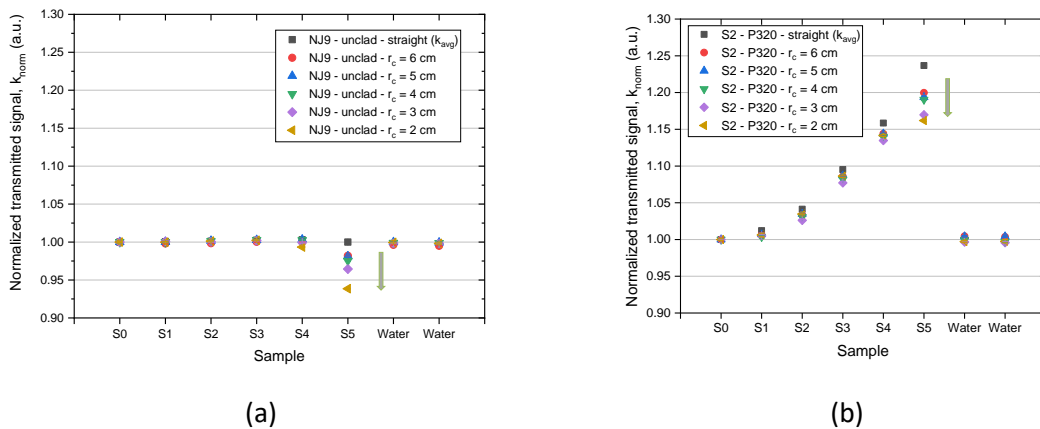


Figure 4.38 Sensor's response to RI variation with curvature - bending radius (r_c) from 6 cm to 2 cm, and comparison with a straight configuration (no bending), followed by two washing steps with distilled water: (a) unclad POF (NJ9); (b) sensor S2 (P320).

For both sensors, a decrease in the transmitted light was obtained with the decrease of the bending radius from 6 cm to 2 cm, showing the increased light loss by scattering due to the fibre's curvature as already discussed in Chapter 2 (section 2.4.1.4).

Results show that in the case of the unclad POF (NJ9) an enhancement on the sensor's sensitivity was obtained, between 1.39 – 1.41, maximum for a bending radius of 2 cm (variation of 5.49 % in the transmitted light for an RI variation of ~ 0.02). For sensor S2, polished with sandpaper P320, also a decrease in the sensor's response was observed with decreasing bending radius, although leading to lower sensitivity. As the response of this sensor increases with increasing RI due to the roughness of the sensing region, when applying a bending the two phenomena will compete leading to lower sensitivity with RI variation. For sensor S2, a variation of RI of around ~ 0.02 RIU caused a variation on the sensor's response of 7.83 % for the straight configuration and 2.04 % for a bending radius of 2 cm. What is important to verify is that roughness allows to increase the sensitivity of POF sensor's in all refractive index range between 1.3326 – 1.41, while bending an unclad POF only allows to increase the sensor's response in the RI range between 1.39 – 1.41, and probably at higher RI's until reaching the refractive index of the fibre's core (Lúcia Bilro *et al.*, 2011).

Initially, the idea was to perform the sensor's characterization with curvature for the sensors that revealed similar sensitivities with RI variation, whose sensing region had been polished with sandpapers of different grit sizes (S2 – P320, S6 – 12 μm and S7 – 5 μm). This would allow to deduce the influence of roughness combined with curvature in the performance of POF-RI sensors. Even though, from the obtained results was validated that roughness and curvature have two opposite effects in light transmission in POF's and, therefore, the other sensors were not characterized to RI with curvature variation as no improvement in the sensitivity was expected.

4.3.3 Conclusions and future work

Straight POF sensors were manufactured only by changing the roughness of the sensing region. Simple, fast and low-cost methods were used. Sandpapers with grit size higher than 5 μm allowed to obtain POF sensors with a resolution lower than 5.25×10^{-4} RIU and sensitivities between 1.9 – 7.1 au.RIU⁻¹, dependent on the external refractive index.

The reproducibility of the manufacturing process can be improved, also probably leading to an improve in the sensor's reproducibility (similar sensitivities for sensors prepared in similar way). One option can be the development of a mechanical polishing setup, allowing the rotation of the POF with controlled speed while polishing with sandpapers of known grit size.

Sensing region's roughness and bending are competitor phenomenon's, therefore, when applying bending smooth surfaces are advised. The refractive index range of interest combined with the best configuration for the foreseen application will determine the best procedure for the development of the POF sensors.

Further developments on chemical sensing were foreseen through the deposition of selective layers. The preliminary studies on the coating of polished unclad POFs with proteins were conducted and the results will be presented in Chapter 5.

4.4 Conclusions

Two POF sensing platforms were developed and their performance optimized for refractive index sensing, based on straight and D-shaped configurations. These POF sensors were easy to produce by simple, fast and low cost procedures.

The performance of the POF sensors is strongly dependent on roughness of the sensing region and external refractive index. Sensor's response becomes independent to external refractive index when finer polishing films were used and a linear behaviour was observed. The performance of the D-shaped POF sensors was further evaluated with the length of the sensing region revealing its direct dependency.

Performance optimization was based in the enhancement of light interaction with the external medium by modifying the POF structure and lowering the transmission capability in a controlled way. This was possible by changing the roughness of the sensing region.

In general, higher performances were obtained for D-shaped POF sensors after polishing the sensing surface with sandpaper P600 and resolutions of 10^{-3} – 10^{-4} RIU were obtained. Straight POF sensors polished with a sandpaper of 5 μm grit size or higher showed lower sensitivity (1.9 – 7.1 au.RIU⁻¹) in comparison with the D-shaped POF sensors (1.2 – 10.4 au.RIU⁻¹), although with much lower resolution values ($< 5.25 \times 10^{-4}$ RIU instead of $< 5.37 \times 10^{-3}$ RIU, dependent on external RI).

Manufacturing procedures can be improved, related with the polishing procedures and the obtained interface between the sensing region and the unpolished POF. Only one polishing film should be used together with an automated setup in order to improve manufacturing reproducibility. In case of straight configurations, a mechanical polishing setup which allows the rotation of the POF with controlled speed while polishing with sandpapers of known grit size could be developed. In D-shaped configurations, the planar support to which the POFs are embedded should be optimized in order to prevent light losses that do not contribute to sensing capabilities (interface clad-unclad polished region). One possibility is to create a very smooth macro bending in the limits of the sensing region making the unpolished POF enter the planar support, preventing its polishing. In that case, the D-shaped region could be defined easier and be limited to the sensing region.

The best configuration will depend on the foreseen application. A D-shaped POF sensor was coated with a sensitive layer for chemical detection, making use of its planar surface for spin coating deposition, while the immobilization of proteins on the surface of unclad straight POFs was evaluated by immersing the samples in protein solutions. Results will be presented in Chapter 5.

Chapter 5 POF chemical sensing and biosensing

5.1 Introduction

The coating of modified POFs with sensitive and selective layers allows the development of chemical sensors and biosensors for the selective detection and quantification of a chemical specie or family.

After the positive results achieved with the developed POF sensing platforms, described in the Chapter 4, the conditions are now positive for the development of POF chemical sensors and/or biosensors.

Different layers were chosen to be deposited on the surface of POFs: molecularly imprinted polymers (MIPs) and proteins. A previous reported MIP which showed viability for PFASs detection (Nunzio Cennamo, D'Agostino, *et al.*, 2018) was chosen as sensing layer for proof-of-concept and validation of the optical platform for viable POF-MIP integration for chemical detection. The studies conducted on chemical sensing by D-shape POF-MIP sensors are described in section 5.2. D-shaped POF sensors were developed, characterized and optimized for RI sensing. A molecular imprinted polymer (MIP), chosen as selective layer, was deposited in the sensing region of the sensors and the D-shaped POF-MIP sensors were characterized with PFOA solutions of increasing concentration (0 - 200 ppb).

Biosensors development for the detection of contaminants was foreseen through the coating of modified POFs with mutant proteins of interest. The obtained results with the preliminary studies on protein immobilization on the surface of modified straight POFs are in section 5.3.

5.2 D-shaped POF chemical sensors for the detection of perfluorooctanoate (PFOA/PFO⁻)

D-shaped POF chemical sensors for the detection of perfluorooctanoate (PFOA/PFO⁻) were developed in collaboration with Italian researchers.

5.2.1 Introduction and state of the art

Perfluoroalkylated substances (PFASs, with chemical formula $C_nF_{2n+1}-R$), also known as perfluorinated chemicals (PFCs), are widely used in industrial and consumer applications such as stain and water resistant coatings for fabric and carpets, oil-resistant coatings for food contact and cookware, among others (European Commission, 2010). Perfluorooctanesulfonic acid (PFOS, $C_8F_{17}SO_3^-$) and perfluorooctanoic acid (PFOA, $C_7F_{15}COO^-$) are important perfluorinated organic surfactants which belong to this family, see Figure 5.1.

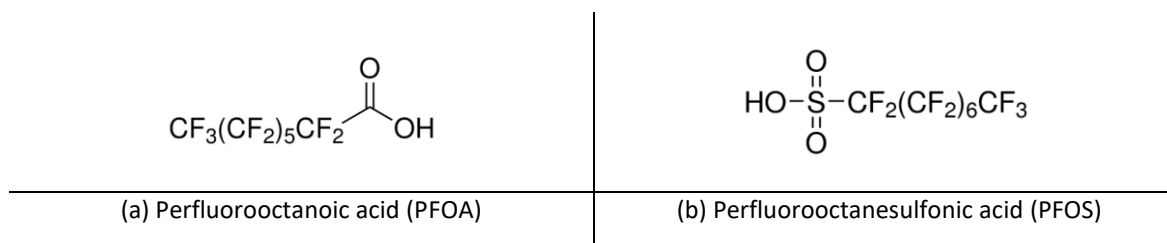


Figure 5.1 Structural formulas: (a) perfluorooctanoic acid, PFOA; (b) perfluorooctanesulfonic acid (PFOS).

In aqueous media, perfluorooctanoic acid (PFOA) stays in equilibrium with perfluorooctanoate ($\text{C}_7\text{F}_{15}\text{COO}^-$), the conjugate base, as well as perfluorooctanesulfonic acid (PFOS) and perfluorooctanesulfonate, ($\text{C}_8\text{F}_{17}\text{SO}_3^-$). In this chapter, PFOA/PFOS refers to the acid as well as to its conjugate base.

On 21 February 2008, the Scientific Panel on Contaminants in the Food chain adopted a scientific opinion ‘PFOS, PFOA and their salts’ and on 17 March 2010 the Commission Recommendation 2010/161/EC was adopted on the monitoring of perfluoroalkylated substances in food (European Commission, 2010).

In 2013, the Member State Committee identified PFOA as a persistent, bioaccumulative and toxic substance (PBT) in accordance with Article 57(d) of Regulation (EC) No 1907/2006a, and PFOA was included in the Candidate List of Substances of Very High Concern (SVHC) for possible inclusion in Annex XIV to Regulation (EC) No 1907/2006, REACH (European Commission, 2017). In 2017, the following entry relative to perfluorooctanoic acid (PFOA) and its salts was added to the Annex XVII to the REACH Regulation: “shall not be manufactured, or placed on the market as substances on their own from 4 July 2020” (European Commission, 2017).

The United States has health advisory levels for PFOA/PFOS of 0.07 $\mu\text{g}/\text{L}$. At the time of the proposal for a Directive of the European Parliament and of the Council on the quality of water intended for human consumption, in 2018, there was no legislative approach regulating PFASs, and there was no conclusive list of all the substances available. The WHO (World Health Organization) Europe report recommended adopting maximum parametric values for perfluorooctanesulfonic acid (PFOS) of 0.4 $\mu\text{g}/\text{L}$ and perfluorooctanoic acid (PFOA) of 4 $\mu\text{g}/\text{L}$. The Commission proposed the regulation of the whole group of PFASs, suggesting values of 0.1 $\mu\text{g}/\text{L}$ for individual PFASs and 0.5 $\mu\text{g}/\text{L}$ for PFASs in total (Annex I, part B - Chemical parameters). (European Commission, 2018)

Fluorochemicals are persistent contaminants which are not removed efficiently during wastewater treatment. Effluents from wastewater treatment plants (WWTPs) and Glatt River water in Switzerland were found to have perfluorooctanesulfonate (PFOS), which was detected in all samples, followed by perfluorohexane sulfonate (PFHxS) and perfluorooctanoate (PFOA) (Huset *et al.*, 2008). PFAS contamination affecting the groundwater, surface water and drinking water in the Veneto region, Italy, was discovered in 2013. Member States were required to establish and submit to the Commission (by December 2018) a monitoring and preliminary programme of measures for PFOS in surface waters (European Parliament, 2019). In 2016, a reported study by Lindim *et al.* showed that European’s major rivers were highly contaminated with PFOS and PFOA. The predicted PFOS levels in all the eleven rivers under study were consistently above the proposed surface water environmental quality standard (EQS) for inland waters, 0.65 ng/L (Lindim, van Gils and Cousins,

2016). In 2019, a study reported by Junttila *et al.* showed that PFASs were widely present in the Finish aquatic environment (Junttila *et al.*, 2019).

Perfluorooctanoic acid (PFOA) and perfluorooctanesulfonic acid (PFOS) are the most commonly detected compounds and generally occur with the highest concentrations in environmentally exposed organisms (Dewitt *et al.*, 2012). Furthermore, PFOA and PFOS have been detected worldwide in human blood (Eriksen *et al.*, 2011).

Therefore, these contaminants are very persistent and refractory to different biological and chemical treatments and their presence in the environmental matrix can give rise to toxic and bio accumulative effects, particularly to mammalian species. Immune-toxic effects of PFASs to cellular systems and animals are largely demonstrated, and different epidemiologic research studies have shown the potential effects of these chemical compounds on various human immune diseases (Dewitt *et al.*, 2012) (Corsini *et al.*, 2012). Health concerns for PFASs include cancer, reproductive and developmental effects, endometriosis, bioaccumulation, immunotoxicity, ulcerative colitis, and thyroid disease (Richardson and Kimura, 2016).

The common analytical methods for PFASs determination are based on chromatographic techniques coupled with mass spectrometry detection (Scott *et al.*, 2006) (Huset *et al.*, 2008) (Saito *et al.*, 2010) (Onghena *et al.*, 2012) (Young *et al.*, 2013) (Trojanowicz and Koc, 2013). Sensors based on electrochemistry (Chen *et al.*, 2013) (Zhang *et al.*, 2014) (Gong *et al.*, 2015), spectroscopy-based and enzyme-linked immunosorbent assay (ELISA)-based analysis (Wu *et al.*, 2018) have also been described. All of the mentioned methods are time-consuming, expensive and they often require a non-easy pre-treatment step. Richardson *et al.* reported two reviews regarding water analysis, in 2016 and 2018, where the problems concerning PFOA and PFASs are addressed as well as the analytical methods commonly used (Richardson and Kimura, 2016) (Richardson and Ternes, 2018).

POF sensors and biosensors for the detection of PFOA and PFASs can be found in the literature, see Table 5.1. Cennamo *et al.* reported in 2018 a POF biosensor for the detection of PFOA and PFOS in seawater samples. An LOD of 0.16 ppb was obtained for PFOA in buffer solution (20 mM sodium phosphate buffer (PBS, phosphate buffered saline), pH 7.4) and an LOD of 0.21 ppb was obtained in prepared seawater samples (460 mM sodium chloride solution, NaCl) (Nunzio Cennamo, Zeni, Tortora, *et al.*, 2018).

PFOA/PFASs detection in aqueous medium was also reported by Cennamo *et al.* in 2018. D-shaped POFs coated with gold and a molecularly imprinted polymer (MIP) allowed the detection of these contaminants with a wavelength-based optical setup. In this case, an LOD of 0.13 ppb was obtained for PFOA detection and an LOD of 0.15 ppb was obtained for a PFAS matrix (Nunzio Cennamo, D'Agostino, *et al.*, 2018). PFOA detection in aqueous medium using an optical fibre was also reported by Faiz *et al.* in 2019. The optical fibre end face was coated with Polyvinylidene Fluoride (PVDF) thin film and Fabry-Perot interference was monitored allowing to characterize the sensor's performance. (Faiz *et al.*, 2019)

Aforementioned studies did not report sensor parameters such as resolution, reversibility, recovery time, and selectivity. In summary, there is a need of low-cost alternatives for in-situ detection of these contaminants. These can be developed using POF sensors, by allowing remote, on-line and in-site monitoring, using cheaper and simpler intensity based setups.

Table 5.1. POF sensors for PFOA detection / sensing characteristics of different methods used for the detection and quantification of PFOA.

| Method | Analyte | Matrix | Response time | Sensitivity at low c (nm/ppb) | LOD (ppb) | Reference |
|--|---------|---|---------------|---------------------------------|-----------|---|
| SPR POF biosensor (wavelength based) | PFOA | Buffer solution | 10 min | 29.82 | 0.16 | (Nunzio Cennamo, Zeni, Tortora, <i>et al.</i> , 2018) |
| | | prepared seawater samples | | 22.59 | 0.21 | |
| SPR POF MIP (wavelength based) | PFOA | Aqueous solutions | 10 min | 22.14 | 0.13 | (Nunzio Cennamo, D'Agostino, <i>et al.</i> , 2018) |
| | PFASs | Standard matrix (11 PFASs) in distilled water | | 18.99 | 0.15 | |
| Optical fibre end face with PVDF thin film (FPI) | PFOA | Aqueous medium | - | - | - | (Faiz <i>et al.</i> , 2019) |

5.2.2 Optical sensing platform

D-shaped POFs were selected for the deposition of the MIP layer by spin coating and thermal polymerization, as the planar surface allows for easy deposition procedures as previously reported by Cennamo *et al.* (Nunzio Cennamo, D'Agostino, *et al.*, 2018).

The POFs were cut to 20 cm with a fibre optic cutter and were embedded in grooves engraved on planar supports (6 cm length, 1 cm high and 1 cm wide).

The surface of the fibres embedded in the planar surface was polished with a sandpaper of 22 μm grit size (P800) obtaining the desired D-shaped sensors (D16, D17, D18), see Figure 5.2.

Sandpaper of 10 μm (P2000) and 5 μm (LFG5P) grit sizes were also used for the final polishing procedure of the sensor D18. Sensor D19 was only polished with sandpaper of 10 μm and 5 μm .



Figure 5.2 Produced D-shaped sensors (D16 – D19).

The D-shaped POF sensors were characterized using a commercial setup similar to the one depicted in Figure 4.3, section 4.2.2.1.1. This commercial intensity based sensing setup comprised an LLS LED light source (627 nm), a POF coupler (50:50), two DET10A-M Si Biased detectors and a Picoscope (PicoScope® 6, Pico Technology Ltd.) connected to a laptop which allowed to record the data, see Figure 5.3.

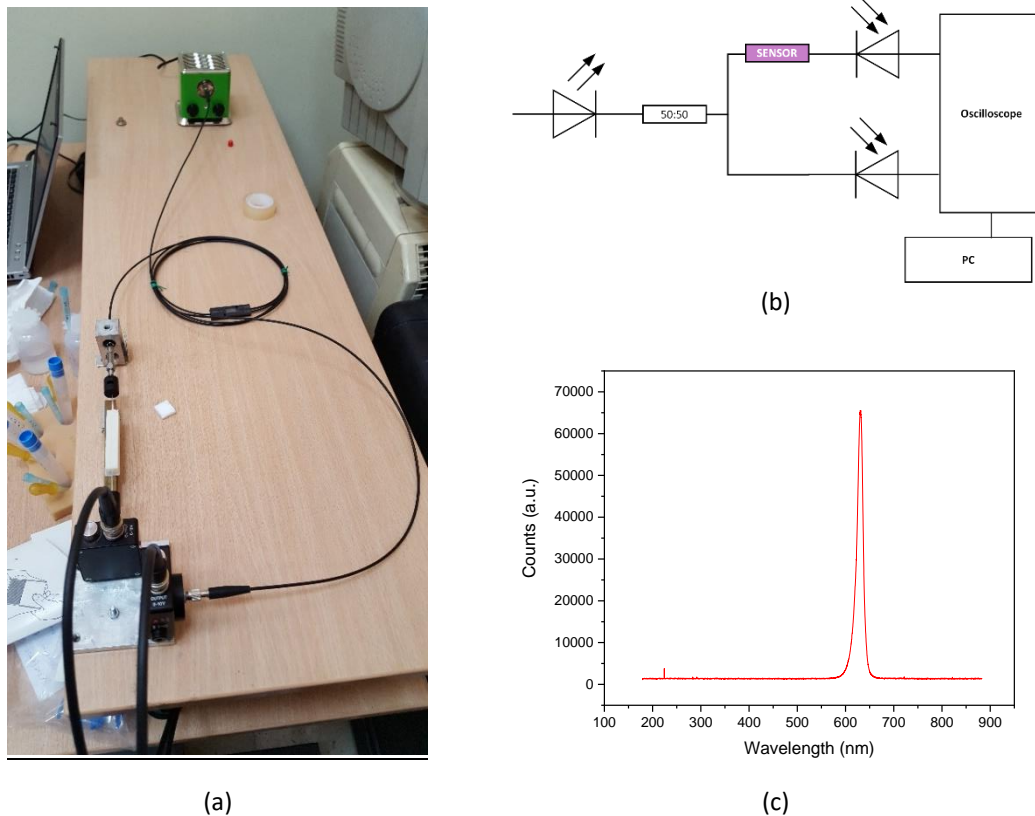


Figure 5.3 Intensity based optical sensing system: (a) photograph of the experimental setup; (b) schematic representation; (c) LED spectrum (LLS LED, 627 nm).

Output data, time and voltages of the reference and sensor signals, V_{ref} and V_{sensor} respectively, were logged into a laptop by means of Picoscope' software. The self-referenced transmitted signal (k) was used to correct source fluctuations and variations due to external conditions, as previously defined in section 3.8, Chapter 3.

5.2.3 Refractive index characterization

Prior to the deposition of the MIP layer, the sensitivity and resolution of the manufactured D-shaped POF sensors for RI sensing was obtained.

The sensors were characterized in transmission with the optical setup mentioned above, using glycerin solutions of increasing refractive index, from 1.332 to 1.395. The solutions of glycerin were prepared using distilled water and the refractive index was measured with an Abbe Refractometer.

First, the stability of the sensor's response with time was verified with distilled water covering the sensing region (as already described in Chapter 4). For the RI characterization, glycerin solutions of increasing refractive index were placed in the D-shaped POF's sensing region and the sensor's response of 5 min monitoring was obtained ($k \pm \delta k$), average value and standard deviation, according with Equation 3.7. The normalized transmitted signal ($k_{norm} \pm \delta k_{norm}$) was calculated as defined by Equation 3.8 and Equation 3.9.

The sensing region of the D-shaped POF sensors was washed twice with the glycerin solution prior to the monitoring of the sensor's response, to eliminate any residues of the previous solution.

Three replicated measurements of the sensor's responses to refractive index (n_{ext}) variation were performed and the average value and standard deviation were calculated, $k_{avg} \pm \delta k_{avg}$, see Figure 5.4. An exponential fit was applied to the obtained results.

The parameters obtained from the exponential fit as well as the maximum standard deviation of the sensor's response in all RI characterizations ($\delta k_{norm_{max}}$) can be found in Table 5.2. The reproducibility of the sensors responses was evaluated by the relative error, calculated using Equation 3.10, see Table 5.3.

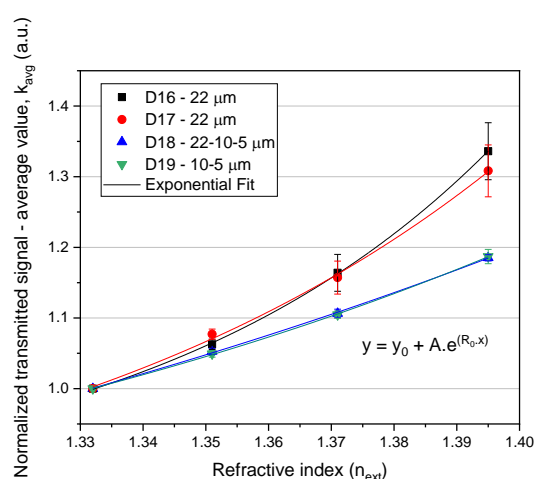


Figure 5.4 Response of the D-shaped POF sensors (D16 – D19) in glycerin solutions with increasing refractive index and exponential fit.

Table 5.2. RI response of D-shaped POF sensors: parameters of the exponential fit and maximum standard deviation of the sensor responses.

| Sensor | $\delta k_{norm_{max}}$ (a.u.) | R_0 | A | Adj. R^2 |
|--------|-----------------------------------|------------------|-----------------------------------|------------|
| D16 | 6.19×10^{-3} | 17.78 ± 1.20 | $(0.85 \pm 1.45) \times 10^{-11}$ | 0.99968 |
| D17 | 3.07×10^{-2} | 12.62 ± 4.16 | $(1.25 \pm 7.56) \times 10^{-08}$ | 0.99577 |
| D18 | 3.62×10^{-3} | 4.70 ± 2.22 | $(1.02 \pm 3.57) \times 10^{-03}$ | 0.99869 |
| D19 | 4.00×10^{-3} | 7.18 ± 1.27 | $(2.30 \pm 4.41) \times 10^{-05}$ | 0.99958 |

Table 5.3. Relative error of the RI characterizations, calculated using Equation 3.10.

| Sensor | Maximum response $k_{avg_{max}}$ (a.u.) | Maximum error $\delta k_{avg_{max}}$ (a.u.) | Relative error (%) |
|--------|--|--|-----------------------|
| D16 | 1.336 | 0.0404 | 3.02 |
| D17 | 1.308 | 0.0367 | 2.81 |
| D18 | 1.185 | 0.0060 | 0.51 |
| D19 | 1.187 | 0.0101 | 0.85 |

Sensors D16 and D17, only polished with sandpaper P800 ($\sim 22\mu\text{m}$) showed higher variation in the sensor's responses with increasing RI (31% – 34%). In accordance with the results presented in Chapter 4, sensors D18 and D19, polished with sandpapers of lower grit size, showed lower variation on the sensor's responses (19%) but higher reproducibility in the RI characterizations, as the relative error was lower than 0.85%.

The sensitivity (S) and resolution (Δn) of the sensors were calculated and depicted in Figure 5.5.

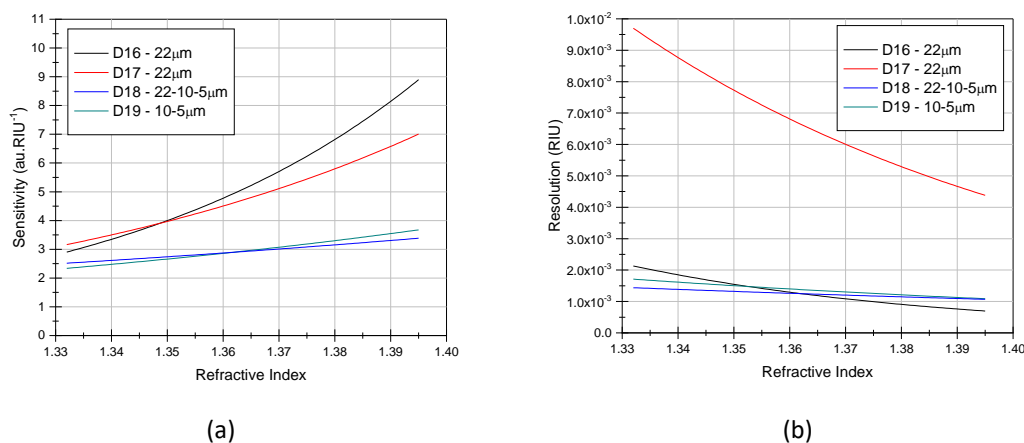


Figure 5.5 Sensitivity (a) and resolution (b) of the D-shaped POF sensors.

Sensors D16 and D17, polished with sandpaper P800, showed higher sensitivity to RI variation while sensors D18 and D19, polished with sandpapers of lower grit size, showed lower sensitivity in all the refractive index range, as already expected. All sensors showed resolutions of 10^{-3} RIU, although for sensor D17 the obtained resolution was higher than 4×10^{-3} RIU for all the RI range. Sensors D18 and D19 have resolutions between 1.7×10^{-3} RIU and 1.1×10^{-3} RIU. Sensor D16 has a resolution between 2×10^{-3} RIU and 7×10^{-4} RIU, being lower than 1×10^{-3} RIU for RI higher than 1.375.

Taking into account the obtained results, a chemical layer based on molecular imprinted technology was deposited on the sensing region of the D-shaped POF sensors D16 and D17, as described in the next section.

5.2.4 Sensitive MIP layer

The developed MIP was previously deposited on a D-shaped SPR-POF sensor and characterized, confirming the suitability of this layer for the chemical detection of perfluorooctanoate (PFOA/PFO⁻) and perfluorinated alkylated substances (PFASs). The D-shaped SPR-POF-MIP sensor showed a limit of detection (LOD) of 0.13 – 0.15 ppb (Nunzio Cennamo, D'Agostino, *et al.*, 2018). The same pre-polymeric mixture without the template (NIP, non-imprinted polymer) was deposited in the exact same way on the surface of a D-shaped SPR-POF sensor and the results obtained by the characterization in solutions of PFOA were compared (MIP and NIP). Results have shown that by increasing the concentration of PFOA no variation in the resonance wavelength was observed for the D-shaped SPR-POF-NIP sensor, while a decrease of about 3.8 nm was observed for a

concentration of 4 ppb with the D-shaped SPR-POF-MIP sensor (Nunzio Cennamo, D'Agostino, *et al.*, 2018)(N. Cennamo *et al.*, 2018).

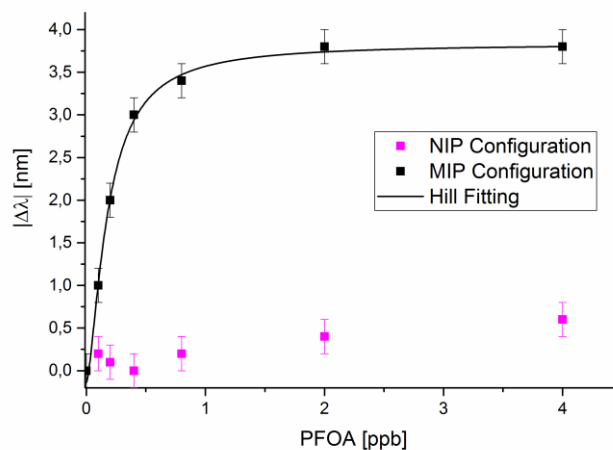


Figure 5.6 Validation results of the MIP used in this study, by an SPR-POF-MIP sensor - wavelength variation with concentration of PFOA (N. Cennamo *et al.*, 2018). (MIP – molecular imprinted polymer; NIP – non-imprinted polymer)

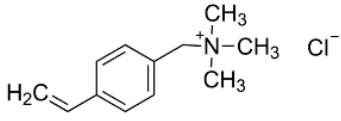
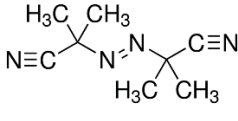
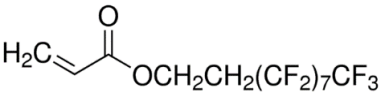
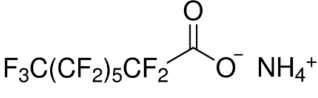
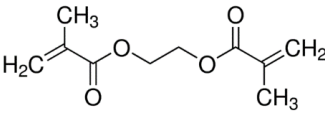
After validation of the suitability of this MIP layer for chemical sensing with POF by SPR technology, its deposition on the surface of D-shaped POF sensors was conducted, allowing the development and characterization of D-shaped POF-MIP sensors for chemical sensing using a low-cost intensity based sensing setup.

5.2.4.1 Chemical reagents

(Vinylbenzyl)trimethylammonium chloride (VBT) [26616-35-3], 2,2-azobisisobutyronitrile (AIBN) [78-67-1], 1H,1H,2H,2H-Perfluorodecyl acrylate (PFDA) [27905-45-9], ammonium perfluorooctanoate (PFO-NH₄) [3825-26-1] were obtained from Sigma–Aldrich and used without any further purification. Ethylene glycol dimethacrylate (EDMA) [97-90-5] (Sigma–Aldrich cod. 335681) was distilled in vacuum prior to use in order to remove stabilizers. All other chemicals were of analytical reagent grade. The solvent was deionized water. Stock solutions were prepared by weighing the solids and dissolving in ultrapure water (Milli-Q).

In the following table are the structural formulas of the chemical reagents used in the preparation of the molecular imprinted polymer (MIP).

Table 5.4. Structural formulas of the chemical reagents.

| | |
|---|--|
|  |  |
| (Vinylbenzyl)trimethylammonium chloride (VBT) | 2,2-azobisisobutyronitrile (AIBN) |
|  |  |
| 1H,1H,2H,2H-Perfluorodecyl acrylate (PFDA) | ammonium perfluorooctanoate (PFO-NH ₄) |
|  | |
| Ethylene glycol dimethacrylate (EDMA) | |

5.2.4.2 Pre-polymeric mixture – preparation and deposition

The pre-polymeric mixture of the molecular imprinted polymer (MIP) was prepared with ammonium perfluorooctanoate (PFO-NH₄) as the template, VBT and PFDA as the functional monomers, EDMA as the cross-linker and AIBN as the radical initiator (see Table 5.4). AIBN is a common reagent for the initiation of radical reactions, as decomposes (at temperatures above 60 °C) forming isobutyronitrile radicals:

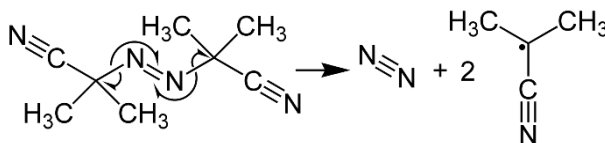


Figure 5.7 Decomposition of the Azobisisobutyronitrile (AIBN) in nitrogen and isobutyronitrile radicals.

The reagents were mixed at the following molar ratio 1_(Template):4_(VBT):5_(PFDA):50_(EDMA). The mixture was uniformly dispersed by sonication (visually homogeneous milky solution). Deionized water was added (volume ratio H₂O:EDMA = 1:17.5). Finally, the AIBN was added to the solution in non-stoichiometric ratio.

The pre-polymeric mixture was stored in the fridge. Before MIP deposition, the pre-polymeric mixture was removed from the fridge and kept at room temperature for 15 minutes, protected from light. Then it was placed in a sonic bath for about 5 min.

The MIP layer was deposited on sensors D16 and D17 as hereafter described. The D-shaped POF sensor was placed in the spin coater, see Figure 5.8(a). A known volume of the pre-polymeric mixture (100 μ L) was dropped over the D-shaped sensing region and spun for 1 min 20 s at 800 rpm (acceleration 50 rpm/s). The D-shaped sensor was removed from the spin coater and placed in the oven, see Figure 5.8(b). The thermal polymerization was carried out overnight (\sim 16 h) at 72 $^{\circ}$ C.

The next day, the sensor was left to slowly reach the room temperature.

The obtained polymeric film was washed and the template molecule was extracted, leaving the imprinting sites free for rebinding. The obtained D-shaped POF-MIP sensor is schematically represented in Figure 5.8(c). The interaction length (D-shaped sensing region) was 6 cm.

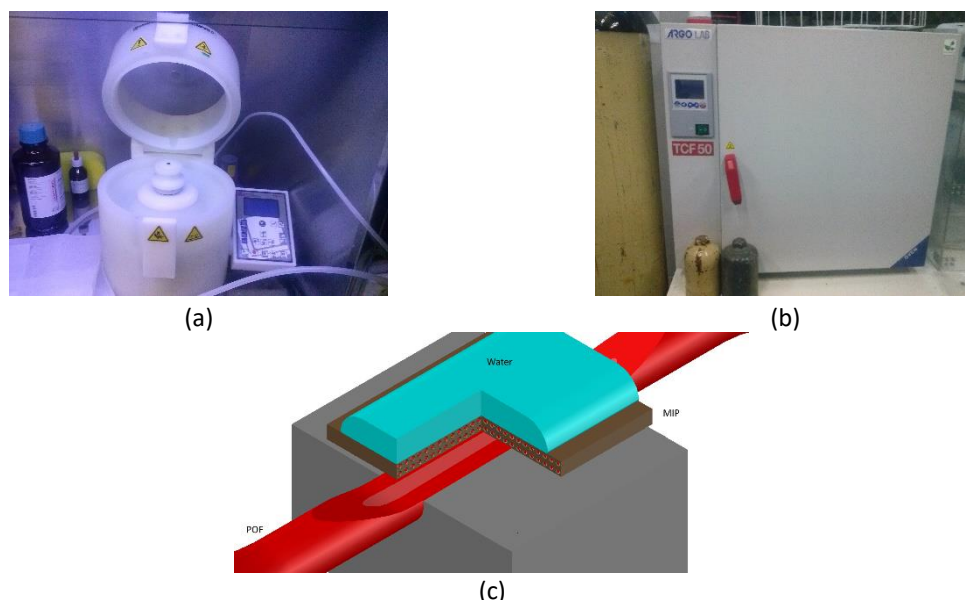


Figure 5.8 (a) Spin coater; (b) oven – thermal polymerization; (c) schematic representation of the D-shaped POF-MIP sensor.

The washing and extraction procedures were performed in two steps. First, the MIP layer was washed with 96% v/v ethanol in order to remove the un-polymerized monomers, by pouring 5 mL of ethanol on the D-shaped POF-MIP sensor. In a second step, the template was extracted from the MIP by washing with hydrochloric acid (HCl) solution (2% w/w) and 96% v/v ethanol. The extraction step was conducted by pouring 1.5 mL of HCl solution, 5 mL of ethanol, 1.5 mL of HCl and 5 mL of ethanol. Finally, the D-shaped POF sensors were poured with deionized water and left to dry at room temperature.

This synthetic receptor was designed to recognize C4 to C12 PFASs at low concentration, and the MIP sensor's response was similar to PFOA or C4 to C12 PFASs, as reported in (Nunzio Cennamo, D'Agostino, *et al.*, 2018). As perfluorooctanoate (PFO⁻) was used as the template, the recognition is focused on C8. Although the polymer can absorb PFASs between C4 to C12 at concentrations lower than 2 ppb. The recognition is due to the ionic interaction common to all PFASs (carboxylic

and sulphonic anion) and Van der Waals interactions due to the -F groups. The amount of perfluorinated carbons is determined by the length of the C-C chain. The change in the refractive index, determined by the number of -CF₂- groups, is such as to allow a similar response within the range of interest to be obtained. (Nunzio Cennamo, D'Agostino, *et al.*, 2018)(N. Cennamo *et al.*, 2018)

5.2.5 PFOA/PFO detection

D-shaped POF-MIP sensors were characterized with PFOA solutions of increasing concentration, from 0 ppb (distilled water) to 200 ppb. All the measurements were performed in a laboratory at room temperature (23 °C).

A standard measuring protocol was implemented, based on three steps: 1) incubation step, for chemical-interaction between the analyte and the MIP (10 minutes at room temperature); 2) washing step with distilled water (blank), in order to obtain the same bulk refractive index; 3) recording step for the data (with distilled water covering the sensing region).

This protocol was necessary in order to measure the response determined by the specific binding (analyte/receptor interaction) on the sensing surface, and not by the changes of the bulk refractive index or by non-specific binding between the surface of the sensor and the analyte.

For comparison, one D-shaped POF sensor (with no MIP deposited at its surface) was also characterized with solutions of PFOA.

The monitoring of the sensor's responses to increasing concentration of PFOA was performed for 1 min (after 10 min of incubation time and the washing step). The average value and standard deviation of the sensor's responses ($k \pm \delta k$) and the normalized transmitted signal ($k_{norm} \pm \delta k_{norm}$) were calculated.

The normalized transmitted signal obtained for the D-shaped POF sensors with and without the MIP layer, with increasing concentration of PFOA, are shown in Table 5.5 and Figure 5.9.

Table 5.5. D-shaped POF sensors (with and without the MIP layer) – output signal normalized to 0 ppb (blank), by incubating PFOA solutions with increasing concentration.

| PFOA concentration (ppb) | Normalized transmitted signal ($k_{norm} \pm \delta k_{norm}$) | | |
|--------------------------|--|-----------------|---------------------|
| | D-shaped POF-MIP sensors | | D-shaped POF sensor |
| | D16 | D17 | D18 |
| 0 | 1.0000 ± 0.0008 | 1.0000 ± 0.0027 | 1.0000 ± 0.0019 |
| 0.1 | 0.9998 ± 0.0013 | 0.9979 ± 0.0020 | 1.0004 ± 0.0015 |
| 0.2 | 0.9888 ± 0.0007 | 0.9925 ± 0.0029 | - |
| 0.5 | 0.9736 ± 0.0012 | 0.9844 ± 0.0022 | 0.9955 ± 0.0015 |
| 1 | 0.9458 ± 0.0015 | 0.9815 ± 0.0020 | 0.9983 ± 0.0017 |
| 2 | - | 0.9787 ± 0.0063 | - |
| 4 | - | 0.9704 ± 0.0021 | - |
| 200 | 0.9323 ± 0.0008 | 0.9700 ± 0.0019 | 0.9922 ± 0.0060 |

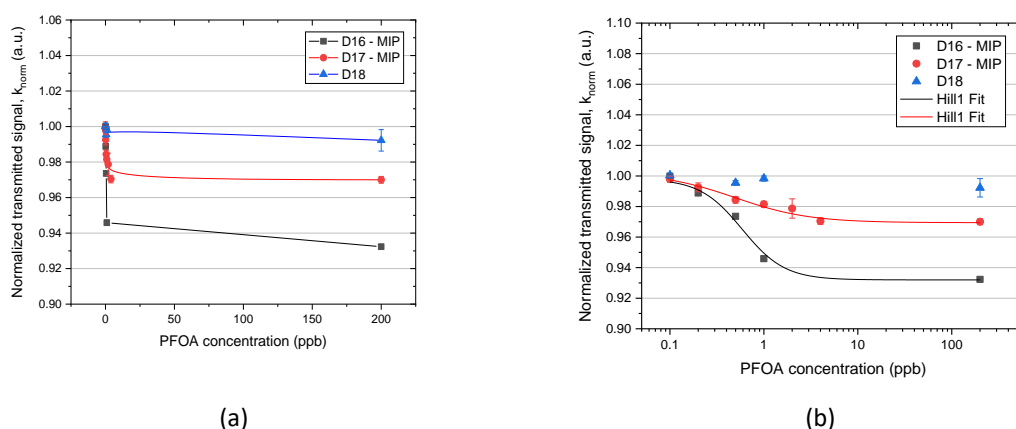


Figure 5.9 D-shaped POF sensor's response to PFOA concentration, with (D16-MIP, D17-MIP) and without (D18) the MIP layer: (a) linear scale; (b) semi-logarithmic scale and Hill Fit.

The D-shaped POF-MIP sensors (D16-MIP, D17-MIP) show a decrease in the normalized transmitted signal with increasing concentration of PFOA. On the other hand, when a D-shaped POF sensor without an MIP layer (D18) was characterized with the same concentrations of PFOA, no significant variation in the transmitted signal was observed.

These results confirm that the binding between the MIP receptor and the analyte (PFOA) is present and the variation in the sensor's response is not due to an unspecific binding between the analyte and the surface of the POF's core, nor variation of the bulk's refractive index while performing the monitoring of the sensor's response.

When the concentration of the analyte increases, the output transmitted signal decreases. Taking into account the obtained results with the RI characterization previously performed, an increase in the external refractive index led to an increase in the sensor's response. Therefore, a decrease in the sensor's response means that a decrease in the refractive index of the MIP layer occurred with the binding of analyte. This was also verified with the D-shaped SPR-POF-MIP sensor, using the same MIP layer (Nunzio Cennamo, D'Agostino, *et al.*, 2018). Furthermore, POF's cladding are often doped with fluorinated compounds in order to decrease the refractive index of this layer (Ishigure *et al.*, 2002)(Yao, Li and Huang, 2014).

Sensors D16-MIP and D17-MIP showed different responses with increasing concentration of PFOA solutions, although the behaviour was similar. From the RI characterizations performed (section 5.2.3) it was expected higher sensitivity from sensor D16-MIP.

Sensor D16-MIP was again characterized with solutions of PFOA, see Figure 5.10 and Table 5.6. Previously, the template was extracted from the MIP layer as described in section 5.2.4.2, by washing with hydrochloric acid (HCl) solution (2% w/w) and 96% v/v ethanol. Several washings steps were performed with distilled water and the sensor was left to dry at room temperature.

Table 5.6. – Output signal normalized to 0 ppb (blank) of the sensor D16-MIP (test 1 and test 2) in PFOA solutions with increasing concentrations.

| PFOA concentration (ppb) | Normalized transmitted signal ($k_{norm} \pm \delta k_{norm}$) | |
|--------------------------|--|-----------------|
| | D16-MIP | |
| | Test 1 | Test 2 |
| 0 | 1.0000 ± 0.0008 | 1.0000 ± 0.0063 |
| 0.1 | 0.9998 ± 0.0013 | 0.9855 ± 0.0046 |
| 0.2 | 0.9888 ± 0.0007 | 0.9899 ± 0.0045 |
| 0.5 | 0.9736 ± 0.0012 | 0.9842 ± 0.0047 |
| 1 | 0.9458 ± 0.0015 | 0.9784 ± 0.0045 |
| 2 | - | 0.9764 ± 0.0045 |
| 200 | 0.9323 ± 0.0008 | 0.9653 ± 0.0043 |

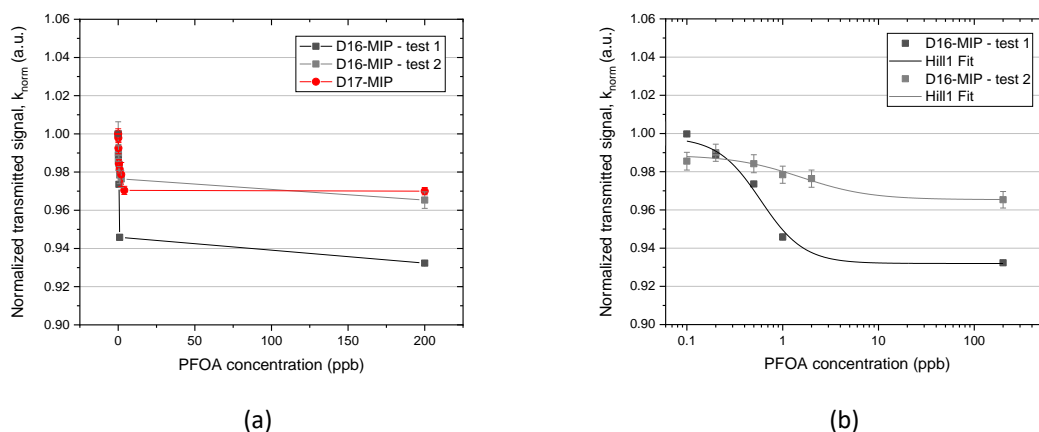


Figure 5.10 Response of the sensor D16-MIP in solutions with increasing concentrations of PFOA: (a) test 1 and test 2, and comparison with the response of the sensor D17-MIP, in linear scale; (b) test 1 and test 2 in semi-logarithmic scale, with the Hill Fit.

Decrease of the response in the second calibration of the sensor D16-MIP in solutions of PFOA indicates that no total recovery occurred with MIP extraction, i.e. the template was not totally removed from the MIP layer during the extraction procedure.

The responses for the D-shaped POF-MIP sensors in the first calibration are well fitted by the Hill equation reported below (see Figure 5.9(b) and Figure 5.10(b)):

$$k_{norm} = k_{start} + (k_{end} - k_{start}) \frac{c^n}{K_{Hill}^n + c^n} \quad \text{Equation 5.1}$$

where k_{start} is the value obtained without PFOA (blank), k_{end} is the plateau value obtained at high concentrations, c is the concentration of the analyte and k_{norm} is the sensor's response at the concentration c of PFOA. The two parameters K_{Hill} and n are descriptors of the standardization curve. The Hill fitting parameters are listed in Table 5.7.

Table 5.7. D-shaped POF-MIP sensors – Hill Fit parameters.

| Sensor | k_{start} | k_{end} | K_{Hill} | n | Reduced χ^2 | Adj. R^2 |
|------------|---------------------|---------------------|---------------------|---------------------|------------------|------------|
| D16 | 0.9981 ± 0.0075 | 0.9320 ± 0.0036 | 0.5893 ± 0.1195 | 1.9258 ± 0.7836 | 17.51075 | 0.98008 |
| | 0.9888 ± 0.0078 | 0.9654 ± 0.0052 | 1.5649 ± 1.2796 | 1.2151 ± 1.6853 | 1.36119 | 0.71673 |
| D17 | 1.0022 ± 0.0066 | 0.9694 ± 0.0017 | 0.4953 ± 0.2299 | 1.1000 ± 0.4174 | 0.79336 | 0.97064 |

From Equation 5.1 it is possible to notice that, if $n \sim 1$ and at low concentration ($c \ll K_{Hill}$), the dose-response curve is linear, with sensitivity $\frac{\Delta k_{max}}{K_{Hill}}$, defined as the “sensitivity at low concentration”, as shown in Equation 5.2:

$$k_{norm} - k_{start} = \frac{(k_{end} - k_{start})}{K_{Hill}} \cdot c = \frac{\Delta k_{max}}{K_{Hill}} \cdot c \quad \text{Equation 5.2}$$

Standard curves like the ones obtained in Figure 5.9 and Figure 5.10, with the Hill parameters listed in Table 5.7, are commonly used for chemical sensors and biosensors, and their physical meaning can be related to the adsorption due to the combination of the template at specific sites, when the number of receptor sites available for the combination with the substrate is limited (Nunzio Cennamo, D’Agostino, *et al.*, 2018)(N. Cennamo *et al.*, 2018).

Binding of species onto homogeneous substrates can be described by Hill equation (Hill, 1910), assuming that adsorption is a cooperative phenomenon where different binding sites on the same macromolecule can be influenced by ligand binding ability at one site on the macromolecule. (Foo and Hameed, 2010)

According to (Crawford and Quinn, 2017) “adsorption can be defined as a process in which a material (adsorbate) travels from a gas or liquid phase and forms a superficial monomolecular layer on a solid or liquid condensed phase (substrate)”.

The interaction between pollutants and adsorption layers are described by equilibrium relationships, known as adsorption isotherms. Although the Langmuir adsorption isotherm includes several assumptions (adsorbed layer is one molecule in thickness; adsorption can only occur at a fixed number of localized sites; all sites possess equal affinity for the adsorbate; no lateral interaction occurs between the layer and the adsorbate), graphically is characterized by a plateau, an equilibrium saturation, due to the fact that once a molecule occupies a site, no further adsorption can take place at that site. (Foo and Hameed, 2010)(Langmuir, 1917)(Langmuir, 1918)

The limit of detection (LOD) can be calculated as the ratio of three times the associated error of the initial sensor’s response (blank, δk_{start}) and the sensitivity at low concentration $\left(\frac{\Delta k_{max}}{K_{Hill}}\right)$ (N. Cennamo *et al.*, 2018). Using the Hill equation for the quantitative description of the calibration curves facilitates the procedure of comparison of the sensitivities of sensors designed for detection of the same substance (Kurganov *et al.*, 2001).

Table 5.8 shows the sensitivity at low concentration and the LOD for PFOA detection in water by the developed D-shaped POF-MIP sensors.

Table 5.8. D-shaped POF-MIP sensors – sensitivity at low concentration and limit of detection (LOD).

| PFOA detection in water ($c \ll K_{Hill}$ and $n \sim 1$) | | |
|--|--------|-------------------------|
| Hill Parameters | Values | D-shaped POF-MIP sensor |
| Sensitivity at low c (au.ppb ⁻¹) | 0.11 | D16-MIP |
| $\left \frac{\Delta k_{max}}{K_{Hill}} \right $ | 0.07 | D17-MIP |
| LOD (ppb) | 0.20 | D16-MIP |
| $\frac{3 \times \delta k_{start}}{\text{sensitivity at low } c}$ | 0.28 | D17-MIP |

An LOD of 0.20 ppb and 0.28 ppb have been obtained for sensors D16-MIP and D17-MIP, respectively, showing that intensity based D-shaped POF-MIP sensors have the capability to detect PFOA with very low concentrations. In the work reported by Cennamo et al. the same MIP was deposited on D-shaped SPR-POF sensors and an LOD of 0.13 ppb was achieved with solutions of PFOA using wavelength-based sensing (Nunzio Cennamo, D'Agostino, *et al.*, 2018). Although the LOD obtained with the intensity based POF-MIP sensors is higher than the one obtained with the SPR-POF-MIP sensor, promising developments can be foreseen with these low-cost POF sensing platforms.

5.2.6 Conclusions

D-shaped POF-MIP sensors were developed and tested, for the first time, for the detection of PFOA in water. The obtained results validate the suitability of these sensing platforms for the development of chemical sensors based on POFs. Furthermore, the intensity based detection scheme allow low-cost chemical sensing associated with very simple manufacturing procedures.

It should be pointed out that indirect sensing of PFOA concentration was performed by the RI variations that occurred in the MIP layer due to the specific interaction between the recognition sites and the analyte. In this case, the refractive index of the MIP layer decreased leading to a decrease in the transmitted light (lower sensor's response) with the increase of PFOA concentration.

The obtained LOD is the same order of magnitude as the maximum value proposed for individual PFASs (0.1 ppb) and lower than the maximum value proposed to total PFASs (0.5 ppb) (European Commission, 2018). As already mentioned, the developed MIP was designed to recognize long chain PFASs (from C4 to C12) at low concentration, making it suitable to address the maximum allowed parametric values imposed by the European Commission.

Future developments include: evaluate and improve the reproducibility of the sensor's manufacture; evaluate the stability of the MIP layer on the sensor's surface; improve the

regeneration of the MIP layer; characterization of D-shaped POF-NIPs and comparison with the response of D-shaped POF-MIPs (compare the un-selective and selective binding); evaluate the time of life of the D-shaped POF-MIP sensors; develop new strategies for ON/OFF sensing.

5.3 Protein immobilization on POF's surface

Preliminary studies on the coating of POFs with proteins were conducted. To increase the interaction between the protein layer and the optical transmitted signal, the cladding was removed using solutions of acetone and distilled water, as already described in Chapter 3 (section 3.3.3). Taking into account the results achieved and presented at Chapter 4, the roughness of the sensing region was increased by polishing with sandpapers of known grit size.

The samples of POF were immersed in protein solutions of *Escherichia coli* (*E. coli*) cell extracts, under stirring. At the same time and in the same conditions, controls were performed using POF samples immersed in buffer solutions, in the absence of proteins. A simple and easy methodology using protein staining solution was performed to confirm the coating of the POFs with proteins and to evaluate the dependency with the experimental conditions.

Several parameters were evaluated: POF sample (POF with cladding / unclad POF / unclad polished POF), buffer solution (phosphate or tris(hydroxymethyl)aminomethane, Tris), time (1h, 2h, 3h, overnight) and temperature (room temperature or at 4°C). Figure 5.11 depicts an overview of the experimental procedures and Figure 5.12 of the experimental conditions.

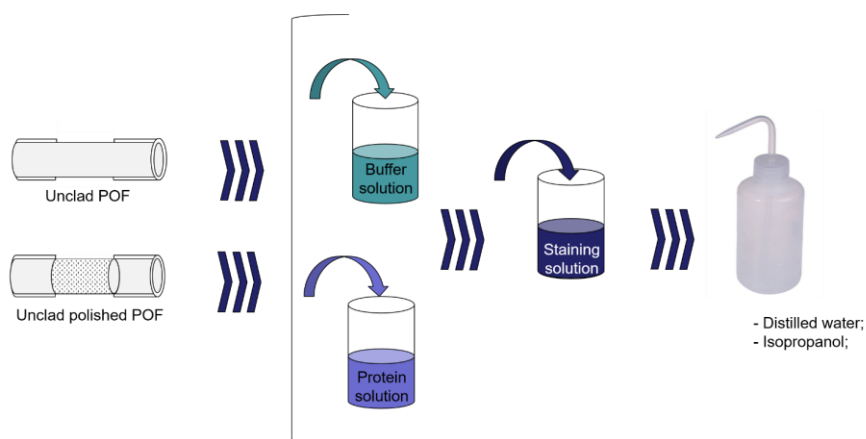


Figure 5.11 Overview of the experimental procedures.

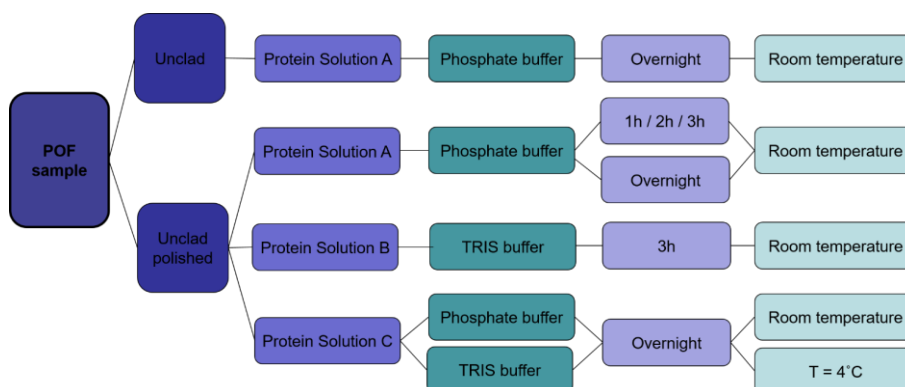


Figure 5.12 Overview of the experimental conditions.

The surface of the POF samples was analysed by optical microscopy and the transmission spectra of the modified samples was measured using a Warm White Fibre-Coupled LED and a spectrometer.

This simple technique allowed to confirm and evaluate the coating of the POF's with proteins and its dependency with the experimental conditions.

5.3.1 Introduction and state of art

The coating of POFs with proteins for the selective detection of contaminants was again foreseen. The idea underlining this study was proteins' selectivity due to modification procedures, reported by (Otrelo-Cardoso *et al.*, 2017). Based on this work, the immobilization of a mutant protein of interest for the selective detection of tungstate (WO_4^{2-}) was foreseen and preliminary studies on the coating of POF's surface were performed with "model proteins" from Escherichia coli (E-coli).

Tungsten is a transition metal (group VI of the periodic table) with desirable characteristics (strength, flexibility, high melting point, good conductivity) which caused a rise in its use for different applications and consequently higher exposure (occupational – mines and industry, implanted medical devices, environmental and military). In the environment tungsten exists as a mineral (such as wolframite, $[\text{FeMn}]\text{WO}_4$, and scheelite, CaWO_4) while in solution mostly exists as tungstate (WO_4^{2-}) under alkaline conditions or as polytungstate in more acidic conditions or higher concentrations. The entry of tungsten into the water systems can occur due to runoff from rocks and soil, as well by disposal of contaminated garbage from industry. (Bolt and Mann, 2016)

Tungsten is an emerging environmental toxicant and our understanding of the risks to human health associated with exposure are still limited (Bolt and Mann, 2016). Bolt and Mann presented a review in 2016 discussing the potential toxicity of tungsten, alone and in combination with other metals, the main routes of exposure for humans and consequent health problems associated.

Tungsten detection usually requires expensive equipment (such as ICP-mass spectrometry) and few works are reported on new detection methodologies that can be applied directly on the field

(Otrelo-Cardoso *et al.*, 2017). In 2015, Alvarado-Gómez *et al.* reported a biosensor for the detection of tungsten in water, nevertheless, for concentrations higher than 1.0 μM , the presence of interferers must be taken into account, such as selenium, iron or aluminium (Alvarado-Gómez *et al.*, 2015).

In 2017, Otrelo-Cardoso *et al.* reported the modification of protein TupA from *Desulfovibrio alaskensis* G20 and consequent high selectivity to tungstate, suggesting the suitability of the mutant protein (R118K) for a biosensor recognition element for tungsten detection. *DaG20* TupA is highly specific for tungstate and molybdate (WO_4^{2-} , MoO_4^{2-}) and not for other oxyanions such as sulphate, phosphate or perchlorate (SO_4^{2-} , PO_4^{3-} , ClO_4^- , respectively) while the mutant R118K shows high affinity and selectivity for tungstate. (Otrelo-Cardoso *et al.*, 2017)

Making a synergy between POF sensing capabilities with the high affinity and selectivity of the mutant protein, a highly selective and low-cost sensor for tungsten/tungstate could be developed. The preliminary studies on the coatings of POFs with proteins were performed with model proteins from *E. coli*.

E. coli is a bacteria, a motile rod belonging to the Enterobacteriaceae family (Link, Robison and Church, 1997)(Octavia and Lan, 2014). It is found in the down intestinal tract of humans and warm-blood animals but can be grown easily in the laboratory.

Proteins are a sequence of amino acids, which contain in their structure an amino group ($-\text{NH}_2$), a carboxylic group ($-\text{COOH}$) and a residue group (R) which is responsible for the amino acid properties, see Figure 5.13(a,b) as an example. The chemical bond between two amino acids is known as peptide bond and occurs between the amino and the carboxylic groups, see Figure 5.13(c).

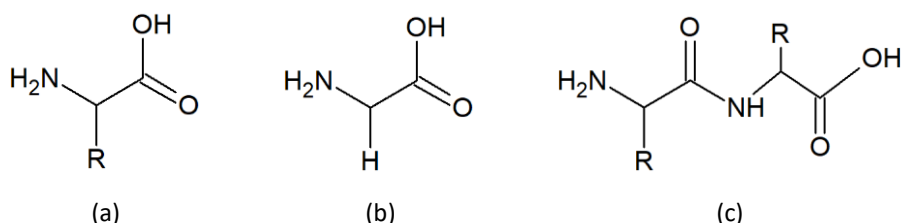


Figure 5.13 (a) General chemical structure of an amino acid; (b) glycine, Gly ($\text{R} = \text{H}$), the simplest amino acid; (c) example of a peptide bond between two amino acids as represented in (a).

Physical adsorption and covalent bonding are two possibilities for protein immobilization on PMMA surfaces. Physical adsorption is based on non-covalent interaction, allowing the coverage of a surface with proteins by mutual attraction.

As already described in Chapter 3, and based on the work reported by Fixe *et al.* (Fixe *et al.*, 2004), it is expected that the amino groups ($-\text{NH}_2$) chemically bind to the methyl esters group (COOCH_3) from the PMMA, see Figure 5.14.

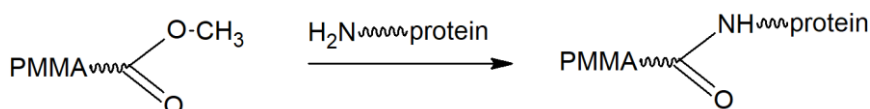


Figure 5.14 Amination of PMMA surfaces with proteins, adapted from Fixe *et al.* (Fixe *et al.*, 2004).

In 1999, Tan *et al.* studied the use of polymer coated glass for the improvement of protein immobilization to the surface for optical biosensing applications (Tan *et al.*, 1999) as generally polymers allow for protein adsorption. PMMA presents a relatively lower protein adsorption capacity as compared to other polymeric substrates, such as polystyrene (PS) widely used for protein immobilization applications (Tsougeni *et al.*, 2010).

To improve the adsorption of proteins to PMMA surface, use of oxygen plasma treatment is suggested (Tsougeni *et al.*, 2010) (Vesel, Elersic and Mozetic, 2012) or laser ablation (Ma *et al.*, 2011).

Tsougeni *et al.* reported the improvement on protein binding capacity by nano-texturing of PMMA by oxygen plasma treatment, related with the increased surface area due to the plasma-induced roughness. Studies were performed with two model proteins (biotinylated bovine serum albumin, b-BSA, and rabbit gamma-globulins, RgG) by reaction with a fluorescently labelled dye, showing the independency of the enhanced protein binding with the protein used. (Tsougeni *et al.*, 2010)

Ma *et al.* reported the enhancement on the protein - PMMA binding by creation of patterns with femtosecond laser ablation, by studying the adsorption of fluorescein isothiocyanate (FITC) – labelled bovine serum albumin (BSA). (Ma *et al.*, 2011)

The amount of adsorbed proteins and the overall adsorption kinetics are dependent on the surface properties of the solid substrate (e.g., hydrophobicity, hydrophilicity, surface charge, and functional groups) as well as the physiological adsorption conditions (e.g., temperature, pH, and concentration of bulk protein solutions). Higher the bulk protein concentration higher is the amount of adsorbed proteins; furthermore, hydrophobic surfaces such as PMMA or PS immobilize larger amounts of proteins than hydrophilic surfaces such as PHEMA (poly(2-hydroxyethyl methacrylate)). (Kim, Qian and Al-Saigh, 2011)

Vesel *et al.* reported the immobilization of protein streptavidin to the surface of PMMA using both approaches – physical adsorption and chemical coupling, also evaluating the immobilization efficiency by oxygen plasma treatment. In both cases, the samples were incubated around 2 h in solutions of protein in buffer solution, but a reaction with EDC (1-ethyl-3-(3-dimethylaminopropyl) carbodiimide) was promoted for the chemical coupling between the amino part of the streptavidin and the carboxylic group created by the plasma treatment. Results showed that the oxygen plasma treatment allows for increased protein immobilization to the surface and chemical coupling is more efficient than physical adsorption, observed after washing with buffer solution. (Vesel, Elersic and Mozetic, 2012)

In 1996, Chang *et al.* reported the development of an optical fibre biosensor for the detection of Protein A produced by *Staphylococcus aureus*, an important pathogen. In this case, the unclad portion of the POF was incubated in a solution of anti-(protein-A) immunoglobulin G (IgG) in PBS (phosphate buffered saline), after which was incubated with bovine serum albumin (BSA) to block the unoccupied sites on the fibre surface. (Chang *et al.*, 1996) In this case, the protein BSA was directly immobilized on the fibre surface only to block the unoccupied sites and the antigen-antibody reaction was monitored by conjugating fluorescein isothiocyanate with anti-(protein A).

Several POF sensors reported in the literature make use of proteins for bacteria and antibody detection, however the protein may not be deposited directly on the POF's surface (Lopes *et al.*,

2018)(Nunzio Cennamo *et al.*, 2013). Lopes et al. reported a U-shaped POF biosensor for the detection (on/off) of sulphate-reducing bacteria (SRB), by the monitoring of the light variation due to the immunocapture of *Desulfovibrio alaskensis* (*D. alaskensis*) by specific antibodies (anti *D. alaskensis*) immobilized on the POF's surface (Lopes *et al.*, 2018). In the immobilization procedure, a layer of Staphylococcal Protein A was deposited on the modified POF's surface before the immobilization of the antibody, according with (Anderson *et al.*, 1997) and (Fixe *et al.*, 2004). The binding sites were also blocked using bovine serum albumin (BSA), to avoid non-specific binding.

Kratz et al. reported a study related with the effectiveness of different solvents to remove protein layers (BSA and lysozyme) adsorbed at the surface of different materials, including PMMA – ultrapure water, isopropanol, sodium dodecyl sulphate (SDS), RIPA-buffer and Tween-20. Results showed that the solvent should be chosen taken into account the combination of protein and substrate material, nevertheless ultrapure water is a quite effective solvent for BSA while for lysozyme the effectiveness depends on the substrate material. (Kratz *et al.*, 2015)

5.3.2 Optical sensing platform

Straight unclad POFs were chosen as optical sensing platforms as they allowed to monitor refractive index variations with resolutions of 10^{-4} RIU, lower than the ones obtained with D-shaped POF sensors, when both platforms presented similar sensitivities (Chapter 4).

The samples of POF were cut to the desired length with a POF cutter and the cladding was removed using solutions of acetone and water as already described (section 3.3.3).

The roughness of the sensing region was increased by polishing with sandpaper P600, as generally better sensing performances were achieved after soft polishing with sandpapers of this grit size (Chapter 4, section 4.2.3.2). The unclad polished POF samples were cleaned with distilled water and optical paper prior to use.

The spectra of the light transmitted through the POF samples was analysed in transmission using the experimental setup described in section 3.4.3.3: Warm White Fibre-Coupled LED (MWWHF1), two bare fibre adapters (BARE-05-1000) and a Fibre Optic Spectrometer (Ocean Optics USB4000) connected to a laptop, see Figure 5.15. The spectra were analysed with the SpectraSuite software, from Ocean Optics.



Figure 5.15 Experimental setup: warm White-LED, bare fibre adapters, POF sample and an optical fibre spectrometer.

5.3.3 Buffer, protein and staining solutions

Solutions of Escherichia coli (E-coli) cell extracts were used in these experiments. The bacterial cells were grown in culture medium. Sonication allowed to break the cellular structures which was followed by centrifugation, in order to separate the two existing phases – soluble and insoluble. The soluble phase, consisting of a high concentration pool of proteins, is usually stabilized with a buffer solution. In this case, phosphate and Tris (Tris(hydroxymethyl)aminomethane) buffer solutions were used. The proteins and buffer solutions used in this study are described in Table 5.9.

Table 5.9. Protein and buffer solutions.

| Protein solution | Buffer solution |
|------------------|---|
| Pr-A | 50 mM Phosphate / 0.5 M NaCl / 20 mM Imidazole pH = 7.4 |
| Pr-B | 100 mM Tris / 0.5 M NaCl / 3 mM DTT / 100 mM Imidazole pH = 8.2 |

The samples of POF were immersed in the protein solutions always under stirring (50 rpm), performed with a Multi-functional orbital shaker (PSU-20i), see Figure 5.16.



Figure 5.16 Samples of POF immersed in buffer and protein solutions, under stirring (Multi-functional orbital shaker, PSU-20i).

A blue-staining solution was used as a visual marker to verify the immobilization of the proteins to the POF samples. This solution was already prepared and available to use. The Coomassie blue R250 present in the staining solution is a commonly used dye as selectively binds to proteins without causing permanent chemical modification, allowing the proteins to be de-stained and recovered for further analysis. The colour intensity after staining can be related with the protein's concentration. Blank samples were always immersed in the staining solution at the same time, allowing to compare the obtained results.

The transmission of light through the staining solution was analysed. This allowed to verify the variation in the intensity of the light that is transmitted (I) and reached the spectrometer. Therefore, the wavelengths in which the absorbance (A) occurs could be identified. The light source, a glass vial and the spectrometer were fixed to the laboratory table, as depicted in Figure 5.17.

Distilled water was added to the glass vial and the transmission spectrum was recorded (I_{water}). The water was removed with a plastic pipette, the phosphate buffer was added and the spectrum was recorded (I_{buffer}). Using the same procedures, the staining solution was added to

the glass vial and the spectrum was registered (I_{S1}). The staining solution was diluted and the spectrum was registered again (I_{S2}, I_{S3}). A continuous fluctuation in the obtained spectrum was verified, which was related with the suspended particles in the solution that were directly affecting the transmission measurements. The staining solution $S3$ was filtrated and the spectrum was registered again ($I_{S3\text{ filtrated}}$).



Figure 5.17 Experimental setup for the measurement of the transmission spectra.

The obtained transmission spectra are depicted in Figure 5.18(a). The spectra obtained with distilled water and buffer solution are identical. The intensity of the transmitted light diminished with the staining solution, which means that light is absorbed or scattered. Higher the concentration of the staining solution lower was the transmitted light.

In order to determine the wavelength at which light was absorbed, scattering was not considered and the absorbance (A) was calculated using the Equation 5.3 (only for qualitative analysis). The absorption of light was maximum around 550 nm – 560 nm due to the staining solution and no absorbance was observed for the buffer solution, see Figure 5.18(b).

$$A = -\log \frac{I_{\text{solution}}}{I_{\text{water}}} \quad [a. u.] \quad \text{Equation 5.3}$$

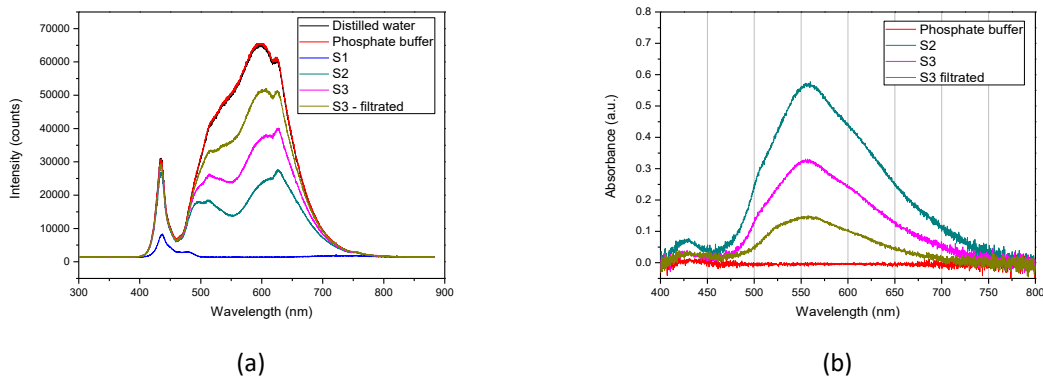


Figure 5.18 Transmission (a) and absorbance (b) spectra obtained with distilled water, phosphate buffer and staining solutions of different concentrations ($S1, S2, S3$ and $S3\text{ filtrated}$).

5.3.4 Influence of the immersion time

5.3.4.1 Immersion time: 1h

Three samples of unclad polished POF (P1, P2 and P3) with 4 cm were placed in Eppendorf's of 1.5 mL and immersed for 1 h with stirring (50 rpm). The sample P1 was immersed in phosphate buffer while samples P2 and P3 were immersed in solutions of protein (Pr-A) in phosphate buffer, see Table 5.10. The samples were washed by placing in Eppendorf's with phosphate buffer and manual stirred. The samples were removed and left to dry in identified Eppendorf's.

Table 5.10. POF samples (P1 – P3): conditions of preparation.

| POF Sample | | Protein / buffer solution | Washing |
|------------|------|---------------------------|------------------|
| P1 | P600 | Phosphate, 1h | Phosphate buffer |
| P2 | | Pr-A in phosphate, 1h | |
| P3 | | | |

The transmission spectrum of the samples was recorded before and after the immersion in buffer and protein solutions, see Figure 5.19. No changes in the transmission spectra were observed. Unless the protein or the buffer solution had characteristic absorption, no changes in the shape of the obtained spectra were expected.

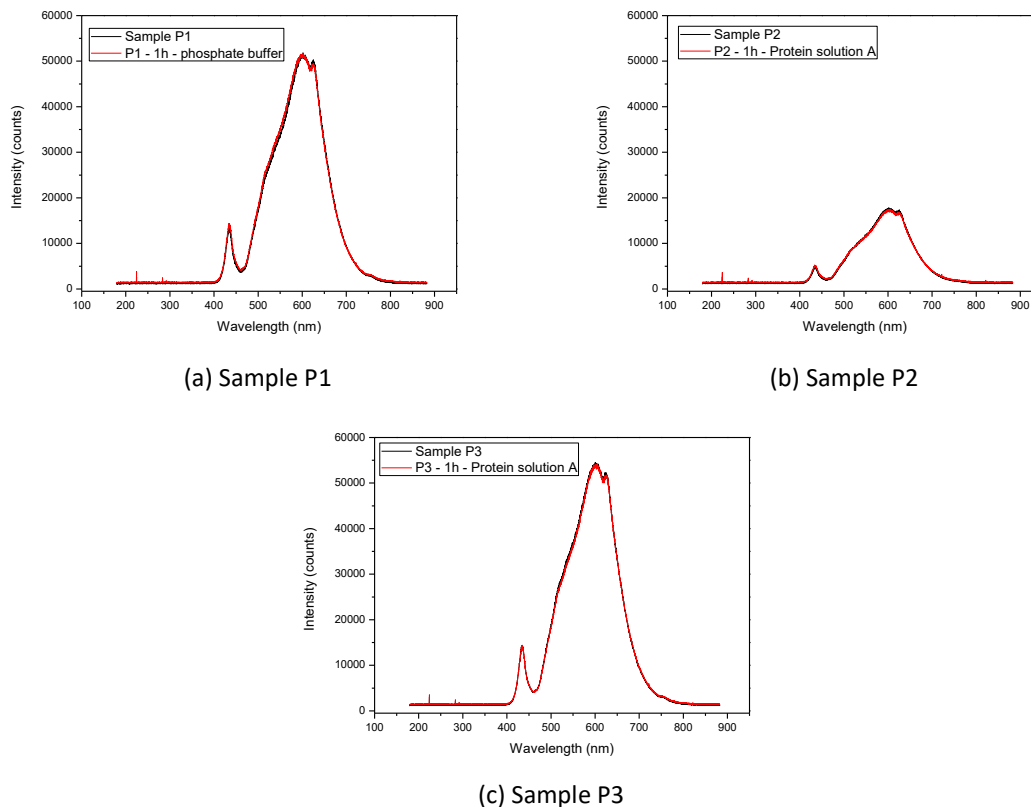


Figure 5.19 Transmission spectra obtained before and after immersion of the POF samples in phosphate buffer and protein solution A for 1h.

In order to verify the adsorption or non-selective binding of the staining solution to the unclad polished POF in the absence of proteins, the sample P1 was immersed in an Eppendorf with blue-staining solution for 1 h.

The sample was removed and a blue colour was seen with the naked eye, see Figure 5.20(a). The sample was washed with distilled water which slightly diminished the blue colour, Figure 5.20(b), and was further washed with squirts of isopropanol and optical paper, Figure 5.20(c). Intensity of initial blue colour diminished after washing with distilled water and was completely removed after washing with isopropanol.

This reveals that after immersion for 1 h in the blue-staining solution, an unclad polished POF previously immersed in phosphate buffer does not acquire a permanent staining.

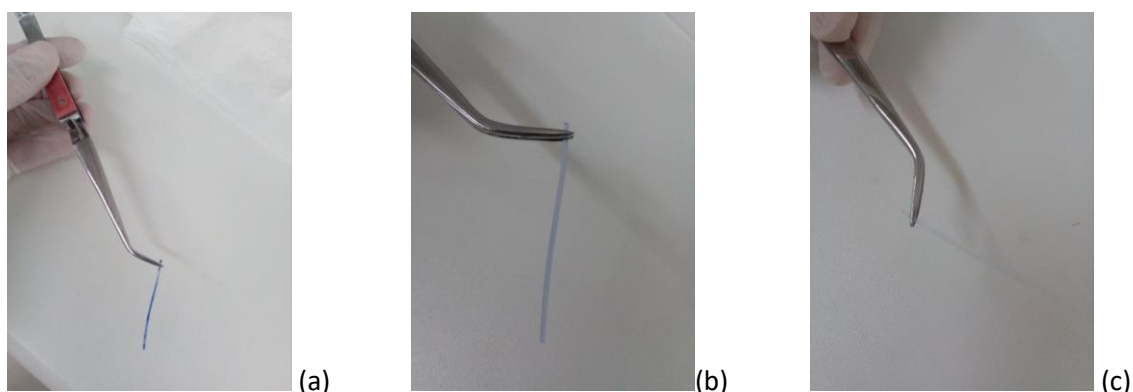


Figure 5.20 Sample P1, unclad polished POF immersed in phosphate buffer for 1h, after (a) immersion in staining solution (1h); (b) washing with distilled water; (c) washing with isopropanol.

The transmission spectra were recorded before and after the washing procedures with water and isopropanol. The tips of the sample were cut. Despite blue staining of the POF being visible after incubation in the staining solution, no difference in absorption of light was observed between stained and washed colourless fibres, see Figure 5.21.

Un-selective binding caused by immersion in the staining solution for 1 h was not enough to affect absorption of the light that travels through the POF. The immersion time of 30 min in the staining solution should be enough to cause the staining of the proteins immobilized to the POF.

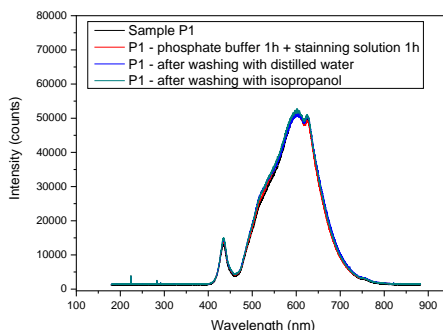


Figure 5.21 Transmission spectra obtained for sample P1 in different procedure steps.

5.3.4.2 Immersion time: overnight

POF samples were immersed in phosphate buffer or solution of protein (Pr-A) and left overnight (~17 h) at room temperature with stirring. The samples P2 and P3 were again immersed in the solution of protein A, as well as one unclad POF sample with 4 cm, P4 (not polished). Sample P5 was prepared, an unclad polished POF with 4 cm, and was immersed in phosphate buffer overnight.

Table 5.11. Preparation conditions of POF samples (P2 – P5).

| POF Sample | | Protein / buffer solution | Washing | Staining | Washing |
|------------|--------|---------------------------|------------------|----------|--------------------------------|
| P2* | P600 | Pr-A in phosphate, 17h | - | 30 min | Distilled water Isopropanol |
| P3* | | | Phosphate buffer | | |
| P4 | Unclad | - | | | |
| P5 | P600 | Phosphate, 17h | - | | |

* These POF samples were immersed again in protein solution.

The samples P2, P4 and P5 were placed directly in an Eppendorf with staining solution, for 30 min. The sample P3 was washed in an Eppendorf with phosphate buffer (manual stirring) before being placed in the staining solution. When a sample is placed directly in the staining solution after being immersed in protein solution, as occurred with samples P2 and P4, unspecific binding is expected between the staining solution and protein that is not attached to the POF. A stronger colour could be expected, which would disappear through washing.

The samples were removed from the staining solution, washed with squirts of distilled water and placed in identified Eppendorf's to dry. The polished POF samples that were immersed in protein solution (P2, P3) revealed a stronger colour, while the unpolished POF sample immersed in protein (P4) and the polished POF sample immersed in phosphate buffer (P5) presented less colour at naked eye, see Figure 5.22(a). The samples were further washed with isopropanol which removed the blue colour present in the samples P4 and P5, see Figure 5.22(b). These results are in accordance with the previously obtained for the sample P1, for 1 h of immersion time.

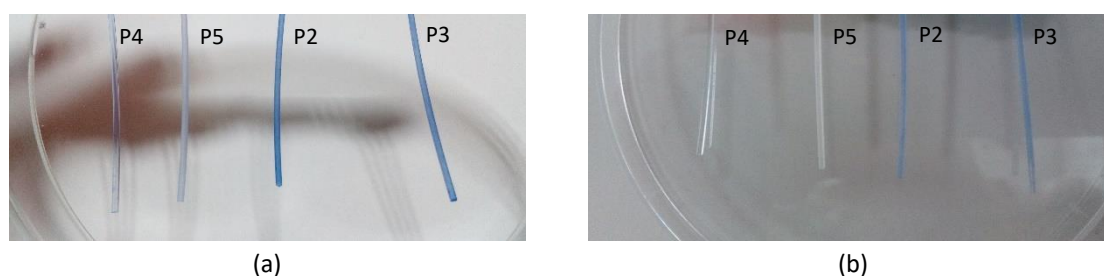


Figure 5.22 Unclad (P4) and unclad polished (P5,P2,P3) POF samples after being immersed in protein solution (P4,P2,P3) and in buffer solution (P5) overnight, after washing with squirts of distilled water (a) and isopropanol (b).

No significant difference was observed in the blue colour acquired by the samples P2 and P3 and also for the samples P4 and P5. This reveals two important aspects:

(i) only polished POF samples allow for protein immobilization in the considered immersion time (P2 and P3). The sample P4, an unclad POF immersed in protein solution, presented a similar colour than sample P5 immersed only in buffer solution.

(ii) washing the samples with buffer solution before immersion in the staining solution is not mandatory. Even if unspecific binding occurs, the stained proteins that are not attached to the POF are removed through washing with distilled water. Only sample P3 was previously washed with buffer solution and presents a similar colour when comparing with sample P2, immersed directly in the staining solution.

The samples were observed with optical microscopy after the washing procedures with distilled water and isopropanol, see Figure 5.23. The surface roughness is easily observed in the microscopic images for the samples polished with sandpaper P600, samples P2, P3 and P5. The sample P4 (unclad POF) reveals a smooth surface. After washing the samples with distilled water the polished samples immersed in protein solution (P2 and P3) present a very strong blue colour.

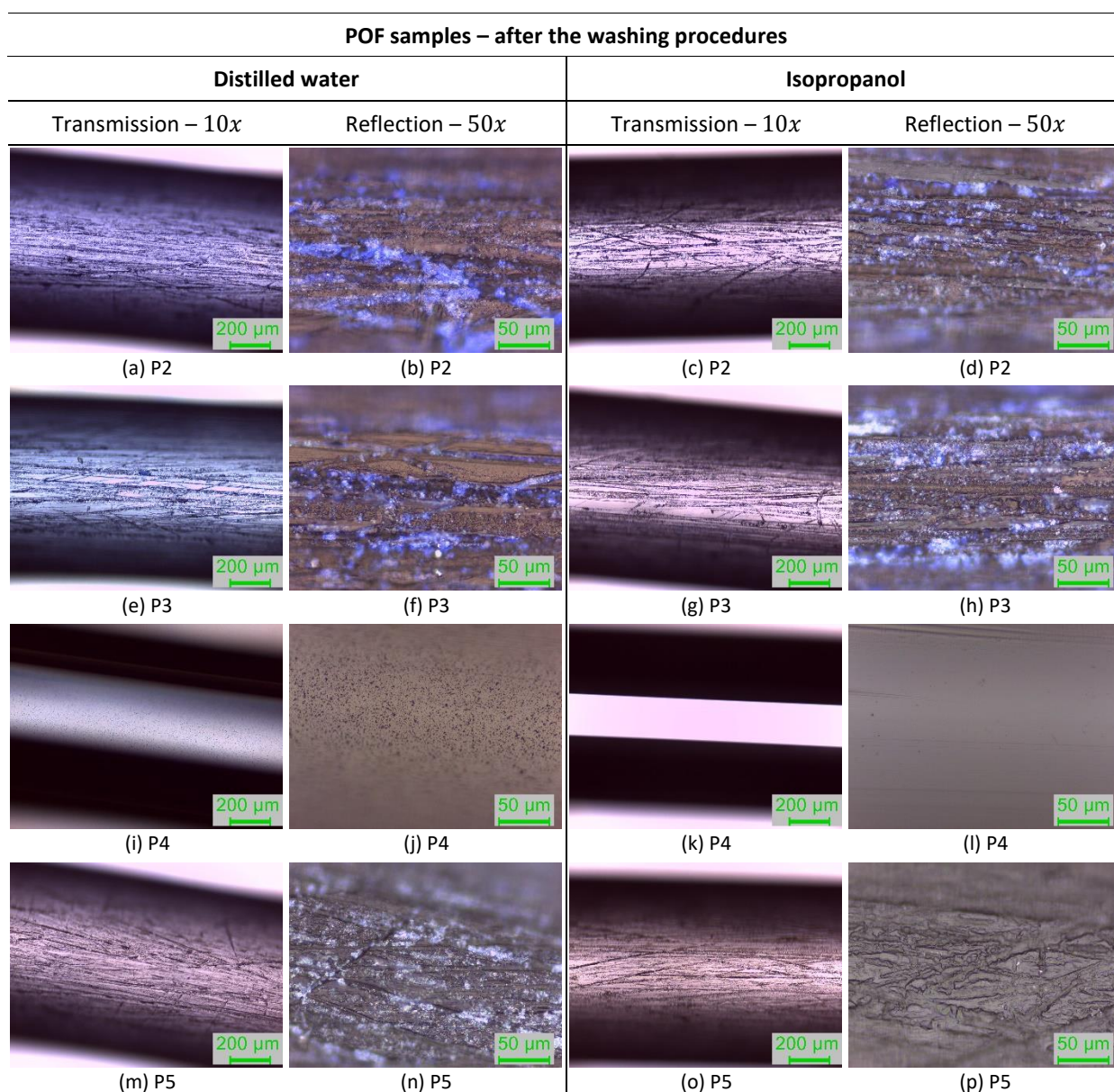


Figure 5.23 Images of optical microscopy - POF samples immersed in protein solution (P2,P3,P4) and buffer solution (P5) overnight, washed with distilled water and isopropanol: Sample P2 (a,b,c,d); Sample P3 (e,f,g,h); Sample P4 – unclad POF (i,j,k,l); Sample P5 (m,n,o,p).

The transmission spectra of the samples after the washing procedures (distilled water and isopropanol) are depicted in the Figure 5.24. The samples left overnight in protein solution (P2, P3 and P4) and washed with distilled water showed absorption of light between 500 – 700 nm. After washing with isopropanol, the light transmission increased at these wavelengths. The sample P5, immersed overnight in buffer solution did not reveal a variation in the transmission of light after the washing procedures. These results show that, even if samples P4 and P5 showed similar colours at naked eye after the washing procedures, absorption of light only occurred for the sample immersed in protein solution (P4).

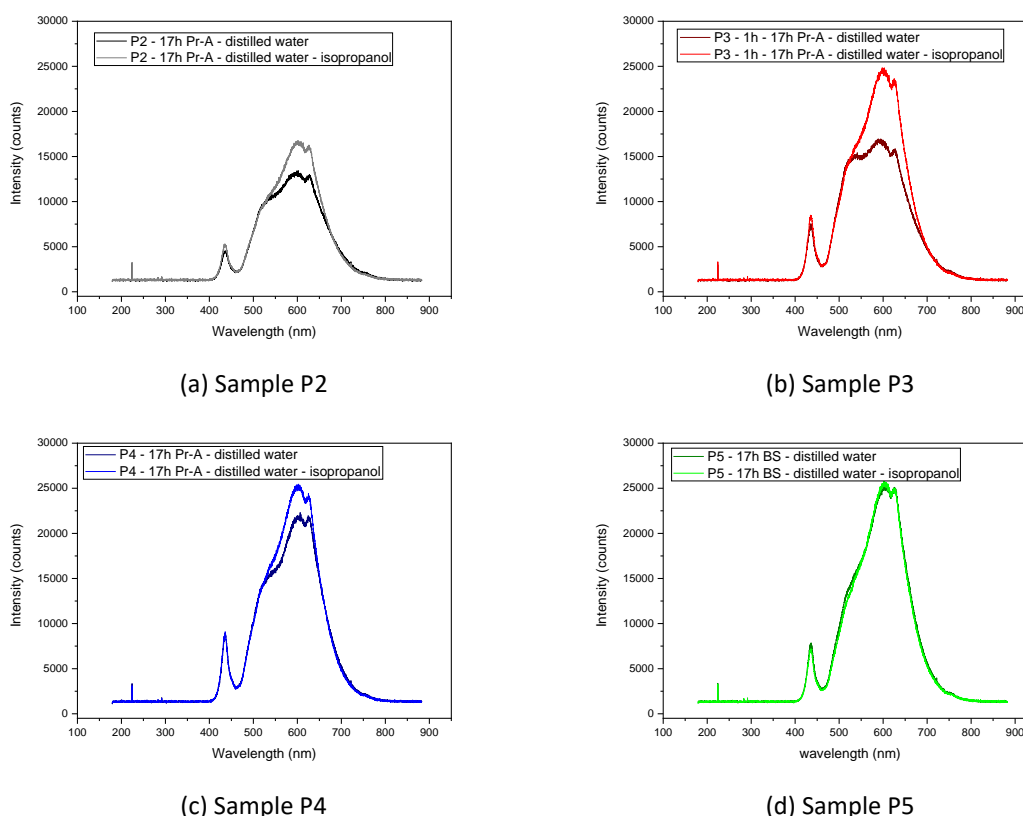


Figure 5.24 Transmission spectra obtained after washing with distilled water and with isopropanol of the POF samples immersed overnight in protein solution (Pr-A) or buffer solution (BS).

The results obtained for sample P2 were compared with the ones obtained before immersion in the protein solution, see Figure 5.25. Figure 5.25(a) shows that after washing with isopropanol, the transmission spectra is very similar with the one previously obtained for the sample before immersion in the protein solution. The absorbance (A) was calculated (Equation 5.4) and is depicted in Figure 5.25(b). In this case, the reference used to calculate the absorbance was the sample's spectrum before immersion in the protein solution (sample P2):

$$A = -\log \frac{I_{\text{modified sample}}}{I_{\text{sample}}} \quad [a. u.] \quad \text{Equation 5.4}$$

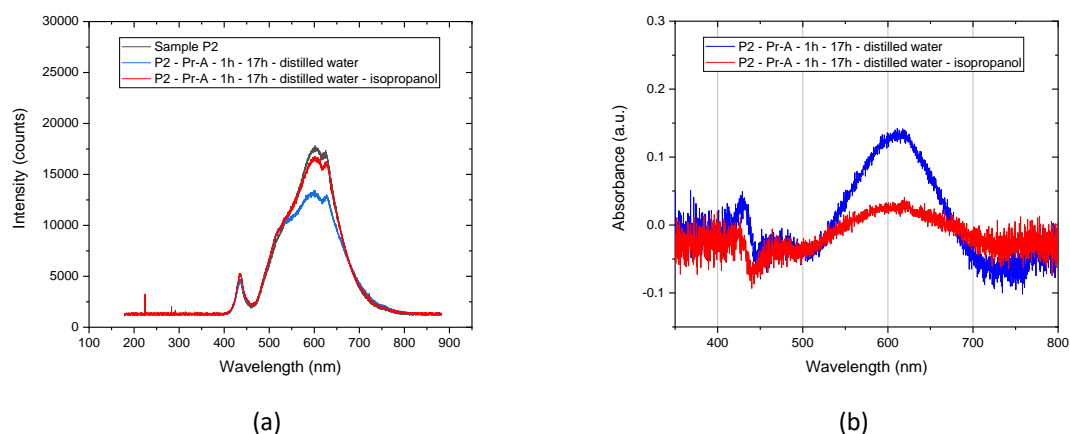


Figure 5.25 (a) Transmission spectra obtained for sample P2 after immersion in the protein solution overnight and washing with distilled water and with isopropanol - comparison with the spectra obtained before immersion in the protein solution (sample P2); (b) calculated absorbance (reference – sample P2, without any modification procedure, see Equation 5.4).

Although the blue colour was not completely removed from the sample P2 due to the washing procedure with isopropanol, the absorption of light decreased significantly after this step. From these results we can conclude that stained proteins are removed from the POF's surface through this washing procedure, although not completely. Furthermore, the variation in the transmission spectra obtained after the washing procedures, with distilled water and isopropanol, can be used to confirm the presence of stained proteins in the POF's surface, associated with the blue colour observed at naked eye (qualitative analysis).

Figure 5.26 allows to compare the shape of the samples' spectra before and after washing with isopropanol. The samples P2 and P3, both immersed in protein solution (Pr-A) overnight, reveal an identical spectrum after washing with isopropanol, see Figure 5.26(b). Before, after washing only with distilled water, the spectra have different intensities although the shape is similar, with light absorption between 500 nm and 700 nm, see Figure 5.26(a).

When comparing the samples P3 and P5 (polished samples immersed in protein and buffer solutions, respectively), with the sample P4 (an unclad POF immersed in protein solution), one can see that the absorption is higher for the polished sample in protein solution (P3), followed by the unclad POF in protein solution (P4). When these samples were washed with isopropanol, the transmission of the light increased for the samples immersed in protein solution (P2,P3,P4) and the shape of the spectra obtained for the samples P3 and P4 was identical, see Figure 5.26(d). These results reveal that polishing the POF samples allows more protein immobilization and confirms that washing with squirts of isopropanol decreases the quantity of immobilized protein.

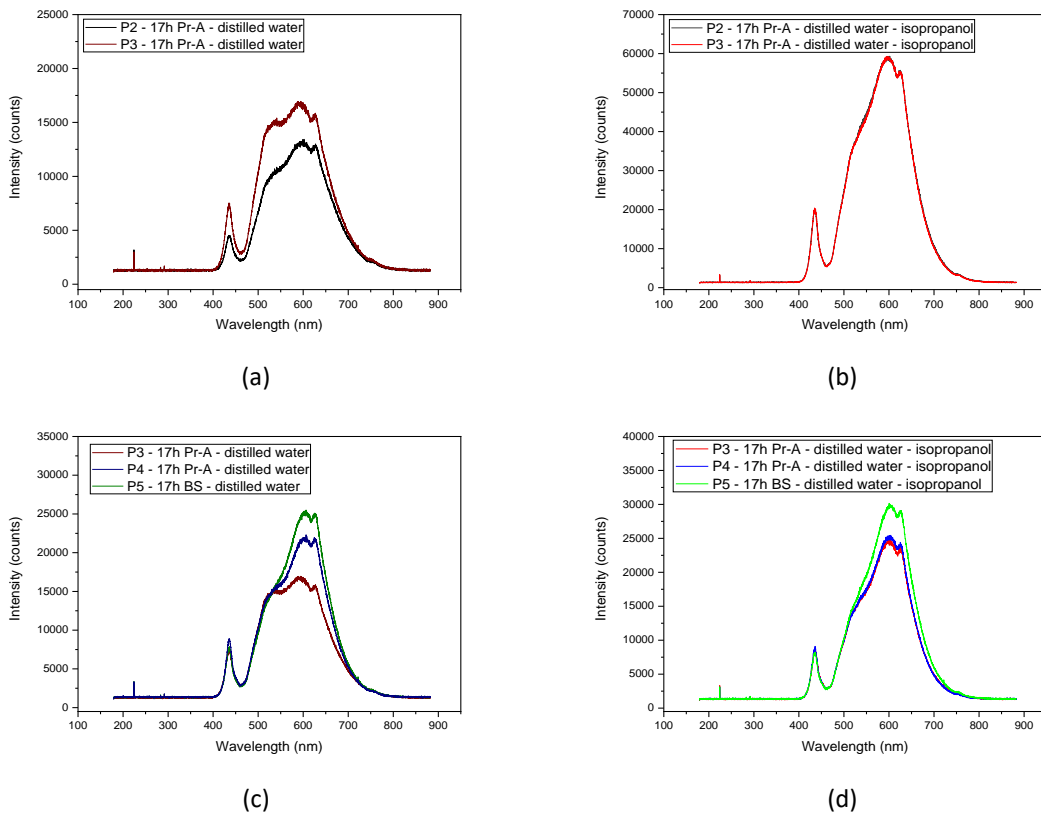


Figure 5.26 Comparison of the transmission spectra obtained after washing with distilled water (a,c) and isopropanol (b,d) – samples immersed overnight in protein solution, Pr-A (P2,P3,P4) and buffer solution, BS (P5).

The absorbance (A) was calculated and depicted in Figure 5.27. The reference used to calculate the absorbance for each sample was the spectra obtained after the washing procedure with distilled water. The calculated absorbance is only indicative, as the obtained spectra is not exactly the same when measured several times for the same sample. This variation can be related with the removal of the POF samples from the experimental setup between measurements and the variation of the light intensity in the optical source.

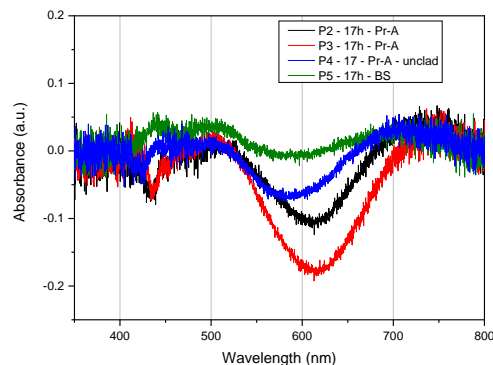


Figure 5.27 Absorbance of the samples after washing with distilled water and isopropanol (immersion overnight in protein solution, Pr-A and in buffer solution, BS).

The decrease observed in the absorbance means that the transmission of light increased, at those wavelengths, after washing with isopropanol.

These results confirm the coating of POF samples with proteins, which can be observed at naked eye, by optical microscopy and by the variation of the light that is transmitted through the POF samples. The polishing of the POF's surface allows for more protein immobilization, probably related with the increase of the surface area or creation of sites for protein agglomeration.

5.3.4.3 Immersion time: 1h / 2h / 3h

Nine samples of POF with 4 cm were prepared (P6 – P14). The cladding was removed in the central zone (2 cm length) with acetone and distilled water. The unclad region was polished with sandpaper P600. These two zones, POF with cladding and unclad polished POF, would allow to easily verify the variation in the colour caused by the stained proteins on the POF's surface. The samples were washed with squirts of distilled water and optical paper.

The samples were placed in Eppendorf's of 1.5 mL, filled with protein solution (Pr-A) or phosphate buffer (Table 5.9) and left for 1h, 2h and 3h with stirring (50 rpm), see Table 5.12. The variation in the blue colour observed at naked eye may allow to verify the dependence of the protein immobilization to the POF's surface with immersion time.

The samples P8, P11 and P14 were washed by manual stirring with phosphate buffer after removal from the protein solution (unspecific binding would be removed through this washing step with the buffer solution).

All the samples were immersed in staining solution for 30 min. After the removal from the staining solution, the samples were cleaned with squirts of distilled water and optical paper. The tips of the POF samples were cut and the samples were placed in identified Eppendorf's to dry.

The samples were analysed at naked eye and the transmission spectra was recorded. The samples were further washed with squirts of isopropanol, cleaned with optical paper and again analysed.

Table 5.12. POF samples (P6 – P14): conditions of preparation.

| POF Sample | Immersion time | Protein / buffer solution | Washing | Staining | Washing |
|------------|----------------|---------------------------|------------------|----------|----------------------|
| P6 | 1h | Phosphate buffer | - | 30 min | Water Isopropanol |
| P7 | | Pr-A in phosphate | - | | |
| P8 | | | Phosphate buffer | | |
| P9 | 2h | Phosphate buffer | - | | |
| P10 | | Pr-A in phosphate | - | | |
| P11 | | | Phosphate buffer | | |
| P12 | 3h | Phosphate buffer | - | | |
| P13 | | Pr-A in phosphate | - | | |
| P14 | | | Phosphate buffer | | |

Two regions are very clear in the POF samples. Only the unclad polished region became blue after the samples were immersed in the staining solution. The cladded POF kept clear and transparent. The POF samples immersed in protein solution always reveal a stronger blue colour than the samples immersed in phosphate buffer. After washing with isopropanol the blue colour

disappears from the samples immersed in phosphate buffer contrary to the samples immersed in the protein solution, see Figure 5.28 and Figure 5.29.

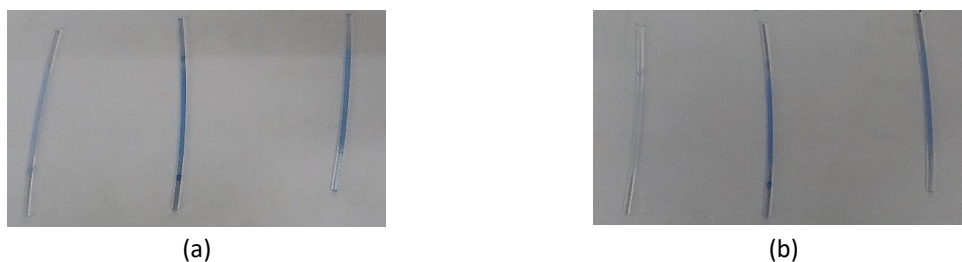


Figure 5.28 POF samples P6, P7 and P8 (from the left to the right) immersed for 1h in buffer and protein solutions, after washing with distilled water (a) and isopropanol (b).

Furthermore, the samples immersed in protein solution for 3 h (P13, P14) present a stronger colour when compared with the samples immersed for 1 h (P7, P8) and 2 h (P10, P11), see Figure 5.29. Nevertheless, at naked eye no difference can be noticed between the colour of the samples immersed for 1 h and 2 h in protein solution.

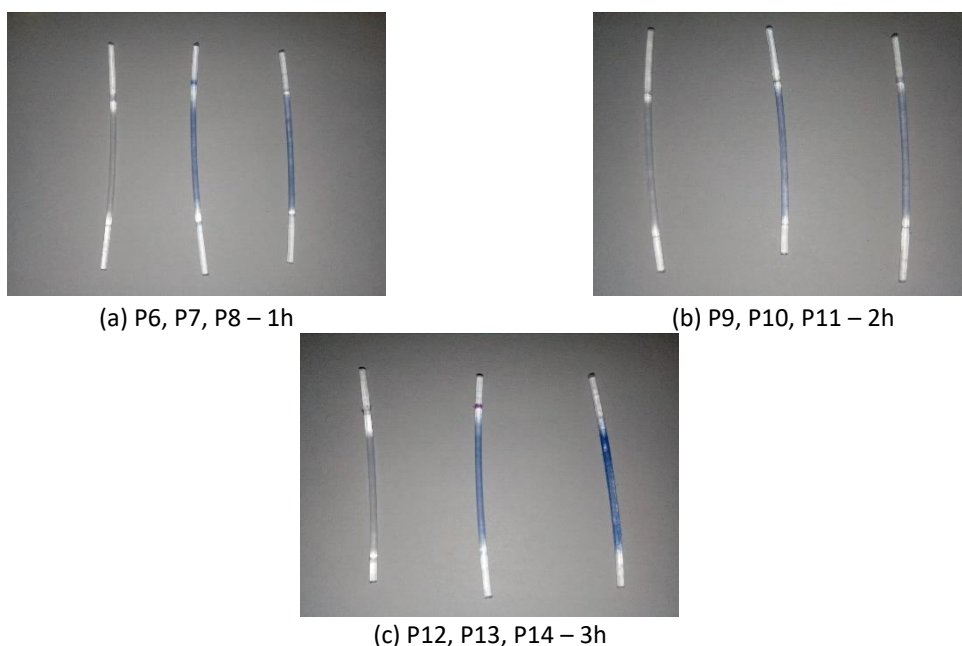


Figure 5.29 POF samples immersed in buffer and protein solutions for 1 h (a), 2 h (b) and 3 h (c), after washing with squirts of distilled water and isopropanol.

No difference was observed in the colour of the samples previously washed with buffer solution (P8,P11,P14) when comparing with the samples placed directly in the staining solution (P7,P10,P13), except for sample P14 which presented a stronger colour.

The samples immersed for 3 h were observed by optical microscopy after the washing procedures, see Figure 5.30. From the images obtained with optical microscopy it was verified that the surface of sample P14 was more covered with stained proteins than sample P13. Furthermore, the surface of sample P14 seems rougher, which can be related with the stronger blue colour acquired.

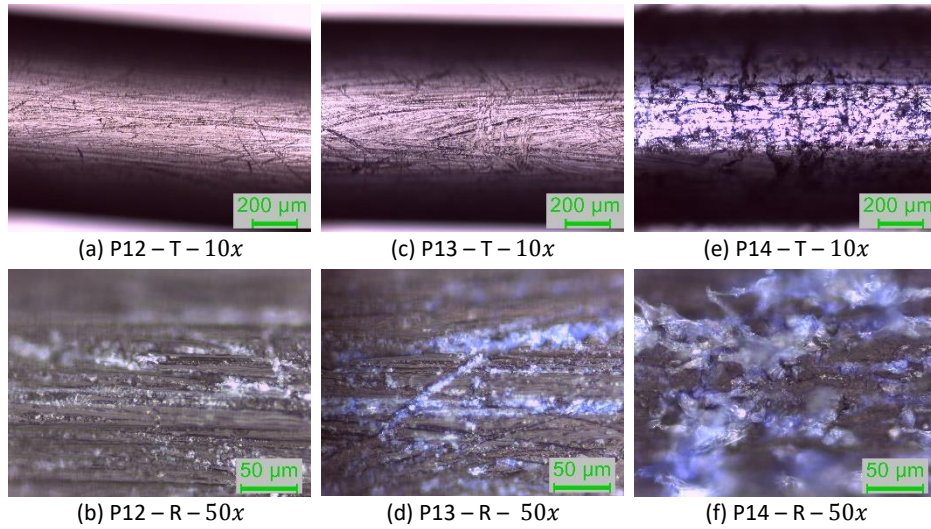


Figure 5.30 Images of optical microscopy, transmission (T) and reflection (R) – POF samples immersed for 3 h in phosphate buffer (P12) and in protein solution Pr-A (P13,P14), after washing with distilled water and isopropanol.

The transmission spectra of the samples after the washing procedures (distilled water and isopropanol) were recorded in transmission and the results are depicted in the Figure 5.31. There was no significant variation in the obtained spectra. Although the blue colour present in the samples immersed in the protein solution, a strong absorption of light was not verified.

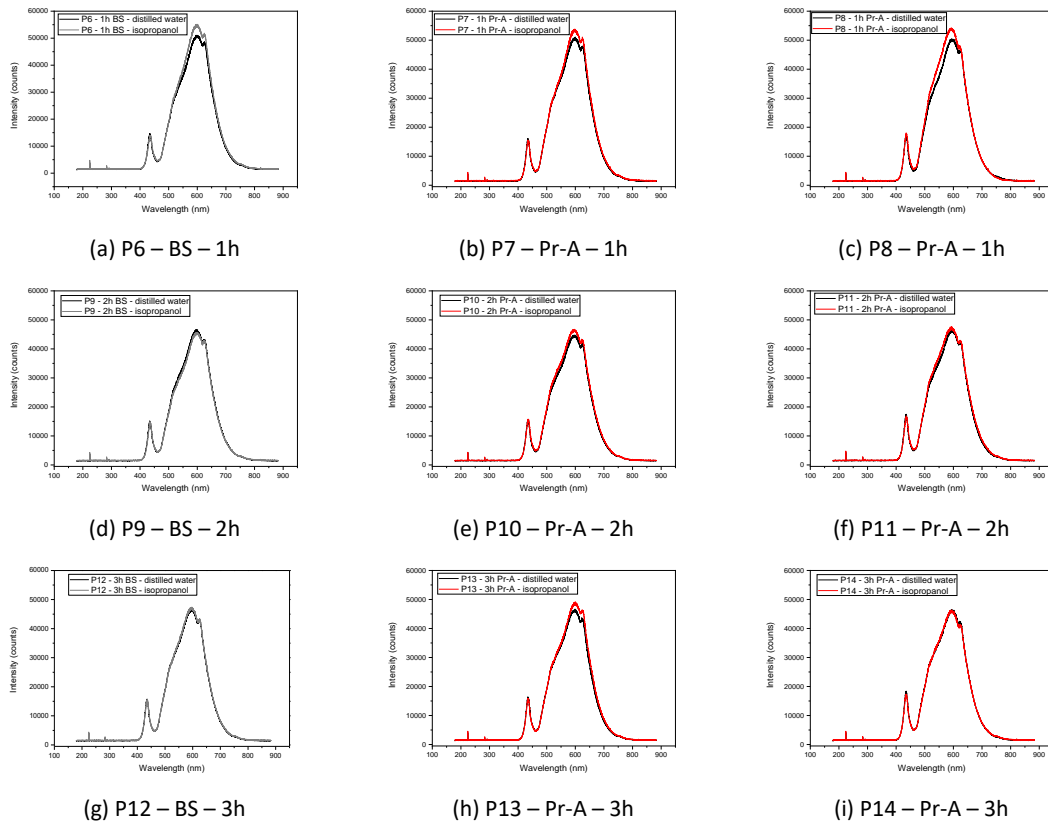


Figure 5.31 Transmission spectra obtained after washing with distilled water and with isopropanol - POF samples immersed in buffer (BS) and protein solutions (Pr-A) for 1 h, 2 h and 3 h.

The light transmitted through the samples was also analysed using another setup. Instead of connecting the POF with the fibre adapters, as depicted in the Figure 5.32(a,b,c), the POF was placed vertically between the light source and the spectrometer, see Figure 5.32(d,e,f). This allowed to collect in the spectrometer the light transmitted through the POF instead of the light that travelled in the POF.

The spectra after the washing procedure with isopropanol was recorded using this setup and the results are depicted in the Figure 5.33. This setup brought some difficulties with the measurements, as it was very difficult to place the POF exactly occupying the space of the transmitted light, sometimes causing white light to reach the spectrometer.

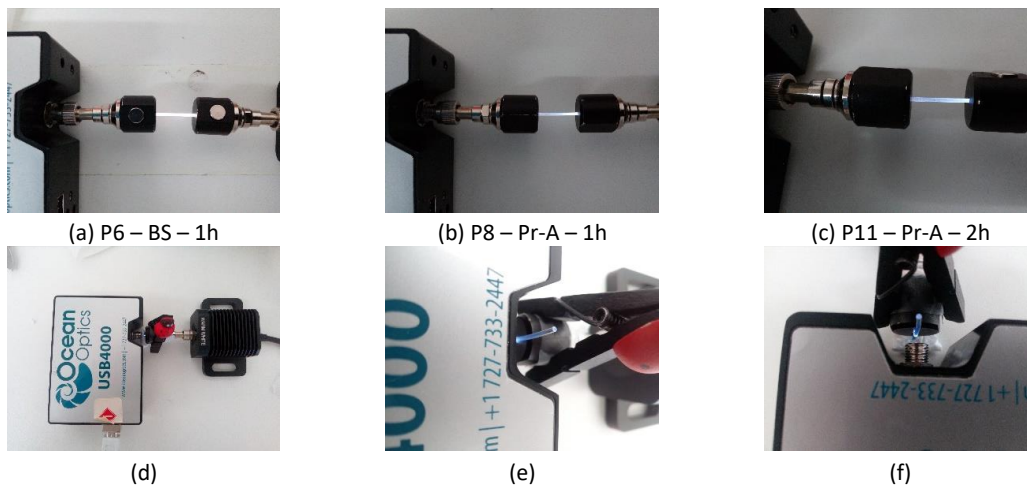


Figure 5.32 Experimental setups used to record the transmission spectra: (a,b,c) POF placed horizontally fixed by the POF adapters; (d,e,f) POF placed vertically between the light source and the spectrometer.

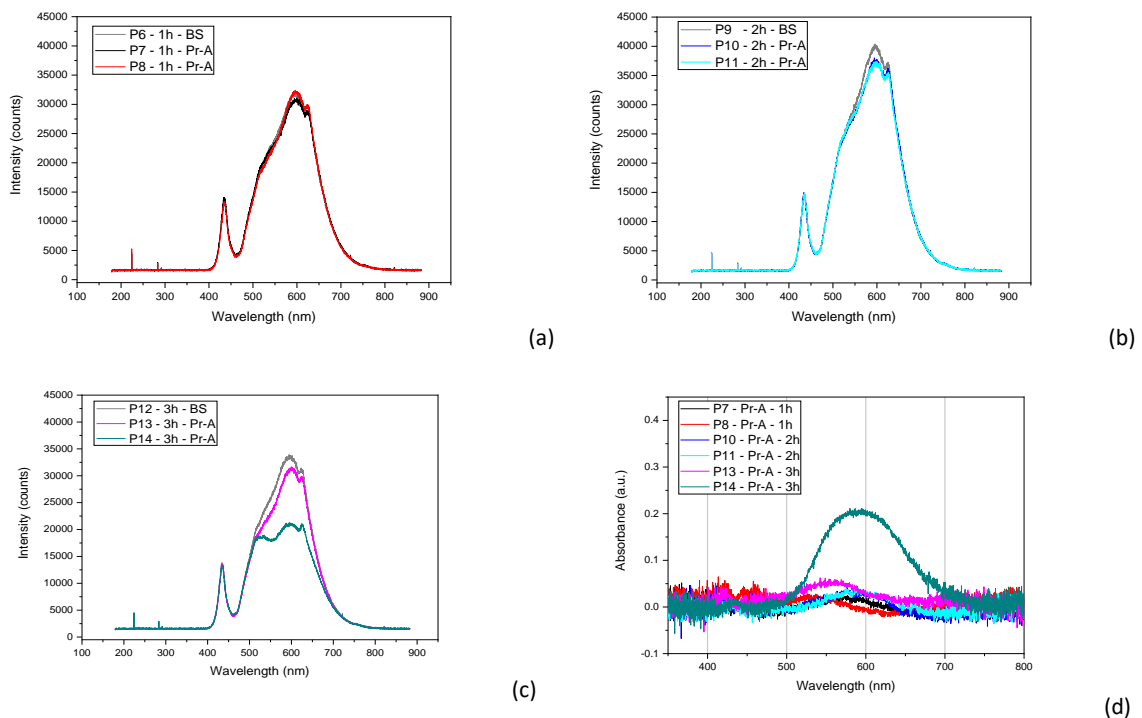


Figure 5.33 POF samples placed vertically between the light source and spectrometer, after washing with distilled water and isopropanol: (a,b,c) transmission spectra; (d) absorbance spectra.

Only for the sample P14, immersed in protein solution for 3 h, was observed a strong absorption of light in the region between 500 nm and 700 nm, see Figure 5.33(c). The absorbance was calculated for all the samples immersed in protein solution (Pr-A), based in Equation 5.4 and using the spectra obtained with the POF sample immersed in buffer solution (BS) as reference, see Figure 5.33(d).

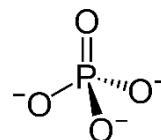
5.3.5 Influence of the buffer solutions: phosphate and Tris

In order to evaluate the influence of the buffer solution on the immobilization of proteins to the POF's surface, two buffer solutions were used: phosphate and Tris.

Tris is the short name for Tris(hydroxymethyl)aminomethane, $(NH_2C(CH_2OH)_3)$. Contrary to phosphate (PO_4^{3-}), used in the protein solution A, Tris contains an amino group ($-NH_2$) which can bind to the POF's surface and compete with the proteins, see Figure 5.14. If this happens, less protein would be immobilized on the POF's surface when Tris buffer is used in comparison to the case when phosphate buffer is used.



(a) Tris - $(NH_2C(CH_2OH)_3)$



(b) Phosphate - (PO_4^{3-})

Figure 5.34 Structural formula of (a) Tris (Tris(hydroxymethyl)aminomethane) and (b) Phosphate.

The following studies were performed using the same protein solution with the two different buffers, phosphate and Tris. This was achieved by the dialysis of the protein solution B, which allowed to change the buffer solution (section 5.3.5.2). The POF samples were immersed in the different solutions overnight and the immobilization of the proteins on the POF's surface was evaluated at room temperature and at 4°C.

5.3.5.1 Pr-B and Tris buffer – immersion time: 3 h

The first test performed consisted in the immersion of POF samples in protein solution B (Pr-B) prepared with Tris buffer and the results were compared with the ones previously obtained with protein solution A (Pr-A) in phosphate buffer.

Two samples of POF were prepared (P15 and P16). Unclad POFs with 4 cm were polished with sandpaper P600 and cleaned with squirts of distilled water and optical paper. The samples were modified as hereafter described and the conditions of preparation can be found in Table 5.13.

The samples were placed in Eppendorf's of 1.5 mL, one filled with Tris buffer (P15) and the other with protein solution B (P16), see Table 5.9. The samples were left for 3 h at room temperature with stirring (50 rpm). After removal from the protein solution the sample P16 was washed with Tris buffer by manual stirring inside an Eppendorf (unspecific binding would be removed through this washing step).

The samples were immersed in staining solution for 30 min, washed with squirts of distilled water and left to dry. The tips of the POF samples were cut and the samples were washed with squirts of isopropanol and left to dry in identified Eppendorf's. At naked eye it was observed that both samples were blue, although sample P16 showed a stronger blue colour when compared with sample P15, see Figure 5.35(a).

The samples were washed again with isopropanol and optical paper and observed at naked eye. There was no variation in the blue colour of the sample P16, on the contrary the blue colour was completely removed from sample P15, see Figure 5.35(b). Only squirts of isopropanol do not completely remove un-specific binding while isopropanol and optical paper allow for complete removal of the staining solution from POF's only immersed in buffer solution.

The colour of these samples was compared with the samples immersed for 3 h in phosphate buffer and protein solution A (P12, P13, P14), see Figure 5.35(c). At naked eye, the blue colour of the samples immersed in the different protein solutions is very similar.

Table 5.13. POF samples (P15, P16): conditions of preparation.

| POF Sample | | Immersion time | Protein / buffer solution | Washing | Staining | Washing |
|------------|------|----------------|---------------------------|-------------|----------|--------------------------------|
| P15 | P600 | 3h | Tris buffer | - | 30 min | Distilled water Isopropanol |
| P16 | | | Pr-B in Tris | Tris buffer | | |

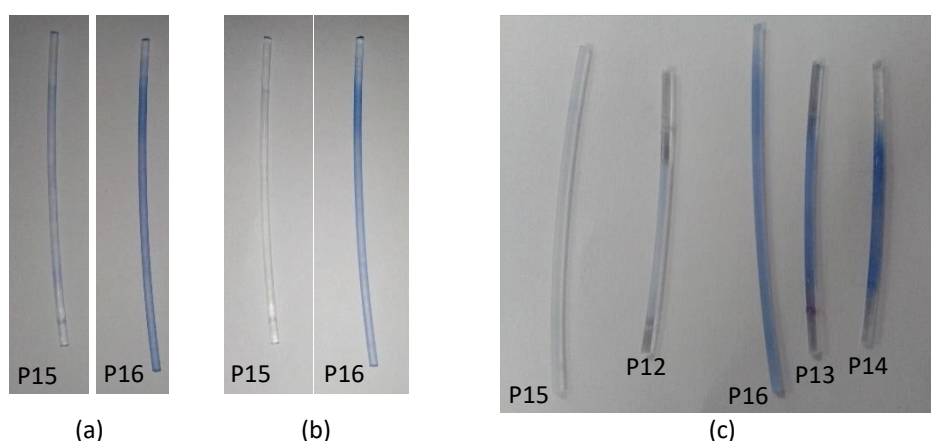


Figure 5.35 POF samples immersed for 3 h in Tris buffer (P15) and protein solution B (P16), after washing with squirts of isopropanol (a), and further washed with isopropanol and optical paper (b); comparison with the samples immersed for 3 h in phosphate buffer (P12) and protein solution A (P13,P14).

Samples P15 and P16 were also analysed by optical microscopy, see Figure 5.36. The blue colour is only present in the sample that was immersed in the protein solution.

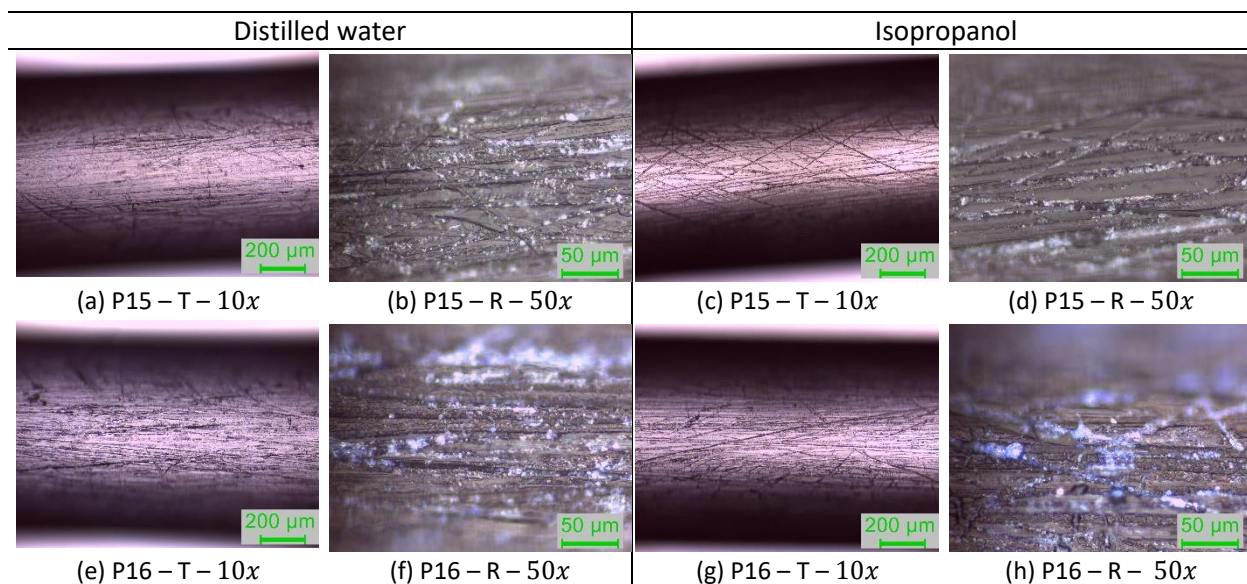
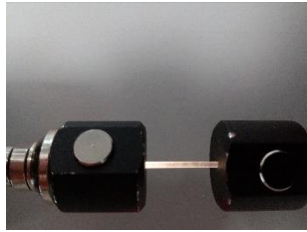


Figure 5.36 Microscope images, transmission (T) and reflection (R) - sample immersed in Tris buffer (P15 - a,b,c,d) and in protein solution B with Tris buffer (P16 - e,f,g,h), after washing with distilled water and with isopropanol.

The spectra of the light transmitted through the POF samples were recorded by placing the POF horizontally fixed by the POF adapters. The transmission spectra of one unclad polished POF was recorded as well as the spectra of the samples P15 and P16 after washing with isopropanol, see Figure 5.37(c). Results show that the spectrum obtained with the sample immersed in Tris buffer (P15) is very similar to the spectrum of the unclad polished POF and absorption of light occurred only for the sample immersed in the protein solution B (P16).

Absorbance was calculated based on Equation 5.4, using the spectrum obtained for the sample immersed in Tris buffer as reference (sample P15) and is depicted in Figure 5.37(d).

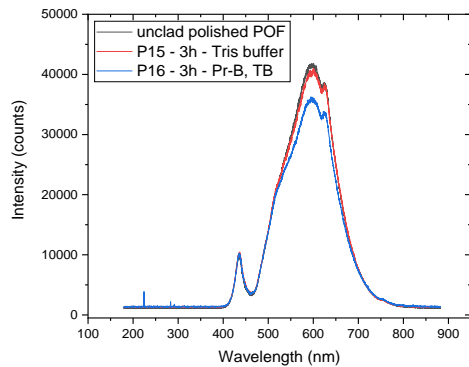
The POF samples were placed vertically between the light source and the spectrometer, as depicted in Figure 5.32(d,e,f), and the transmission spectra were analysed (see Figure 5.37(e)). To compare samples P14 and P16, immersed for 3 h in protein solutions A and B with phosphate and Tris buffer, respectively, the absorbance was calculated based on Equation 5.4, only for qualitative analysis (spectra obtained for the samples only immersed in buffer solution were used as reference), see Figure 5.37(f).



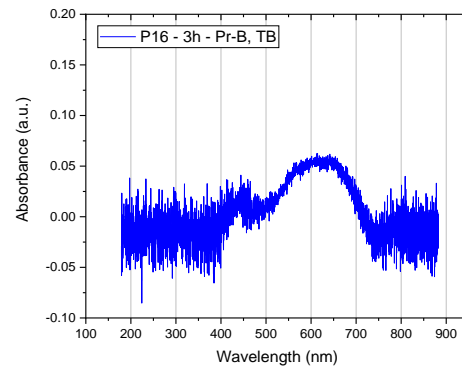
(a) Sample P15 (Tris buffer)



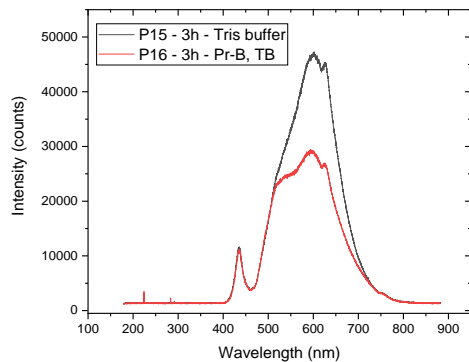
(b) Sample P16 (Pr-B in Tris buffer)



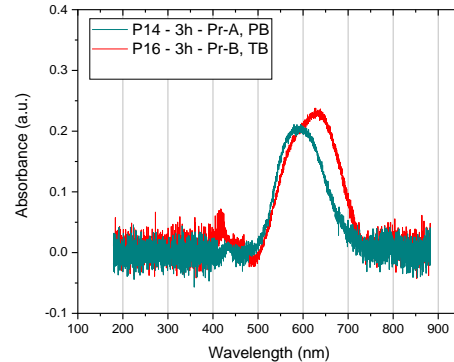
(c)



(d)

POF samples placed horizontally on the experimental setup

(e)



(f)

POF samples placed vertically on the experimental setup

Figure 5.37 POF samples immersed 3 h in Pr-B with Tris buffer (TB): (a,b) samples placed horizontally in the experimental setup; (c) transmission spectra and comparison with an unclad polished POF (setup – horizontal); (d) absorbance spectra (setup – horizontal, reference: sample immersed in Tris buffer); (e) transmission spectra (setup – vertical); (f) absorbance spectra of sample P16 and comparison with sample P14 (setup – vertical, reference: samples immersed in buffer solution).

Samples immersed for 3 h on protein solution almost do not reveal light absorption due to the stained proteins immobilized on the POF's surface when placed horizontally in the optical setup. By placing the POF samples vertically a stronger absorption around 600 nm was observed.

Furthermore, protein solutions were different (Pr-A and Pr-B). For this reason, a protein solution was prepared using both buffer solutions (phosphate and Tris). The experimental procedures and obtained results are described in the next section.

5.3.5.2 Pr-C – phosphate and Tris buffer

To evaluate the influence of the buffer solution on the immobilization of the proteins to the POF's surface, different buffers were used with the same protein solution – phosphate and Tris. The protein solution B was previously prepared in Tris buffer and, for that reason, dialysis was performed to substitute the Tris buffer by phosphate buffer.

Firstly, Tris buffer was added to the protein solution B in order to obtain a total volume of 50 mL – from now on known as protein solution C, Pr-C.

Around 25 mL of the Pr-C with Tris buffer were placed inside a “snake skin”, depicted in Figure 5.38. The “snake skin” was closed, placed inside a glass vial filled with 300 mL of phosphate buffer and left for 1 h with magnetic stirring at 4°C, see Figure 5.38. The solution was removed and more 300 mL of phosphate buffer were added to the glass vial and left for 1 h with magnetic stirring at 4°C. This procedure was repeated one more time corresponding to three washing procedures with phosphate buffer.



Figure 5.38 Dialysis of the protein solution C: (a) experimental setup; (b) glass vial filled with phosphate buffer and the “snake skin” containing the original protein solution C with Tris buffer.

The dialysed solution C now containing the phosphate buffer was removed from the “snake skin” and stored in the laboratory refrigerator, along with the original solution Pr-C with Tris buffer. The protein solutions Pr-C with phosphate and Tris buffer are described in the Table 5.14.

Table 5.14. Protein solution C with Tris and phosphate buffer.

| Protein solution | Buffer solution | |
|------------------|---|----------|
| Pr-C | 50 mM Phosphate / 0.5 M NaCl / 20 mM Imidazole | pH =7.1 |
| | 100 mM Tris / 0.5 M NaCl / 3 mM DTT / 100 mM Imidazole | pH = 8.2 |

Samples of POF were prepared and placed in Eppendorf's filled with buffer or protein solution and left overnight. The same protein solution (Pr-C) was used with phosphate and Tris buffer.

Four samples of POF with 12 cm were selected and the cladding was removed in 2 cm of the central region. The unclad portion of the POFs was polished with sandpaper P600 and the samples were washed with distilled water and cleaned with optical paper.

The samples were placed in Falcon tubes of 10 mL filled with phosphate buffer (P17), protein solution C with phosphate buffer (P18), Tris buffer (P19) and protein solution C with Tris buffer (P20). The samples were left overnight at room temperature, after which were removed and placed in staining solution for 30 min. The samples placed in protein solution were firstly washed with the respective buffer solution.

The samples were washed with distilled water and left to dry in identified Eppendorf's. The samples were further washed with isopropanol and optical paper. The conditions of preparation can be found in the Table 5.15.

Table 5.15. POF samples (P17 – P20) – conditions of preparation.

| POF Sample | | Immersion time and temperature | Protein / buffer solution | Washing | Staining | Washing |
|------------|------|--------------------------------|---------------------------|------------------|----------|--------------------------------|
| P17 | P600 | Overnight at room temperature | Phosphate buffer | - | 30 min | Distilled water Isopropanol |
| P18 | | | Pr-C in phosphate | Phosphate buffer | | |
| P19 | | | Tris buffer | - | | |
| P20 | | | Pr-C in Tris | Tris buffer | | |

The samples were analysed at naked eye and by optical microscopy, see Figure 5.39 and Figure 5.40. Only sample P20, immersed overnight in protein solution with Tris buffer, showed a strong blue colour (sample P18, immersed overnight in protein solution with phosphate buffer, showed a much lighter blue colour).

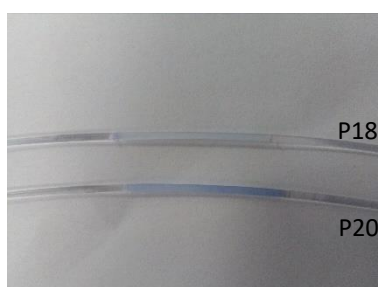


Figure 5.39 POF samples immersed in protein solution Pr-C with phosphate buffer (P18) and Tris buffer (P20) overnight, at room temperature.

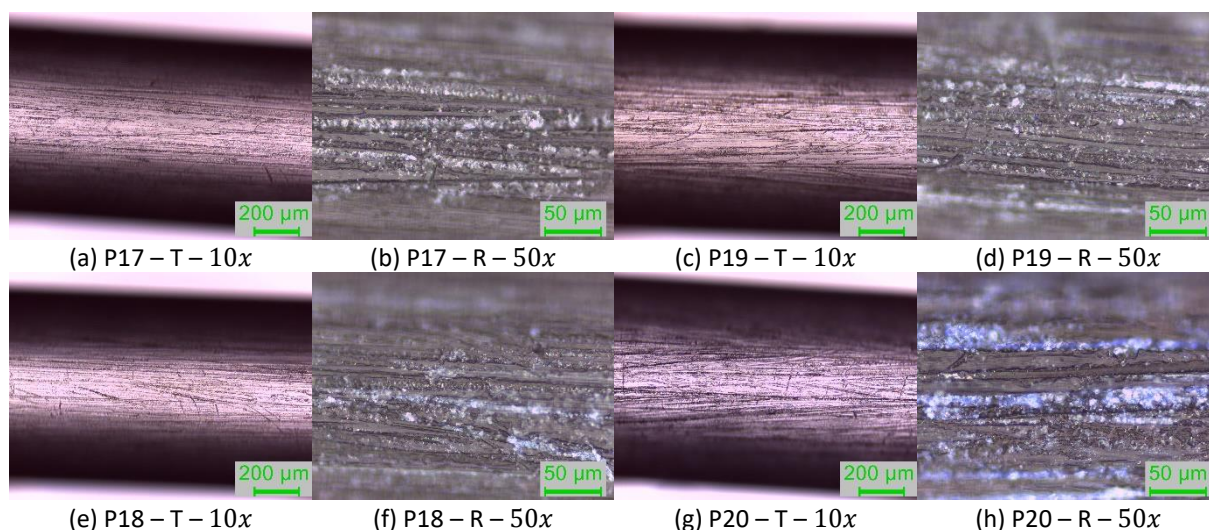
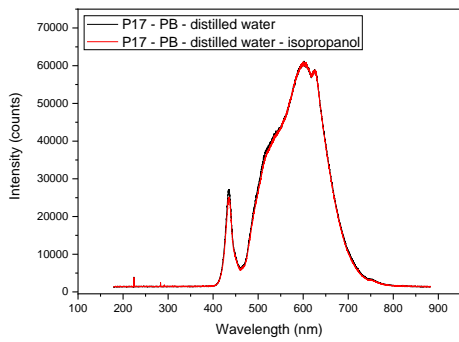


Figure 5.40 Images of optical microscopy, transmission (T) and reflection (R) – samples P17 and P19, P18 and P20, immersed in buffer and protein solutions, respectively, at room temperature, after washing with isopropanol and optical paper.

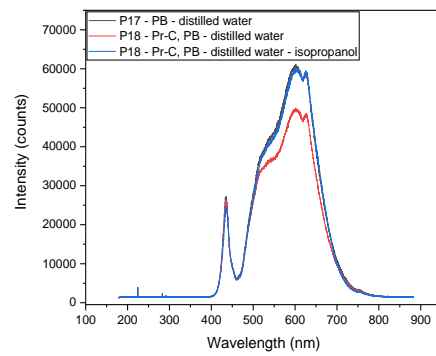
The spectra of the light transmitted through the prepared samples were registered. The samples were washed with squirts of isopropanol while placed in the optical setup and softly cleaned with optical paper. The spectra were registered again and the results are depicted in the Figure 5.41. This procedure intended to verify the variation in the transmission spectra without removing the sample from the experimental setup.

Variation on the light transmitted through the POF samples after the washing procedures was not observed for the samples left overnight in buffer solution (P17 and P19), see Figure 5.41 (a,c). Moreover, the spectra obtained for the samples immersed in buffer solution was similar and independent of the buffer solution used (phosphate or Tris), see Figure 5.41 (e).

The samples left overnight in protein solution (P18 and P20) showed absorption of light between 500 – 700 nm, and an increase of the transmitted light was observed after washing with isopropanol, see Figure 5.41 (b,d). Furthermore, the spectra obtained for these samples after washing with isopropanol was similar to the ones obtained for the samples immersed overnight in buffer solution – showing one more time that the washing procedure with isopropanol removes stained proteins immobilized on the POF's surface. Figure 5.41 (f) depicts the spectra obtained for the samples immersed on both protein solutions, after washing with distilled water.

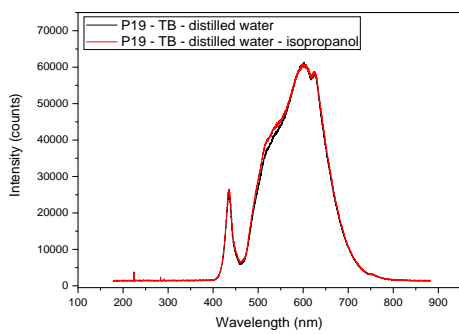


(a)

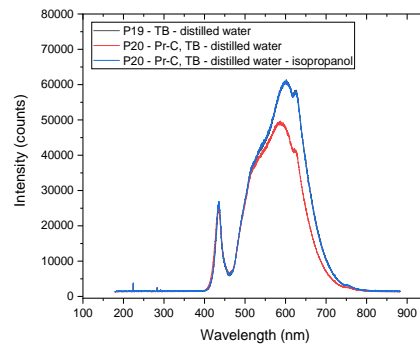


(b)

Sample P17 – phosphate buffer (PB) and sample P18 – Pr-C in phosphate buffer

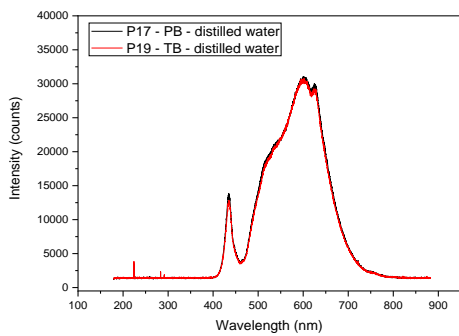


(c)

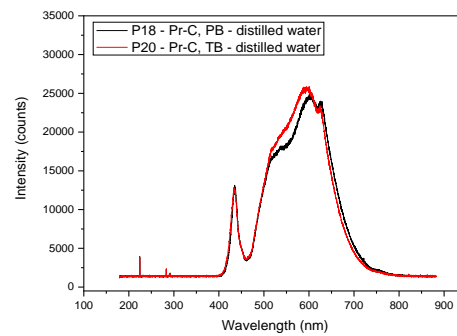


(d)

Sample P19 – Tris buffer (TB) and sample P20 – Pr-C in Tris buffer



(e) Sample P17 and P19 - buffer solutions



(f) Sample P18 and P20 - protein solutions

Figure 5.41 Transmission spectra obtained after washing with distilled water and isopropanol - POF samples immersed overnight at room temperature in protein (Pr-C) and buffer solutions (PB, TB).

The absorbance (A) was calculated based on Equation 5.4 and is depicted in the Figure 5.42, being only indicative. The spectra of the samples immersed in buffer solution were used as reference and the maximum of absorbance occurred around 600 nm.

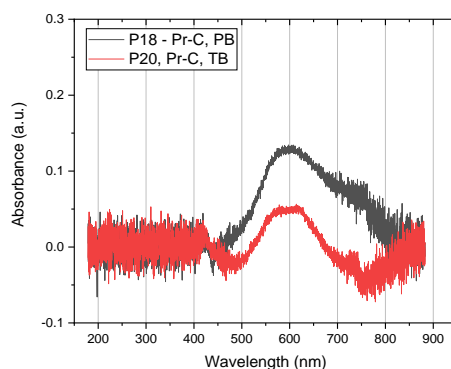


Figure 5.42 Absorbance - samples immersed in protein solution overnight at room temperature, after washing with distilled water and isopropanol (reference: samples immersed in buffer solution).

5.3.6 Influence of the temperature

The results presented in the section above were performed at room temperature. In order to evaluate the influence of temperature in the protein immobilization on POF's, the same procedure was applied but using another temperature condition: $T=4^{\circ}\text{C}$.

The samples were placed in Eppendorf's filled with phosphate buffer (P21), protein solution C with phosphate buffer (P22), Tris buffer (P23) and protein solution C with Tris buffer (P24). The samples were left overnight in a cold room with a temperature of 4°C , with stirring. The experimental setup is depicted in the Figure 5.43.

The next day the samples were removed and placed in staining solution for 30 min. The samples placed in protein solution (P22, P24) were firstly washed with the respective buffer. All the samples were washed with squirts of distilled water and left to dry in identified Eppendorf's. The samples were further washed with isopropanol and optical paper. The conditions of preparation are summarized in the Table 5.16.

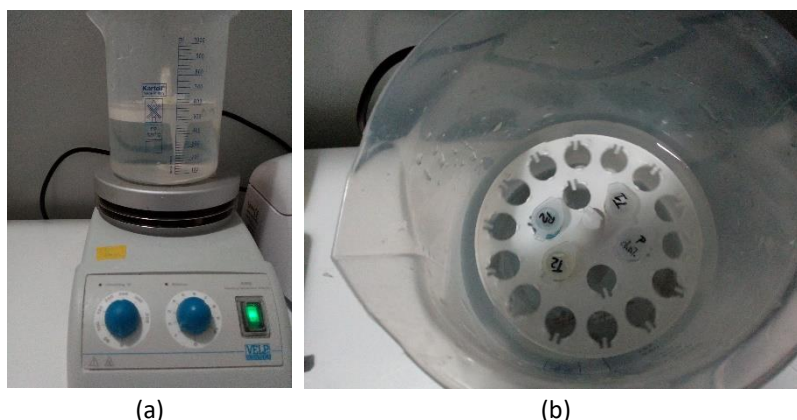


Figure 5.43 Experimental setup – POF samples immersed in buffer and protein solutions, overnight at 4°C with stirring: (a) plastic vial containing water, a magnetic stirrer and floating plastic support; (b) top view, the samples are inside the Eppendorf's placed in the floating plastic support.

Table 5.16. POF samples (P21 – P24) – conditions of preparation.

| POF Sample | | Immersion time and temperature | Protein / buffer solution | Washing | Staining | Washing |
|------------|------|--------------------------------|---------------------------|------------------|----------|------------------------------------|
| P21 | P600 | Overnight at T = 4°C | Phosphate buffer | - | 30 min | Distilled water Isopropanol |
| P22 | | | Pr-C in phosphate | Phosphate buffer | | |
| P23 | | | Tris buffer | - | | |
| P24 | | | Pr-C in Tris | Tris buffer | | |

The samples were analysed at naked eye and by optical microscopy, see Figure 5.44 and Figure 5.45. Samples immersed in protein solution show a stronger blue colour after washing with distilled water which is not completely removed after washing with isopropanol and cleaning with optical paper. On the contrary, the blue colour of samples P21 and P23, immersed in buffer solution, was removed completely by washing with isopropanol and cleaning with optical paper, as expected.

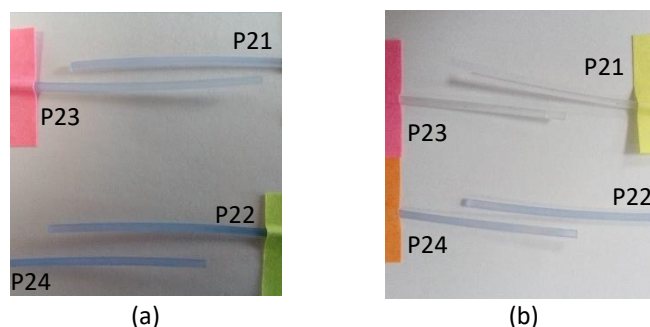


Figure 5.44 POF samples immersed overnight at 4°C in buffer and protein solutions (Pr-C with phosphate and Tris buffer) after (a) washing with distilled water and (b) washing with isopropanol and cleaning with optical paper.

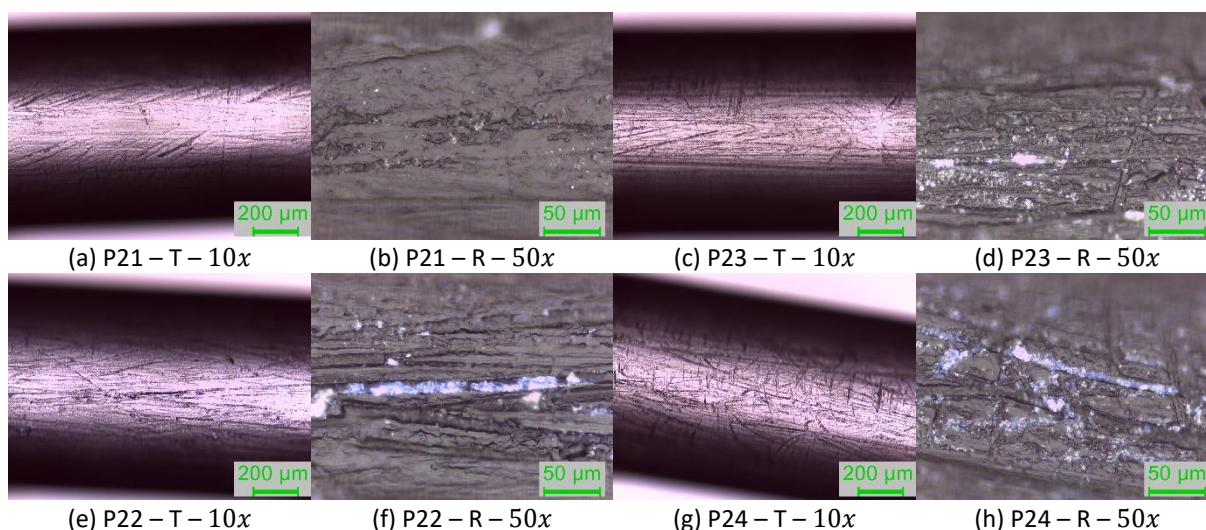
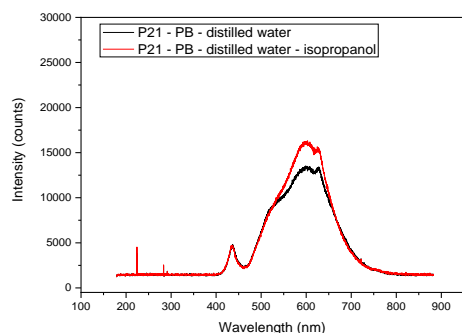
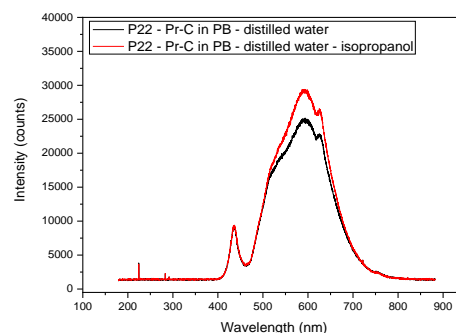


Figure 5.45 Microscope images, transmission (T) and reflection (R), of the samples P21 and P23, P22 and P24, immersed overnight in buffer and protein solutions (respectively) at 4°C, after washing with isopropanol and optical paper.

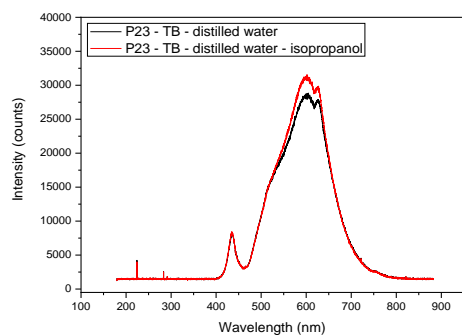
The spectra of the light transmitted through the prepared samples were registered. The same procedure used for the samples immersed overnight at room temperature was used and results are depicted in Figure 5.46. Variation on the transmitted light was obtained for all the samples after the washing procedure with isopropanol.



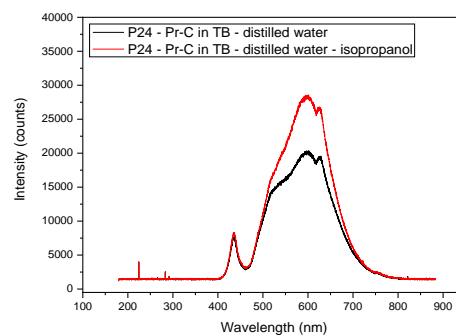
(a) Sample P21 – phosphate buffer (PB)



(b) Sample P22 – Pr-C in phosphate buffer



(c) Sample P23 – Tris buffer (TB)



(d) Sample P24 – Pr-C in Tris buffer

Figure 5.46 Transmission spectra obtained after washing with distilled water and isopropanol - POF samples immersed overnight at 4°C in protein solution (Pr-C) or buffer solution.

The spectra obtained for all samples after washing with isopropanol was compared (see Figure 5.47(a)). The spectra obtained for the samples immersed in buffer solution (P21,P23) is identical, as well as the spectra obtained for the samples immersed in protein solution (P22,P24). Light absorption occurred for the samples immersed in protein solution when comparing with the samples immersed in buffer solution.

The absorbance (A) was calculated based on Equation 5.4 and is depicted in Figure 5.47(b). The spectra of the samples immersed in buffer solution were used as reference and the maximum of absorbance also occurred around 600 nm.

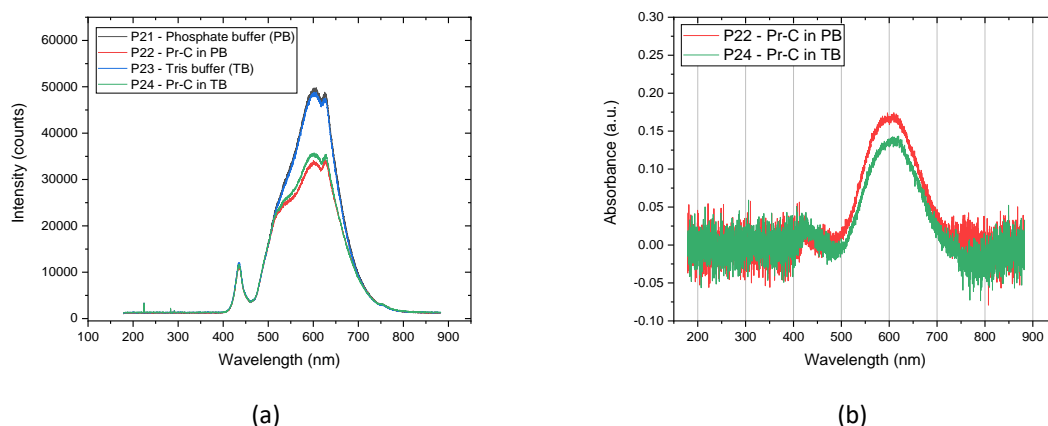


Figure 5.47 POF samples immersed overnight at 4°C in protein solution (Pr-C) or buffer solution: (a) transmission spectra obtained for all samples after washing with distilled water and isopropanol; (b) absorbance spectra obtained for samples immersed in the protein solution (reference: samples immersed in buffer solution).

Further studies should be performed in order to understand the influence of temperature and buffer solution in the immobilization of proteins on the POF's surface.

5.3.7 Conclusions

The coating of modified POFs with proteins was achieved with success. The presence of proteins was verified at naked eye through the blue colour present in the samples immersed in protein solution (stained with Coomassie Blue R250), in contrast with the samples only immersed in buffer solution, after washing with isopropanol.

The polishing of the POF's surface allowed to improve the immobilization of proteins. Samples of POF with cladding did not allow protein binding to the surface. Unclad POFs immersed in solutions of protein became colourless after washing with isopropanol, although absorption of light was observed. As reported in the literature, the increase of surface roughness allows to increase protein immobilization due to the increase of surface area (Tsougeni *et al.*, 2010). From the images of optical microscopy, it seems that surface roughness allowed the agglomeration of proteins at specific sites, even if at naked eye the samples were seeming totally covered with stained proteins. Changes on surface roughness along the POF sample can be responsible for variations on protein immobilization and, consequently, on the blue colour observed.

Higher concentration of proteins on the POF's surface was obtained with higher immersion time and, consequently, stronger was the colour observed and the absorbance of light. No significant variation was observed in the sample's colour due to immersion in protein solution between 1 h and 3 h, but a stronger blue colour was obtained through immersion overnight.

Moreover, higher concentration of proteins on the POF's surface should also be achieved by immersing in solutions with higher protein concentration. Unfortunately, was not possible to compare the protein concentration of the solutions used in these studies.

Temperature and buffer solution can affect the binding of the proteins to the POF although a more detailed study should be performed.

Further developments are focused on the coating of POFs with target proteins selective to water contaminants, contributing to the development of low-cost POF chemical sensors and biosensors.

5.4 Conclusions

These studies allowed to verify the characteristics and capabilities of two different layers that can be used for chemical detection with POFs by low-cost sensing methodologies and technologies. Although the proteins immobilized on the POF's surface are not able to be used as a recognition layer (model proteins), it allowed to understand the conditions involved in the manipulation and analysis of POF biosensors.

The configuration of the D-shaped POF platform allows for easy deposition of selective layers, i.e. MIP's by spin coating and thermal polymerization. On the other hand, straight modified POF's allow for lower resolution values in sensing but there is the need of successful immobilization of the layer on the POF's surface. The strategy of using a specific dye allows to determine, easily and fast, if immobilization/coating occurs or not.

MIP layers are more resistant and the sensor was re-used, although recovery on the sensor's response was not obtained. As reported on the literature, a balance must be attained between the sensor's selectivity and recovery. On the other hand, MIPs are a good possibility for ON/OFF sensing, especially if they include a responsive dye for the layer-target interaction.

In the case of using proteins as a recognition layer, due to the removal of stained proteins with isopropanol, lower resistance seems to be present and more care should be taken in handling and storage. Moreover, the time of life of this type of sensor is an important question, as it should be stored in the cold and temperature can cause protein's denaturation.

A chemical sensor, as defined in Chapter 2, should give an automatic response in short time and comprise the following characteristics: free from sample treatment, able to work in complex samples (selectivity) and reversibility. Time of life (in operation) is also an important parameter as well as the chemical and mechanical stability. The ability to work in complex and real samples is the high demand of the (POF) chemical sensors reported in the literature and developed in laboratories.

The major conclusion is that POF chemical sensing is possible using simple and low-cost methods, and promising results can be achieved with further studies. Nevertheless, the characteristics of the selective layer are fundamental to achieve good and reliable results. A synergy is needed between the POF sensing technology and other areas of knowledge due to the vast interdisciplinary knowledge that is needed in sensor's development.

Chapter 6 Conclusions and future developments

6.1 Major conclusions

The main objective of this work was the development of intensity based POF sensors for water quality assessment, including detection of refractive index (RI) variations and quantification of contaminants.

POF sensors were developed using simple and low-cost procedures, such as chemical etching with solutions of acetone and distilled water and/or polishing using sandpapers with different grain sizes. Two POF based platforms were presented: D-Shape and straight based configurations. The principle of operation was based on the variation of the transmitted light through the modified section of the fibre due to RI variations of the liquid being monitored. A portable optical setup was used, which allows in-site and remote sensing. The low-cost sensing system allows real time monitoring through Bluetooth technology and the data is saved through a LabVIEW application, which can be further analysed. The intensity based detection system incorporated a reference POF allowing for a self-referenced signal, avoiding small source fluctuations. The stability of the transmitted signal was verified, as well as the reproducibility on the sensor's responses and signal recovery with washing procedures with distilled water.

The studies described in the Chapter 3 allowed to better understand the complexity that is inherent to MIPs development and the grafting of an MIP to POF's surface.

Immersion of unclad DB-1000 PMMA POFs in a solution of ethanol in water (30%) at 57°C causes solvent adsorption leading to the increase of mass and thickness and the appearance of cracks. These procedures do not increase fibre's sensitivity to external medium (RI variation) although evident damage of the fibre occurs.

Grafted polymerized fibres (NJ-MIP, Chapter 3) showed that the polymerization process also causes damage to the fibre's morphology, increasing the light loss, but simultaneously enhancing the sensitivity to external medium. At the same time, fibres polymerized for increased time did not reveal higher responses, on the contrary, as if the polymer growth diminished the fibre's sensitivity to external medium variations.

MIP-POFs obtained with the grafting polymerization did not reveal high sensitivity to the template analyte. Sample NJ2-MIP, polymerized for 5h, showed a sensitivity of around 0.05 a.u.M⁻¹ to ammonium anion (template analyte), with a maximum response of 2.8% at 0.6 M. Some selectivity towards ammonium ion was observed when mixed solutions of the different analytes were used. At the same time, increased response was obtained for two interferents (D-(+)-glucose and sodium chloride) in the individual solutions. Furthermore, POF-MIP NJ2 displayed response in the solutions of sucrose with refractive index varying from 1.33 to 1.41 with high sensitivity (6 – 14 au.RIU⁻¹) and a resolution below 5×10⁻⁴ RIU. No saturation was observed in these experimental conditions.

These results highlighted the need for further development of optical platforms with characteristics suitable for chemical sensing namely high sensitivity to the external medium refractive index and low resolution value. Furthermore, optimization of the sensing layer composition and deposition methods is necessary to ensure sensitivity, selectivity, detection limit and reproducibility required for the practical applications of sensors. Fine-tuning of both parts, optical platform and sensing layer is important to warrant desired sensor performance.

The work focused on the development and optimization of the POF platforms and study of their feasibility for chemical sensing.

The optimization of the sensing capabilities of the POF platforms to RI variation was performed by adjustment of the sensing region roughness and length.

Generally, straight modified POF sensors polished with a sandpaper of 5 μm grit size or higher showed lower sensitivity ($1.9 - 7.1 \text{ au.RIU}^{-1}$) in comparison with D-shaped POF sensors ($1.2 - 10.4 \text{ au.RIU}^{-1}$), although with lower resolution values ($< 5.25 \times 10^{-4} \text{ RIU}$ instead of $< 5.37 \times 10^{-3} \text{ RIU}$, dependent on external RI).

Chemical detection was performed. POFs with a D-shaped configuration combined with a previous validated MIP allowed the detection of PFOA/PFO⁻ in aqueous solutions and a LOD of 0.20 – 0.28 ppb was obtained. Indirect sensing of PFOA concentration was performed by the RI variations that occurred on the MIP layer due to the specific interaction between the recognition sites and the analyte. Although still higher than the LOD obtained with a D-shaped SPR-POF-MIP sensor using the same MIP (0.13 – 0.15 ppb) (Nunzio Cennamo, D'Agostino, *et al.*, 2018), the obtained results validate the use of POF-MIPs as low-cost sensing platforms for chemical detection. The obtained LOD is the same order of magnitude as the maximum value proposed for individual PFASs (0.1 ppb) and lower than the maximum value proposed to total PFASs (0.5 ppb) (European Commission, 2018).

Furthermore, preliminary assessment of the modified straight POFs coated with proteins for sensing layer development was performed. The success of the coating was verified with naked eye using a binding-specific dye (Coomassie Blue R250). Increasing surface roughness allowed to increase protein immobilization on the fibre's surface probably due to the increase on surface area (Tsougeni *et al.*, 2010) combined with the enhancement on light interaction.

Using bio-layers for chemical detection has some drawbacks due to instability of molecules such as proteins, which denaturise easily. As a result, POF biosensors should be stored in cold and time of life can therefore be a problem.

The obtained results show a promising future for the development of low-cost POF chemical sensors and biosensors, as different layers can be coated on POF's surface allowing for the detection of different analytes/contaminants.

The configuration of the D-shaped POF platform allowed easy deposition of an MIP by spin coating and thermal polymerization. On the other hand, straight modified POFs allowed for lower sensing resolution although successful immobilization of the layer on the POF's surface must be addressed in more detail.

6.2 Future developments

Possibility of POF chemical sensing using simple and low-cost methods was demonstrated, and very promising results were obtained. Sensing layer characteristics are fundamental to achieve good and reliable results. A synergy is needed between POF sensing technology and other areas of knowledge due to the vast interdisciplinary knowledge that is needed in sensor's development.

Preparation procedures of the POF sensors shall be improved, in particular polishing steps allowing to obtain required surface morphology of the sensing region and defined interface between the sensing region and the unpolished POF. Ideally, only one polishing film should be used implemented in an automated setup in order to improve manufacturing reproducibility. In case of straight configurations, a mechanical polishing setup which allows the rotation of the POF with controlled speed while polishing with sandpapers of known grit size can be developed. In D-shaped configurations, the planar support to which the POFs are embedded should be optimized in order to prevent light losses, interface clad-unclad polished region, that do not contribute to sensing capabilities. One possibility is to create a very smooth macro bending in the limits of the sensing region making the unpolished POF enter the planar support, preventing its polishing. In that case, the D-shaped region could be easier to define and to limit the sensing region.

MIPs are complex sensitive layers which require time consuming optimization. Cooperation with research teams with experience of MIP development is of interest for the development of POF-MIP chemical sensors. The lack of MIP regeneration (complete extraction of the analyte) suggests that POF-MIP sensors can be useful for on/off applications instead of continuous monitoring of water quality. Furthermore, the integration of fluorescent dyes in the polymer matrix or use fluorescent monomers can be a good possibility for an easy and visual on/off possibility.

Deposition of modified selective proteins is a promising direction for future biosensors development, as was demonstrated by the successful immobilization of proteins on POF's surface. POF biosensors revealed some possible drawbacks in terms of storage, operating temperature and time of life.

Further studies may allow to overcome the inherent difficulties and develop new sensing configurations for reliable, fast, simple, low cost, intensity based POF chemicals sensors for contaminants detection in water.

References

- Ahmad, O. S. *et al.* (2018) 'Molecularly Imprinted Polymers in Electrochemical and Optical Sensors', *Trends in Biotechnology*. Elsevier Ltd, pp. 1–16. doi: 10.1016/j.tibtech.2018.08.009.
- Aitkulov, A. *et al.* (2018) 'All-POF Chemical H₂S Sensor Designed for Smartphone Operation', in *2018 IEEE SENSORS*. IEEE, pp. 1–4. doi: 10.1109/ICSENS.2018.8630301.
- Aitkulov, A. and Tosi, D. (2019) 'Optical Fiber Sensor Based on Plastic Optical Fiber and Smartphone for Measurement of the Breathing Rate', *IEEE Sensors Journal*. IEEE, 19(9), pp. 3282–3287. doi: 10.1109/JSEN.2019.2894834.
- Al-Qazwini, Y. *et al.* (2016) 'Refractive index sensor based on SPR in symmetrically etched plastic optical fibers', *Sensors and Actuators A: Physical*, 246, pp. 163–169. doi: 10.1016/j.sna.2016.04.064.
- Ali, U., Karim, K. J. B. A. and Buang, N. A. (2015) 'A Review of the Properties and Applications of Poly (Methyl Methacrylate) (PMMA)', *Polymer Reviews*, 55(4), pp. 678–705. doi: 10.1080/15583724.2015.1031377.
- Alvarado-Gómez, A. L. *et al.* (2015) 'A chronoamperometric screen printed carbon biosensor based on alkaline phosphatase inhibition for W(IV) determination in water, using 2-phospho-L-ascorbic acid trisodium salt as a substrate', *Sensors (Switzerland)*, 15(2), pp. 2232–2243. doi: 10.3390/s150202232.
- Anderson, G. P. *et al.* (1997) 'Effectiveness of protein A for antibody immobilization for a fiber optic biosensor', *Biosensors and Bioelectronics*, 12(4), pp. 329–336. doi: 10.1016/S0956-5663(96)00074-7.
- Angelini, E. *et al.* (2010) 'Plasma modified POF sensors for in situ environmental monitoring of museum indoor environments', *Applied Physics A*. Springer-Verlag, 100(3), pp. 975–980. doi: 10.1007/s00339-010-5691-3.
- Arcas, A. *et al.* (2018) 'Surface Plasmon Resonance and Bending Loss-Based U-Shaped Plastic Optical Fiber Biosensors', *Sensors*. Multidisciplinary Digital Publishing Institute, 18(2), p. 648. doi: 10.3390/s18020648.
- Asahi Kasei (2001) *High-Performance Plastic Optical Fiber LUMINOUS POF*. Available at: <https://www.promelec.ru/UPLOAD/fck/file/Asahi.pdf> (Accessed: 16 January 2020).
- Asahi Kasei (2013) *DB-1000 Asahi Optical Fiber*. Available at: <https://i-fiberoptics.com/fiber-detail-asahi.php?id=3644&sum=168> (Accessed: 15 October 2019).
- Asher, S. A. *et al.* (1998) 'Mesoscopically periodic photonic-crystal materials for linear and nonlinear optics and chemical sensing', *MRS Bulletin*, 23(10), pp. 44–50. doi: 10.1557/S0883769400029596.
- Asher, S. A. and Holtz, J. H. (1997) 'Polymerized colloidal crystal hydrogel film as intelligent chemical sensing materials', *Nature*, 389(6653), pp. 829–832. doi: 10.1038/39834.
- Axelsson, H. *et al.* (1995) 'Measurement of Aromatic Hydrocarbons with the DOAS Technique', *Applied Spectroscopy*, 49(9), pp. 1254–1260. doi: 10.1366/0003702953965254.
- Azkune, M. *et al.* (2018) 'U-Shaped and Surface Functionalized Polymer Optical Fiber Probe for Glucose Detection', *Sensors*, 18(34). doi: 10.3390/s18010034.
- Baldini, F. *et al.* (eds) (2006) *Optical Chemical Sensors (Proceedings of ASCOS 2014), Series II: Mathematics, Physics and Chemistry - Vol 224*. Springer & NATO Public Diplomacy Division. doi: 10.1007/1-4020-4611-1.
- Barringer, A. R. and Davies, J. H. (1977) 'Satellite monitoring of atmospheric cases', *J.BRIT.INTERPLANETARY SOC.*, 30(5), pp. 178–183.
- Beres, C. *et al.* (2011) 'Tapered plastic optical fiber-based biosensor - Tests and application', *Biosensors and Bioelectronics*. Elsevier B.V., 30, pp. 328–332. doi: 10.1016/j.bios.2011.09.024.
- Bhowmik, K. and Peng, G.-D. (2019) 'Polymer Optical Fibers', in *Handbook of Optical Fibers*. Springer Nature Singapore Pte Ltd., pp. 1–51. doi: 10.1007/978-981-10-1477-2_38-1.

References

- Bilro, L., Alberto, N., *et al.* (2010) 'A simple and low-cost cure monitoring system based on a side-polished plastic optical fibre', *Measurement Science and Technology*, 21(11), p. 117001. doi: 10.1088/0957-0233/21/11/117001.
- Bilro, L., Prats, S. A., *et al.* (2010) 'Design and performance assessment of a plastic optical fibre-based sensor for measuring water turbidity', *Measurement Science and Technology*, 21(10), p. 107001. doi: 10.1088/0957-0233/21/10/107001.
- Bilro, L., Oliveira, J. G., *et al.* (2011) 'A reliable low-cost wireless and wearable gait monitoring system based on a plastic optical fibre sensor', *Measurement Science and Technology*. IOP Publishing, 22(4), p. 045801. doi: 10.1088/0957-0233/22/4/045801.
- Bilro, Lúcia *et al.* (2011) 'Analytical Analysis of Side-Polished Plastic Optical Fiber as Curvature and Refractive Index Sensor', *Journal of Lightwave Technology*, 29(6), pp. 864–870. doi: 10.1109/JLT.2011.2105462.
- Bilro, L. (2011) *Metrologia óptica com fibra polimérica*. University of Aveiro. Available at: <http://hdl.handle.net/10773/3611>.
- Bilro, L., Alberto, N., *et al.* (2011) 'Side-polished plastic optical fibre as refractive index, cure and viscosity sensor', in Costa, M. F. (ed.). International Society for Optics and Photonics, p. 800142. doi: 10.1117/12.892099.
- Bilro, L. *et al.* (2012) 'Optical sensors based on plastic fibers.', *Sensors (Basel, Switzerland)*, 12(9), pp. 12184–207. doi: 10.3390/s120912184.
- Bilro, L. *et al.* (2013) 'TURBIDITY MEASURING SENSOR AND METHOD'.
- Binu, S. *et al.* (2009) 'Fibre optic glucose sensor', *Materials Science and Engineering: C*. Elsevier B.V., 29(1), pp. 183–186. doi: 10.1016/j.msec.2008.06.007.
- Biran, I., Yu, X. and Walt, D. R. (2008) 'Optrode-based fiber optic biosensors (bio-optrode)', in Ligler, F. S. and Taitt, C. R. (eds) *Optical Biosensors: Today and Tomorrow*. 2nd editio. Elsevier B.V., pp. 3–82. doi: 10.1016/B978-044453125-4.50003-6.
- Bolt, A. M. and Mann, K. K. (2016) 'Tungsten: an Emerging Toxicant, Alone or in Combination', *Current Environmental Health Reports*. Current Environmental Health Reports, 3, pp. 405–415. doi: 10.1007/s40572-016-0106-z.
- Boogert, F. J. *et al.* (2013) 'Assessing the potential of a newly-developed turbidity sensor for estimating sediment yields from recently burnt catchments', *Flamma*, 4(3), pp. 139–141.
- Bundalo, I.-L. *et al.* (2016) 'All-plastic fiber-based pressure sensor', *Applied Optics*, 55(4), p. 811. doi: 10.1364/AO.55.000811.
- Buurman, E. T. *et al.* (1989) 'Replacement of potassium ions by ammonium ions in different micro-organisms grown in potassium-limited chemostat culture', *Archives of microbiology*, 152(1), pp. 58–63. doi: 10.1007/BF00447012.
- Camli, S. T. *et al.* (2010) 'Fine-tuning of functional poly(methylmethacrylate) nanoparticle size at the sub-100nm scale using surfactant-free emulsion polymerization', *Colloids and Surfaces A: Physicochemical and Engineering Aspects*, 366(1–3), pp. 141–146. doi: 10.1016/j.colsurfa.2010.05.037.
- Cao-Paz, A. M. *et al.* (2010) 'A multi-point sensor based on optical fiber for the measurement of electrolyte density in lead-acid batteries.', *Sensors (Basel, Switzerland)*. Multidisciplinary Digital Publishing Institute (MDPI), 10(4), pp. 2587–608. doi: 10.3390/s100402587.
- Carrasco, S. *et al.* (2015) 'Fiber-Optic Array Using Molecularly Imprinted Microspheres for Antibiotic Analysis', *Chem. Science*, 6(5), pp. 3139–3147. doi: 10.1039/C5SC00115C.
- Caucheteur, C., Guo, T. and Albert, J. (2015) 'Review of plasmonic fiber optic biochemical sensors: improving the limit of detection', *Analytical and Bioanalytical Chemistry*, pp. 3883–3897. doi: 10.1007/s00216-014-8411-6.
- Cennamo, N. *et al.* (2011) 'Low cost sensors based on SPR in a plastic optical fiber for biosensor implementation', *Sensors (Basel, Switzerland)*, 11(12), pp. 11752–60. doi: 10.3390/s111211752.
- Cennamo, Nunzio *et al.* (2013) 'An innovative plastic optical fiber-based biosensor for new

bio/applications. The case of celiac disease', *Sensors and Actuators B*, 176, pp. 1008–1014. doi: 10.1016/j.snb.2012.10.055.

Cennamo, N. *et al.* (2013) 'Sensors based on surface plasmon resonance in a plastic optical fiber for the detection of trinitrotoluene', *Sensors and Actuators B: Chemical*. Elsevier B.V., 188, pp. 221–226. doi: 10.1016/j.snb.2013.07.005.

Cennamo, N. *et al.* (2014) 'High selectivity and sensitivity sensor based on MIP and SPR in tapered plastic optical fibers for the detection of l-nicotine', *Sensors and Actuators, B: Chemical*. Elsevier B.V., 191, pp. 529–536. doi: 10.1016/j.snb.2013.10.067.

Cennamo, Nunzio, Pesavento, M., *et al.* (2015) 'An easy way to realize SPR aptasensor: A multimode plastic optical fiber platform for cancer biomarkers detection', *Talanta*. Elsevier, 140, pp. 88–95. doi: 10.1016/j.talanta.2015.03.025.

Cennamo, Nunzio, De Maria, L., *et al.* (2015) 'Monitoring of Low Levels of Furfural in Power Transformer Oil with a Sensor System Based on a POF-MIP Platform', *Sensors*. Multidisciplinary Digital Publishing Institute, 15(4), pp. 8499–8511. doi: 10.3390/s150408499.

Cennamo, N. *et al.* (2015) 'Sensitive detection of 2,4,6-trinitrotoluene by tridimensional monitoring of molecularly imprinted polymer with optical fiber and five-branched gold nanostars', *Sensors and Actuators, B: Chemical*. Elsevier B.V., 208, pp. 291–298. doi: 10.1016/j.snb.2014.10.079.

Cennamo, N. *et al.* (2016) 'Markers Detection in Transformer Oil by Plasmonic Chemical Sensor System Based on POF and MIPs', *IEEE Sensors Journal*, 16(21), pp. 7663–7670. doi: 10.1109/JSEN.2016.2603168.

Cennamo, Nunzio, Pesavento, M., *et al.* (2017) 'Comparison of different photoresist buffer layers in SPR sensors based on D-shaped POF and gold film', in *25th International Conference on Plastic Optical Fibers (POF 2016), Proc. of SPIE Vol. 10323*, p. 103234F. doi: 10.1117/12.2265603.

Cennamo, N. *et al.* (2017) 'Intensity-based plastic optical fiber sensor with molecularly imprinted polymer sensitive layer', *Sensors and Actuators B: Chemical*. Elsevier B.V., 241, pp. 534–540. doi: 10.1016/j.snb.2016.10.104.

Cennamo, Nunzio, Maria, L. De, *et al.* (2017) 'SPR Chemosensors Based on D-Shaped POFs and MIPs: Investigation on Optimal Thickness of the Buffer Layer', *Proceedings*. Multidisciplinary Digital Publishing Institute, 1(8), p. 816. doi: 10.3390/proceedings1080816.

Cennamo, Nunzio, Zeni, L., Tortora, P., *et al.* (2018) 'A High Sensitivity Biosensor to detect the presence of perfluorinated compounds in environment', *Talanta*. Elsevier B.V., 178(October 2017), pp. 955–961. doi: 10.1016/j.talanta.2017.10.034.

Cennamo, Nunzio, D'Agostino, G., *et al.* (2018) 'A Molecularly Imprinted Polymer on a Plasmonic Plastic Optical Fiber to Detect Perfluorinated Compounds in Water', *Sensors*. Multidisciplinary Digital Publishing Institute, 18(6), p. 1836. doi: 10.3390/s18061836.

Cennamo, Nunzio, Zeni, L., Andò, B., *et al.* (2018) 'A novel chemical optical sensor based on molecularly imprinted polymer, optical fibers and inkjet printing technology', in *2018 IEEE International Instrumentation and Measurement Technology Conference (I2MTC)*. IEEE, pp. 1–5. doi: 10.1109/I2MTC.2018.8409619.

Cennamo, N. *et al.* (2018) 'A simple and low-cost optical fiber intensity-based configuration for perfluorinated compounds in water solution', *Sensors (Switzerland)*, 18(9). doi: 10.3390/s18093009.

Cennamo, N., Zeni, L., *et al.* (2019) 'Detection of naphthalene in sea-water by a label-free plasmonic optical fiber biosensor', *Talanta*. Elsevier B.V., 194, pp. 289–297. doi: 10.1016/j.talanta.2018.10.051.

Cennamo, N., Pesavento, M., *et al.* (2019) 'Polishing Process Analysis for Surface Plasmon Resonance Sensors in D-Shaped Plastic Optical Fibers', in B. Andò *et al.* (eds.) (ed.) *Sensors. CNS 2018. Lecture Notes in Electrical Engineering, vol 539*, Springer, Cham. Springer, Cham. doi: 10.1007/978-3-030-04324-7_32.

References

- Cennamo, N., Mattiello, F. and Zeni, L. (2019) 'A Novel Intensity-Based Sensor Platform for Refractive Index Sensing', in Andò B. et al. (eds) *Sensors. CNS 2018. Lecture Notes in Electrical Engineering*. Springer, Cham, pp. 269–273. doi: 10.1007/978-3-030-04324-7_35.
- Cennamo, N. and Zeni, L. (2014) 'Bio and Chemical Sensors Based on Surface Plasmon Resonance in a Plastic Optical Fiber', in Yasin, M. (ed.) *Optical Sensors - New Developments and Practical Applications*. IntechOpen, pp. 119–140. doi: 10.5772/57148.
- Chang, Y. H. et al. (1996) 'Detection of Protein A Produced by Staphylococcus aureus with a Fiber-optic-based Biosensor', *Bioscience, Biotechnology, and Biochemistry*, 60(10), pp. 1571–1574. doi: 10.1271/bbb.60.1571.
- Chen, L. et al. (2016) 'Molecular imprinting: perspectives and applications', *Chem. Soc. Rev.* Royal Society of Chemistry, 45(8), pp. 2137–2211. doi: 10.1039/C6CS00061D.
- Chen, L. D. et al. (2013) 'Fluorous Membrane Ion-Selective Electrodes for Perfluorinated Surfactants: Trace-Level Detection and in Situ Monitoring of Adsorption', *Analytical Chemistry*, 85(15), pp. 7471–7477. doi: 10.1021/ac401424j.
- Chen, L., Xu, S. and Li, J. (2011) 'Recent advances in molecular imprinting technology: current status, challenges and highlighted applications', *Chem. Soc. Rev.*, 40(5), pp. 2922–2942. doi: 10.1039/C0CS00084A.
- Chu, F. et al. (2009) 'Characterization of a dissolved oxygen sensor made of plastic optical fiber coated with ruthenium-incorporated solgel', *Applied Optics*. Optical Society of America, 48(2), p. 338. doi: 10.1364/AO.48.000338.
- Chu, F. and Yang, J. (2012) 'Coil-shaped plastic optical fiber sensor heads for fluorescence quenching based TNT sensing', *Sensors and Actuators A: Physical*, 175, pp. 43–46. doi: 10.1016/j.sna.2011.12.028.
- Cieplak, M. and Kutner, W. (2016) 'Artificial Biosensors: How Can Molecular Imprinting Mimic Biorecognition?', *Trends in Biotechnology*, 34(11), pp. 922–941. doi: 10.1016/j.tibtech.2016.05.011.
- Corres, J. M. et al. (2015) 'Analysis of lossy mode resonances on thin-film coated cladding removed plastic fiber', *Optics Letters*, 40(21), pp. 4867–4870. doi: 10.1364/OL.40.004867.
- Corsini, E. et al. (2012) 'In vitro characterization of the immunotoxic potential of several perfluorinated compounds (PFCs)', *Toxicology and Applied Pharmacology*. Elsevier Inc., 258(2), pp. 248–255. doi: 10.1016/j.taap.2011.11.004.
- Crawford, C. B. and Quinn, B. (2017) 'The interactions of microplastics and chemical pollutants', *Microplastic Pollutants*. Elsevier, pp. 131–157. doi: 10.1016/B978-0-12-809406-8.00006-2.
- Dehghani, S. et al. (2018) 'Aptamer-based biosensors and nanosensors for the detection of vascular endothelial growth factor (VEGF): A review', *Biosensors and Bioelectronics*, 110, pp. 23–37. doi: 10.1016/j.bios.2018.03.037.
- Deng, S. et al. (2016) 'A low-cost, portable optical sensing system with wireless communication compatible of real-time and remote detection of dissolved ammonia', *Photonic Sensors*, 6(2), pp. 107–114. doi: 10.1007/s13320-016-0291-2.
- Derazshamshir, A. and Yavuz, H. (2017) 'Molecular Imprinting of Macromolecules for sensing applications'. doi: 10.3390/s17040898.
- Dewitt, J. C. et al. (2012) 'Immunotoxicity of Perfluorinated Compounds: Recent Developments', *Toxicologic Pathology*, 40(2), pp. 300–311. doi: 10.1177/0192623311428473.
- Divagar, M. et al. (2018) 'Graphene oxide coated U-bent plastic optical fiber based chemical sensor for organic solvents', *Sensors and Actuators, B: Chemical*. Elsevier B.V., 262, pp. 1006–1012. doi: 10.1016/j.snb.2018.02.059.
- Duarte, D. A. P., Nogueira, R. N. and Bilro, L. (2019) 'Optical Fiber Sensing Principles', in Werneck, M. M. and Allil, R. C. S. B. (eds) *Plastic Optical Fiber Sensors: Science, Technology and Applications*. Boca Raton: Taylor & Francis, pp. 67–92. doi: 10.1201/b22357.
- Elias, S. N., Arsad, N. and Abubakar, S. (2015) 'Nitrite detection using plastic optical fiber (POF); an early stage investigation towards the development of oral cancer sensor using POF', *Optik -*

- International Journal for Light and Electron Optics*. Elsevier GmbH., 126(21), pp. 2908–2911. doi: 10.1016/j.ijleo.2015.07.038.
- Elosua, C. *et al.* (2017) 'Micro and Nanostructured Materials for the Development of Optical Fibre Sensors', *Sensors*, 17(10), p. 2312. doi: 10.3390/s17102312.
- Emiliyanov, G. *et al.* (2013) 'Selective Serial Multi-Antibody Biosensing with TOPAS Microstructured Polymer Optical Fibers', *Sensors*. Multidisciplinary Digital Publishing Institute, 13(3), pp. 3242–3251. doi: 10.3390/s130303242.
- Emslie, C. (1988) 'Review Polymer optical fibres', *Journal of Materials Science*, 23, pp. 2281–2293.
- Eriksen, K. T. *et al.* (2011) 'Determinants of Plasma PFOA and PFOS Levels Among 652 Danish Men', *Environmental Science & Technology*. American Chemical Society, 45(19), pp. 8137–8143. doi: 10.1021/es100626h.
- European Commission (2010) *Commission Recommendation of on the Monitoring of Perfluoroalkylated Substances in Food, Official journal of the European Union*. Available at: <http://eur-lex.europa.eu/LexUriServ/LexUriServ.do?uri=OJ:L:2010:068:0022:0023:EN:PDF>.
- European Commission (2017) *COMMISSION REGULATION (EU) 2017/1000, Official Journal of the European Union*.
- European Commission (2018) *Proposal for a DIRECTIVE OF THE EUROPEAN PARLIAMENT AND OF THE COUNCIL on the quality of water intended for human consumption (recast)*. Available at: <http://www.right2water.eu/>. (Accessed: 8 July 2019).
- European Parliament (2019) *Petition No 0496/2018 by G.P. (Italian) on the proposal for a directive of the European Parliament and the Council on the quality of water intended for human consumption*. Available at: http://www.euro.who.int/__data/assets/pdf_file/0018/340704/FINAL_pfas-report-20170530-h1200.pdf (Accessed: 8 July 2019).
- Faiz, F. *et al.* (2019) 'Perfluorooctanoic (PFOA) Acid Detection in Aqueous Medium using Polyvinylidene Fluoride (PVDF) Thin Film on Optical Fiber Endface', in. The Optical Society, p. EW4A.3. doi: 10.1364/es.2019.ew4a.3.
- Feng, D.-J. *et al.* (2014) 'D-Shaped Plastic Optical Fiber Sensor for Testing Refractive Index', *IEEE Sensors*, 14(5), pp. 1673–1676. doi: 10.1109/JSEN.2014.2301911.
- Feng, D. *et al.* (2014) 'Refractive index sensor based on plastic optical fiber with tapered structure', *Applied optics*, 53(10), pp. 2007–2011. doi: 10.1364/AO.53.002007.
- Ferreira, M. F. S. *et al.* (2017) 'Fabry-Perot cavity based on polymer FBG as refractive index sensor', *Optics Communications*. Elsevier B.V., 394(November 2016), pp. 37–40. doi: 10.1016/j.optcom.2017.03.011.
- Ferreira, R. X. *et al.* (2013) 'Advanced Sensor and Method to Measure Turbidity', in *RIAO/OPTILAS 2013*. Porto.
- Fixe, F. *et al.* (2004) 'Functionalization of poly(methyl methacrylate) (PMMA) as a substrate for DNA microarrays.', *Nucleic Acids Research*, 32(1), pp. 1–8. doi: 10.1093/nar/gng157.
- Foguel, M. V. *et al.* (2015) 'A molecularly imprinted polymer-based evanescent wave fiber optic sensor for the detection of basic red 9 dye', *Sensors and Actuators, B: Chemical*. Elsevier B.V., 218, pp. 222–228. doi: 10.1016/j.snb.2015.05.007.
- Foo, K. Y. and Hameed, B. H. (2010) 'Insights into the modeling of adsorption isotherm systems', *Chemical Engineering Journal*. Elsevier, 156(1), pp. 2–10. doi: 10.1016/J.CEJ.2009.09.013.
- Fu, J. *et al.* (2015) 'Current status and challenges of ion imprinting', *Journal of Materials Chemistry A*. Royal Society of Chemistry, 3(26), pp. 13598–13627. doi: 10.1039/C5TA02421H.
- Fujii, Y. *et al.* (2007) 'Development of new optical fiber toluene sensor', in Wang, A., Zhang, Y., and Ishii, Y. (eds). *International Society for Optics and Photonics*, p. 68291Z. doi: 10.1117/12.758019.
- Gámez, F. *et al.* (2011) 'Vibrational study of isolated 18-crown-6 ether complexes with alkaline-

References

earth metal cations', *International Journal of Mass Spectrometry*, 308, pp. 217–224. doi: 10.1016/j.ijms.2011.06.015.

Garcia-Ivars, J. *et al.* (2017) 'Nanofiltration as tertiary treatment method for removing trace pharmaceutically active compounds in wastewater from wastewater treatment plants', *Water Research*. Elsevier Ltd, 125, pp. 360–373. doi: 10.1016/j.watres.2017.08.070.

Gholizadeh, M. H., Melesse, A. M. and Reddi, L. (2016) 'A Comprehensive Review on Water Quality Parameters Estimation Using Remote Sensing Techniques.', *Sensors (Basel, Switzerland)*, 16(8), p. 1298. doi: 10.3390/s16081298.

Gong, J. *et al.* (2015) 'A highly sensitive photoelectrochemical detection of perfluorooctanic acid with molecularly imprinted polymer-functionalized nanoarchitected hybrid of AgI–BiOI composite', *Biosensors and Bioelectronics*. Elsevier, 73, pp. 256–263. doi: 10.1016/J.BIOS.2015.06.008.

Gong, W. *et al.* (2019) 'Experimental and theoretical investigation for surface plasmon resonance biosensor based on graphene/Au film/D-POF', *Optics Express*, 27(3), pp. 3483–3495. doi: 10.1364/oe.27.003483.

Gowri, A. *et al.* (2019) 'U-bent plastic optical fiber probes as refractive index based fat sensor for milk quality monitoring', *Optical Fiber Technology*, 47, pp. 15–20. doi: 10.1016/j.yofte.2018.11.019.

Gowri, A. and Sai, V. V. R. (2016) 'Development of LSPR based U-bent plastic optical fiber sensors', *Sensors and Actuators, B: Chemical*. Elsevier B.V., 230, pp. 536–543. doi: 10.1016/j.snb.2016.02.074.

Grassini, S. *et al.* (2015) 'Design and Deployment of Low-Cost Plastic Optical Fiber Sensors for Gas Monitoring', *Sensors*, 15, pp. 485–498. doi: 10.3390/s150100485.

Gravina, R., Testa, G. and Bernini, R. (2009) 'Perfluorinated Plastic Optical Fiber Tapers for Evanescent', pp. 10423–10433. doi: 10.3390/s91210423.

Haupt, K. and Mosbach, K. (2000) 'Molecularly imprinted polymers and their use in biomimetic sensors.', *Chem. Rev.*, 100(7), pp. 2495–2504. doi: 10.1021/cr990099w.

Henry, O. Y. F., Cullen, D. C. and Piletsky, S. A. (2005) 'Optical interrogation of molecularly imprinted polymers and development of MIP sensors: A review', *Analytical and Bioanalytical Chemistry*, 382(4), pp. 947–956. doi: 10.1007/s00216-005-3255-8.

Hill, A. V. (1910) 'The possible effects of the aggregation of the molecules of haemoglobin on its dissociation curves', *The Journal of Physiology*, 40, pp. iv–vii.

Homola, J., Koudela, I. and Yee, S. S. (1999) 'Surface plasmon resonance sensors based on diffraction gratings and prism couplers: sensitivity comparison', *Sensors and Actuators, B: Chemical*, 54(1), pp. 16–24. doi: 10.1016/S0925-4005(98)00322-0.

Hu, X. *et al.* (2014) 'Tilted Bragg gratings in step-index polymer optical fiber', *Optics Letters*. Optical Society of America, 39(24), p. 6835. doi: 10.1364/OL.39.006835.

Huset, C. A. *et al.* (2008) 'Occurrence and Mass Flows of Fluorochemicals in the Glatt Valley Watershed, Switzerland', *Environmental Science & Technology*, 42(17), pp. 6369–6377. doi: 10.1021/es703062f.

Ishigure, T. *et al.* (2002) 'High-Bandwidth Graded-Index Polymer Optical Fiber With High-Temperature Stability', *JOURNAL OF LIGHTWAVE TECHNOLOGY*, 20(8), p. 1443. doi: 10.1109/JLT.2002.800798.

Jalal, H. A., Yu, J. and Nnanna, A. G. A. (2012) 'Fabrication and calibration of Oxazine-based optic fiber sensor for detection of ammonia in water', *Applied Optics*, 51(17), pp. 3768–3775. doi: 10.1364/AO.51.003768.

Jasim, A. A. *et al.* (2014) 'Refractive index and strain sensing using inline Mach–Zehnder interferometer comprising perfluorinated graded-index plastic optical fiber', *Sensors and Actuators A: Physical*. Elsevier B.V., 219, pp. 94–99. doi: 10.1016/j.sna.2014.07.018.

Jin, Y. and Granville, A. M. (2016) 'Polymer Fiber Optic Sensors – A Mini Review of their

- Synthesis and Applications', *Biosensors & bioelectronics*, 7(1). doi: 10.4172/2155-6210.1000194.
- Jing, N. *et al.* (2015) 'Refractive Index Sensing Based on a Side-Polished Macrobending Plastic Optical Fiber', *IEEE Sensors Journal*, 15(5), pp. 2898–2901. doi: 10.1109/JSEN.2014.2385308.
- Junttila, V. *et al.* (2019) 'PFASs in Finnish Rivers and Fish and the Loading of PFASs to the Baltic Sea', *Water*. Multidisciplinary Digital Publishing Institute, 11(4), p. 870. doi: 10.3390/w11040870.
- Kawa, T. *et al.* (2017) 'Temperature sensing based on multimodal interference in polymer optical fibers: Room-temperature sensitivity enhancement by annealing', *Japanese Journal of Applied Physics*, 56(7), p. 078002. doi: 10.7567/JJAP.56.078002.
- Khalaf, A. L. *et al.* (2016) 'Modified plastic optical fiber coated graphene/polyaniline nanocomposite for ammonia sensing', in *2016 IEEE 6th International Conference on Photonics (ICP)*. IEEE, pp. 1–3. doi: 10.1109/ICP.2016.7510030.
- Khalaf, A. L. *et al.* (2017) 'Room temperature ammonia sensor using side-polished optical fiber coated with graphene/polyaniline nanocomposite', *Optical Materials Express*, 7(6), p. 1858. doi: 10.1364/OME.7.001858.
- Kim, C. *et al.* (2016) 'Detection of organic compounds in water by an optical absorbance method', *Sensors*, 16(1), p. 61. doi: 10.3390/s16010061.
- Kim, J., Qian, W. and Al-Saigh, Z. Y. (2011) 'Measurements of water sorption enthalpy on polymer surfaces and its effect on protein adsorption', *Surface Science*, 605(3–4), pp. 419–423. doi: 10.1016/j.susc.2010.11.011.
- Kitazawa, M., Kreidl, J. F. and Steele, R. E. (eds) (1991) 'Plastic Optical Fibers (Conference Review)', in *Proceedings of SPIE*. The International Society for Optical Engineering.
- Koike, Y. and Koike, K. (2011) 'Progress in low-loss and high-bandwidth plastic optical fibers', *Journal of Polymer Science, Part B: Polymer Physics*, 49(1), pp. 2–17. doi: 10.1002/polb.22170.
- Korposh, S. *et al.* (2014) 'Selective vancomycin detection using optical fibre long period gratings functionalised with molecularly imprinted polymer nanoparticles.', *The Analyst*, 139(9), pp. 2229–36. doi: 10.1039/c3an02126b.
- Kratz, F. *et al.* (2015) 'Cleaning of biomaterial surfaces: Protein removal by different solvents', *Colloids and Surfaces B: Biointerfaces*, 128, pp. 28–35. doi: 10.1016/j.colsurfb.2015.02.016.
- Kulkarni, A. *et al.* (2010) 'Thin film-coated plastic optical fiber probe for aerosol chemical sensing applications', *Sensors and Actuators B: Chemical*, 150(1), pp. 154–159. doi: 10.1016/j.snb.2010.07.026.
- Kurganov, B. . *et al.* (2001) 'Criterion for Hill equation validity for description of biosensor calibration curves', *Analytica Chimica Acta*. Elsevier, 427(1), pp. 11–19. doi: 10.1016/S0003-2670(00)01167-3.
- Kurilić, S. M. *et al.* (2015) 'Assessment of typical natural processes and human activities' impact on the quality of drinking water', *Environmental Monitoring and Assessment*, 187(11). doi: 10.1007/s10661-015-4888-5.
- Langmuir, I. (1917) 'The constitution and fundamental properties of solids and liquids', *JACS*, 39, pp. 1848–1906.
- Langmuir, I. (1918) 'Adsorption of gases on plane surfaces of glass, mica and platinum', *Journal of the American Chemical Society*, 40(9), pp. 1361–1403.
- Le, T. D. H. *et al.* (2017) 'Contribution of waste water treatment plants to pesticide toxicity in agriculture catchments', *Ecotoxicology and Environmental Safety*. Elsevier Inc., 145, pp. 135–141. doi: 10.1016/j.ecoenv.2017.07.027.
- Leal-Junior, A., Frizera, A., Lee, H., Mizuno, Y., Nakamura, K., Leitão, C., *et al.* (2018) 'Design and characterization of a curvature sensor using fused polymer optical fibers', *Optics Letters*, 43(11), p. 2539. doi: 10.1364/ol.43.002539.
- Leal-Junior, A., Frizera, A., Lee, H., Mizuno, Y., Nakamura, K., Paixão, T., *et al.* (2018) 'Strain, temperature, moisture, and transverse force sensing using fused polymer optical fibers', *Optics Express*. Optical Society of America, 26(10), p. 12939. doi: 10.1364/OE.26.012939.

References

- Leal-Junior, A. G., Frizera, A., *et al.* (2018) 'Design considerations, analysis, and application of a low-cost, fully portable, wearable polymer optical fiber curvature sensor', *Applied Optics*, 57(24), p. 6927. doi: 10.1364/ao.57.006927.
- Leal-Junior, A. G., Theodosiou, A., *et al.* (2018) 'Polymer Optical Fiber Sensors Approaches for Insole Instrumentation', in Carrozza M., Micera S., P. J. (ed.) *Proceedings of the 4th International Symposium on Wearable Robotics, WeRob2018*. Pisa, Italy: Springer, Cham, pp. 470–474. doi: 10.1007/978-3-030-01887-0_91.
- Leal-Junior, A. G., Díaz, C. R., Marques, C., *et al.* (2019) '3D-printed POF insole: Development and applications of a low-cost, highly customizable device for plantar pressure and ground reaction forces monitoring', *Optics & Laser Technology*. Elsevier, 116, pp. 256–264. doi: 10.1016/J.OPTLASTEC.2019.03.035.
- Leal-Junior, A. G., Díaz, C. R., Leitão, C., *et al.* (2019) 'Polymer optical fiber-based sensor for simultaneous measurement of breath and heart rate under dynamic movements', *Optics & Laser Technology*. Elsevier, 109, pp. 429–436. doi: 10.1016/J.OPTLASTEC.2018.08.036.
- Leal-Junior, A. G., Frizera, A. and José Pontes, M. (2018) 'Sensitive zone parameters and curvature radius evaluation for polymer optical fiber curvature sensors', *Optics and Laser Technology*. Elsevier Ltd, 100, pp. 272–281. doi: 10.1016/j.optlastec.2017.10.006.
- Lednev, I. K., Hester, R. E. and Moore, J. N. (1997) 'Benzothiazolium styryl dyes containing a monoazacrown ether: Protonation and complexation with metal and ammonium cations in solution', *Journal of the Chemical Society, Faraday Transactions*, 93(8), pp. 1551–1558. doi: 10.1039/A607389A.
- Li, D. and Wang, L. (2010a) 'Cellulose acetate polymer film modified microstructured polymer optical fiber towards a nitrite optical probe', *Optics Communications*. North-Holland, 283(14), pp. 2841–2844. doi: 10.1016/J.OPTCOM.2010.04.005.
- Li, D. and Wang, L. (2010b) 'Fluorescence Hydrogen Peroxide Probe Based on a Microstructured Polymer Optical Fiber Modified with a Titanium Dioxide Film', *Applied Spectroscopy*. Society for Applied Spectroscopy, 64(5), pp. 514–519.
- Li, N. *et al.* (2017) 'Removal of antibiotic resistance genes from wastewater treatment plant effluent by coagulation', *Water Research*, 111, pp. 204–212. doi: 10.1016/j.watres.2017.01.010.
- Lieberman, R. A. (1993) 'Recent progress in intrinsic fiber-optic chemical sensing II', *Sensors and Actuators B: Chemical*. Elsevier, 11(1–3), pp. 43–55. doi: 10.1016/0925-4005(93)85237-5.
- Lindim, C., van Gils, J. and Cousins, I. T. (2016) 'Europe-wide estuarine export and surface water concentrations of PFOS and PFOA', *Water Research*. Pergamon, 103, pp. 124–132. doi: 10.1016/J.WATRES.2016.07.024.
- Link, A. J., Robison, K. and Church, G. M. (1997) 'Comparing the predicted and observed properties of proteins encoded in the genome of Escherichia coli K-12', *Electrophoresis*, 18, pp. 1259–1313.
- Liu, G. *et al.* (2015) 'Side-Hole Plastic Optical Fiber for Testing Liquid's Refractive Index', *IEEE Sensors Journal*. IEEE, 15(5), pp. 2902–2905. doi: 10.1109/JSEN.2014.2382294.
- Liu, G. and Feng, D. (2016) 'Evanescent wave analysis and experimental realization of refractive index sensor based on D-shaped plastic optical fiber', *Optik - International Journal for Light and Electron Optics*. Elsevier GmbH., 127(2), pp. 690–693. doi: 10.1016/j.ijleo.2015.10.129.
- Liu, Z., Nalluri, S. K. M. and Stoddart, J. F. (2017) 'Surveying macrocyclic chemistry: from flexible crown ethers to rigid cyclophanes', *Chemical Society Reviews*. Royal Society of Chemistry, 46(9), pp. 2459–2478. doi: 10.1039/C7CS00185A.
- Lopes, N. *et al.* (2015) 'Fiber optic sensor modified by grafting of the molecularly imprinted polymer for the detection of ammonium in aqueous media', *Scientific and Technical Journal of Information Technologies, Mechanics and Optics*, 15(4), pp. 568–577. doi: 10.17586/2226-1494-2015-15-4-568-577.
- Lopes, N. de J. C. (2014) *Sensor em fibra ótica para a análise do íão amônio na água*. University

of Aveiro. Available at: <http://hdl.handle.net/10773/13403>.

Lopes, R. N. *et al.* (2018) 'Plastic optical fiber immunosensor for fast detection of sulfate-reducing bacteria', *Measurement*. Elsevier, 125, pp. 377–385. doi: 10.1016/j.measurement.2018.04.088.

Lukosz, W. (1995) 'Integrated optical chemical and direct biochemical sensor', *Sensors and Actuators, B: Chemical*, 29, pp. 37–50. doi: 10.1016/0925-4005(95)01661-9.

Luo, D. *et al.* (2016) 'Concrete beam crack detection using tapered polymer optical fiber sensors', *Measurement*. Elsevier Ltd, 88, pp. 96–103. doi: 10.1016/j.measurement.2016.03.028.

Luo, Y. *et al.* (2017) 'Fabrication of Polymer Optical Fibre (POF) Gratings', *Sensors*. Multidisciplinary Digital Publishing Institute, 17(3), p. 511. doi: 10.3390/s17030511.

Ma, X. *et al.* (2011) 'Enhanced protein binding on femtosecond laser ablated poly(methyl methacrylate) surfaces', *Applied Physics Letters*, 98(17), p. 171101. doi: 10.1063/1.3583981.

Maciak, E., Sufa, P. and Stolarczyk, A. (2014) 'A low temperature operated NO₂ gas POF sensor based on conducting graft polymer', *Photonics Letters of Poland*, 6(4), pp. 124–126. doi: 10.4302/plp.2014.4.04.

Markos, C. *et al.* (2013) 'High-Tg TOPAS microstructured polymer optical fiber for fiber Bragg grating strain sensing at 110 degrees', *Optics Express*, 21(4), pp. 4758–4765. doi: 10.1364/OE.21.004758.

Memon, S. F. *et al.* (2018) 'Measurement of Ultralow Level Bioethanol Concentration for Production Using Evanescent Wave Based Optical Fiber Sensor', *IEEE Transactions on Instrumentation and Measurement*, 67(4), pp. 780–788. doi: 10.1109/TIM.2017.2761618.

Menzies, R. T. and Chahine, M. T. (1974) 'Remote atmospheric sensing with an airborne laser absorption spectrometer.', *Applied optics*, 13(12), pp. 2840–9. doi: 10.1364/AO.13.002840.

Merchant, D. F., Scully, P. J. and Schmitt, N. F. (1999) 'Chemical tapering of polymer optical fibre', *Sensors and Actuators A: Physical*, 76(1–3), pp. 365–371. doi: 10.1016/S0924-4247(99)00008-4.

Miller-Chou, B. a. and Koenig, J. L. (2003) 'A review of polymer dissolution', *Progress in Polymer Science (Oxford)*, 28, pp. 1223–1270. doi: 10.1016/S0079-6700(03)00045-5.

Min, R. *et al.* (2018) 'Fast Inscription of Long Period Gratings in Microstructured Polymer Optical Fibers', *IEEE Sensors Journal*, 18(5), pp. 1919–1923. doi: 10.1109/JSEN.2018.2791663.

Mitsubishi Chemical Co. (2000) *GHCP4001 Eska™ Premier Simplex High-Performance Plastic Optical Fiber Cable*. Available at: <https://i-fiberoptics.com/fiber-detail.php?id=51&sum=80> (Accessed: 15 October 2019).

Mizuno, Y. *et al.* (2017) 'Pilot demonstration of refractive index sensing using polymer optical fiber crushed with slotted screwdriver', *IEICE Electronics Express*, 14(21), pp. 1–7. doi: 10.1587/elex.14.20170962.

Moo, Y. C. *et al.* (2016) 'New development of optical fibre sensor for determination of nitrate and nitrite in water', *Optik - International Journal for Light and Electron Optics*. Elsevier GmbH., 127(3), pp. 1312–1319. doi: 10.1016/j.ijleo.2015.09.072.

Morey, W. W., Dunphy, J. R. and Meltz, G. (1991) 'Multiplexing fiber bragg grating sensors', *Fiber and Integrated Optics*, 10(4), pp. 351–360. doi: 10.1080/01468039108201715.

Mosbach, K. and Ramström, O. (1996) 'The Emerging Technique of Molecular Imprinting and Its Future Impact on Biotechnology', *Nature Biotechnology*. Nature Publishing Group, 14(2), pp. 163–170. doi: 10.1038/nbt0296-163.

Nagata, J. *et al.* (2007) 'Development of polymer optical waveguide-type alcohol sensor', in Wang, A., Zhang, Y., and Ishii, Y. (eds). *International Society for Optics and Photonics*, p. 682920. doi: 10.1117/12.758025.

Nnanna, A. A. and Jalal, A. H. (2012) 'Oxazine-based sensor for contaminant detection, fabrication method'. Available at: <http://www.freepatentsonline.com/20120288953.pdf> (Accessed: 25 October 2019).

References

- Nogueira, R. *et al.* (2015) 'New advances in polymer fiber Bragg gratings', *Optics & Laser Technology*, 78, Part A, pp. 104–109. doi: 10.1016/j.optlastec.2015.08.010.
- Octavia, S. and Lan, R. (2014) 'The Family Enterobacteriaceae', in *The Prokaryotes*. Berlin, Heidelberg: Springer Berlin Heidelberg, pp. 225–286. doi: 10.1007/978-3-642-38922-1_167.
- Oliveira, N. *et al.* (2016) 'Development and characterization of a low cost sediment concentration optical sensor', in *25th International Conference on Plastic Optical Fibers (POF 2016)*, p. PP30.
- Oliveira, R., Bilro, L., *et al.* (2016) 'Bragg Gratings Inscription in Highly Birefringent Microstructured POFs', *IEEE Photonics Technology Letters*, 28(6), pp. 621–624. doi: 10.1109/LPT.2015.2503241.
- Oliveira, R., Aristilde, S., *et al.* (2016) 'Intensity liquid level sensor based on multimode interference and fiber Bragg grating', *Measurement Science and Technology*, 27(12). doi: 10.1088/0957-0233/27/12/125104.
- Oliveira, R. *et al.* (2017) 'Multiparameter POF Sensing Based on Multimode Interference and Fiber Bragg Grating', *Journal of Lightwave Technology*, 35(1), pp. 3–9. doi: 10.1109/JLT.2016.2626793.
- Oliveira, R. *et al.* (2018) 'Polymer Optical Fiber Sensors and Devices', in Peng, G.-D. (ed.) *Handbook of Optical Fibers*. Springer, Singapore, pp. 1–40. doi: 10.1007/978-981-10-1477-2_1-1.
- Oliveira, R., Bilro, L. and Nogueira, R. (2018) 'Fabry-Pérot cavities based on photopolymerizable resins for sensing applications', *Optical Materials Express*, 8(8), p. 2208. doi: 10.1364/OME.8.002208.
- Oliveira, R., Bilro, L. and Nogueira, R. N. (2019) 'Principles of Polymer Optical Fibers', in Werneck, M. M. and Allil, R. C. S. B. (eds) *Plastic Optical Fiber Sensors: Science, Technology and Applications*. Boca Raton: Taylor & Francis, pp. 21–66. doi: 10.1201/b22357.
- Onghena, M. *et al.* (2012) 'Analysis of 18 perfluorinated compounds in river waters: Comparison of high performance liquid chromatography–tandem mass spectrometry, ultra-high-performance liquid chromatography–tandem mass spectrometry and capillary liquid chromatography–mass spectrometry', *Journal of Chromatography A*. Elsevier, 1244, pp. 88–97. doi: 10.1016/J.CHROMA.2012.04.056.
- Otrelo-Cardoso, A. R. *et al.* (2017) 'Highly selective tungstate transporter protein TupA from *Desulfovibrio alaskensis* G20', *Scientific Reports*, 7(5798), pp. 1–12. doi: 10.1038/s41598-017-06133-y.
- Paz, A. M. C. *et al.* (2007) 'Plastic optical fiber sensor for real time density measurements in wine fermentation', *Instrumentation and Measurement Technology Conference - IMTC 2007*, pp. 1–5. doi: 10.1109/IMTC.2007.379330.
- Peng, L. *et al.* (2011) 'Gaseous ammonia fluorescence probe based on cellulose acetate modified microstructured optical fiber', *Optics Communications*, 284(19), pp. 4810–4814. doi: 10.1016/j.optcom.2011.06.015.
- Pereira, V. *et al.* (2013) 'Multiparameter Optical Monitoring of Madeira Wine', *International Journal of Online Engineering (iJOE)*, 9(S8), p. 62. doi: 10.3991/ijoe.v9iS8.3389.
- Pesavento, M. *et al.* (2017) 'Towards the development of cascaded surface plasmon resonance POF sensors exploiting gold films and synthetic recognition elements for detection of contaminants in transformer oil', *Sensing and Bio-Sensing Research*, 13, pp. 128–135. doi: 10.1016/j.sbsr.2017.01.003.
- Peters, K. (2011) 'Polymer optical fiber sensors—a review', *Smart Materials and Structures*, 20(1), p. 013002. doi: 10.1088/0964-1726/20/1/013002.
- Pospíšilová, M., Kuncová, G. and Trögl, J. (2015) 'Fiber-optic chemical sensors and fiber-optic bio-sensors', *Sensors (Switzerland)*, 15(10), pp. 25208–25259. doi: 10.3390/s151025208.
- Pulido, C. and Esteban, Ó. (2013) 'Tapered polymer optical fiber oxygen sensor based on fluorescence-quenching of an embedded fluorophore', *Sensors and Actuators B: Chemical*, 184, pp.

64–69. doi: 10.1016/j.snb.2013.04.061.

Qazi, H. H. *et al.* (2019) 'Surface roughness and the sensitivity of D-shaped optical fibre sensors', *Journal of Modern Optics*, 66(11), pp. 1244–1251. doi: 10.1080/09500340.2019.1610521.

Ramani, V. and Kuang, K. S. C. (2019) 'An evaluation of the performance of a lens-based plastic optical fiber strain sensor', *Engineering Research Express*. IOP Publishing, 1(1), p. 015018. doi: 10.1088/2631-8695/ab2eb7.

Rezende, A. *et al.* (2018) 'Polymer Optical Fiber Goniometer: A New Portable, Low Cost and Reliable Sensor for Joint Analysis', *Sensors*. Multidisciplinary Digital Publishing Institute, 18(12), p. 4293. doi: 10.3390/s18124293.

Richardson, S. D. and Kimura, S. Y. (2016) 'Water Analysis: Emerging Contaminants and Current Issues', *Analytical Chemistry*, 88, pp. 546–582. doi: 10.1021/acs.analchem.5b04493.

Richardson, S. D. and Ternes, T. A. (2018) 'Water Analysis: Emerging Contaminants and Current Issues', *Analytical Chemistry*, 90, pp. 398–428. doi: 10.1021/acs.analchem.7b04577.

Rico-Yuste, A. and Carrasco, S. (2019) 'Molecularly Imprinted Polymer-Based Hybrid Materials for the Development of Optical Sensors', *Polymers*, 11(7), p. 1173. doi: 10.3390/polym11071173.

Rithesh Raj, D. *et al.* (2015) 'Ammonia sensing properties of tapered plastic optical fiber coated with silver nanoparticles/PVP/PVA hybrid', *Optics Communications*. Elsevier, 340, pp. 86–92. doi: 10.1016/j.optcom.2014.11.092.

Rivera, L. *et al.* (2009) 'Simple dip-probe fluorescence setup sensor for in situ environmental determinations', *Sensors and Actuators, B: Chemical*, 137(2), pp. 420–425. doi: 10.1016/j.snb.2009.01.064.

Rivero, P. J., Goicoechea, J. and Arregui, F. J. (2018) 'Optical fiber sensors based on polymeric sensitive coatings', *Polymers*, 10(3), pp. 1–26. doi: 10.3390/polym10030280.

Saito, K. *et al.* (2010) 'Determination of perfluorooctanoic acid and perfluorooctane sulfonate by automated in-tube solid-phase microextraction coupled with liquid chromatography-mass spectrometry', *Analytica Chimica Acta*, 658(2), pp. 141–146. doi: 10.1016/j.aca.2009.11.004.

Sawada, H., Tanaka, A. and Wakatsuki, N. (1989) 'Plastic optical fiber doped with organic fluorescent materials', *Fujitsu Scientific and Technical Journal*, 25(2), pp. 163–169.

Scott, B. F. *et al.* (2006) 'Analysis for perfluorocarboxylic acids/anions in surface waters and precipitation using GC-MS and analysis of PFOA from large-volume samples', *Environmental Science and Technology*, 40(20), pp. 6405–6410. doi: 10.1021/es061131o.

Scully, P. J. *et al.* (2007) 'Optical fibre biosensors using enzymatic transducers to monitor glucose', *Measurement Science and Technology*. IOP Publishing, 18(10), pp. 3177–3186. doi: 10.1088/0957-0233/18/10/S20.

Sequeira, F. *et al.* (2014) 'Molecularly imprinted polymer grafted on a polymeric optical fibre for ammonium sensing', in *International Conference on Applications of Optics and Photonics - AOP 2014*, p. 72.

Sequeira, F., Nogueira, R. N. and Bilro, L. (2019) 'Chemical Sensing with POF', in Werneck, M. M. and Allil, R. C. S. B. (eds) *Plastic Optical Fiber Sensors: Science, Technology and Applications*. Boca Raton: Taylor & Francis, pp. 251–266. doi: 10.1201/b22357.

Sequeira, F. R. C. *et al.* (2013) 'Experimental assessment of a plastic optical fibre based turbidity sensor', in *Riao/Optilas*. Porto, Portugal.

Sherazi, T. A. (2016) 'Graft Polymerization', in Drioli, E. and Giorno, L. (eds) *Encyclopedia of Membranes*. Berlin, Heidelberg: Springer, pp. 886–887. doi: 10.1007/978-3-662-44324-8_274.

Shin, J.-D. and Park, J. (2015) 'High-sensitivity refractive index sensors based on in-line holes in plastic optical fiber', *Microwave and Optical Technology Letters*, 57(4), pp. 918–921. doi: 10.1002/mop.28991.

Silva-López, M. *et al.* (2005) 'Strain and temperature sensitivity of a single-mode polymer optical fiber', *Optics Letters*, 30(23), p. 3129. doi: 10.1364/OL.30.003129.

Some, S. *et al.* (2013) 'Highly Sensitive and Selective Gas Sensor Using Hydrophilic and

References

Hydrophobic Graphenes', *Scientific Reports*. Nature Publishing Group, 3(1), p. 1868. doi: 10.1038/srep01868.

Späth, A. *et al.* (2010) 'Molecular recognition of organic ammonium ions in solution using synthetic receptors', *Beilstein J. Org. Chem*, 6(32). doi: 10.3762/bjoc.6.32.

Sultangazin, A. *et al.* (2017) 'Design of a Smartphone Plastic Optical Fiber Chemical Sensor for Hydrogen Sulfide Detection', *IEEE Sensors Journal*, 17(21), pp. 6935–6940. doi: 10.1109/JSEn.2017.2752717.

Swinehart, D. F. (1962) 'The Beer-Lambert Law', *Journal of Chemical Education*, 39(7), pp. 333–335. doi: 10.1021/ed039p333.

Tan, T. T. M. *et al.* (1999) 'Coating of polystyrene thin film on glass for protein immobilization in optical biosensor applications', in Lieberman, R. A., Asundi, A. K., and Asanuma, H. (eds) *Proc. SPIE 3897, Advanced Photonic Sensors and Applications*. International Society for Optics and Photonics, pp. 150–157. doi: 10.1117/12.369299.

Taylor, E. W. (1987) 'Optical waveguide diffraction grating sensor', in Trainor, D. W. and Chicklis, E. P. (eds) *Instrumentation in the Aerospace Industry*. ISA, pp. 143–147.

Teng, C. *et al.* (2017) 'Investigation of refractive index sensors based on side-polished plastic optical fibers', *Optical Fiber Technology*. Elsevier Inc., 36, pp. 1–5. doi: 10.1016/j.yofte.2017.01.008.

Teng, C. *et al.* (2019) 'Refractive Index Sensor Based on Twisted Tapered Plastic Optical Fibers', *Photonics*. Multidisciplinary Digital Publishing Institute, 6(2), p. 40. doi: 10.3390/photonics6020040.

Theodosiou, A. *et al.* (2018) 'Bragg gratings and Fabry-Perot cavities in low-loss multimode CYTOP polymer fibre', *IEEE Photonics Technology Letters*, 1135(c), pp. 1–1. doi: 10.1109/LPT.2018.2820381.

Thomas, K. J. *et al.* (2008) 'Raman spectra of polymethyl methacrylate optical fibres excited by a 532 nm diode pumped solid state laser', *Journal of Optics A: Pure and Applied Optics*, 10, p. 5. doi: 10.1088/1464-4258/10/5/055303.

Thompson, T. *et al.* (2012) 'Chemical safety of drinking-water: assessing priorities for risk management', *Int. J. Environ. Stud.*, 69(6), pp. 1–2. doi: 10.1080/00207233.2011.565947.

Tilaki, R. A. D. and Kahe, D. (2012) 'Removal of Ammonium Ions from Water by Raw and Alkali Activated Bentonite', in Pavelkova, D., Strouhal, J., and Pasekova, M. (eds) *Advances in Environment, Biotechnology and Biomedicine*, pp. 169–174.

Tiwari, A. and Uzun, L. (eds) (2017) *Advanced molecularly imprinting materials*. Scrivener Publishing LLC.

Tiwari, S., Singh, M. K. and Pandey, P. C. (2017) 'Refractive index sensor based on spiral-shaped plastic optical fiber', *IEEE Sensors Journal*, 17(6), pp. 1692–1695. doi: 10.1109/JSEN.2016.2646802.

Ton, X. A. *et al.* (2015) 'A disposable evanescent wave fiber optic sensor coated with a molecularly imprinted polymer as a selective fluorescence probe', *Biosensors and Bioelectronics*. Elsevier, 64, pp. 359–366. doi: 10.1016/j.bios.2014.09.017.

Tow, K. H. *et al.* (2017) 'Towards a new generation of fibre optic chemical sensors based on spider silk threads', p. 103231E. doi: 10.1117/12.2264438.

Trojanowicz, M. and Koc, M. (2013) 'Recent developments in methods for analysis of perfluorinated persistent pollutants.', *Mikrochimica acta*. Springer, 180(11–12), pp. 957–971. doi: 10.1007/s00604-013-1046-z.

Tsougeni, K. *et al.* (2010) 'Plasma nanotextured PMMA surfaces for protein arrays: Increased protein binding and enhanced detection sensitivity', *Langmuir*, 26(17), pp. 13883–13891. doi: 10.1021/la101957w.

Uzun, L. and Turner, A. P. F. (2016) 'Molecularly-imprinted polymer sensors: Realising their potential', *Biosensors and Bioelectronics*. Elsevier, 76, pp. 131–144. doi: 10.1016/j.bios.2015.07.013.

Varma, H. K. *et al.* (2003) 'In vitro calcium phosphate growth over surface modified PMMA film', *Biomaterials*, 24(2), pp. 297–303. doi: 10.1016/S0142-9612(02)00318-6.

- Vesel, A., Elersic, K. and Mozetic, M. (2012) 'Immobilization of protein streptavidin to the surface of PMMA polymer', *Vacuum*. Elsevier Ltd, 86(6), pp. 773–775. doi: 10.1016/j.vacuum.2011.07.019.
- Wan, W., Wagner, S. and Rurack, K. (2016) 'Fluorescent monomers: "bricks" that make a molecularly imprinted polymer "bright"', *Analytical and Bioanalytical Chemistry*, 408(7), pp. 1753–1771. doi: 10.1007/s00216-015-9174-4.
- Wandemur, G. *et al.* (2014) 'Plastic optical fiber-based biosensor platform for rapid cell detection', *Biosensors and Bioelectronics*. Elsevier, 54, pp. 661–666. doi: 10.1016/j.bios.2013.11.030.
- Wang, J. and Wang, L. (2010) 'Carbon dioxide gas sensor derived from a 547-hole microstructured polymer optical fiber preform', *Optics Letters*, 35(19), p. 3270. doi: 10.1364/OL.35.003270.
- Wang, L. and Zhang, Z. (2008) 'The study of oxidization fluorescence sensor with molecular imprinting polymer and its application for 6-mercaptopurine (6-MP) determination', *Talanta*, 76(4), pp. 768–771. doi: 10.1016/j.talanta.2008.04.024.
- Wang, Q. and Zhao, W.-M. (2018) 'A comprehensive review of lossy mode resonance-based fiber optic sensors', *Optics and Lasers in Engineering*. Elsevier, 100, pp. 47–60. doi: 10.1016/J.OPTLASENG.2017.07.009.
- Wang, X.-D. and Wolfbeis, O. S. (2016) 'Fiber-Optic Chemical Sensors and Biosensors (2013-2015)', *Analytical Chemistry*, 88(1), pp. 203–227. doi: 10.1021/acs.analchem.5b04298.
- Weinert, A. (1999) *Plastic Optical Fibers: principles, components, installation*. Edited by Siemens. Publicis MCD Verlag.
- Whitcombe, M. J., Kirsch, N. and Nicholls, I. A. (2014) *Molecular imprinting science and technology: A survey of the literature for the years 2004-2011*, *Journal of Molecular Recognition*. doi: 10.1002/jmr.2347.
- Woyessa, G. *et al.* (2016) 'Single mode step-index polymer optical fiber for humidity insensitive high temperature fiber Bragg grating sensors', *Optics Express*. Optical Society of America, 24(2), p. 1253. doi: 10.1364/OE.24.001253.
- Wu, J. *et al.* (2018) 'Analytical methods of perfluorosulfonic acids (PFSAs) and perfluorocarboxylic acids (PFCAs) in environmental water samples', *Environmental Chemistry*, 37(8), pp. 1851–1859. doi: 10.7524/j.issn.0254-6108.2017122901.
- Wulff, G. (1995) 'Molecular Imprinting in Cross-Linked Materials with the Aid of Molecular Templates— A Way towards Artificial Antibodies', *Angewandte Chemie International Edition in English*. John Wiley & Sons, Ltd, 34(17), pp. 1812–1832. doi: 10.1002/anie.199518121.
- Xue, P. *et al.* (2019) 'Refractive Index Sensing Based on a Long Period Grating Imprinted on a Multimode Plastic Optical Fiber', *IEEE Sensors Journal*, 19(17), pp. 7434–7439. doi: 10.1109/JSEN.2019.2915361.
- Xue, S. *et al.* (2007) 'Theoretical, Numerical, and Experimental Analysis of Optical Fiber Tapering', *Journal of Lightwave Technology*, 25(5), pp. 1169–1176. doi: 10.1109/JLT.2007.893028.
- Yan, H. and Row, K. H. (2006) 'Characteristic and Synthetic Approach of Molecularly Imprinted Polymer', *International Journal of Molecular Sciences*, 7, pp. 155–178. doi: 10.3390/i7050155.
- Yang, D. *et al.* (2017) 'Fatigue crack monitoring using plastic optical fibre sensor', *Procedia Structural Integrity*, 5, pp. 1168–1175. doi: 10.1016/j.prostr.2017.07.029.
- Yang, X. *et al.* (2011) 'Oxygen gas optrode based on microstructured polymer optical fiber segment', *Optics Communications*, 284(13), pp. 3462–3466. doi: 10.1016/j.optcom.2011.03.036.
- Yao, W., Li, Y. and Huang, X. (2014) 'Fluorinated poly(meth)acrylate: Synthesis and properties', *Polymer*. Elsevier, 55(24), pp. 6197–6211. doi: 10.1016/J.POLYMER.2014.09.036.
- Yeh, P. *et al.* (2017) 'Applications of LEDs in optical sensors and chemical sensing device for detection of biochemicals, heavy metals, and environmental nutrients', *Renewable and Sustainable Energy Reviews*. Elsevier Ltd, 75, pp. 461–468. doi: 10.1016/j.rser.2016.11.011.

References

Young, W. M. *et al.* (2013) 'Determination of Perfluorochemicals in Fish and Shellfish Using Liquid Chromatography–Tandem Mass Spectrometry', *Journal of Agricultural and Food Chemistry*, 61(46), pp. 11166–11172. doi: 10.1021/jf403935g.

Yuan, W. *et al.* (2011) 'Improved thermal and strain performance of annealed polymer optical fiber Bragg gratings', *Optics Communications*. Elsevier B.V., 284(1), pp. 176–182. doi: 10.1016/j.optcom.2010.08.069.

Zeni, L. *et al.* (2018) '[INVITED] Slab plasmonic platforms combined with Plastic Optical Fibers and Molecularly Imprinted Polymers for chemical sensing', *Optics & Laser Technology*, 107, pp. 484–490. doi: 10.1016/j.optlastec.2018.06.028.

Zhang, H. *et al.* (2011) 'Detection of Acetone Vapor Using Graphene on Polymer Optical Fiber', *Journal of Nanoscience and Nanotechnology*, 11(7), pp. 5939–5943. doi: 10.1166/jnn.2011.4408.

Zhang, T. *et al.* (2014) 'Electrochemical Biosensor for Detection of Perfluorooctane Sulfonate Based on Inhibition Biocatalysis of Enzymatic Fuel Cell', *Electrochemistry*, 82(2), pp. 94–99. doi: 10.5796/electrochemistry.82.94.

Zhang, W. and Webb, D. J. (2014) 'Humidity responsivity of poly(methyl methacrylate)-based optical fiber Bragg grating sensors', *Optics Letters*, 39(10), pp. 3026–3029. doi: 10.1364/OL.39.003026.

Zhong, N. *et al.* (2013) 'Effects of surface roughness on optical properties and sensitivity of fiber-optic evanescent wave sensors.', *Applied optics*, 52(17), pp. 3937–45. doi: 10.1364/AO.52.003937.

Zhong, N. *et al.* (2019) 'A highly sensitive photocatalytic plastic optic-fiber sensor for selective detection of phenol in aqueous solutions', *Sensors and Actuators, B: Chemical*. Elsevier, 285, pp. 341–349. doi: 10.1016/j.snb.2019.01.042.

Zhou, Q., Tabacco, M. B. and Rosenblum, K. W. (1991) 'Development of chemical sensors using plastic optical fiber', in *Proc. SPIE 1592, Plastic Optical Fibers*, pp. 108–113. doi: 10.1117/12.50998.

Zhuang, Q. *et al.* (2016) 'Water-equivalent fiber radiation dosimeter with two scintillating materials', *Biomedical Optics Express*, 7(12), pp. 4919–4927. doi: <http://dx.doi.org/10.1364/BOE.7.004919>.

Ziemann, O. *et al.* (2008) *POF Handbook: Optical short range transmission systems*. Second Edi. Springer. doi: 10.1007/978-3-540-76629-2.

Zubia, J. and Arrue, J. (2001) 'Plastic optical fibers: An introduction to their technological processes and applications', *Optical Fiber Technology*, 7(2), pp. 101–140.

Zubia, J., Garitaonaindía, G. and Arrúe, J. (2000) 'Passive device based on plastic optical fibers to determine the indices of refraction of liquids', *Applied Optics*, 39(6), p. 941. doi: 10.1364/AO.39.000941.